C-H activation mediated by Transition Metals

Vom Fachbereich Chemie
der Technischen Universität Kaiserslautern
zur Verleihung des akademischen Grades
"Doktor der Naturwissenschaften" (Dr. rer. nat.)
genehmigte

DISSERTATION

Vorgelegt von

Dawei Zhao

Tag der mündlichen Prüfung: 24.11.16

Dekan:	Prof. Dr. Christoph van Wüllen
Vorsitzender:	Prof. Dr. Stefan Ernst
Gutachter:	1.Prof. Dr. Christoph van Wüllen
	2.Prof. Dr. Markus Gerhards

D 386

(2016)

Contents

Abbreviations

σ ..... bond orbital

σ-CAM ..... σ-complex assisted metathesis

σ^* ..... antibonding orbital

AMLA ..... ambiphilic meta ligand activation

AO ..... atomic orbital

B3 ..... B3LYP/def2-TZVP

BO ..... bond-order

bpym ..... bpympyrimindine

BQ ..... benzoquinone

CGTO ..... contracted Gaussian-type orbital

CMD ..... concerted metalation deprotonation

Co^{2+} complex . Co^{2+}(H^{i}PrMal66) complex

D3 ..... B3LYP-D3/def2-TZVP

DFT ..... density functional theory

DODS ..... Different Orbitals for Different Spins

EA ..... elctrophilic activation

ECP ..... effective core potential

Hbpym ..... protonated bpympyrimindine

HK ..... Hohenberg Kohn

IR^{c} ..... stretching frequency of the cis C-H bond

IR^{t} ..... stretching frequency of the trans C-H bond

IR^{α} ..... stretching frequency of the α-C-H bond

IR^{δ} ..... stretching frequency of the δ-C-H bond

KIE ..... kinetic isotope effect

KS ..... Kohn and Sham

LP ..... lone pair

MASBM ..... metal assited σ-bond metathesis

MO ..... molecular orbital

NAO ..... natural atom orbital

NBO ..... natural bond orbital

NHO ..... natural hybrid orbital

Ni^{3+} complex . $Ni^{3+}(H^{i}PrMal66)$ complex

NLS ..... natural Lewis structure

NO ..... natural orbital

NPA ..... natural population analysis

OA ..... oxidative addition

OATS ..... oxidative added transition state

Occ(σ ..... occupancy in the antibonding orbital of the C-H bond

Occ(σ) ..... occupancy in the bond orbital of the C-H bond

OHM ..... oxidative hydrogen migration

OWSO ..... occupancy-weighted symmetric orthogonalization

PES ..... potential surface scan

pic$^-$ ..... η^2-N,O-picolinate

QM-RP ..... quantum mechanical-rapid prototyping

RE ..... reductive elimination

SBM ..... σ-metathesis

SD ..... slater determinante

TFA$^-$ ..... trifluoracetate

TM ..... transition metal

TS ..... transition state

TSR ..... two-state reactivity

VB ..... valence bond

List of Figures

1 Introduction

1.1 C-H cleavage and functionalization

Hydrocarbons, especially saturated hydrocarbons, are the main constituents of crude oil and natural gas. Conversion of saturated hydrocarbons from fossil or biogenic resources to more valuable feedstock is one of the central challenges[1]. Success of C-H functionalization can potentially revolutionize the industrial manufacture of fine chemicals. New types of hydrocarbon transformations can help reduce petroleum pollution and other important environmental problems. Mild and selective transformations of C-H bonds will undoubtedly influence the chemical field, including synthesis of natural products, agrochemicals, polymers, and feedstock commodity chemicals, leading to improved economy and increased overall efficiency[2]. Direct formations of C-C and carbon-heteroatom bonds from inactivated C-H bonds via C-H functionalizations have enormous potential for advancing the field of chemical synthesis. Direct C-H functionalizations can drastically shorten possible routes in natural product synthesis by providing unprecedented disconnections and have potential to streamline synthetic schemes by eliminating the need for preparations and isolations.

Reactions of C-H bonds, their cleavage and functionalization fascinated chemists for years. Two factors limit the selective functionalization of a C-H bond: the inert nature of the C-H bond and selectivity control.

The strong, unpolar and general unreactive nature of a C-H bond make it highly challenging to cleave directly, both heterolytically or homolytically. This chemical inertness originates from the fact that the constituent atoms of saturated alkanes are all held together by strong C-C and C-H bonds, so that no empty orbital of low energy or filled orbital of high energy are available to possibly participate in a chemical reaction. This is different in the cases of olefines, alkynes, and aromats, which offer π and π^* orbitals that can interact with other species[3].

For example, the homolytic bond dissociation enthalpy of methane at 25°C is 440 kJ/mol (ca. 420 kJ/mol for other primary C-H bonds)[4]. Direct functional-

izations of C-H bonds suffer from the fact that new bonds in viable products are generally weaker than the C-H bonds in the parent hydrocarbons. However many transition metals(TMs) have been discovered to catalyze C-H-cleavages. Most of the functionalization reactions of C-H-bonds with TM complexes occur at remarkably mild conditions with high selectivity in contrast to almost all the other presently employed processes.

The TM-mediated C-H functionalizations typically involve two steps: oxidative addition(OA) followed by reductive elimination(RE) leading to functionalization. The energetic cost of cleaving the C-H bond is compensated, at least partly, by the formation of strong M-H and M-C bonds in the intermediate R-M-H species[4].

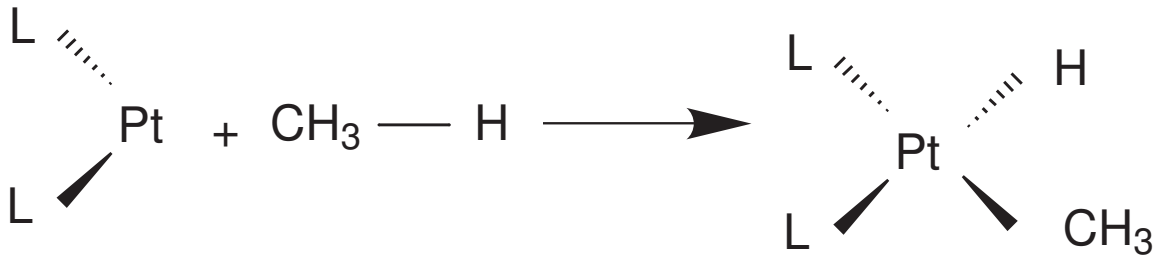

Figure 1.1: Pt-mediated methane oxidative addition

As shown in the Figure 1.1, Platin(Pt)-H and Pt-CH_3 bond enthalpy in neutral square-planar Pt^{2+}-complexes are about 306-314 kJ/mol and 251-268 kJ/mol, respectively and the entropy loss of oxidative addition is about 42 kJ/mol. It seems that with assistance of a TM a thermodynamical neutral C-H cleavage is feasible[4].

The common uses of organometallic catalysts under remarkable mild conditions, which lead to C-H functionalization, reflect as well that metal-mediated C-H cleavages and functionalizations are thermodynamically feasible.

Another evidence for this conclusion is the unusual selectivity of the TM-mediated C-H functionalization. The bond dissociation enthalpy for a primary C-H bond (420 kJ/mol) is smaller than for H-C_6H_5 (460 kJ/mol), but C-H functionalization of benzene is still preferred. And in plenty of reactions primary C-H bonds are preferred to secondary and tertiary C-H bonds to cleave, even if the dissociation enthalpy of a primary C-H bond is higher[4].

All the evidences indicate that the selectivity, which is driven by kinetic bias, are the key consideration in catalyst research for C-H functionalizations.

1.2 Development of synthetic applications

Since C-H functionalizations could potentially be a uniquely powerful synthetic tool, the increase in the depth and breadth of the research is enormous in recent decades. The efforts of most experimental chemists focus on influencing steric and electronic features to expand the usage and scope of reactions and optimize the selectivity and efficiency by changing oxidants, metal ions, ligands, solvents, directing groups and protecting groups.
The most powerful and most widely used catalysts are Palladium(Pd)-based[5–7]. We will briefly review palladium-catalyzed C-H functionalizations, as to highlight significant advances in this field and document challenges that remain to be addressed.

The versatility of palladium-catalyzed C-H functionalizations have hugely expanded its scope in the past few years. Direct conversions of C-H bonds into C-O, C-N, C-S, C-halogen, C-B, and C-C bonds is possible. The most common strategy is the use of substrates that contain coordinating ligands(directing group). These ligands bind to the metal center and a proximal C-H bond is activated by the metal, leading to desired functionalizations. Ligand-directed C-H functionalizations at Pd centers allow diverse bond constructions (e.g. C-O, C-N, C-S, C-halogen, C-C). Most of those reactions can be performed in the presence of air and water, greatly enhancing the versatility and practicality of this chemistry.

The scope of directing groups has been greatly expanded recently: imines, oxime ethers, azonbenzene derivatives, nitrogen heterocycles, amides, carboxylic acids, esters, alcohols, etc. can all be used as effective directing groups. This greatly extends the utility of Pd-mediated C-H functionalizations. Only a few less basic functionalities as directing groups remain a challenge: aldehydes, ketones, oxygen containing heterocycles[8].

Pd-catalyzed ortho-oxygenation reactions can be performed with a variety of different oxidants. The first of these is $PhI(OAc)_2$, which is tolerant of many functional groups, is shown in Figure 1.2 in the next page. Polymer-immobilized $ArI(OAC)_2$ as the oxidant offers the advantage that it can be recovered from the reaction mixture and be recycled. The use of IOAc as oxidant achieves excellent yields and high selectivities for functionalizations of N-methylamines and N-methylanilines. Using inorganic peroxides (Oxone or $K_2S_2O_8$) as oxidants is an attractive alternative to costly iodine-based reagents. From financial and practical aspects, using air as the oxidant

is most attractive. It has recently been reported that under an atmosphere of O_2 benzylic C-H bonds can be effectively acetoxylated[8].

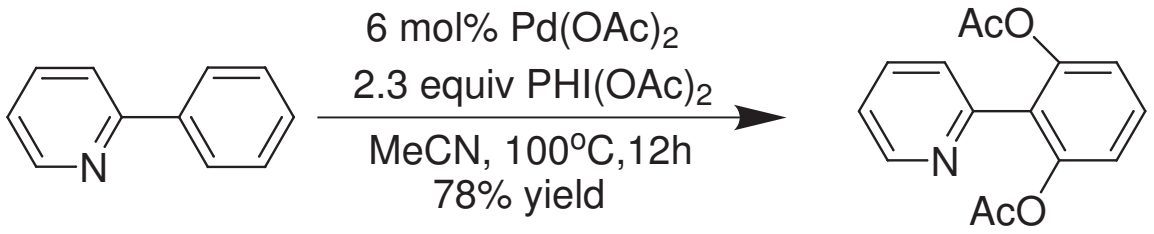

Figure 1.2: Pd-catalyzed ortho-oxygenation with $PhI(OAc)_2$ as oxidant

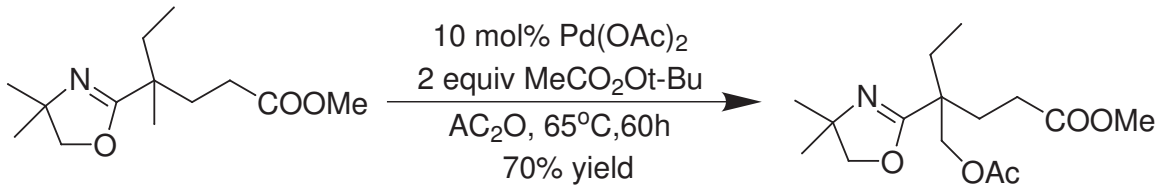

Figure 1.3: Pd-catalyzed sp^3-C-H bond acetoxlation

With combination of Oxone and $Pd(OAc)_2$ not only sp^2-C-H bonds but also inactive sp^3-C-H bonds can be efficient acetoxlated which use Ac_2O as a crucial promoter[9] as shown in the Figure 1.3.

The formation of C-N bonds from C-H bonds is very important due to the importance of C-N bonds in many biologically relevant molecules[10]. The most exciting C-N bond constructions are intramolecular C-N bond formations, leading to a heterocycle. Pd-catalyzed cyclizations of N-alkylanilines in presence of $PhI(OAc)_2$ proceed efficiently at room temperature. And tosylhydrazones, phenethyltriflamides, lactams can all be used as directing groups leading to high yields of intramolecularly aminated products. And those reactions show good functional group compatibility and tolerant with many functional groups on the aromatic ring: halogens, acetyl, cyano and nitro substituentes. A variety of lactams were formed in high yields using $Pd(OAc)_2$ as catalyst[8].

The most widely studied area in the field is C-C bond formations. Various catalytic cycles have been developed to accomplish the olefination, arylation, alkylation, and carbonylation of C-H bonds. $C(sp^2)-C(sp^2), C(sp^2)-C(sp^3), C(sp^3)-C(sp^3)$ coupling methods have been reported[5,8].

The most exciting strategies in this field are Pd-catalyzed ligand-directed cross-coupling without requirement for prefunctionalization of the reagents. In these trans-

formations diverse functional groups can be used as directing groups: pyridine, quinoline, pyrimidine, pyrazole, acetannilides, pivalanilides, among others. Ag_2CO_3 was employed as oxidant. In some of these reactions a promoter(benzoquinone(BQ)) is required, but the role of the promoter is still unknown. The authors believe that the promoter is used to facilitate the C-C bond formation in the reductive elimination step of the catalytic cycle.

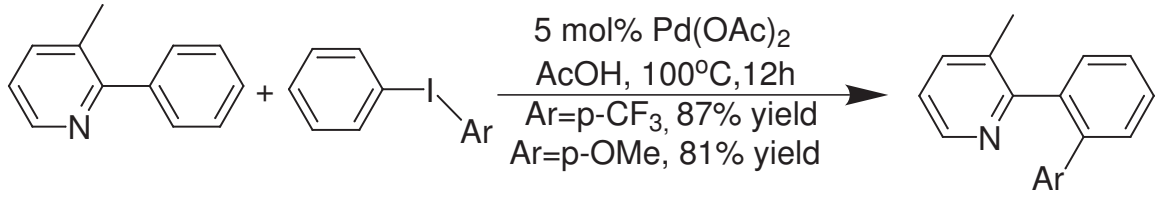

Figure 1.4: Pd-catalyzed sp^2-phenylation

As shown in Figure 1.4, sp^2-phenylations can be catalyzed by diphenyliodonium salts with the use of diverse directing groups: arylpylidines, quinolines, pyrrolidinones, oxazolidinones, and benzodiazepines. Several key experiments show that the catalytic reaction shows a first-order dependence on iodide, a second-order dependence on Pd, and an inverse third-order dependence on arylpyridine. This is consistent with the rate law that the rate-limiting step is the formation of a dimeric Pd^{2+}-complex[11]. Using stoichiometric amounts of AgOAc in conjugation with ArI the arylation of substituted anilides, benzoxazoles, benzonic acid derivates can be achieved. All of these transformations show broad scope and functional group compatibility.

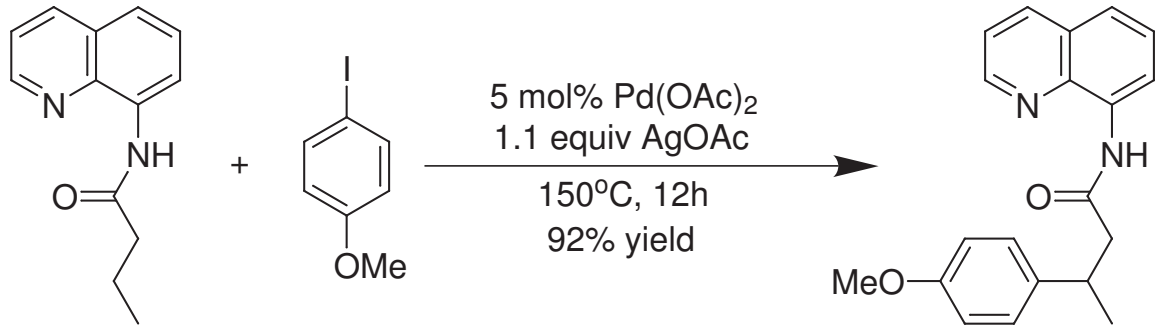

Figure 1.5: Pd-catalyzed sp^3-C-H bond arylation

With the combination of AgOAc and Ar-I, inactive sp^3-C-H bonds can be catalytically arylated by Pd with diverse directing groups: pyridines, aminquinolines and picolinamides as shown in Figure 1.5, sp^3-C-H arylation of caboxylic acids can be

achieved with arylboronic esters, but the regioselectivity and mixture of mono-and diarylated products remain a challenge.

With phosphine ligands the combination of Pd^{2+} and Ar-I catalyzes the arylation of α-methyl groups, while at least one additional α-substituent is required to achieve efficient catalysis as shown in Figure 1.6.

sp^3-C-H bonds adjacent to the nitrogen in amines can be oxidatively aklylated through an iminium ion intermediate, using Pd^{2+} species as catalyst[12]. It is reported that sp^3-allylic C-H bonds undergo oxidative alkylation reactions utilizing Pd^{2+} complexes as a catalyst[13]. Still oxidative cross-coupling reactions of simple aliphatic C-H bonds by Pd-species remains to be a challenging problem.

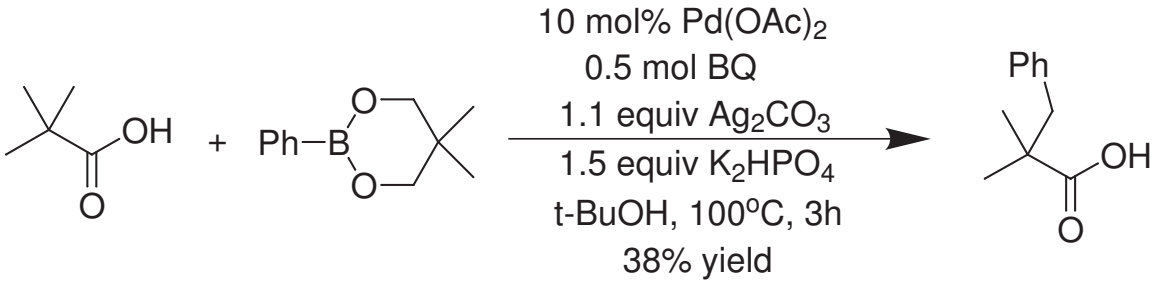

Figure 1.6: Pd-catalyzed sp^3-C-H bond arylation

Only sp^2-C-H bonds can be alkenylated with Palladium as catalyst as shown in Figure 1.7. The ortho-alkenylation of benzylamines and acetanilides can be achieved with electron-deficient alkenes. In these transformations $Cu(OAc)_2$ or benzoquinone is used as oxidant and terminal α,β-unsaturated esters as the source of alkenyl groups.

Only sp^2-C-H bonds can be carbonylated under an atmosphere of CO with Pd as

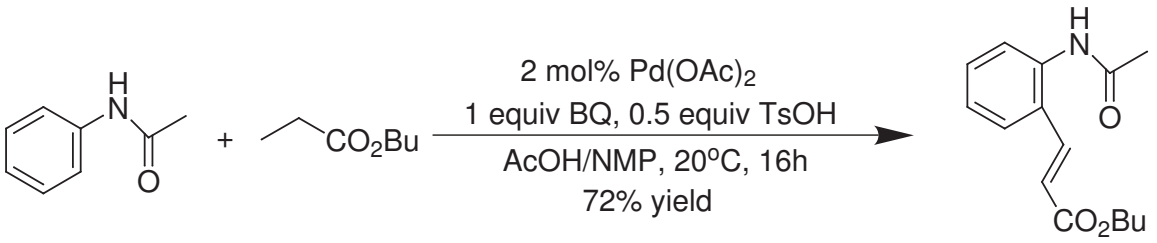

Figure 1.7: Pd-catalyzed sp^2-C-H bond alkenylation

shown in the Figure 1.8. Amines and carboxylate can be used as directing groups and $Cu(OAc)_2$ and benzoquinones are used as oxidant. A interesting fact is that when changing the solvent instead of carbonylated products cyclic imidates were formed in high yields.

The only example of a Pd-catalyzed C-H alkynlation is the reaction of anilides with bromalkynes. Using AgOTf and K_2CO_3 as additives a number of substituted anilides could be ortho-alkynlated in high yield.

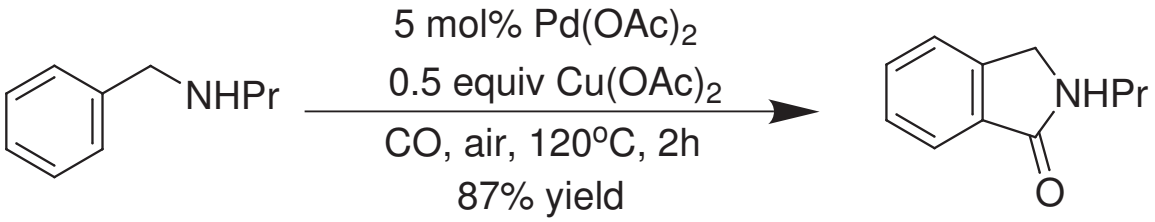

Figure 1.8: Pd-catalyzed cabonylation

Most Pd-catalyzed ortho-alkylations are accomplished with SnR_4 and Boronic acids. $Cu(OAc)_2$ was used as the terminal oxidant and Benzoquinone as a key promoter. The author believes that benzoquinone accelerates both cyclopalladation and C-C bond formation[14]. Recently reported meta-C-H bond functionalizations use a class of easily removable nitrile-containing templates[15]. The end-on interaction between the linear nitrile group and the metal center relieves the strain of the cyclophane-like transition state and overrides ortho-directing effects.

Despite all progresses in this field, sp^3- versus sp^2-C-H functionalization will clearly require more investigations[3]. Sanford (2010) concludes that the extensive versatility of Pd catalysts in contrast to other TM metals predominantly stems from the tolerance with a wide variety of directing group, compatibility with oxidants, air, water, and the selectivity in the functionalizations of cyclopalladated intermediates. However the origin for the differences remains a challenge to investigation, the interplay between catalyst, ligands, solvent, additives, and substrates remain a challenge to be addressed.

Improvements in regioselectivity, efficiency and expanding the scope of directing groups in this field will be closely tied to mechanistic investigations. The mechanistic understanding of these transformations and developments of novel reactions will greatly facilitate the design of catalysts to improve the versatility and practicality of these catalytic transformations.

1.3 Development of mechanistic aspects

A thorough understanding of the mechanism of C-H functionalization processes remains a key consideration, and computational modeling plays a central role in pro-

viding insight into the processes.[16] Computational studies give information that is difficult, if not impossible, to obtain directly from experiments. Computational modeling of mechanic pathways give key information on characteristics of the transition state(TS) and intermediates on the potential energy surface(PES). It allows the evaluation of energy barriers ($\Delta E^{\ddagger}$) and activation barriers ($\Delta G^{\ddagger}$).

Transition state determinations lead to a better understanding of reaction mechanisms that can suggest rate-limiting steps of catalytic cycles and provide insights into reactivities. With these transition states a lot of reaction cycles have been proposed and the understanding of mechanisms can lead to the development of new conditions and reagents.

The electronic structure of the TS allows the characterizations of mechanisms of reactions in terms of bonds that are broken and formed. Computations of full energy profiles give access to rate determining steps for transformations of interest. Intermediates, which may be too unstable to be observed, can be computationally analyzed. All this information allows to propose modifications of both catalysts and experimental conditions to improve the reactivity and the selectivity of catalysts.

Catalytic cycles include a series of elementary, stoichiometric reactions: oxidative addition, reductive elimination, migratory insertion, β-hydrogen elimination, metathesis and more. The development of methods to link these step together leads to many catalytic processes used today.

The C-H bond-breaking step is assumed to be the most difficult transformation in the multi-step process of C-H functionalization due to the inertness of the C-H bond. The mechanism of this step is generally considered to fall into one of four general categories: oxidative addition(OA), σ-bond-metathesis(SBM), 1,2-addition or electrophilic activation(EA). In many cases these mechanisms compete with each other[3].

Computational studies suggest that C-H cleavage processes can be assisted by heteroatoms in a ligand, which can reduce the energy barrier. A plenty of novel reactions has been developed: σ-CAM(complex assisted metathesis), OATS(oxidative added transition state), OHM(oxidative hydrogen migration), AMLA (ambiphilic meta ligand activation) and MASBM(metal assisted σ-bond metathesis). Most of these newly discovered reactions emphasize the dual role of metal and ligand (as intramolecular base), this makes SBM processes more accessible and improves the selectivity and activity of catalysts[17].

We will briefly review theoretical studies of the Shilov reaction, to highlight some significant advancements in this field and document challenges that remain to be addressed.

Before the discovery of the Shilov reaction, it was believed that direct functionalization of inert C-H bonds could only be accomplished with metal surfaces, strong oxidants or radical reagents. The Shilov reaction showed that inert C-H bonds of some alkanes can be functionalized by $[Pt(Cl)_4]^{2-}$ in acidic aqueous conditions. These transformations show an unusual selectivity: primary C-H > secondary C-H > tertiary C-H, which is opposite to the trends of the dissociation energies[3,4,16]. Theoretical studies have shown that the nature of the ligands and their spatial arrangement around the metal center strongly influence the reaction mechanism[18].

Using DFT and ab initio methods C-H functionalizations of methane by $Pt(Cl)_2$ was theoretically studied[19]. The overall activation barrier of 27 kcal/mol agrees with the experimental value of 28 kcal/mol. All, σ-bond metathesis, AMLA and oxidative addition mechanisms are possible in this transformation. The unusual selectivity is caused by the higher polarity and strength of the Pt-(n-alkyl) bond, in other words, the thermodynamically favored intermediates are formed. It was shown as well that the solvent (water) plays a critical role in the transformations by ligand exchanges and proton transfers.

Zhu and Ziegler with computational studies have shown that coordinations of methane on Pt centers, rather than cleavages of C-H bonds are the rate-determining step[20–22].

The ligand effect (Cl^- substituted by X^-, X=F, Cl, Br, I, NO_2, and CN) was theoretically investigated before[20,21]. Reactivities of PtX_2 catalyst increase in the order of ligands $F^-<Cl^-<Br^-<I^-<NO_2^-<CN^-$, which is located trans to the methane[22]. The origin of the trends in the reactivity is suggested to originate from the strength of the trans-ligand bond to Pt^{2+}, enhancing the energy barrier associated with C-H cleavages. It reveals that cis/trans isomerisms in the active Pt aqua species play as well a key role.

Nevertheless, gas-phase studies of the methane activation by ligated transition metal cations $(MX_n)^+$ show a reverse C-H reactivities($F^->Cl^->Br^- >I^-$). The reason for these trends in reactivity is explained as the electronegativity of the halogen atom and the corresponding reaction enthalpy of the formation of HX[1].

Further developments of the Shilov chemistry lead to catalytic oxidations of methane to methanol possible[23,24]. $[Pt(Cl)_2(bpym)]$(bpym=bipyrimindine) can catalytically oxidize methane using concentrated sulfuric acid as solvent and oxidant under high

temperatures ($180 - 220°C$). The substitution of a bpym ligand by methane is the rate-determining step with an energy barrier of 34 kcal/mol, when chloride ligands are situated cis to methane[25]. When the chloride ligand is trans to methane, the energy barrier increases to 44 kcal/mol. This again shows the strong influence of trans ligands.
The nature of C-H cleavage mechanisms (OA or SBM) depends on cis/trans isomerisms of catalysts and the nature of the ligands. The change of ligands (Cl to OSO_3H, bpym to ammoniac) cab cause changes of favored mechanisms.

The pH-value influences the oxidation of methane as well. The energy barrier is significantly reduced by protonation (from 39.0 kcal/mol for $[Pt(Hbpym)(Cl)(OSO_3H)]^+$ to 27.9 kcal/mol$[Pt(Hbpym)(Cl)(OSO_3H_2)]^{2+}$, Hbpym = protonated bipyrimidine). The methane coordination on the Pt center is the rate-determining step of the C-H functionalization in all these reaction systems. The overall energy barrier can be separated into 27 kcal/mol for methane coordinations and 5 kcal/mol for C-H cleavages.

Calculations predicted that $[Pt(pic)(TFA)_2]^-$ ($pic^- = \eta^2$-N,O-picolinate, TFA^- =trifluoracetate) can promote methane coordinations. The experiments confirmed that the $[Pt(pic)(TFA)_2]^-$ catalyst is 300 times more active than $[Pt(bpym)(TFA)_2]$. The energy barrier for the coordination of benzene of 14 kcal/mol is reduced to 5k cal/mol using pic^- as ligands[26], which shows the power of synergy when experiment and theory work together.

QM-RP (quantum mechanical rapid prototyping) is a new computational approach to discover new catalysts, that follows a five-steps flow[27]:

- complete and detailed descriptions of the reaction mechanism for a well known experimental system
- characterizations of the catalytic bottlenecks
- new catalyst screening, using a variety of metals, ligands, cocatalysts, or solvents
- catalyst refinement
- experimental test

The QM-RP was used for the development of the methane oxidation. Calculations show strong influences of pH values and inhibitions of the reaction by water solvating the ground states of the reactants. With Ir^{3+} and a pincer NNC ligand the overall energy barrier of C-H functionalization can be reduced to less than 30 kcal/mol without

being poisoned by water. Experiments confirm that this catalyst shows excellent activities for the methane oxidation[28].
In absence of chloride, amine, and aqua ligands oxidationa of methane to acetic acid can be accomplished with dissolved Pd^{2+} in concentrated H_2SO_4 in the presence of O_2 and CO at 453 K[29]. The rate determing step ($\Delta G^{\ddagger} = 41.5\ kcal/mol$) is the concerted metalation deprotonation(CMD) of methane, in which the formation of the Pd-CH_3 bond is concomitant with a proton transfer to the η^2-OSO_3H^- ligand.

However, developments in the study of mechanisms are still at an early stage, a number of major challenges must be overcome. In Shilov reactions all mechanical studies indicate that the rate determining step is methane coordinations on Pt centers. However which factors influence the coordination step and how the Pt centers influence C-H bonds is not well understood. C-H bond coordinations on metals lead to a so-called σ-complex, which appears to be involved in most of C-H functionalization reactions, regardless of reaction mechanisms. Balcells(2010)[16] pointed out that there are three fundamental aspects to consider in C-H functionalization processes, despite large differences among the various mechanisms.

- how to bring the C-H bond into the proximity of the metal
- mechanism of the C-H bond cleavage in the metal coordination
- thermodynamic stability of the organometallic product

The first two points are connected to the C-H coordination step[2,30–32]. Most computational studies call this step a coordination step and don't realize that in this step the coordinated C-H bonds are strongly influenced by the transition metal (TM) centers, which lets most TM-mediated C-H cleavages and functionalizations to occur under mild conditions. The coordination to metal centers results in altered and/or enhanced reactivities of C-H bonds, through associated changes in the relative energies of their orbitals or their polarity[3].

Many examples of C-H functionalizations at TM centers under remarkably mild conditions make it evident that interactions between metal centers and coordinated C-H bonds are critical factors that make the fundamental difference of TM-mediated C-H functionalization processes and other presently employed processes.

Since a understanding of interactions between a TM center and a coordinated C-H bond is essential for designing improved C-H functionalization reactions, Bergman (2007) concludes that this coordination step is the biggest issue of all mechanistic questions about C-H functionalization processes[2]. Unfortunately C-H bonds bind weakly

to metals, so the intermediates in C-H functionalization processes have short lifetimes. Direct experimental evidences and studies of these complexes are problematic, but a substantial body of evidences suggests that these complexes do exist.

Clearly a need for further investigations of these σ-complexes remains, especially into interactions between metal centers and coordinated C-H bonds in the complexes.

1.4 Agostic interaction

First we differentiate between the terms C-H functionalizations and C-H activations. We use C-H activations to describe a process, in which the strength of a C-H bond is reduced, this is especially indicated by a significant lowering of the corresponding C-H stretching modes in IR spectra. C-H cleavages and functionalizations are consequences of C-H activations with or without assistances of other species in TM-mediate catalytic processes.

A hydrocarbon coordinating to a metal leads to the so-called σ-complex, which appears to be involved in most C-H functionalization reactions. Realizing that the C-H bond coordination and the σ-complex formation is an important process leading to eventual C-H activations, the term agostic interaction was coined by Brookhart and Green. It describes interactions that come from two-electron, three-center bonding interactions between a metal center and a C-H bond, which is held in proximity of the metal center[3,33].

The presence of the metal atoms imparts certain properties to the C-H bond in its proximity, leading to C-H activations or cleavages. This is why most transition metal-mediated C-H cleavages and functionalizations processes react under mild conditions, in contrast to all other C-H functionalization processes.

We do not consider hydride-bond like situation, in which the M-H-C angle is close to 180°. Despite the significance of agostic interactions, especially C-H bond activation effects, agostic interactions are proved difficult to characterize[34–36].

X-ray diffraction studies suffer from the low scattering factor of hydrogen atoms experimentally and the difficulties in locating hydrogen atoms, which means that the position of hydrogen atoms can only be determinated approximately. Uncertainties in M-H and C-H distances are more than 10 pm[34]. It can lead to unreliable conclusions identifying agostic interactions with X-ray diffraction spectroscopy.

NMR spectroscopy can be used to reveal redistributions of the bonding electron density during developments of an agostic interaction. The fluxionality of most C-H

bonds means that only the strongest agostic interactions can be characterized at low temperatures[37].

The best way to identify agostic interactions is using vibrational spectroscopy. Stretching frequencies of a C-H bond show a proper relationship with strengths of interactions[38]. A frequency reduction of a C-H stretching mode is the diagnostic evidence for an agostic interaction. However coupling of individual C-H oscillators leading to delocalized normal modes, overtones and fermi resonances may complicate determinations. Only partial deuteriations of a agostic C-H bond, which decoupl his oscillator from other C-H-vibrations, can give reliable evidences for strengths of the agostic C-H bond[39].

In spite of all experimental difficulties most agostic interactions have been identified using geometrical distortions, particularly reduced M-C and M-H distances and the deformation of M-C-H angles. Shift of NMR signals of H-atoms was also used to identify agostic interactions[34–36,40].

On the computational side one of the main problems with HOMO and LUMO analysis of agostic interactions are clearly connected to the fact that molecular orbitals (MO) delocalize over all atoms of a molecule. Based on HOMO-LUMO analysis only the involvement of orbitals can be discussed. But the delocalization nature of MOs prevent the clear understanding of natures and consequences of the interactions[34–36].

With generalized compliance matrixes, strengths of α-agostic bonds for some small molecules is determinated to be similar to a typical hydrogen bond ($\leq$10 kcal/mol)[3,41]. By investigations of charge-density distributions in d^0 complexes, experimentally and theoretically, the author concluded that C-H activations are caused by negative hyperconjugative delocalizations of M-C bonding electrons and not by C-H bond donations[34]. The author concluded as well that characterizations of agostic interactions and understanding of their fundamental natures even for simple systems remain exclusive.

Based on different structural and spectroscopic properties some additional terms were coined: pregostic[42] and anagostic interaction[35]. For example anagostic interactions refer to any M-H-C interactions that are not agostic.
Numerous definitions of agostic interactions exist.

- Agostic is used to discuss the various manifestations of covalent interactions between C-H groups and transition metal centers in organometallic compounds, in which a hydrogen atom is covalently bonded simultaneously to both a carbon and to a transition metal atom[33].

- Agostic interactions are characterized by distortions of an organometallic moiety which brings an appended C-H bond into close the proximity with a metal center[34].

- Agostic interactions are generally characterized as a T-shaped (near perpendicular) attack of a metal on a C-H-bond[43].

Much of debates have centered around characterizations of agostic interactions and which orbitals are involved in the HOMO-LUMO analysis. The fundamental nature of agostic interactions are more difficult to rationalize. Avoiding these debates we use a general definition from Weinhold[43]: The agostic interaction describe the interaction of transition metals in a side-on (T-shaped) manner with nearby alkyl C-H bonds, and this type of interactions will be named "hyperconjugative interactions" in this thesis.

With calculated IR-Spectra and normal mode analyse, agostic interactions can be characterized by the lowering of C-H stretching frequencies, which suggests C-H bond activations. Unless otherwise mentioned, symmetric stretching frequencies of the C-H bond will be noted, when more C-H oscillators are coupled. We will focus on C-H activation effects in specific molecules and try to determine the critical factor that cause C-H activations.
The mechanism of C-H activations is simple. In the Dewar-Chatt-Duncanson model it results from two synergic transfers of electron densities:

- donations from the C-H bonding(σ) orbital into a symmetry-adapted vacant orbital of L_nM

- backdonations from an occupied orbital of L_nM into the C-H antibonding(σ^*) orbital

The L_nM-systems have both donor and acceptor orbitals, interactions with C-H-σ and -σ^* orbitals can act synergistically. Such self-reinforcing charge flows enables a significantly strong interaction, which may lead to strong C-H activations.

Both of these type of interactions tend to reduce the C-H bond strength, leading to an elongated C-H distance and a lowering of its vibrational frequency. The strength of C-H activations depends on the actual nature and magnitude of the two contributions to the transfer of electron densities: σ-donations from and backdonations into the C-H bond should lead to decrease of occupancy number in C-H-σ orbital and increase of occupancy number in C-H-σ^* orbital respectively, and further lead to C-H activations. Since C-H activation effects from donations of a C-H-σ orbitals can be diminished by

interactions with ambient bonds, the so called relaxation effects, it is general believed that occupancy number reductions of a C-H-σ orbital is not the critical factor leading to C-H activations[43].

This mechanism indicates that analyse of occupancy numbers in C-H-σ and C-H-σ^* orbitals permit us to decide whether σ-donations or backdonations is the critical factor for activations of the coordinated C-H bonds. Interactions causing changes of the occupancy numbers are perturbative donor-acceptor interactions, involving a filled orbital σ and an unfilled orbital σ^*. It is usually so small that it can be well approximated by a simple second order perturbative expressions ($\Delta E^2_{\sigma\sigma^*}$) used in the NBO program[44].

$$\Delta E^2_{\sigma\sigma^*} = -q * \frac{\langle\sigma|\hat{F}|\sigma^*\rangle^2}{E_{\sigma^*} - E_\sigma} \tag{1.4.1}$$

$\hat{F}$ is the Fock operator, E_{σ^*} and E_σ are the energies of natural bond orbitals (NBO), q is the occupancy number in the filled orbital. The strength of the $\hat{F}$ can be visualized in terms of the overlap of both orbitals on the basis of the Mulliken-type approximation.

$$\langle\sigma|\hat{F}|\sigma^*\rangle \approx k\langle\sigma|\sigma^*\rangle \tag{1.4.2}$$

It depends strongly both on distances and orientations. k is a constant of order unity in atomic units. But the overlap alone should not be the true origin for the C-H activation, since it does not answer the question why C-H bonds come closer to metal centers.

The formula suggests that the orbital energy difference of E_{σ^*} and E_σ could be the critical factor that controls the interaction strength and the change of orbital occupancy number. Analyse of orbital compositions provides further informations on which orbitals of the TM center are strongly participated in the C-H activation step.

When energies of these orbitals can be modified by changing ligands or other methods, then strengths of C-H activations can be selectively modified. In other words occupancy numbers of the C-H-σ and -σ^* orbital of the coordinated C-H bond, interactions between the TM and the coordinated C-H bond and the orbital compositions of interacted TM orbital can be used as a fundamental framework to analyze the C-H activation effect. For this reason we will use these informations calculated by the NBO program to analyze C-H activation effects.

1.5 Purpose

Firstly a few (Ni^{3+}-ligand-complexes) and (Co^{2+}-ligand-complexes) are investigated as prototypes with a presumptive d^7-configuration at the metal center, since in the infrared (IR)-spectroscopy of the Ni^{3+}-pyridine-complex a peak of 2789 cm^{-1} is explicitly identified as a reduced stretching mode of a C-H bond, which is coordinated at the Ni center with the pyridine ligand located trans to the coordinated C-H bond.

We carry out NBO analyse on the Ni^{3+}-complexes by changing the trans standing pyridine to other ligands(DMF, OAc^-, CN^-, MeO^-) with structures calculated at B3LYP/def2-TZVP[45,46] level of theory. We then extend the study to Co^{2+}-complexes with different ligands. We focus on the orbital interactions between coordinated C-H bonds and TM centers, which should induce C-H-activation.

Then we analyze a model system CH_3MX (X=F, Cl, Br, I, H), in which M include all transition metal atoms from group 4 to group 10. We use this model system to investigate sp^3-C-H bond activation effects, which are assumedly induced by interactions between TMs and coordinated C-H bonds. This model system is simple and experimentally available, therefore can be extended to include all TMs. The study of this system can provide insights into fundamental aspects of C-H activation phenomena by identifying the role played by metal centers and substituents.

In this model system three factors influence interactions between metal atoms and C-H bonds. The ring pressure (rigidity of molecular skeleton) is a hindrance for the closer approach of the C-H bond to the metal center. The other two factors originate from the orbital overlap effects, which are of the quantum mechanical nature. The destabilizing factor is Pauli repulsion (steric hindrance), which prefers a long distance between C-H bond and metal center. The only stabilizing factor is hyperconjugation (can also be called as agostic interaction, orbital mix, charge transfer, donor-acceptor effect), which causes the closer approach of C-H bonds to metal centers.

During C-H coordinations at metal centers the entropy contribution for oxidative addition amounts to 42kJ/mol at the room temperature, this amount is believed to mainly stem from the coordination of the C-H bond. In this model system CH_3MX this entropy loss vanishes due to direct bonding between the C-Atom and the metal atom, but the ring pressure cause that the coordinated C-H bond is far from a free coordination. It is assumed that in this model system the C-H coordination is in a beginning stage when the direct mutual electronic influences of the C-atom and the

TM atom are neglected. Study of this system can provide good insights into C-H activations, especially in the beginning stage.

Replacing the methyl group of CH_3MX to a *n*-butyl group releases the most ring pressures, since five-membered rings are easier to form without high ring pressure. In this system an equilibrium between hyperconjugations and Pauli repulsions leads to that a C-H bond is expected to approach closer to the metal center and C-H activation is expected to be stronger.

Most descriptions of chemical reactivities are based on spin conservations that the rate-determining step proceeds on a surfaces with a uniform spin multiplicity, i.e., reactants, intermediates, transition states, and products all have same spin states. Theoretical studies indicated that often the reactants, intermediates, transition states, and products have ground states of different spin multiplicities. Therefore participations of more than a single spin surface in the reaction pathways are proposed as a key factor in the organometallic chemistry and oxidation catalysis[1,16,47,48]. Hence the two-state reactivity(TSR) model has been proposed to rationalize of several intriguing feature of chemistry:

- opposite trends of oxidation of phosphines and alkanes by Fe complexes[49]
- unusual kinetic isotope effect(KIE) patterns for some Fe complexes ($k_H/k_D > 7$)[50]
- inverse temperature dependence of reactions[51,52]

In these cases the overall reactivity observed experimentally can only be rationalized under participations of the TSR model. In the TSR model two spin states, which are close in energy, interplay, lowering energy barriers of rate-determining steps. Excited states are less stable but more reactive, because energy barriers associated with rate-determining steps are lower.
The spin multiplicity, under which the actual C-H activations and possible C-H cleavages occur, is unknown, all spin multiplicities of the model system should be investigated.

Understanding of factors controlling C-H activations leads to rational choices about how to modify existing catalysts and design new catalysts. In early stages of a C-H bond coordination to a TM atom, interations between metal atoms and C-H bonds are crucial for a C-H functionalization process with a low activation barrier, therefore the model systems will be extensively explored. The study of these model systems is

a basic research, dealing with isolated gasphase systems, but the way of understanding mechanisms and analyzing factors controlling C-H activations in more complex molecules should be the same.

2 Method

2.1 Natural Bond Orbital (NBO) analysis

2.1.1 Hyperconjugation

Two-electron/two-orbital hyperconjugative interactions (hyperconjugations)[53–59] describe electronic consequences of delocalizations of a saturated σ-orbital and can be expressed in term of energetic differences between a perfectly with a single Lewis structure described, localized system and a real molecule. It can also be interpreted as energetic lowering by probably additional resonance structures in the valence bond (VB) theory and is similar with configuration interactions between electronic configurations in the molecular orbital (MO) theory (in a localized configurational assignment). It implies that the real many-electron wavefunction(Ψ) of plenty molecules can not be accurately expressed by a Slater Determinant (SDs) formed with localized orbitals .[60–66]

These "correlated" many-electron wavefunctions can be imagined to be accurately expressed by a dominant Lewis-type contribution $\Psi^{(L)}$, which corresponds to the dominant valence structure in the VB theory, and secondary non-Lewis corrections $\Psi^{(NL)}$.[43,65,67]

$$\Psi = \Psi^{(L)} + \Psi^{(NL)} \tag{2.1.1}$$

Therefore in order to describe hyperconjugations a localized configurational assignment will be used to replace the canonical MO configuration.

$$\Psi^{(L)} = |(\sigma_{AB})^2(\sigma_{CD})^2...| \tag{2.1.2}$$

$\Psi^{(L)}$ can be seen as a SD of localized filled orbitals of a given Lewis structural diagram. Each localized orbital σ_{AB} is built from a combination of orthonormal bonding hybrides h_A, h_B,

$$\sigma_{AB} = c_A h_A + c_B h_B \tag{2.1.3}$$

Then a general perturbative approach can be used to analyze the quantum mechanical Schrödinger equation.

$$H_{op}\Psi = H_{op}(\Psi^{(L)} + \Psi^{(NL)}) = E^{(L)}\Psi^{(L)} + E^{(NL)}\Psi^{(NL)} \tag{2.1.4}$$

The idealized Lewis model wave function $\Psi^{(L)}$ should satisfy the model Schrödinger equation:

$$H_{op}^{(L)}\Psi^{(L)} = E^{(L)}\Psi^{(L)} \tag{2.1.5}$$

The system energy E can be written as

$$E = E^{(L)} + E^{(NL)} \tag{2.1.6}$$

and system Hamiltonian as

$$H_{op} = H_{op}^{(L)} + H_{op}^{(NL)} \tag{2.1.7}$$

$E^{(L)}$ describes the part of the energy of the single localized Lewis structure, and $E^{(NL)}$ describes the energetic corrections due to resonance delocalizations. A systematic perturbative analysis of the resonance corrections to the energy ($E^{(NL)}$) can be expressed from known properties of the model Lewis system.
The unperturbed $\Psi^{(L)}$ is an idealized single-configuration many-electron wavefunction formed of localized orbitals. In this limit, the eq. 2.1.5 leads to a corresponding Lewis-type one electron eigenvalue equation,

$$H_{op}^{(L)}\Omega_i = \varepsilon_i\Omega_i \tag{2.1.8}$$

The first N eigenfunctions $\Omega^{(L)}$ accord to filled Lewis-type orbitals with corresponding orbital energies ε_i, and will be seen as donor orbitals. The remaining non-Lewis-type orbitals $\Omega^{(NL)}$ corresponding to formally vacant orbitals and will be referred as acceptor orbitals.
In a resonance-free(idealized) world of $H_{op}^{(L)}$,

$$\int \Omega^{(L)} H_{op}^{(L)} \Omega^{(NL)} d\tau = 0 \tag{2.1.9}$$

which is due to their mutual orthogonality of the chosen eigenfunctions. For a real 1e-hamiltionian operator $\hat{F}_{op}$ (i.e. of Fock, Kohn-Sham, or related type for other theory

levels) non-vanishing donor-acceptor interactions come up,

$$\int \Omega^{(L)} \hat{F}_{op}^{(0)} \Omega^{(NL)} d\tau \neq 0 \tag{2.1.10}$$

That means that electronic delocalizations (also resonance structures other than $\Psi^{(L)}$) can lead to energetic lowering, this effect can also be called as resonance-type donor-acceptor orbial-mix effects.

2.1.2 NAO (natural atom orbital)

A sequence of transformations are performed by NBO analysis[68], and a series of various localized basis sets (NAOs, natural hybrid orbitals (NHOs), natural bond orbitals (NBOs)) are formed from input basis sets χ_i (atomic basis set and delocalized canonical MOs). All of those localized orbitals are orthonormal sets that span the full space of the input basis set. And the calculated wavefunction and operators of the system can be equally exactly expressed by those localized orbital sets as the input basis set.

By formations of NAOs from the input atomic basis set (AOs) a occupancy-weighted symmetric orthogonalization (OWSO)[69] procedure is imposed. And the subsequent formation of NHOs and NBOs involves only a unitary transformation, so that orthogonality is automatically maintained.

Non-Hermitian terms in the second-quantized form of the Hamiltionian can be induced by using non-orthogonal orbitals, since field operators for nonorthogonal AOs do not satisfy proper Fermi-Dirac commutation relations. The assumption of orthogonality for the underlying orbitals of elementary VB theory is therefore an essential prerequisite for the physical and mathematical consistency of perturbative analyse of chemical phenomena.[70,71]

Transformations of non-orthogonal atomic basis sets χ to orthogonal NAOs Φ_i is imposed by the OWSO procedure.

$$T_{OWSO}\chi_i = \Phi_i, \langle \Phi_i | \Phi_j \rangle = \delta_{ij} \tag{2.1.11}$$

Mathematical properties of minimizing the occupancy-weighted, mean-squared deviations of the Φ_i from the parent non-orthogonal basis function χ_i is essential by OWSO procedure.

$$min\{\sum \omega \int |\Phi_i - \chi_i| d\tau\} \tag{2.1.12}$$

The weighting factor ω can be interpreted as the occupancy of χ (diagonal expectation value of the first order reduced density operator $\hat{\Gamma}$)

$$\omega = <\chi_i|\hat{\Gamma}|\chi_i> \tag{2.1.13}$$

The final NAOs are obtained by removing interatomic overlaps by the OWSO procedure. NAOs are localized 1-center orbitals that can be described as effective natural orbitals of a atom in the molecular environment. Two important physical effects are incorporated by NAOs, which distinguish them from the usually atomic basis orbitals:

- Spatial diffusenesses of NAOs are optimized for effective atomic charges in molecular environments.
- NAOs of a atom preserve orthogonality to its own atomic core as well as the outer nodes and preserve orthogonality to filled orbitals on other atoms.

Both features are necessary for the proper Fermi-Dirac anticommutators of the associated second-quantized NAO field operators.
The orthonormal NAOs ($\Phi_i^{(A)}$) provide the basis for natural population analysis (NPA), in which populations of a atom A ($q^{(A)}$) is given by

$$q^{(A)} = n - \sum_i q_i^{(A)} = n - \sum_i <\Phi_i^{(A)}|\hat{\Gamma}|\Phi_i^{(A)}> \tag{2.1.14}$$

with n as nuclear charges of the atom. NPA is numerical stable and agrees with other theoretical and experimental measures of charge distributions,[72] and corrects many of deficiencies of the well-known Mulliken population analysis.[67]

2.1.3 NBO and estimates of hyperconjugations

After the NAO basis is formed, the NBO program seeks further for an optimal natural Lewis structure (NLS). Firstly NAOs of high occupancy ($\geq$1.999e) are removed as core orbitals K_A in one-center blocks $\Gamma^{(A)}$, then lone-pair orbitals (LPs), which have a occupancy higher than a pair threshold ($\geq$1.90). Then in all two-center blocks $\Gamma^{(AB)}$, bond orbitals $\sigma_{(AB)}$ are sought, whose occupancy exceeds a threshold ρ_{thresh}. The search may be further extended to three-center blocks or the ρ_{thresh} will be reduced if an insufficient electron density is found in the one- and two-center blocks.
For example a 2-center in-phase bond orbital ($\sigma_{(AB)}$) can be decomposed into a normalized hybrid orbital h_A and h_B from each atom shown in the Equation 2.1.3. Hybrids

from each center participating in different bonds are symmetrically orthogonalized to remove interatomic overlaps. This procedure also leads to a series of out-of-phase antibonding orbitals σ^*_{AB} NBOs.

$$\sigma^*_{AB} = c_B h_A - c_A h_B \tag{2.1.15}$$

Occupied NBOs form also an orthonormal set of localized maximum occupancy orbitals(same as NAOs), which can give the equally accurate description of many-electron wavefunctions as the input basis set. Neither forms of the bonding hybrids nor locations of localized bonds and lone pairs are preseted. All possible options are sought for a variationally optimal bonding pattern that places maximum occupancies in the leading Lewis-type NBOs. These Lewis-type NBOs should outweigh the localized Natural Lewis Structure (NLS) representation of the wavefunction (typically >99.9% of the total electron density for common organic molecules). The remaining "non-Lewis"-type NBOs complete spans of the basis set and describe delocalization effects.

NBOs provide a VB-type description of the wavefunction, which is closely linked to classical Lewis structure concepts. The only input to the NBO algorithms is atomic basis sets and calculated canonical molecular wavefunctions (through its first-order reduced density operator Γ[73]), which implies that NBOs are uniquely determinated by the many-electron wave function Φ.

The occupancies of NBOs are generally non-degenerate, and important resonance delocalization corrections to the idealized Lewis structure are reflected by the occupancy variations in term of NBO analysis. Valence antibonds σ^*_{AB} are non-Lewis type orbitals and they are the most important acceptor orbitals that contributing to resonance stabilizations, which should be key orbitals to understanding delocalization effects.

The localized Lewis-type wavefunction $\Psi^{(L)}$ is formed from a set of localized electron pairs $(K_A)(n_A)(\sigma)_{AB}$, which commonly accounts for $> 99\%$ of the total electron density leading to small corrections to the Lewis-type picture so that can be well approximated by a simple second-order perturbative expressions of interactions of a filled orbital σ_i and a unfilled orbital σ^*_j.

$$\Delta E^{(2)}_{ij} \approx -n^{(0)}_i \frac{<\sigma_i|\hat{F}|\sigma^*_j>^2}{\varepsilon_j - \varepsilon_i} \tag{2.1.16}$$

The filled orbital σ_i may be a occupied LP orbital or a bond(σ) orbital , and σ_j^* may be a antibonding(σ^*) orbital or a vacant LP orbital, $n_i^{(0)}$ is the occupancy of the filled orbital.

NAOs, NHOs and NBOs are distinguish with the associated pre-NAOs, pre-NHO and pre-NBOs. NAOs, NHOs, NBOs are strictly mutually orthonormal since any proper physical Hermitian operator demands, but for example pre-NAOs differ from NAOs only in omission of the final interatomic orthogonalization step. Therefore pre-NAOs are mutually orthogonal on a single atom, but have non-vanishing overlap with NAOs on distinct atoms, so that it allows to connect the valuable concept of overlaps with hyperconjugations.

A Fock matrix element can be estimated in terms of the corresponding overlap integral by Mulliken approximations,

$$<\sigma_i|\hat{F}|\sigma_j^*> \approx k<\overline{\sigma_i}|\overline{\sigma_j^*}> = kS_{ij} \tag{2.1.17}$$

where k is a constant of order unity in atomic units, σ may be the NBOs, NHOs or NAOs and $\overline{\sigma}$ is the corresponding pre-NBO, pre-NHO or pre-NAOs. By substituting Eq.2.1.17 into the Eq.2.1.16, hyperconjugation can be expressed as

$$\Delta E_{ij}^{(2)} \approx -n_i^{(0)} \frac{k^2<\overline{\sigma_i}|\overline{\sigma_j^*}>^2}{\varepsilon_j - \varepsilon_i} = -n_i^{(0)} \frac{k^2 S_{ij}^2}{\varepsilon_j - \varepsilon_i} \tag{2.1.18}$$

The associated charge transfer from the σ_i- into the σ_j^*-orbital can also be determinated

$$q \approx \frac{\Delta E_{ij}^{(2)}}{\varepsilon_j - \varepsilon_i} \simeq -n_i^{(0)} \frac{k^2 S_{ij}^2}{(\varepsilon_j - \varepsilon_i)^2} \tag{2.1.19}$$

In the case of closed-shell singlet species near equilibrium geometry $n_i^{(0)}$ in eq. 2.1.18 is two, which means that the Lewis NBOs are paired occupied, since the α-spin orbital is equal to the β-spin orbital in all the properties. For open-shell species the NBO analysis incorporates the DODS concept (Different Orbitals for Different Spins), in which no relationship between orbitals of the two spin sets are presumed, since distinct exchange forces will general lead to spatially distinct orbitals in the both spin system. In accordance with the general DODS concept α and β spin sets should have different orbital forms, spatial distributions, energies, and bonding properties for an open-shell system.

2.2 Density Functional Theory (DFT)

DFT[74,75] is a standard technique with low computational costs and useful accuracies used in most branches of chemistry and material research. The most popular used in quantum chemistry is B3LYP method, and PBE is the most popular used method in material sciences.

Basis for DFT is the Hohenberg Kohn (HK) theorem which proves that the ground state electronic energy is determined completely by the one-electron ground state density $\rho(r)$. There is a one-to-one correspondence between the electron density and the energy.

The introduction of orbitals, which suggested by Kohn and Sham (KS), are the foundation for the modern DFT method used today. KS equation defines a self-consistent equation that to be solved to find the energy-minimizing orbitals, whose density is defined to be exactly that of the real system:

$$(-\frac{1}{2} \bigtriangledown^2 + v_s(r))\Phi_i(r) = \varepsilon_i \Phi_i(r) \tag{2.2.1}$$

and

$$v_s(r) = v_{nuc}(r) + \int d^3r' \frac{\rho(r')}{|r - r'|} + v_{XC}[\rho](r) \tag{2.2.2}$$

with $v_{XC}(r) = \delta E_{XC}/\delta\rho(r)$.

By use of the HK theorem the ground-state energy can be expressed by those KS orbitals.

$$E_{DFT} = T_s[\rho] + E_{ne}[\rho] + J[\rho] + E_{XC}[\rho] \tag{2.2.3}$$

where $T_s[\rho]$ is the kinetic energy of KS orbitals, $E_{ne}[\rho]$ is the attraction between the nuclei and electrons, $J[\rho]$ is the Column energy of electrons, E_{XC} is the unknown exchange-correlation functional, which must be approximated.

The key success of the KS theory is that the kinetic energy is split into two parts, one can be calculated with KS orbitals, and a small correction term $T[\rho] - T_S[\rho]$, which is absorbed into the exchange-correlation functional E_{XC}.

$$E_{XC} = (T[\rho] - T_S[\rho]) + (E_{ee}[\rho] - J[\rho]) \tag{2.2.4}$$

The first parenthesis in Eq. 2.2.4 is corrections to the kinetic energy, and the second contains correlation and exchange energies. Different approximations to exchange-correlation energy functionals lead to different methods of KS-DFT.

2.2.1 Dispersion corrections to DFT

Dispersion forces are poorly described by standard KS-DFT functionals, they do not show the correct R^{-6} but rather an exponentially limiting behavior in the long distance limit. The method of dispersion corrections as an add-on to standard KS-DFT (DFT-D3)[76–78]) has be proved as a robust method to accurately, consistently describe inter- and intramolecular systems of all chemically relevant elements of the periodic system. Most important parameters (pairwise dispersion coefficients, cut-off radii) are computed from first principles, therefore DFT-D3 is minimal empiric and has the property of a minor computation time in comparison to KS-DFT methods.
The total DFT-D3 energy is given by

$$E_{(\text{DFT-D3})} = E_{\text{KS-DFT}} - E^{(2)}_{\text{disp}} - E^{(3)}_{\text{disp}} \tag{2.2.5}$$

where $E_{(\text{DFT-D3})}$ is the self-consistent energy calculated by KS-DFT method, $E^{(2)}_{disp}$ is the sum of the dispersion correction energy of all two-atom terms, $E^{(3)}_{disp}$ is the sum of the dispersion correction energy of all three-atom terms. $E^{(3)}_{disp}$ term will be in general neglected, since it has only a minor impact on the energy.
The two-body dispersion correction are given by

$$E^{(2)}_{disp} = \sum_{A \neq B} \sum_{n=6,8,10,\ldots} s_n \frac{C^{AB}_n}{R^n_{AB}} f_{damp}(R_{AB}) \tag{2.2.6}$$

where the first sum runs over all atom pairs in the system, C^{AB}_n is the averaged nth-order dispersion coefficients (orders n=6,8,10,...) for atom pair AB, and R_{AB} is their internuclear distance, s_n is a density functional dependent scaling factor, $f_{damp}(R_{AB})$ is the damping function in order to avoid near singularities for small R_{AB} and double-counting effects of correlation at intermediate distances.
The dispersion coefficients C^{AB}_6 are computed *ab initio* by time-dependent DFT (TD-DFT),

$$C^{AB}_6 = \frac{1}{3} \int_0^\infty \alpha^A(i\omega)\alpha^B(i\omega)d\omega, \tag{2.2.7}$$

where $\alpha(i\omega)$ is the averaged dipole polarizability at imaginary frequency ω. And higher-multipole terms (C^{AB}_8, C^{AB}_{10}, ...) will be computed by recursion relations.
The new used default damping function in the DFT-D3 treatments, which is proposed

by Becke and Johnson (BJ)[79,80], substitutes in the Eq. 2.2.6 for $n = 6, 8$ leading to

$$E_{disp}^{(2)} = -\frac{1}{2}\sum_{A\neq B}(s_6\frac{C_6^{AB}}{R_{AB}^6 + [f(R_{AB}^0)]^6} + s_8\frac{C_8^{AB}}{R_{AB}^8 + [f(R_{AB}^0)]^8}) \tag{2.2.8}$$

with

$$f(R_{AB}^0) = a_1 R_{AB}^0 + a_2 \tag{2.2.9}$$

a_1 and a_2 are free fit parameters, and the cut-off radius R_{AB}^0 for atom pair AB is given by

$$R_{AB}^0 = \sqrt{\frac{C_8^{AB}}{C_6^{AB}}} \tag{2.2.10}$$

In this case there are three free parameters (s_8, a_1, a_2) to be determinated for each functional and s_6 is set to unity for GGA (generalized gradient approximation) and hybrid functionals.

2.3 Basis sets

Since investigated molecules in this thesis contain 4d and 5d transition metal elements, a suitable basis set is necessary for a consistent, efficient and accurate description of the molecules. This basis set should be flexible and efficient enough by use of techniques such as contracted Gaussian-type orbitals (CGTOs), split valence basis set and effective core potentials (ECPs) in order to efficiently describe the molecules without compromising accuracies of chemical relevant properties.[74] The use of ECPs for heavy atoms is very important to take account of scalar relativistic effects[81,82] without using full relativistic calculations. Replacing core electrons by ECP leads to that the valence orbitals should also be new optimized and replaced by a set of nodeless pseudo-orbitals.

The def2-TZVP[45,83,84] (triple zeta valence + polarisation) basis set satisfies all the above mentioned requirements. The number of primitives GTOs functions is determinated by an accuracy maintain of better than 1 mE_h in atomic Hartree-Fock(HF) energies, which means that all atoms can be accurately and consistently described mit the basis set. Segmented contractions was used with orbital exponents and contraction coefficients optimized for atomic HF ground states, so that less primitives GTO are used in comparison to general contractions.

For d elements only 1f function is used as polarisationsfunction, and 1p function is

use to polarize the H atom. For example def2-TZVP basis set had sizes $[6s4p3d1f]$ for 4d and 5d element. Numerous test shows that those contractions suffice for DFT treatments. DFT calculations of first-order properties with def2-TZVPP bases, which is a little larger than def2-TZVP, are close to the basis set limit with DFT methods.

Small-Core ECPs[46,85] were used for 4d and 5d elements, which substitutes 28 and 60 core orbitals respectively, so that the scalar relativistic effects can be described and high accuracy of results can be achieved by using a fraction of the cost of a calculation involving all electrons.

A large test set of more than 300 compounds indicates that results close to the basis set limit are obtained with the def2-TZVP basis set at the DFT level[83]. The good accuracy and high flexibility with relatively few primitives justify the choice of the basis set.

3 Results

3.1 Investigation of Ni^{3+}- and Co^{2+}- complexes

Appearing of a new peak, which lies at 2789cm^{-1} in the IR spectrum, indicates that a C-H bond is probably activated, when the Ni^{2+}-(N,N'-Bis-[2-(1-hydroxyimino-ethyl)-phenyl]-2-isopropyl-2-methyl-malonamide-dianion) complex (singlet d^8 electronic system on the nickel-atom, abbreviated as Ni^{2+} complex below) is oxidized to the Ni^{3+}-(N,N'-Bis-[2-(1-hydroxyimino-ethyl)-phenyl]-2-isopropyl-2-methyl-malonamide-dianion)-pyridine complex (doublet d^7 electronic system on the nickel-atom, abbreviated as Ni^{3+}-pyridine complex below, the structure is shown in Figure 3.1). Compared with the calculated spectrum at B3LYP/def2-TZVP (B3) level, this activated peak can be assigned to stretching frequencies of the tertiary C-H bond, which lies above the nickel atom. Such C-H activations can also be observed in the similar Ni^{3+}- and Co^{2+}-complexes with many other ligands, in all of these complexes the metal atoms have a doublet d^7 electronic system.

Figure 3.1: The structure of the Ni^{3+} complex

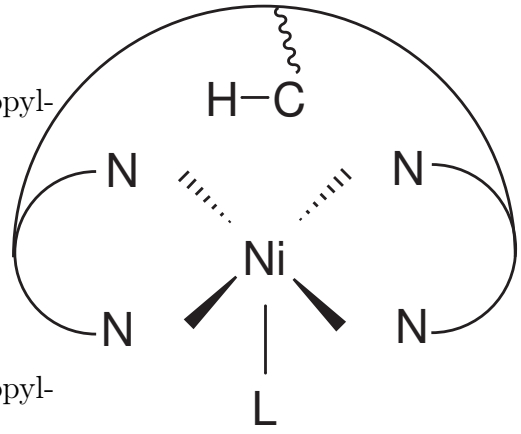

3.1.1 Ni^{3+}-complexes in the doublet state

The with X-ray diffractions determined structure of the complexes[86] is compared in Table 3.1 with the calculated structure. Compared to the calculation at the B3LYP/def2-TZVP (B3) level, all deviations from the experimental data are strongly reduced at the B3LYP-D3/def2-TZVP (D3) level, where dispersion corrections are

Table 3.1: Structure (experimental and calculated) of Ni^{3+}-ligand complexes. IR column shows stretching frequencies of the activated C-H bond, d(Ni-C) column represents the distance between the Ni atom and the C atom of the activated C-H bond, d(Ni-L) column shows the distance between the Ni atom and the ligand. (exp) line represents experimental data determinated with X-ray diffractions, (B3) and (D3) line represent the calculated data with B3LYP and B3LYP-D3 method respectively.

Ni^{3+}-Ligand	IR(C-H)	d(Ni-C)	d(Ni-H)	d(Ni-L)
unit	[1/cm]	pm	pm	pm
pyridine(exp)	2789	290	202	205
pyridine(D3)	2777	290	202	210
pyridine(B3)	2811	302	215	213
DMF(exp)	2753	285	203	n.a.
DMF(D3)	2757	288	200	210
DMF(B3)	2792	299	212	210

added to the standard KS-DFT. The same scale factor (0.9613) [87] will be used for IR spectrum calculated at the both levels. Agreements of bond lengths related with the activated C-H bond are strongly improved at the D3 level, and distances between Ni atom and the C-H bond will be reduced in general with the dispersion correction. Between the Ni atom and isopropyl unit there is no covalent bond, the Ni-C and Ni-H distances are floppy modes which makes the dispersion correction so important.

Table 3.2: Occupancy numbers of the C-H-σ-orbital in β-spin channel. IR columns show the calculated stretching frequencies at D3 level of the activated C-H bond without scaling. Occ(σ) columns show the occupancy numbers of C-H-σ-orbital in β-spin channel. Δ column shows differences between the data calculated with structures got at the B3 and D3 levels.

Ni^{3+}-Ligand	IR	Occ(σ)		
		D3	B3	Δ
unit	[cm^{-1}]		[a.u.]	
p-nitro-pyridine	2871	0.947	0.959	0.011
pyridine	2889	0.949	0.960	0.011
p-DMA-pyridine	2897	0.952	0.962	0.010
acetate	2964	0.962	0.969	0.007
CN^-	2989	0.965	0.971	0.006
MeO^-	2989	0.968	0.973	0.005

Compared C-H activations with occupancy numbers of the C-H orbitals shows that only occupancy numbers of the C-H-σ orbital in the β-spin varies significantly with C-H activations. Occupancy variations of other orbitals (the C-H-σ^* orbitals in the both spins and the C-H-σ orbitals in α-spin) are 10 times smaller, therefore interactions

between these three orbitals and Ni valence orbitals can be excluded as the main reason for the C-H activations. Comparisons of occupancy numbers of the C-H-σ orbital in the β-spin with the IR stretching frequencies of the C-H bond are listed in Table 3.2 showing that occupancy numbers of the C-H bond calculated at both levels are different, however both of them show that occupancy numbers of C-H-σ orbital in the β-spin correlate properly with the the C-H activations. The more pronounced occupancy lowering in the D3 calculation is certainly a consequence of the shorter Ni-CH distance compared to the B3 calculation.

Hyperconjugations between the C-H-σ orbital and vacant Ni orbitals in the β-spin

Table 3.3: Hyperconjugations between the C-H-σ-orbital and vacant Ni hybrid orbitals in β-spin. B3 and D3 represent the calculated data with structure got at the B3 and D3 level respectively. IR column shows unscaled calculated stretching frequencies of the activated C-H bond. ΔE^2_{ij} column shows sums of the hyperconjugation between the C-H-σ-orbital and vacant Ni hybrid orbitals in β-spin channel.

Ni^{3+}-Ligand	D3		B3	
	IR	ΔE^2_{ij}	IR	ΔE^2_{ij}
unit	1/cm	kcal/mol	1/cm	kcal/mol
p-nitro-pyridine	2871	5.55	2897	4.04
pyridine	2889	5.51	2908	3.88
p-DMA-pyridine	2897	5.13	2922	3.57
acetate	2964	5.08	2976	3.43
CN^-	2989	4.48	2991	3.12
MeO^-	2989	3.65	3002	2.52

are shown in Table 3.3, indicating that this type of interactions can be identified as the reason for the C-H activation, and it is the only type of interactions, which correlates properly with the C-H activations. Electron withdrawing ligands leading to the increased C-H activations suggests that interactions between the C-H-σ orbital and the unoccupied d_{z^2} orbital at the Ni atom (z-axis parallel to the Ni-CH connection) in the β-spin channel is responsible for the C-H activation. Although the structure calculated at both methods are different, but NBO analyse with these structure leads to the same conclusion that hyperconjugations between the C-H-σ orbital and vacant Ni orbitals in the β-spin channel induce the C-H activations.

3.1.2 Co^{2+}-complexes in the doublet state

Table 3.4: Structure (experimental and calculated) of Co^{2+}-complexes. IR column shows stretching frequencies of the activated C-H bond, d(Co-C) column represents the distance between the Co atom and the C atom of the activated C-H bond, and so on, d(Co-L) column shows the distance between the Co atom and the ligand. (exp) line represents experimental data determinated with X-ray diffractions, (B3) and (D3) line represent the calculated data at B3 and D3 level respectively, and 0.9613 is taken as the scaling factor for the calculated IR frequencies.

Co^{2+}-Ligand	IR	Co-C	Co-H	Co-L
	[cm^{-1}]	pm	pm	pm
Pyridine(exp)	2816	304	228	216
Pyridine(D3)	2856	297	210	221
Pyridine(B3)	2891	300	220	226
DMF(exp)	2812	296	215	220
DMF(D3)	2851	293	205	233
DMF(B3)	2869	302	215	234

Structure (experimental and calculated) of the Co^{2+}-complexes (d^7 electronic system, isoelectronic to the Ni^3+-complex) is compared in Table 3.4. Although the calculated structure at the B3 level shows smaller deviations from experimental structure than that at the D3 level in general, deviations in the stretching frequency of the C-H bond between the experimental and calculated are smaller at the D3 level.

In Table 3.5 occupancy numbers of the C-H-σ-orbital the in β-spin are compared

Table 3.5: Occupancy numbers of the C-H-σ orbital in the β-spin channel. IR columns show the calculated stretching frequencies of the activated C-H bond at D3 level without scaling. Occ(σ) columns show the occupancy numbers of C-H-σ-orbital in β-spin channel. Δ column shows differences of the occupancy numbers, which are calculated with the structure optimized with the B3 and D3 levels.

Co^{2+}-Ligand	IR	Occ(σ)		
		D3	B3	Δ
unit	[cm^{-1}]		[a.u.]	
noligand	2921	0.958	0.963	-0.005
ethanol	2955	0.960	0.965	-0.006
DMF	2965	0.966	0.966	0
p-Nitro-Pyridine	2964	0.961	0.967	-0.006
p-DMA-Pyridine	2968	0.960	0.967	-0.006
pyridine	2971	0.961	0.966	-0.005

with the C-H activation, a strict correlation between the occupancy number and the

C-H activation can not be discovered.

Hyperconjugations between the C-H-σ-orbital and vacant Co orbitals in the β-spin

Table 3.6: Hyperconjugations between the C-H-σ-orbital and vacant Co orbitals in the β-spin. IR column shows the unscaled calculated stretching frequencies of the activated C-H bond at D3 level. ΔE^2_{ij} column shows sums of the hyperconjugation between the C-H-σ-orbital and vacant Ni hybrid orbitals in β-spin. Δ column shows differences between the data calculated at the B3 and D3 levels.

Co^{2+}-Ligand	IR	ΔE^2_{ij}		
		D3	B3	Δ
unit	[1/cm]	[kcal/mol]		
noligand	2921	6.48	5.27	1.21
ethanol	2955	6.03	4.82	1.21
DMF	2965	5.88	4.47	1.41
p-Nitro-Pyridine	2964	4.82	3.90	0.92
p-DMA-Pyridine	2968	4.83	3.79	1.04
pyridine	2971	4.72	3.91	0.82

are shown in Table 3.6 showing the same conclusion got from the Table 3.3. In spite of quantitative differences in the calculated structures at different levels, the same conclusion can be drawn that hyperconjugations between the C-H-σ-orbital and vacant Co orbitals in β-spin should induce the C-H activation.

3.1.3 Summary

Investigations of the Co^{2+} and Ni^{3+}-complexes (all have d^7 electronic system) show that the calculated structure and IR frequencies at the B3 level are slightly different from that calculated at the D3 level, however NBO analyse with structures got at the different levels shows the same conclusion that hyperconjugations between the C-H-σ-orbital and vacant metal orbitals in β-spin should induce the C-H activation.
This observation can also explain why the C-H bond are more activated in the Ni^{3+}-DMF complex than in the Co^{2+}-DMF complex. In both complexes metal atoms have d^7 electronic structure, and the only difference is that nucleus charge of Ni^{3+} is higher, which leads lower energies of orbitals in the Ni^{3+} cation than that in Co^{2+} cation. It reduces energy gaps between the C-H-σ-orbital and vacant valence metal orbitals and should lead to the more strongly activated C-H bond in the Ni^{3+}-complex.

3.2 Comparison and determination of structure optimize methods

As described in the Section 1.5, the model systems CH_3MX and n-C_4H_9MX will be used to study interactions between the metal atoms and C-H bonds in the molecules, which should lead to C-H activations, in which M include all transition metal atom from group 4 to group 10 and X=F, Cl, Br, I, H. At the beginning geometries of CH_3ZrX molecules (X=F, Cl, Br, I, H) will be optimized with different methods (CCSD(T), B3LYP(B3), B3LYP-D3(D3) using def2-TZVP-basis/def2-ecp basis set. Then the resulting structure parameters get compared in order to determine, which method is more appropriate for the further investigations.

CCSD(T) is an accurate but very time consuming method, which provides a very good description of molecules near the equilibrium geometry. It provides an accurate description of dispersion and correlation (both dynamic and static correlation) effects, but can only be used for small molecules.

The accuracy and reliability of the B3LYP/def2-TZVP/def2-ecp method level are known from experiences, it can describe static and dynamic correlation relatively well, but can not correctly describe long-range dispersion forces.

The method of dispersion correction (D3) as an add-on to B3LYP density functional (B3LYP-D3) describes the dispersion effect as well, this extension has been tested thoroughly and applied successfully to thousands of different systems including inter- and intramolecular interactions ranging from rare gas dimers to huge graphene sheets.

Through the comparisons we want to determinate which method (B3 or D3) is more appropriate to describe the model systems. All the IR frequencies are provided without scaling, unless otherwise mentioned.

Triplet CH_3ZrF is the ground state and takes an eclipsed form as the absolute minimum. The C-H bond (C-H^t), which stands trans to the Zr-F bond, is more activated than the cis standing C-H bond (C-H^c). As expected, the structure comparison in Table 3.7 shows that the D3 correction only has a weak influence on the structure, since the molecule is small and does not have floppy modes. Almost all deviations of the bond length lie inside the error limit (2pm). There are some points worthy to note:

- Except the C-H bond lengths, all the parameters calculated with the B3-method show better agreement with the CCSD(T)-method than those calculated with the D3-method.

Table 3.7: Structure comparison of triplet CH_3ZrF optimized with different methods. The CCSD(T) row shows calculated structure parameters optimized at the CCSD(T)/def2-TZVP/def2-ecp level. The ΔB3 (or ΔD3) column displays differences between CCSD(T) and B3 (D3), i.e., ΔB3 = CCSD(T) − B3. C-H^t lies trans to the Zr-F bond, C-H^c lies cis to the Zr-F bond. The IR^t entries show the frequency of the trans-C-H stretching mode. D(Zr-H^t) shows the distance between the Zr-atom and the H-atom of the C-H^t-bond, D(C-H^t) is the bond-length of the C-H^t-bond, and so on.

	IR^t	D(C-H^t)	D(Zr-H^t)	D(Zr-C)	IR^c	D(C-H^c)	D(Zr-H^c)
unit	cm^{-1}		pm		cm^{-1}	pm	
CCSD(T)	2945.6	110.5	281.1	224.9	3073.9	109.6	292.4
ΔB3	-8.5	0.4	2.6	2.5	-7.9	0.4	5.3
ΔD3	34.5	0.1	3.1	3.3	11.8	0.1	9.5

- Since B3LYP/TZ and CCSD(T)/TZ have almost the same vibrational scaling factor(0.967 vs 0.964)[88], the C-H vibrational frequency calculated with the B3 method show perfect agreement with that of the CCSD(T) method.
- The C-H stretching frequencies calculated with the D3-method show the biggest deviation ($34.5 cm^{-1}$). Since adding D3 correction is to include dispersion forces, it should not affect the frequency scaling of a normal bond. Hence there is no reason to take another scaling factor for the D3-method as for the B3-method. It shows that small geometry deformations can have a large effect if the M-C distance is in a critical range. This implies that the B3 method is more appropriate to describe the triplet CH_3ZrX-molecules.

Table 3.8: Structure comparisons of CH_3ZrBr optimized with different methods. The CCSD(T) row shows calculated structure parameters optimized at the CCSD(T)/def2-TZVP/def2-ecp level, the ΔB3 (ΔD3) column displays differences between CCSD(T) and B3 (or D3), i.e., ΔB3 = CCSD(T) − B3. The C-H^t bond lies trans to the Zr-F bond, the C-H^c cis to the Zr-F bond. The IR(C-H) entries show the frequency of the C-H stretching mode. D(C-H^t) presents the distance between the C-Atom and the trans H-Atom.

	IR(C-H^t)	D(C-H^t)	D(Zr-H^t)	D(Zr-C)	IR(C-H^c)	D(C-H^c)	D(Zr-H^c)
unit	cm^{-1}		pm		cm^{-1}	pm	
CCSD(T)	2946.4	110.5	279.7	223.9	3085.5	109.6	291.4
ΔB3	-1.1	0.4	4.6	3.0	-6.2	0.4	2.9
ΔD3	8.1	0.3	2.7	2.3	11.9	0.2	3.1

In Table 3.8 the structures and vibrational frequencies of CH_3ZrBr are summarized, showing the similar trend as CH_3ZrF that the B3 method is superior to the D3 method

to describe vibrations of the CH_3ZrBr molecules. However, the deviations of the D3-method compared to the CCSD(T)-method in the bond lengths are relatively smaller than that of the B3-method, which is in contrast to the case of the CH_3ZrF molecule. Comparisons of the other molecules (CH_3ZrX(X= Cl, I, H)) arrive at the same conclusion: the B3-method provides in general better description of IR frequencies but poorer description in bond lengths .

Further along we come to the n-C_4H_9ZrX(X=F, Cl, Br, I, H) molecules. The purpose of the extension from CH_3ZrX to n-C_4H_9ZrX is to seek how C-H activation effects are affected, when the ring pressure is released. We concentrate only on the activated C-H bonds, which have a reduced frequency of stretching modes (less than $3000cm^{-1}$), hence only structure parameters, which are related to those activated C-H bonds, are relevant to compare. The CCSD(T) method is too expensive to use to optimize the structure of n-C_4H_9ZrX molecules, so only structures that were calculated with B3- and D3-method can be compared. It is necessary to compare the two methods due to the fact that calculated distances between the Ni-atom and the C-H bond in the Ni^{3+}-complexes with the D3-method differ largely from the distance calculated with the B3 method (the deviation of the M-H distance varies over 10pm, in Section 3.1).

Figure 3.2 depicts the structure of the n-C_4H_9ZrF-molecule optimized with the D3-method. The figure illustrates only the most activated α-C-H bond, which stands trans to the Zr-F bond, and the most activated δ-C-H bond, which stands cis to the Zr-F bond.

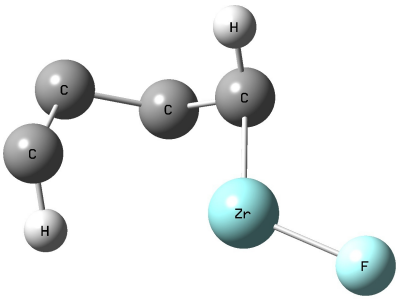

Figure 3.2: The structure of the n-C_4H_9ZrF molecule optimized with the D3 method.

A C-H activation can be identified either from bond lengths, which correlates linear with the bond strengths in electronic structure calculations or from analysis of normal modes. A coupling of individual C-H oscillators can not be avoided, but the more activated a C-H bond is, the weaker is the coupling. By analyse of normal modes even a weakly activated C-H bond can be clearly identified.

The structures optimized with B3- and D3-method are summarized and compared in Table 3.9, showing that:

- The deviations of Zr-δC and Zr-δH distances calculated with the two-methods are large (14.8 and 7.4 pm).

Table 3.9: Structure comparisons of the n-C_4H_9ZrF-molecule, IR(C-H) represents the stretching frequency of the C-H bond, D(C-H) the distance between the C-atom and the H-atom. α-C-H bond represents the C-H bond, which lies in α-position to the Zr-Atom, and so on. D(Zr-δH) shows the distance between the Zr-atom and the H-atom, which belong to the δ-C-H bond.

	IR(δ-C-H)	D(δ-C-H)	D(Zr-δC)	D(Zr-δH)	IR(α-C-H)	D(α-C-H)	D(Zr-αC)	D(Zr-αH)
unit	cm^{-1}		pm		cm^{-1}		pm	
B3	2905.6	110.4	304.8	254.8	2933.5	110.4	224.9	277.8
D3	2911.5	110.4	319.6	262.2	2929.4	110.4	225.0	279.5
Δ	-5.9	0	-14.8	-7.4	4.1	0	0.1	-1.7

- All of the other structure parameters show good agreement, particularly the structure parameters that relate to the activated α-C-H bond.
- The structures optimized with the D3-method, show an unexpected lengthening of the Zr-δ-H distance compared to those calculated with the B3-method.

Table 3.10: Structure comparisons of the n-C_4H_9ZrBr-molecule, IR(δ-C-H) represents the stretching frequency of the δ-C-H bond, D(δ-C-H) the distance between the C-atom and the H-atom of the δ-C-H bond, and so on. D(Zr-δH) stands for the distance between Zr-atom and the H-atom that belongs to the δ-C-H bond.

	IR(δ-C-H)	D(δ-C-H)	D(Zr-δC)	D(Zr-δH)	IR(α-C-H)	D(α-C-H)	D(Zr-αC)	D(Zr-αH)
unit	cm^{-1}		pm		cm^{-1}		pm	
B3	2854.7	110.9	294.4	242.1	2923.8	110.5	223.9	272.9
D3	2884.7	110.7	311.3	275.1	2962.8	109.4	221.7	280.8
Δ	-30.0	0.2	-16.9	-33.1	-39.0	1.1	2.2	-7.9

Table 3.10 shows structure comparisons of the n-C_4H_9ZrBr-molecule, which was optimized with the B3- and D3-methods, suggesting that:

- The deviations of structure are larger in case of the n-C_4H_9ZrBr than in case of the n-C_4H_9ZrF.
- Distance lengthening of the Zr-Atom and the δ-C-H bond is stronger.
- The deviation of the δ-C-H stretching frequency are over 30 cm^{-1}, this is certainly a consequence of the unexpected lengthening of the Zr-δ-CH distance calculated by the D3-method.

It is difficult to determine from the structure comparisons, whether the B3- or the D3-method is more appropriate for the description of the n-C_4H_9ZrX-systems. We prefer the B3-method to the D3-method for following reasons:

- By studying the CH_3ZrX molecules, the B3-method shows better agreement with CCSD(T), the large deviations of C-H bond stretching frequencies between the D3 and CCSD(T)-methods can not be well understood.

- The purpose of the extension to the n-C_4H_9ZrX molecules is to release the ring pressure, in which case a δ-C-H bond should come closer to a Zr atom and the C-H bond should be more activated. We would like to find out how the Zr atom affects the C-H bond strength when the C-H bonds come closer to the Zr atom.

- In the n-C_4H_9ZrBr-molecule calculated with the D3-method, the β-C-H bond is more activated than the δ-C-H bond (the stretching frequencies of the most activated β vs δ-C-H bonds are 2859.4 and 2884.7 cm^{-1} respectively). That is against the chemical principle because a δ-C-H functionalization is in general naturally easier than a β-C-H functionalization. The B3-method provides the right description that the δ-C-H bond is more activated than the β-C-H bond, which is consistent with chemical experience (here the stretching frequencies of the most activated β vs δ-C-H bonds are 2986.1 and 2854.7 cm^{-1} respectively). Such large dispersion effects are unexpected for the investigated small molecules.

Therefore in further investigations all of the structure optimizations and NBO analyse will be carried out at the B3LYP/def2-TZVP/def2-ecp level.

3.3 Group 4 transition metal elements

Table 3.11: Enthalpy comparisons of singlet and triplet states of the CH_3ZrX molecules, all the enthalpies are calculated at the B3LYP/def2-TZVP/def2-ecp levels (Sum of electronic and thermal enthalpies) and presented as the difference ($H_{singlet} - H_{triplet}$) at the corresponding absolute minimum of the molecules without zero-point corrections.

$ZrCH_3X$	triplet		singlet	
unit	kJ/mol	cm^{-1}	kJ/mol	cm^{-1}
-CN	0	2959	44.4	2847
-F	0	2954	25.7	2941
-Cl	0	2951	33.4	2858
-Br	0	2948	36.0	2848
-I	0	2946	38.8	2815

Enthalpies and IR frequencies of the $ZrCH_3X$ molecules (X=H, CN, F, Cl, Br, I) are summarized in Table 3.11, showing that the triplet state of the molecules is the ground state and the singlet state is the first excited state. In the triplet state the C-H bond are less activated than that in the excited(singlet) state. We will study both states by changing metal atoms (Ti, Zr, Hf) and constituents X (H, F, Cl, Br, I, CN). The first goal is to identify critical factors for C-H activations and interpret ligand effects and corresponding effects induced by the metal atoms.

Enthalpy analyse of the n-C_4H_9ZrX molecules reveals the same conclusions:

- The triplet state is the ground state of the molecules.
- The singlet state is the first excited state.
- Enthalpy differences between the triplet state and the singlet state account to about 30 kJ/mol.

3.3.1 The triplet state (ground state)

3.3.1.1 The critical factor for C-H bond activation in the CH_3ZrX-molecules

The structure of the triplet CH_3ZrF-molecule is depicted in Figure 3.3. All the triplet CH_3ZrX molecules (X=H, F, Cl, Br, I, CN) take the eclipsed form as their absolute minimum. An interesting point is that the two trans C-H bonds, which stand trans to the Zr-X bond, are more activated than the cis C-H bond. And in the CH_3ZrH-molecule the Zr-H bond length(187pm) is longer than a normal covalent Zr-H bond(175pm), which explains why smaller product yield is found in the reaction of Zr with methane as compared to the reaction of Zr with methylfluoride[89].

Figure 3.3: The structure of the CH_3ZrF molecule optimized at the B3 level.

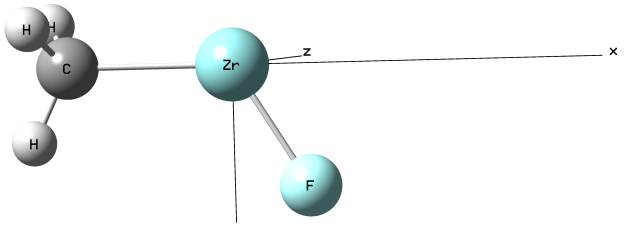

In all the molecules the cartesian axis are fixed as shown in Figure 3.3, the Zr atom lies in the origin, the C atom lies on the X-axis and the X-ligand lies in the XY-plane. The fixation of the cartesian axis will eases later discussions of interactions.

Table 3.12: Structure comparisons of the CH_3ZrX molecules. IR^t presents the stretching frequencies of the C-H bond that stands trans to the Zr-X bond, IR^t_D shows stretching frequencies of the corresponding deuterated C-H bond. IR^c presents the stretching frequencies of the C-H bond that stands cis to the Zr-X bond. Unless otherwise mentioned, only symmetric stretching frequencies are shown. D(Zr-H^t) presents the distance between the Zr atom and the H atom, that belongs to the trans C-H bond, and so on.

CH_3ZrX	IR^t	IR^t_D	D(Zr-H^t)	IR^c	IR^c_D	D(Zr-H^c)
unit	cm^{-1}	cm^{-1}	pm	cm^{-1}	cm^{-1}	pm
-CN	2959	2189	275	3091	2252	284
-H	2959	2191	278	3069	2235	283
-F	2954	2184	278	3082	2247	287
-Cl	2951	2181	276	3089	2253	287
-Br	2948	2178	275	3092	2255	288
-I	2946	2178	274	3093	2257	289

Structures and IR frequencies of the CH_3ZrX molecules are compared in Table 3.12, showing that the trans C-H bond is more activated than the cis C-H bond. Except

in the CH_3ZrCN molecule, it shows that the lower the trans C-H stretching frequency (meaning the more activation), the closer the H atom approaches the Zr atom. The distance between the Zr atom and the H atom of the C-H bond is a good indicator of the overlap between the occupied orbitals of the Zr atom and the antibonding (σ^*) orbital of the C-H bond, implying that the donation from the occupied orbitals of the Zr-atom into the C-H-σ^* orbital is perhaps the critical factor for the C-H activation effect. And the exception in the CH_3ZrCN molecule suggests that overlaps are probably not the only factor affecting C-H activations.

Table 3.13: Bond-orders of the C-H bonds in the CH_3ZrX molecules. In α-spin columns the calculated data of the α-spin are given, and so on. IR^t presents the stretching frequencies of the C-H bond that stands trans to the Zr-X bond, IR^c presents the stretching frequencies of the C-H bond that stands cis to the Zr-X bond. BO^t column shows the bond-order of the C-H bond, that stands trans to the Zr-F bond, and so on. Δ column shows the bond-order difference between the cis and the trans C-H bonds.

			in α-spin			in β-spin		
CH_3ZrX	IR^t	IR^c	BO^t	BO^c	Δ	BO^t	BO^c	Δ
unit	cm^{-1}	cm^{-1}	bond-order			bond-order		
-CN	2959	3091	0.491	0.500	0.009	0.495	0.495	0
-H	2959	3069	0.492	0.497	0.005	0.496	0.496	0
-F	2954	3082	0.493	0.500	0.007	0.500	0.500	0
-Cl	2951	3089	0.490	0.500	0.010	0.495	0.500	0.005
-Br	2948	3092	0.489	0.500	0.011	0.494	0.500	0.006
-I	2946	3093	0.489	0.500	0.011	0.494	0.498	0.004

Bond-order comparisons of the trans (activated) and cis (inactivated) C-H bond are given in Table 3.13, showing that the delocalization effect is stronger in the α-spin than that in the β-spin system. The molecules can be classified into two groups:

- The first group includes CH_3ZrX (X=CN, H, F) molecules, in which the trans C-H bonds are only weakly activated. Comparisons of bond-orders of the trans and the cis C-H bonds shows that mainly the interactions in the α-spin induce the C-H activation. This implies that the donation from occupied Zr orbitals into the C-H-σ^* orbital is the origin for the activation, since the distinction between α- and β-spin channel in the triplet state of the molecules is that two of the Zr valence orbitals (5s or 4d) are occupied in the α-spin, but in the β-spin all of the valence orbitals are unoccupied.

- The second group includes CH_3ZrX (X=Cl, Br, I) molecules, in which the trans C-H bonds are activated in both, α- and β-spin, implying that both the donation from Zr occupied orbitals into the C-H-σ^* orbital and the donation from the C-H-σ orbital into empty valence Zr orbitals make a contribution to C-H activations.

This classification can be explained with the following reasoning:

- The C-H activations begin with electron density donations from Zr occupied orbitals into the C-H-σ^* orbital, since overlaps between those orbital are easy to form, due to the flexibility of the H atoms. It gives only a weak contribution to the C-H activation, but leads to the initial approaches of C-H bonds to metal atoms.

- Further approaches of C-H bonds to the Zr atom lead to overlaps between the C-H-σ and empty Zr orbitals. This releases the increasing electron density pressure of the C-H bond, which is induced by the donation from the occupied Zr orbitals into the C-H-σ^* orbital. This can also been seen from the Table 3.14.

Table 3.14: Occupancies of the activated(trans) C-H bonds in the CH_3ZrX molecules. In α-spin columns the occupancy in the α-spin are given, and so on. IR^t presents the stretching frequencies of the C-H bond that stands trans to the Zr-X bond. The Occ(σ) column gives the occupancy in the C-H bonding orbital, Occ(σ^*) column the occupancy in the C-H antibonding orbital, only occupancy changes related to the CH_3ZrCN molecule are shown.

		in α-spin		in β-spin	
CH_3ZrX	IR^t	Occ(σ)	Occ(σ^*)	Occ(σ)	Occ(σ^*)
unit	cm^{-1}	elemental charge			
-CN	2959				
-H	2959	0.0026	0.0003	0.0021	0
-F	2954	0.0036	0.0005	0.0024	0
-Cl	2951	0.0005	0.0006	-0.0001	0
-Br	2948	-0.0005	0.0009	-0.0009	0
-I	2946	-0.0014	0.0011	-0.0016	0

Occupancies of the activated (trans) C-H bond are summarized in Table 3.14, confirming the conclusions from the bond-order analysis. Observations from the Table 3.14 are that:

- In the α-spin state , the more a C-H bond is activated, the higher the occupancy of a C-H-σ^* orbital is.

- In the β-spin state the occupancy of a C-H-σ^* orbital is uncorrelated with the C-H activation, since there is no occupation at all.
- In the group of the CH_3ZrX (X=CN, H, F) molecules, the donation from Zr occupied orbitals into the C-H-σ^* orbital in the α-spin is clearly the origin for the activation, since the increasing occupancy in the C-H-σ orbital should lead to C-H deactivation, which can not explain the trend of C-H activations.
- In the other group of the CH_3ZrX (X=Cl, Br, I) molecules, the C-H activation may be induced by: the donation from the C-H-σ orbital into empty Zr orbitals in both spins and donation from Zr occupied orbitals into the C-H-σ^* orbital in the α-spin. The critical factor, which dominantly influences the C-H activation, is so far unclear.

3.3.1.2 Analyse of interactions.

Table 3.15: Hyperconjugations of the C-H bonds in the CH_3ZrX molecules in the α-spin. Trans C-H bond columns show the calculated data of the trans C-H bond, which stands trans to the Zr-X bond. IR presents the stretching frequencies of the C-H bond. ΔE^2_{ij} gives second-order perturbative estimation of the hyperconjugation effect between the C-H-σ^* orbital and occupied orbitals of the Zr-atom in the α-spin, $\Delta\varepsilon_{ij}$ gives the energy gap of the two interacted NBOs.

	trans C-H bond			cis C-H bond		
CH_3ZrX	IR	ΔE^2_{ij}	$\Delta\varepsilon_{ij}$	IR	ΔE^2_{ij}	$\Delta\varepsilon_{ij}$
unit	cm^{-1}	kcal/mol	hartree	cm^{-1}	kcal/mol	hartree
-CN	2959	1.22	0.54	3091	0.01	0.85
-H	2959	1.46	0.55	3069	0.25	0.68
-F	2954	1.46	0.55	3082	0.05	0.57
-Cl	2951	1.45	0.55	3089	0.04	0.96
-Br	2948	1.47	0.55	3092	0.05	0.94
-I	2946	1.48	0.55	3093	0.07	0.86

Second-order perturbative estimates of hyperconjugations between the C-H-σ^* orbital and the occupied orbitals of the Zr-atom in the α-spin of the CH_3Zr-X molecules are summarized in Table 3.15, showing the following:

- Comparison of the inactivated (cis) with the activated (trans) C-H bonds shows that the hyperconjugation effect (ΔE^2_{ij}) correlates clearly with the C-H activations, which is induced by the reduced energy gap of the interacting orbitals ($\Delta\varepsilon_{ij}$).

- The ΔE^2_{ij} between the trans C-H-σ^* orbital and the occupied orbitals of the Zr-atom in the α-spin system alone do not show the right tendency to the C-H activation, neither does $\Delta\varepsilon_{ij}$.

At this point we will discuss accuracies of the different terms: occupancies, bond-orders and ΔE^2_{ij} (Second-order perturbative estimate of the hyperconjugation effect).

NBO occupancies associate uniquely with the optimized wavefunction, its variations reflect physically important resonance delocalization effect to the idealized Lewis structure picture. Each NBO is uniquely determined by its defining local-eigenorbital property, therefore the occupancy should be an accurate description of electronic structures of molecules.

Bond-order are derived purely from the information in the first-order density matrix[43], in the broad intermediate region a bond-order correlates with bond-lengths. Therefore bond-orders are an accurately calculated theoretical descriptor of the system, closely correlated with a host of structural, reactive, and electronic properties.

ΔE^2_{ij} is estimated from the second-order perturbation theory of the interaction energy of NBOs according to the Eq. 2.1.18, in the equation the Mulliken approximation, which is only a loose approximation for estimations of the $\langle\sigma_i \mid \hat{F} \mid \sigma^*_j\rangle$, is used. Orbital energy estimations of NBOs (E_j, E_i) is more problematic, since they are composed of NAOs, which are difficult to identify in a molecular environment. Therefore ΔE^2_{ij} and $\Delta\varepsilon_{ij}$ are only semi-quantitative quantities, which should be used critically.

Table 3.16: Further details of the interactions between the C-H-σ^* and occupied Zr orbitals in the α-spin of the CH_3ZrX molecules. IR^t gives the stretching frequencies of the C-H bond standing trans to the Zr-X bond. ΔE^2_{ij} and $\Delta\varepsilon_{ij}$ give the second-order perturbative estimation of hyperconjugation and the energy gap between the C-H-σ^* and the occupied Zr orbitals. hyb. represents the hybridization of the occupied NBO of the Zr atom, which participates in the hyperconjugation.

		NBO1			NBO2		
CH_3ZrX	IR^t	ΔE^2_{ij}	hyb.	$\Delta\varepsilon_{ij}$	ΔE^2_{ij}	hyb.	$\Delta\varepsilon_{ij}$
unit	cm^{-1}	kcal/mol		hartree	kcal/mol		hartree
-CN	2959	0.53	$sd^{0.81}$	0.54	0.69	d	0.54
-H	2959	0.73	$sd^{0.70}$	0.55	0.73	d	0.55
-F	2954	0.59	$sd^{0.55}$	0.55	0.87	d	0.55
-Cl	2951	0.71	$sd^{0.74}$	0.55	0.74	d	0.55
-Br	2948	0.68	$sd^{0.80}$	0.55	0.79	d	0.55
-I	2946	0.63	$sd^{0.89}$	0.55	0.85	d	0.55

Further details of the interactions between the C-H-σ^* and the occupied Zr orbitals in the α-spin of the CH_3ZrX molecules are summarized in Table 3.16. The total interaction between the C-H-σ^* and occupied Zr orbitals in the the α-spin of the CH_3ZrX molecules stem from two interactions (the interactions of NBO1 and NBO2 of the Zr atom with the C-H-σ^* orbital.) The essential parts of NBO1 are the 5s and $4d_{z^2}$ orbitals of the Zr atom with composition

$$0.7890 * 5s + 0.4818 * 4d_{z^2} - 0.2244 * 4d_{x^2-y^2} - 0.2480 * 4d_{xy}$$

in the CH_3ZrF molecule, the NBO1s in the other CH_3ZrX molecules show similar compositions. The essential parts of NBO2 are the $4d_{yz}$ orbitals ($0.8192*4d_{yz} - 0.5619*4d_{xz}$ in the CH_3ZrF molecule), the NBO2s of the other CH_3ZrX molecules show also similar compositions. From the Table 3.16 it is difficult to identify which orbitals (NBO1 or NBO2) have the dominant influence on the C-H activation. But from the analysis of bond-order and occupancy it is evident that the interactions between the C-H-σ^* orbital and the occupied Zr orbitals make the critical contribution to the C-H activation in the CH_3ZrX molecules(X=CN, H, F).

We will pass on the CH_3ZrCN and CH_3ZrH molecules and investigate the hyperconjugation related to the C-H-σ orbital in the rest of the molecules.

Table 3.17: Interactions between the C-H-σ orbital and empty Zr orbitals in the CH_3ZrX molecules. IR^t gives the stretching frequencies of the C-H bond that stands trans to the Zr-X bond. In α-spin columns the calculated data of the α-spin are given, and so on. Sum column represents the sum of all the second-order perturbative estimations of the hyperconjugation effect between the C-H-σ orbital and empty Zr orbitals. ΔE^2_{ij} gives the second-order perturbative estimation of the hyperconjugation effect between the C-H-σ orbital and the Zr-X-σ^* orbital, $\Delta\varepsilon_{ij}$ gives the energy gap between the two interacting NBOs.

		in α-spin			in β-spin		
CH_3ZrX	IR^t	sum	ΔE^2_{ij}	$\Delta\varepsilon_{ij}$	sum	ΔE^2_{ij}	$\Delta\varepsilon_{ij}$
unit	cm^{-1}	kcal/mol		hartree	kcal/mol		hartree
-F	2954	1.27			1.48		
-Cl	2951	1.24	0.69	0.56	1.52	0.65	0.58
-Br	2948	1.34	0.83	0.55	1.62	0.77	0.56
-I	2946	1.44	0.95	0.54	1.74	0.88	0.55

Interactions between the C-H-σ orbital and empty Zr orbitals in the CH_3ZrX molecules are summarized in Table 3.17, showing a clear correlation between the C-H activation and the sum of the interactions in both the α- and β-spin. The energy gap of the

leading interaction is impacted by the change of the constituent(X), the associated hyperconjugation is occurred between the C-H-σ orbital and the Zr-X-σ^* orbital, but such an interaction can not be found in the CH_3ZrF molecule. The Table 3.17 reveals that the different C-H activation in CH_3ZrX (X=F, Cl, Br, I) molecules are induced by the hyperconjugation between the C-H-σ and the Zr-X-σ^* orbital. With the increase in C-H activations energy gaps of this hyperconjugation is reduced, which is affected by the constituent(X).

3.3.1.3 NPA analysis

Table 3.18: NPA of the CH_3ZrX molecules. Trans C-H bond columns show the natural charge of the trans C-H bond, and so on. IR gives the stretching frequency of the C-H bond, q(H) the natural change of the H atom, and so on.

	the trans-C-H bond			the cis-C-H bond	
CH_3ZrX	IR	q(C)	q(H)	IR	q(H)
unit	cm^{-1}	a.u.		cm^{-1}	a.u.
-CN	2959	-1.215	0.223	3091	0.241
-H	2959	-1.218	0.216	3069	0.229
-F	2954	-1.250	0.216	3082	0.232
-Cl	2951	-1.245	0.218	3089	0.237
-Br	2948	-1.248	0.218	3092	0.239
-I	2946	-1.251	0.218	3093	0.240

Natural charges of atoms in the trans and cis C-H bonds in the CH_3ZrX molecules are summarized in Table 3.18, showing that the polarity of the C-H bond is reduced with increased C-H activations compared the trans to the cis C-H bonds in the same molecule. In the different molecules, the more a C-H bond is activated, the less positive is the corresponding H-atom.

3.3.1.4 Group trends in the CH_3MF molecules

Table 3.19: Analysis of group trends in the CH_3MF molecules. IR^t gives the stretching frequencies of the C-H bond that stands trans to the M-X bond, IR^t_D shows stretching frequencies of the corresponding deuterated C-H bond. D(M-H^t) gives the distance between the TM atom and the H atom that belongs to the trans C-H bond. Occ(σ^*) gives the C-H-σ^* orbital occupancy in the α-spin and bond-order gives the trans C-H bond-order in the α-spin. ΔE^2_{ij} represents the sum of all the second-order perturbative estimations of the hyperconjugation effect between the C-H-σ^* orbital and the occupied Zr orbitals in the α-spin.

CH_3TMF	IR^t	IR^t_D	D(M-H^t)	Occ(σ^*)	bond-order	ΔE^2_{ij}
unit	cm^{-1}	cm^{-1}	pm	a.u.	a.u.	kcal/mol
Ti	2974	2200	268	0.00296	0.496	0.83
Zr	2954	2184	278	0.00572	0.493	1.46
Hf	2958	2186	280	0.00579	0.494	1.23

Analysis of group trends is carried out in Table 3.19. From the previous investigation we assume that the C-H activations in the CH_3MF molecules (M=Ti, Zr, Hf) are induced by the interactions between the C-H-σ^* and occupied metal valence orbitals. The Table 3.19 reveals that

- The C-H activation correlates strictly with the bond-order and ΔE^2_{ij} of the α-spin system.
- A approximately proper correlation between the C-H activation and occupancy of the C-H-σ^* orbital in the α-spin can be found as well.

Table 3.20: Further details of interactions between the C-H-σ^* and occupied TM orbitals in the α-spin of the CH_3MX molecules. IR^t gives the stretching frequency of the C-H bond standing trans to the TM-F bond. ΔE^2_{ij} and $\Delta\varepsilon_{ij}$ give the second-order perturbative estimation of hyperconjugation and the energy gap between the C-H-σ^* and occupied TM orbitals. hyb. represents the hybridization of the occupied NBO participating in the hyperconjugation that consists of the TM valence orbitals.

		NBO1			NBO2		
CH_3TMX	IR^t	ΔE^2_{ij}	hyb.	$\Delta\varepsilon_{ij}$	ΔE^2_{ij}	hyb.	$\Delta\varepsilon_{ij}$
unit	cm^{-1}	kcal/mol		hartree	kcal/mol		hartree
Ti	2974	0.48	$sd^{1.40}$	0.58	0.35	d	0.60
Zr	2954	0.59	$sd^{0.55}$	0.55	0.87	d	0.55
Hf	2958	0.31	$sd^{0.35}$	0.57	0.92	d	0.53

Further details of interactions between the C-H-σ^* and occupied TM orbitals in the the α-spin of the CH_3MX molecules are summarized in Table 3.20, showing that with

neither of the interactions the activation trends can be explained. It implies also that both the valence s and valence d orbitals of the metal atoms are participating in C-H activations. The higher trans C-H activation in the CH_3ZrF molecule as compared to CH_3TiF is clearly induced by the raising of the orbital energy of both valence s and valence d orbitals, leading to a smaller energy gap between the C-H-σ^* and occupied TM orbitals. The relativistic effects and associated lanthanide contraction lead to the Hf 6s orbital of lower energy in CH_3HfF as compared to the 5s orbital in the CH_3ZrF molecule. It causes a larger energy gap between between the C-H-σ^* and occupied NBO1 orbitals, leading to reduced trans C-H activation of the CH_3HfF molecule compared to that of CH_3ZrF.

3.3.1.5 The critical factor for C-H bond activation in the *n*-C_4H_9ZrX-molecule

The structure of the triplet *n*-C_4H_9ZrF-molecule is depicted in Figure 3.4, corresponding to a local minimum, since the absolute minimum corresponds to a linear alignment of C-H bonds, which is uninteresting in our investigation. All the triplet *n*-C_4H_9ZrX molecules (X=H, F, Cl, Br, I, CN) take a similar structure. In the figure only the most activated α-C-H bonds that stand trans to the Zr-F bond, and the most activated δ-C-H bonds that stand cis to the Zr-F bond, are shown. In all of the molecules, the cartesian axis are fixed as shown in Figure 3.4: the Zr atom lies in the origin, the C atom, which belongs to the α-C-H bond, lies on the X-axis, and the X-ligand lies in the XY-plane.

Figure 3.4: The structure of the *n*-C_4H_9ZrF molecule optimized with the B3 method.

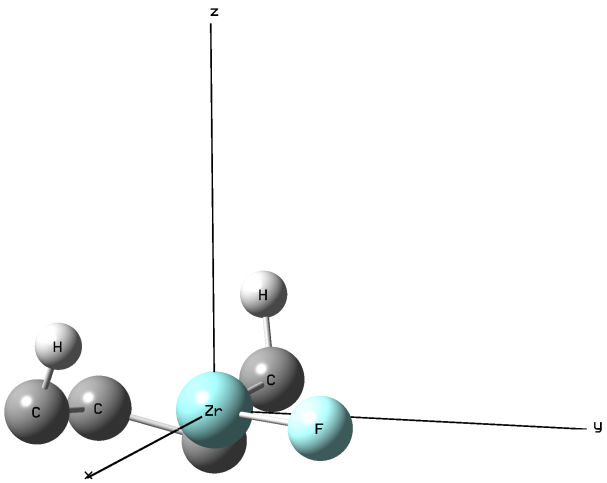

Structures of the *n*-C_4H_9ZrX molecules are summarized in Table 3.21, showing that:

- except *n*-C_4H_9ZrH, compared to the α-C-H bonds the δ-C-H bonds are more activated, the Zr-H distance is reduced, however the Zr-C distance is longer.
- all of the α-C-H bonds are all very weakly activated.

Table 3.21: Structure comparison of the n-C_4H_9ZrX molecules. δ-C-H bond columns show the calculated data of the δ-C-H bond and α-C-H bond show that of the α-C-H bond. IR gives the stretching frequency of the C-H bond. IR_D shows stretching frequencies of the corresponding deuterated C-H bond. D(Zr-H) gives the distance between the Zr atom and the H atom, and so on.

	δ-C-H bond				α-C-H bond			
n-C_4H_9ZrX	IR	IR_D	Zr-H	Zr-C	IR	IR_D	Zr-H	Zr-C
unit	cm^{-1}		pm		cm^{-1}		pm	
-H	2925	2148	263	325	2927	2146	272	222
-F	2906	2135	255	305	2934	2151	278	225
-CN	2864	2101	287	303	2924	2144	269	222
-Cl	2863	2101	244	296	2927	2146	274	224
-Br	2855	2094	242	294	2924	2143	273	224
-I	2845	2087	240	294	2920	2140	271	224

- the more a δ-C-H bonds is activated, the shorter the Zr-C distance gets. With exception of n-C_4H_9ZrCN, the Zr-H distance reduces with increasing C-H activation.
- the δ-C-H bond is much stronger activated than the C-H bond in the corresponding CH_3ZrX.

Table 3.22: Bond-order analyse in the n-C_4H_9ZrX molecules. IR^{δ} gives the stretching frequency of the δ-C-H bond, and so on. In the α-spin columns the bond-order in the α-spin are shown, and so on. The BO(δ) column gives bond-order of the δ-C-H bond, and so on.

			α-spin		β-spin	
	IR^{δ}	IR^{α}	BO(δ)	BO(α)	BO(δ)	BO(α)
unit	cm^{-1}	cm^{-1}	bond order			
-H	2925	2927	0.489	0.495	0.497	0.495
-F	2906	2934	0.490	0.496	0.489	0.495
-CN	2864	2924	0.487	0.495	0.488	0.495
-Cl	2863	2927	0.482	0.495	0.487	0.495
-Br	2855	2923	0.481	0.496	0.486	0.495
-I	2845	2920	0.487	0.496	0.485	0.495

Bond-order comparisons of the δ- to the α-C-H bond of the n-C_4H_9ZrX molecules are summarized in Table 3.22, showing that delocalizations of the δ-C-H bonds are similar in the α- and β-spin, but much stronger than the α-C-H bond. This implies that

interactions between C-H-σ and empty Zr valence orbitals induce the C-H activation, since the occupied Zr valence orbitals exist only in the α-spin, which should only makes a minor contribution to the C-H activation in this case.

Table 3.23: Occupancies of the δ-C-H bonds in the n-C_4H_9ZrX molecules. IR^{δ} gives the stretching frequency of the δ-C-H bond. In the α-spin columns the occupancy in the α-spin is described. Occ(σ) column gives the occupancy difference in the C-H bonding orbital compared to the n-C_4H_9ZrH molecule, Occ(σ^*) column presents occupancy in the C-H anti-bonding orbital (vacant orbital).

		α-spin		β-spin	
	IR^{δ}	Occ(σ)	Occ(σ^*)	Occ(σ)	Occ(σ^*)
unit	cm^{-1}	elemental charge			
-H	2925				
-F	2906	-0.0027	0.0025	-0.0027	0.0001
-CN	2864	-0.0060	0.0065	-0.0065	0.0002
-Cl	2863	-0.0086	0.0066	-0.0089	0.0002
-Br	2855	-0.0099	0.0072	-0.0102	0.0002
-I	2845	-0.0111	0.0080	-0.0114	0.0002

Occupancies of the δ-C-H bonds in the n-C_4H_9ZrX molecules are shown in Table 3.23, showing that the C-H activations in the C-H bonds can be induced by the following factors: reduction of occupancy of the C-H-σ-orbitals in both spins and the occupancy increase of the C-H-σ^*-orbital in the α-spin. Analyse of the bond-order in Table 3.22 suggests that an increase of occupancy of the C-H-σ^*-orbitals should only make a minor contribution to the C-H activation. Therefore in the further investigation only the interactions that induce the reduction of occupancy of the C-H-σ-orbitals, need to be studied in order to identify the critical factor for C-H activations.

3.3.1.6 Analyse of interactions.

Hyperconjugations of the C-H-σ orbital in the n-C_4H_9ZrX molecules are shown in Table 3.24, showing similar patterns in both spin channel. The more C-H is activated, the stronger the interactions between the C-H-σ orbital and empty Zr orbitals gets. $\Delta E^2_{ij}(1)$ is interactions between the C-H-σ orbital and the NBOs, which consist of the empty Zr valence orbitals. The interaction strengths correlate properly with C-H activations, but the more a C-H bond is activated, the larger the energy gap between the interacted orbitals gets. This implies that this interaction could not be the origin for the C-H activation. $\Delta E^2_{ij}(2)$ is interactions between the C-H-σ orbital and the

Table 3.24: Hyperconjugations of the δ-C-H-σ orbital in the n-C_4H_9ZrX molecules. IR^{δ}) gives the stretching frequency of the δ-C-H bond. In the α-spin columns the calculated data of the α-spin are shown, and so on. $\Delta E^2_{ij}(1)$ presents second-order perturbative estimations of the hyperconjugation effect between the C-H-σ orbital and NBO1 (which consists of empty orbitals of the Zr-atom).

		α-spin		β-spin	
	IR^{δ}	$\Delta E^2_{ij}(1)$	$\Delta E^2_{ij}(2)$	$\Delta E^2_{ij}(1)$	$\Delta E^2_{ij}(2)$
unit	cm^{-1}	kcal/mol	kcal/mol	kcal/mol	kcal/mol
-H	2925	0.10	2.32	0.28	2.50
-F	2906	0.26	3.46	0.52	3.47
-CN	2864	0.36	4.67	0.61	4.77
-Cl	2863	0.68	5.40	1.06	5.38
-Br	2855	0.79	5.81	1.11	5.80
-I	2845	0.88	6.30	1.25	6.34

Zr-X-σ^* orbital, with the exception of the n-C_4H_9ZrF molecule. In the n-C_4H_9ZrF molecule an interaction between the C-H-σ orbital and Zr-F-σ^* orbitals do not exist , as seen from the NBO analysis, therefore this interaction is largely different from other NBO in their orbital compositions. The accurate compositon of the NBO2 in the α spin of the n-C_4H_9ZrF molecule is a hybrid LP orbital of Zr atom with accurate compositions of

$$0.4871 * 5s + 0.5943 * 4d_{xy} - 0.4697 * 4d_{x^2-y^2} - 0.4040 * 4d_{z^2}$$

The NBO in the α-spin of n-C_4H_9ZrCl is a Zr-Cl-σ^* orbital, which is composed of $Zr_{sd^{1.77}} + Cl_{sp^{2.35}}$ The accurate composition of the hybrid orbital on the Zr atom is

$$0.5977 * 5s - 0.5701 * 4d_{xy} - 0.4432 * 4d_{x^2-y^2} - 0.3347 * 4d_{z^2}$$

The composition of the other Zr-X-σ^* orbital is similar to that in the α-spin of the n-C_4H_9ZrCl molecule.

This hyperconjugation strength shows a proper correlation with the C-H activation and the energy gap between the interacting orbitals in general are reduced with increasing C-H activation.

3.3.1.7 NPA analysis

Table 3.25: NPA in the n-C_4H_9ZrX molecules. δ-C-H columns show the natural charge differences of the atoms in the δ-C-H bond, and so on. IR gives the stretching frequency of the C-H bond, q(H) gives the natural change of the H atom, and so on. $\Delta(q_H - q_C)$ shows the natural charge difference between the H- and C-atoms.

	the δ-C-H bond				the α-C-H bond			
n-C_4H_9ZrX	IR	$\Delta(q_H - q_C)$	q(C)	q(H)	IR	$\Delta(q_H - q_C)$	q(C)	q(H)
unit	cm^{-1}	a.u.			cm^{-1}	a.u.		
-H	2925	0.763	-0.600	0.163	2927	1.139	-0.940	0.199
-F	2906	0.786	-0.615	0.171	2934	1.159	-0.965	0.194
-CN	2864	0.764	-0.605	0.159	2924	1.141	-0.936	0.205
-Cl	2863	0.779	-0.610	0.169	2927	1.157	-0.961	0.196
-Br	2855	0.767	-0.600	0.167	2924	1.159	-0.962	0.197
-I	2845	0.772	-0.607	0.165	2920	1.162	-0.964	0.198

Natural charges of the atoms in the δ- and α-C-H bonds of the n-C_4H_9ZrX molecules are summarized in Table 3.25, showing that the polarity of the C-H bond is reduced with an increase of C-H activation comparing the δ- to α-C-H bonds in the same molecule.

3.3.1.8 Group trends in the *n*-C_4H_9MF molecules

Table 3.26: Analysis of group trends in the n-C_4H_9MF molecules. IR^{δ} gives the stretching frequency of the δ-C-H bond. M-H gives the distance between the TM atom and the H atom, which belong to the δ-C-H bond, and so on, IR^{δ}_{D} shows stretching frequencies of the corresponding deuterated C-H bond. In the α-spin columns the calculated data of the α-spin is shown, and so on. Occupancy gives occupancies of the δ-C-H-σ orbital and bond-order bond-orders of the δ-C-H bond.

					in the α-spin		in the β-spin	
n-C_4H_9MF	IR^{δ}	IR^{δ}_{D}	D(M-H)	D(M-C)	bond-order	occupancy	bond-order	occupancy
unit	cm^{-1}	cm^{-1}	pm	pm	a.u.			
Ti	2891	2124	232	281	0.489	0.980	0.488	0.980
Zr	2906	2135	305	255	0.490	0.984	0.489	0.983
Hf	2913	2139	323	263	0.489	0.985	0.489	0.985

An analysis of group trends in the n-C_4H_9MF (M=Ti, Zr, Hf) molecules is done in Table 3.26. Only δ-C-H-σ orbital occupancy is represented, since it is known that the C-H activation in the n-C_4H_9ZrF molecules is induced by the interactions between the

C-H-σ and empty Zr valence orbitals. Following pictures can be observed in the Table 3.26.

- The distances between the metal atoms and the δ-H atom reduce with increasing C-H activation.
- The C-H activation correlates properly with the C-H-σ orbital occupancy in both spins.
- The distances between the metal atoms and the δ-C atom do not show a proper correlation with C-H activations.

These observations confirm the conclusion of previous investigation of n-C_4H_9ZrX molecules, that the interactions between the C-H-σ and empty metal valence orbitals are indeed the critical factor inducing the C-H activation.

Table 3.27: The leading interaction between the C-H-σ and empty metal orbitals in the n-C_4H_9MF molecules. IR^{δ} gives the stretching frequency of the δ-C-H bond. In the α-spin columns the calculated data of the α-spin is shown, and so on. ΔE^2_{ij} and $\Delta\varepsilon_{ij}$ give the second-order perturbative estimation of the leading hyperconjugation and the energy gap between the interacting NBOs, hyb. shows the hybridization of the empty NBO of the TM, which participate in the interaction.

		α-spin			β-spin		
n-C_4H_9MF	IR^{δ}	ΔE^2_{ij}	hyb.	$\Delta\varepsilon_{ij}$	ΔE^2_{ij}	hyb.	$\Delta\varepsilon_{ij}$
unit	cm^{-1}	kcal/mol		hartree	kcal/mol		hartree
Ti	2891	4.16	$sd^{1.50}$	0.54	3.87	$sd^{3.19}$	0.58
Zr	2906	3.46	$sd^{3.09}$	0.59	3.47	$sd^{3.71}$	0.61
Hf	2913	2.54	$sd^{5.63}$	0.79	2.80	$sd^{3.77}$	0.67

The leading interactions between the C-H-σ and empty metal orbitals in the n-C_4H_9TMF molecules are summarized in Table 3.27. They show that the stronger the interaction strength is, the more the C-H bond activated is. Within the group hybridizations of the NBOs of the metal atoms changes dramatically in the α-spin. Since the expected similar composition of the NBOs by fixing the cartesian axis can only be found in the β-spin, so only the leading interaction in the β-spin is to be analyzed. It will be assumed that the interactions between the C-H-σ and empty TM orbitals in both spins are similar, which can be supposed from the Table 3.26. The accurate composition of the interacting NBO from the Zr atom in the α-spin is

$$0.4871 * 5s + 0.5943 * 4d_{xy} - 0.4697 * 4d_{x^2-y^2} - 0.4040 * 4d_{z^2}$$

. The interacting NBO from Ti and Hf show similar compositions.

The Table 3.27 shows that the more the δ-C-H bond is activated, the stronger the interaction between the C-H-σ and empty TM orbitals is and the smaller the energy gap between the interacting NBO gets. This implies that the δ-C-H activation is indeed induced by the interactions between the C-H-σ and empty metal orbitals in both spins.

.

3.3.1.9 Summary

By studying the n-C_4H_9ZrX and CH_3ZrX systems (X= H, CN, F, Cl, Br, I) it can be shown that C-H activiations can be classified into two stages:

- In the first stage a C-H bond is only weakly activated, the calculated stretching frequency of the C-H bond is reduced only to about 2900 cm^{-1} (experimental frequencies should lie at about 2850 cm^{-1}). In this stage electron density donations from occupied metal valence orbitals into C-H antibonding (σ^*) orbitals dominantly induce C-H activations, since overlaps between C-H antibonding orbitals and occupied valence TM orbitals are easy to form, due to the flexibility of H atoms. These interactions lead to an approach of C-H bonds to metal atoms and an increase of electron density pressure in the C-H bond. In this stage: Occupied metal valence orbitals of high energy benefit C-H activations, as shown in Table 3.20.

- In the next stage C-H bonds are further activated, since approaches of C-H bonds to metal atoms make overlaps between C-H bonding(σ) orbitals and empty valence metal orbitals possible. And the high electron density pressure of the C-H bond leads also to a strong tendency of the electron density donation from C-H-σ orbitals into empty metal valence orbitals. In this stage this donation is essential for further C-H activations. To strengthen this interaction the energy gap between the C-H bonding orbital and empty metal valence orbitals should be small. In this stage both type of the interactions cooperate and enforce one another: donation from occupied metal valence orbitals into C-H antibonding (σ^*) orbitals and donation from C-H bonding(σ) orbitals into empty metal valence orbitals. From the bond-order analysis in the Table 3.22, the C-H activation is dominantly induced by the interaction between the C-H-σ and empty metal

valence orbitals in this stage. Empty valence TM orbitals of low energy benefit the C-H activations.

Analyse of the natural charge (in Table 3.33 and 3.25) shows that the more a C-H is activated, the less positive is the H atom is of the C-H bond, the more nonpolar the C-H bond is.

3.3.2 The singlet state (first excited state)

3.3.2.1 The critical factor for C-H bond activation in the $ZrCH_3X$-molecule

All the singlet CH_3ZrX molecules (X=F, Cl, Br, I, CN) take the eclipsed form as their absolute minimum, and the trans C-H bond is more activated than that in the corresponding triplet molecules. Since they show similar structure as their triplet counterpart, the structures will not be depicted here. We take Figure 3.3 as the structure of the singlet CH_3ZrX molecules and use as well the same fixation of the cartesian axis.

Table 3.28: Structure comparisons of the singlet CH_3ZrX molecules. IR^t stands for the stretching frequencies of the C-H bond trans to the Zr-X bond, IR^t_D shows stretching frequencies of the corresponding deuterated C-H bond. D(Zr-H^t) gives the distance between the Zr atom and the H atom belonging to the trans C-H bond, and so on.

CH_3ZrX	IR^t	IR^t_D	D(Zr-H^t)	IR^c	IR^c_D	D(Zr-H^c)
unit	cm^{-1}	cm^{-1}	pm	cm^{-1}	cm^{-1}	pm
-F	2941	2176	265	3126	2281	288
-Cl	2858	2125	255	3151	2303	296
-Br	2848	2105	250	3159	2310	299
-CN	2847	2103	249	3160	2311	298
-I	2815	2080	245	3165	2315	302

Structures and IR frequencies of the singlet CH_3ZrX molecules are compared in Table 3.28, showing that the two trans C-H bonds, which lie trans to the Zr-X bond, are more activated than the corresponding cis C-H bond. With increasing C-H activations the H atom approaches more closely to the Zr atom.

Table 3.29: Bond-order comparisons in the CH_3ZrX molecules. IR^t represents the stretching frequency of the C-H bond that stands trans to the Zr-X bond and IR^c gives that of the cis C-H bond. The BO^t column gives the bond-order of the C-H bond trans to the Zr-X bond, and so on.

CH_3ZrX	IR^t	BO^t	IR^c	BO^c
unit	cm^{-1}	a.u.	cm^{-1}	a.u.
-F	2941	0.982	3126	1.000
-Cl	2858	0.965	3151	1.000
-Br	2848	0.965	3159	1.000
-CN	2847	0.969	3160	1.000
-I	2815	0.960	3165	1.000

Bond-order comparisons of the trans and cis C-H bond are shown in Table 3.29, showing that delocalization effects in the trans C-H bonds is stronger than that in the cis C-H bonds. The overall trends of bond-orders of the trans C-H bonds shows a right correlation with C-H activations.

Table 3.30: Occupancies of the C-H bonds in CH_3ZrX molecules. The trans C-H bond column gives the calculated data of the trans C-H bond, and so on. IR gives the stretching frequencies of the C-H bond. The Occ(σ) column gives the occupancy of the C-H-σ orbital, the Occ(σ^*) column the occupancy in the C-H-σ^* orbital. In the trans C-H bond columns only the occupancy changes related to the CH_3ZrF molecule are shown. In the cis C-H bond columns only the occupancy changes related to the trans C-H bond in the same molecule are shown, i.e.
Occ(C-H-σ)=occupancy$_{\text{cis-C-H-}\sigma}$-occupancy$_{\text{trans-C-H-}\sigma}$.

	the trans C-H bond			the cis C-H bond		
CH_3ZrX	IR	Occ(σ)	Occ(σ^*)	IR	Occ(σ)	Occ(σ^*)
unit	cm^{-1}	a.u.		cm^{-1}	a.u.	
-F	2941			3126	0.015	-0.005
-Cl	2858	-0.014	0.005	3151	0.030	-0.009
-Br	2848	-0.020	0.008	3159	0.036	-0.010
-CN	2847	-0.017	0.008	3160	0.033	-0.010
-I	2815	-0.027	0.011	3165	0.043	-0.012

Occupancies of the C-H bonds in the CH_3ZrX molecules are shown in table 3.30, showing that

- with increasing C-H activations of the trans C-H bonds occupancies of C-H-σ orbitals reduce and occupancies of C-H-σ^* orbitals increase. Changes in the C-H-σ orbital is bigger than that in the C-H-σ^* orbital. This confirms the conclusions of the previous investigation on the triplet CH_3ZrX molecules, the donation of the C-H-σ orbital into the vacant Zr orbital may be the critical factor for the C-H activation.

- compared orbital occupancies of the cis C-H bond to the trans C-H bond shows the same picture that occupancy changes in the C-H-σ orbital are dominant.

- the CH_3ZrCN seems to be an exception in the line, the π-ligand(CN) seems to have a different effect on C-H activations as the other σ-ligands.

Table 3.31: Leading Hyperconjugations between the C-H-σ and vacant Zr-X-σ^* orbitals in CH_3ZrX molecules. IR^t gives the stretching frequencies of C-H bonds trans to the Zr-X bond. ΔE^2_{ij} and $\Delta\varepsilon_{ij}$ give the second-order perturbative estimation of hyperconjugation and the energy gap between the C-H-σ and the Zr-X-σ^* orbital. The hyb. column shows the hybridization of the Zr occupied NHO orbital, which participates in the hyperconjugation. The composition columns gives the coefficients of the NAOs that form the NHO on the Zr atom.

					composition			
CH_3ZrX	IR^t	ΔE^2_{ij}	$\Delta\varepsilon_{ij}$	hyb.	5s	$4d_{z^2}$	$4d_{x^2-y^2}$	$4d_{xy}$
unit	cm^{-1}	kcal/mol	hartree					
-F	2941	0.90	0.62	$sd^{6.39}$	0.36	-0.52	-0.54	0.54
-Cl	2858	7.55	0.53	$sd^{3.84}$	-0.45	0	-0.25	0.84
-Br	2848	8.79	0.54	$sd^{2.67}$	-0.52	0.17	-0.13	0.82
-CN	2847	4.94	0.62	$sd^{2.90}$	0.50	0.49	-0.13	-0.13
-I	2815	10.23	0.55	$sd^{2.08}$	-0.56	0.24	0	0.77

3.3.2.2 Analysis of interactions

Hyperconjugations between the C-H-σ and the vacant Zr orbitals atoms in CH_3ZrX molecules are complicated, but in general analyse show that the interaction between the C-H-σ and the vacant Zr-X-σ^* orbital is dominant in all the interactions. Analyse of the interactions in Table 3.31 shows that:

- the CH_3ZrCN molecule is again a exception in the line. This is perhaps due to the variation process in the NBO analysis, which leads to drastic varied compositions of NBO orbitals as compared to the other molecules. It accounts to 9.95 kcal/mol for the CH_3ZrCN molecule, when all the interactions between the C-H-σ and Zr NBOs, which have major contributions by the $4d_{xy}$, $4d_{z^2}$ orbitals (NHO coefficient > 0.7), add up.

- The interactions between C-H-σ and vacant Zr-X-σ^* orbitals in the CH_3ZrX molecules are strong, except for the CH_3ZrF molecule. The interactions correlate well with C-H activations.

- The energy gap between the C-H-σ and the Zr-X-σ^* orbital varies irregularly with C-H activation. But it is known that Zr atoms form stronger Zr-X-σ bonds with light halogens than with heavy halogens and the energies of Zr-X-σ^* NBOs are expected to be higher in the CH_3ZrX molecules including lighter halogens. This should lead to a larger energy gap between the C-H-σ and the Zr-X-σ^* orbitals in CH_3ZrX molecules with lighter halogens.

The secondary interactions between C-H-σ and the vacant orbitals of Zr atoms, which are mostly composed of of the $4d_{xz}$ and $4d_{yz}$ orbital and are not shown here, accounts from 2 to 6 kcal/mol. It implies that the C-H activation should be induced by the interactions between C-H-σ and vacant valence LP orbitals of Zr atoms.

Table 3.32: Leading hyperconjugations between trans C-H-σ^* and occupied Zr orbitals in the CH_3ZrX molecules. IR^t gives the stretching frequencies of the C-H bond trans to the Zr-X bond. ΔE^2_{ij} gives a second-order perturbative estimation of the hyperconjugation effect between the C-H-σ^* orbital and occupied Zr hybrid orbitals, $\Delta\varepsilon_{ij}$ gives the energy gap of the two interacting NBOs. The hyb. column gives the hybridization of the Zr occupied NBO that interact with the C-H-σ^* orbital while the composition columns gives compositions of the NHO on the Zr atom.

					composition		
CH_3ZrX	IR^t	ΔE^2_{ij}	$\Delta\varepsilon_{ij}$	hyb.	5s	$4d_{z^2}$	$4d_{x^2-y^2}$
unit	cm^{-1}	kcal/mol	hartree				
-F	2941	1.59	0.53	$sd^{0.55}$	0.79	0.51	
-Cl	2858	2.39	0.52	$sd^{0.69}$	0.76	0.50	0.32
-Br	2848	2.73	0.51	$sd^{0.74}$	0.75	0.49	0.34
-CN	2847	2.63	0.52	$sd^{0.77}$	0.75		
-I	2815	3.18	0.51	$sd^{0.83}$	0.74	0.49	0.36

Table 3.32 provides information on the leading hyperconjugations between trans C-H-σ^* and the occupied Zr orbital in CH_3ZrX molecules. Comparing Table 3.32 to Table 3.31 one can see that interactions induced by donations of the C-H-σ orbital into the vacant Zr orbitals should make the major contribution to C-H activations. Furthermore donations from the occupied orbital of the Zr atom into the C-H-σ^* orbital should give only a minor contribution to C-H activation.

3.3.2.3 NPA analysis

Natural charges of the atoms in the trans and cis C-H bonds of singlet CH_3ZrX molecules are summarized in Table 3.33, showing that in general polarities of a C-H bond and positivities of H atoms of C-H bonds reduce with increasing C-H activations.

Table 3.33: NPA of the CH_3ZrX molecules. The Trans C-H bond columns show the natural charge of the trans C-H bond, and so on. IR gives the stretching frequency of the C-H bond, q(H) the natural change of the H atom, and so on. $\Delta(q_H - q_C)$ gives the natural charge difference between the H- and C-atoms.

	the trans C-H bond			the cis C-H bond			
CH_3ZrX	IR	$\Delta(q_H - q_C)$	q(H)	IR	$\Delta(q_H - q_C)$	q(H)	q(C)
unit	cm^{-1}	a.u.		cm^{-1}	a.u.		
-F	2941	1.419	0.230	3126	1.434	0.245	-1.189
-Cl	2858	1.403	0.222	3151	1.429	0.248	-1.181
-Br	2848	1.395	0.218	3159	1.426	0.249	-1.177
-CN	2847	1.390	0.208	3159	1.429	0.247	-1.182
-I	2815	1.383	0.212	3164	1.420	0.249	-1.171

3.3.2.4 Group trends in the CH_3MF molecules

Table 3.34: Group trends in the CH_3MF molecules. IR^t gives the stretching frequencies of the C-H bond trans to the TM-X bond, IR^t_D shows stretching frequencies of the corresponding deuterated C-H bond. D(M-H) the distance between the TM atom and the H atom belonging to the trans C-H bond. BO represents the bond-order of the trans C-H bond. In the C-H-σ columns, Occ gives the occupancy of the C-H-σ orbital and ΔE^2_{ij} the sum of all hyperconjugations between the C-H-σ orbital and the vacant metal orbitals, and so on.

					C-H-σ		C-H-σ^*	
CH_3MF	IR^t	IR^t_D	D(M-H)	BO	Occ	ΔE^2_{ij}	Occ	ΔE^2_{ij}
unit	cm^{-1}	cm^{-1}	pm	a.u.		kcal/mol		kcal/mol
Ti	2969	2217	278	0.995	1.987	2.30	0.004	0.94
Zr	2941	2176	265	0.982	1.975	4.95	0.008	1.59
Hf	2942	2176	269	0.989	1.979	4.00	0.006	0.60

Analyse of the group trends of C-H activations in the CH_3MF molecules (M=Ti, Zr, Hf) is carried out in Table 3.34, showing that with increasing activations

- distances between the metal atoms and the trans H atom are reduced.

- bond-orders of the trans C-H bond are reduced as well.
- occupancies of the C-H-σ orbital reduce and occupancies of the C-H-σ^* orbital increase.
- changes of occupancies in the the C-H-σ orbital are bigger than that in the C-H-σ^* orbital, which suggests that donations from C-H-σ orbitals into vacant metal orbitals can be the critical factor for C-H activations.
- the interaction (ΔE_{ij}^2) between the C-H-σ orbital and the vacant TM orbital increases. The sum of the interactions between the vacant metal atom orbital and the C-H-σ orbital correlates properly with C-H activations, but not the sum of the interactions between occupied metal valence orbitals and C-H-σ^* orbitals.

Further determinations of crucial metal atom orbitals that induce the C-H activation, and interpretation of the group trends fail due to the complex appearance in hyperconjugations and complex compositions of interacting NBOs. This is probably connected with a critical area, in which the stretching frequencies of the C-H bond lies. As is known from previous investigations, for the case that a calculated stretching frequency of a C-H bond lies at about 2950 cm^{-1}, C-H activation may be induced by interactions of the C-H bond with empty orbitals of a metal atom or be induced by interactions of the C-H bond with occupied metal valence orbitals. In this case it seems that even more factors compete: the donation from C-H-σ orbitals and the donation into C-H-σ^* orbitals, the valence s and d orbital of the metal atom as well as energies and diffuseness of orbitals of the metal atoms.

3.3.2.5 The critical factor for C-H activation in the *n*-C_4H_9ZrX molecules

All the singlet n-C_4H_9ZrX molecules (X=F, Cl, Br, I, CN) show similar structures as their triplet counterpart, hence structures are not depicted here, we take Figure 3.4 as reference for the structures of the singlet n-C_4H_9ZrX molecules and use the same fixation of the cartesian axis.
All n-C_4H_9MX molecules in general exhibit similar structure, and the most important point on displaying the structure is to show how the cartesian axis is fixed. Fixation of the cartesian axis will ease interpretations of C-H activations, since it should lead to similar orbital compositions in similar molecules. The Figure 3.4 will be taken as pictures for all the n-C_4H_9MX molecules, and this structure accords to a local mini-

mum of the molecules, since the absolute minimum corresponds to a linear alignment of the C-H bonds, which is uninteresting in this thesis.

Table 3.35: Structure comparisons of the n-C_4H_9ZrX molecules, IR^{δ} gives the stretching frequency of the δ-C-H bond, IR^{δ}_{D} shows stretching frequencies of the corresponding deuterated C-H bond. D(Zr-H^{δ}) gives the distance between the Zr atom and the H atom that belongs to the δ-C-H bond, and so on.

n-C_4H_9ZrX	IR^{δ}	IR^{δ}_{D}	Zr-H^{δ}	Zr-C^{δ}	IR^{α}	R^{α}_{D}	Zr-H^{α}	Zr-C^{α}
unit	cm^{-1}	cm^{-1}	pm	pm	cm^{-1}	cm^{-1}	pm	pm
-F	2773	2082	234	278	2924	2143	265	221
-CN	2684	2032	226	266	2921	2141	263	220
-Cl	2679	2018	226	265	2931	2142	266	221
-Br	2654	2002	225	263	2923	2142	265	221
-I	2627	1986	223	260	2923	2142	265	221

Structure comparisons of the n-C_4H_9ZrX molecules is given in Table 3.35, showing that:

- the δ-C-H bonds are very strongly activated, but the α-C-H bonds are only weakly activated.
- comparing the δ- to the α-C-H bond in the same molecule, the δ-C-H bond is more activated and distances between the Zr atom and the H atom of the C-H bonds are shorter, however distances between the Zr atom and the C atom of the C-H bond are longer.
- comparing the δ-C-H activations in the different molecules, both distances between the Zr atom and the C atom and the distances between the Zr atom and the H atom are reduced with increasing C-H activations.

Bond-order comparisons of the n-C_4H_9ZrX molecules are summarized in Table 3.36, showing that delocalizations in the δ-C-H bond are stronger than that in the α-C-H bond.

Occupancies of the C-H bonds in the n-C_4H_9ZrX molecules are shown in Table 3.37, revealing that:

- compared the δ- to the α-C-H bond in the same molecule, occupancies of the C-H-σ orbital are reduced and occupancies of the C-H-σ^* orbital is increased. Both effects can induce C-H activations.

Table 3.36: Bond-order comparisons of the n-C_4H_9ZrX molecules. IR^{δ} gives the stretching frequency of the δ-C-H bond, and so on. BO^{δ} column gives the bond-order of the δ-C-H bond, and so on.

n-C_4H_9ZrX	IR^{δ}	BO^{δ}	IR^{α}	BO^{α}
unit	cm^{-1}	bond-order	cm^{-1}	bond-order
-F	2773	0.964	2924	0.974
-CN	2684	0.963	2921	0.971
-Cl	2679	0.964	2931	0.972
-Br	2654	0.949	2923	0.970
-I	2627	0.949	2923	0.970

Table 3.37: Occupancy of the C-H bonds in the n-C_4H_9ZrX molecules. The δ-C-H bond columns gives the calculated data of the δ-C-H bond, and so on. IR gives the stretching frequencies of the C-H bond. The Occ(σ) column gives the occupancy in the C-H-σ orbital, Occ(σ^*) the occupancy in the C-H-σ^* orbital. In the δ-C-H bond columns only the occupancy changes related to the n-C_4H_9ZrF molecule are shown. In the α-C-H bond columns only the occupancy changes related to the δ-C-H bond in the same molecule are shown , i.e. $Occ(\sigma)=Occ_{(\alpha\text{-C-H-}\sigma)}\text{-}Occ_{(\delta\text{-C-H-}\sigma)}$.

	the δ-C-H bond			the α-C-H bond		
n-C_4H_9ZrX	IR	ΔOcc(σ)	Δ Occ(σ^*)	IR	Δ Occ(σ)	Δ Occ(σ^*)
unit	cm^{-1}	a.u.		cm^{-1}	a.u.	
-F	2773			2924	0.013	-0.018
-CN	2684	-0.013	0.007	2921	0.021	-0.025
-Cl	2679	-0.015	0.009	2931	0.024	-0.029
-Br	2654	-0.018	0.012	2923	0.024	-0.031
-I	2627	-0.021	0.015	2923	0.026	-0.035

- in the different molecules, with increasing activations of the δ-C-H bonds occupancies of the C-H-σ orbital reduce and occupancies of the C-H-σ^* orbital increase in almost the same order. This implies a highly cooperative delocalization, so that the electron donation is reinforced by electron acceptance of the C-H bond to preserve electroneutrality, which induces a strong C-H activation effect.

3.3.2.6 Analyse of interactions

Leading hyperconjugations between δ-C-H-σ^* and occupied Zr valence orbital in n-C_4H_9ZrX molecules are listed in Table 3.38, showing that the interactions correlate strictly with C-H activations. With increasing C-H activations energy gaps of the

Table 3.38: Leading hyperconjugations between δ-C-H-σ^* and occupied Zr valence orbitals in n-C_4H_9ZrX molecules. IR gives the stretching frequencies of the δ-C-H bond. ΔE^2_{ij} gives second-order perturbative estimation of the hyperconjugation effect between the C-H-σ^* orbital and occupied orbitals of the Zr-atom, $\Delta\varepsilon_{ij}$ gives the energy gap of the two interacting NBOs. The hyb. column shows hybridizations and the composition columns show the coefficients of the NAOs.

					composition	
n-C_4H_9ZrX	IR	ΔE^2_{ij}	$\Delta\varepsilon_{ij}$	hyb.	5s	$4d_{z^2}$
unit	cm^{-1}	kcal/mol	hartree			
-F	2773	3.42	0.45	$sd^{0.81}$	0.74	0.60
-CN	2684	4.19	0.44	$sd^{1.28}$	0.66	0.61
-Cl	2679	4.29	0.44	$sd^{1.20}$	0.67	0.63
-Br	2654	4.47	0.43	$sd^{1.35}$	0.65	0.64
-I	2627	4.92	0.43	$sd^{1.61}$	0.62	0.65

two interacting NBOs reduce and valence d-orbital portions of the NBO increases. A smaller energy gap between the C-H-σ^* orbital and the occupied NBO of the Zr-atom can promote occupancy increases of C-H-σ^* orbital. Energy gaps depends on electronegativities (EN) of substituentes X. The higher the electronegativity of a substituent X, the more electron density is attracted from the Zr atom into the X group, therefore the lower the energy of the Zr occupied valence orbitals is, the larger the energy gap is between the C-H-σ^* orbital and occupied orbitals of the Zr-atom, and the less the δ-C-H bond activated is.

Table 3.39: Hyperconjugations between the δ-C-H-σ and Zr-X-σ^* orbitals in n-C_4H_9ZrX molecules. IR gives the stretching frequencies of the δ-C-H bond. ΔE^2_{ij} gives a second-order perturbative estimation of the hyperconjugation effect between the C-H-σ and Zr-X-σ^* orbital, $\Delta\varepsilon_{ij}$ gives the energy gap of the two interacting NBOs. The hyb. column shows the hybridization of the Zr NHO in the Zr-X-σ^* orbital, which interacts with the δ-C-H-σ orbital, and the composition columns gives the coefficient of the NAOs of the Zr NHO.

					composition		
n-C_4H_9ZrX	IR	ΔE^2_{ij}	$\Delta\varepsilon_{ij}$	hyb.	5s	$4d_{z^2}$	$4d_{x^2-y^2}$
unit	cm^{-1}	kcal/mol	hartree				
-F	2773	11.36	0.70	$sd^{2.96}$	-0.50	0.45	0.66
-CN	2684	14.31	0.71	$sd^{1.54}$	0.63	-0.38	-0.54
-Cl	2679	17.74	0.69	$sd^{1.54}$	-0.62	0.36	0.54
-Br	2654	19.06	0.67	$sd^{1.33}$	0.65	-0.34	-0.52
-I	2627	20.69	0.69	$sd^{1.10}$	-0.69	0.30	0.48

Hyperconjugations between δ-C-H-σ and Zr-X-σ^* orbitals in n-C_4H_9ZrX molecules is shown in Table 3.39. The interactions shown in the table is the leading interaction of all the interactions between δ-C-H-σ orbital and vacant Zr valence orbitals. Other interactions are at least four times smaller than this leading interaction. Compared to Table 3.38 it reveals that interactions between δ-C-H-σ and vacant Zr NBOs are largely stronger than those between δ-C-H-σ^* and occupied Zr NBOs, which suggests that the interactions between δ-C-H-σ and vacant Zr NBOs can be identified as the critical interaction for C-H activations.

This conclusion seems inconsistent with the one made from the occupancy comparison in Table 3.37, which suggests that both donations from the C-H-σ orbitals and donations into the C-H-σ^* orbitals are important for C-H activations. In truth this inconsistency can be explained by the fact that donations from C-H-σ orbital can be counterbalanced by donations into C-H-σ^* orbitals though self relaxation of the electron density in the C-H bond.

From Table 3.39 it is known that hyperconjugations between δ-C-H-σ and Zr-X-σ^* orbitals correlates well with C-H activations. Still, the energy gap of the two interacted NBOs seems slightly irregular. However it is known that the stronger a X-ligand forms a bond with the Zr atom, the higher is the energy of the Zr-X-σ^* orbital and the larger the energy gap between the δ-C-H-σ and Zr-X-σ^* orbital gets and the less the C-H bond is activated, which can explains the trends of C-H activations.

From hybridizations and compositions of the Zr NHO is known that both 5s and 4d orbitals make a contribution on C-H activations.

3.3.2.7 NPA analysis

Table 3.40: NPA of n-C_4H_9ZrX molecules. δ-C-H columns gives the natural charge of the δ-C-H bond, and so on. IR gives the stretching frequency of the C-H bond, q(H) gives the natural charge of the H atom, and so on. $\Delta(q_H - q_C)$ gives the natural charge difference between the H- and C-atoms.

	the δ-C-H bond				the α-C-H bond			
CH_3ZrX	IR	$\Delta(q_H - q_C)$	q(C)	q(H)	IR	$\Delta(q_H - q_C)$	q(C)	q(H)
unit	cm^{-1}	a.u.			cm^{-1}	a.u.		
-F	2773	0.815	-0.631	0.184	2924	1.119	-0.908	0.211
-CN	2684	0.808	-0.627	0.181	2921	1.117	-0.902	0.215
-Cl	2679	0.814	-0.630	0.184	2931	1.123	-0.911	0.212
-Br	2654	0.814	-0.631	0.183	2923	1.125	-0.913	0.212
-I	2627	0.816	-0.634	0.182	2923	1.136	-0.923	0.213

Natural charges of the atoms in the δ- and α-C-H bonds of singlet n-C_4H_9ZrX molecules are summarized in Table 3.40, showing that polarities of the C-H bond, and positivities of the H atom are in general reduced with an increase of C-H activations..

3.3.2.8 Group trends in the *n*-C_4H_9MF molecules

Table 3.41: Analysis of group trends(structure). The δ-C-H bond columns gives the calculated data of the δ-C-H, and so on. IR gives the stretching frequency of the C-H bond, IR_D shows stretching frequencies of the corresponding deuterated C-H bond. D(M-H) gives the distance between the metal atom and the H atom.

	the δ-C-H bond				the α-C-H bond			
n-C_4H_9MF	IR	IR_D	D(M-H)	D(M-C)	IR	IR_D	D(M-H)	D(M-C)
unit	cm^{-1}	cm^{-1}	pm	pm	cm^{-1}	cm^{-1}	pm	pm
Ti	2393	1777	198	227	3006	2208	266	210
Zr	2773	2082	234	278	2924	2143	265	221
Hf	2954	2179	279	335	2915	2129	267	220

Structure and IR frequencies of n-C_4H_9MF (M= Ti, Zr, Hf) molecules are listed in Table 3.41. They show that:

- compared the δ-C-H bond to the α-C-H bond in the same molecule, the distance between the metal atom and the H atom reduces, and the distance between the metal atom and the C atom increases with increasing C-H activation.
- Comparing the δ-C-H bond in different molecules, both the distance between the metal atom and the H atom and the distance between metal atom and the C atom are reduced with the increasing C-H activations.

Table 3.42: Comparisons of occupancies and bond-orders in the n-C_4H_9TMF molecules. The δ-C-H bond columns gives the calculated data of the δ-C-H bond. IR gives the stretching frequency of the C-H bond. Occ(σ) gives the occupancy of the C-H-σ orbital and BO gives the bond-order of the C-H bond. In the α-C-H bond columns only changes of the α-C-H that relate to the δ-C-H bond are shown except IR frequencies, i.e. $X = X_{\alpha\text{-C-H}} - X_{\delta\text{-C-H}}$.

	the δ-C-H bond				the α-C-H bond			
n-C_4H_9MF	IR	Occ(σ)	Occ(σ^*)	BO	IR	Occ(σ)	Occ(σ^*)	BO
unit	cm^{-1}	a.u.			cm^{-1}	a.u.		
Ti	2393	1.907	0.076	0.941	3006	0.062	-0.064	0.038
Zr	2773	1.950	0.033	0.964	2924	0.013	-0.018	0.010
Hf	2954	1.975	0.016	0.979	2915	-0.008	-0.001	-0.003

Comparisons of occupancies and bond-orders in the n-C_4H_9MF molecules are carried out in Table 3.42 and shows that:

- compared the δ-C-H bond to the α-C-H bond in the same molecule, occupancies of the C-H-σ orbital reduce, occupancies of the C-H-σ^* orbital increase and bond-orders reduce with increasing C-H activations.
- comparing the δ-C-H bonds in different molecules shows the same behavior. Donations from the C-H-σ orbital and into the C-H-σ orbital vary in the same order with increasing C-H activations.

Since it is known from the analysis of interactions between the Zr atom and the C-H bond in Section 3.3.2.6 that interactions between the δ-C-H-σ and vacant Zr NBOs are the critical factor for C-H activations, only the interaction between C-H-σ and vacant M-F-σ^* orbitals will be investigated.

Details of interactions between the C-H-σ and the vacant Zr-F-σ^* orbitals are listed in Table 3.43, one exception is the interaction in the n-C_4H_9TiF molecule, in which

Table 3.43: Leading hyperconjugations between δ-C-H-σ and M-F-σ^* orbitals in n-C_4H_9MF molecules. IR gives the stretching frequencies of the δ-C-H bond. ΔE^2_{ij} gives second-order perturbative estimations of the hyperconjugation effect between the C-H-σ and M-F-σ^* orbital, $\Delta\varepsilon_{ij}$ gives the energy gap of the two interacting NBOs. The hyb. column shows hybridizations of the NHO of the metal atom in the M-F-σ^* orbital, which interacts with the δ-C-H-σ orbital while the composition columns shows the coefficient of the NAOs of the metal atom.

					composition		
n-C_4H_9MF	IR	ΔE^2_{ij}	$\Delta\varepsilon_{ij}$	hyb.	5s	$4d_{x^2-y^2}$	$4d_{xy}$
unit	cm^{-1}	kcal/mol	hartree				
Ti	2393	25.13	0.59	$sd^{4.29}$	0.43	-0.46	0.67
Zr	2773	11.36	0.70	$sd^{2.96}$	-0.50	0.66	
Hf	2954	3.00	0.99	$sd^{6.83}$	-0.35	0.56	0.56

the interaction accords to an interaction between the C-H-σ and the vacant LP orbital of a Ti atom, no interaction between the C-H-σ and the vacant Ti-F-σ^* orbital can be identified by the NBO program in this molecule.
Table 3.43 shows that the leading interaction between C-H-σ and the vacant Zr orbitals correlates properly with C-H activations. The vacant valence d orbital should make the critical contribution to C-H activation, since the energy of valence d orbital increases on moving from the first to the third transition series, which increase the energy gap between the NBOs, decreasing C-H activation. When the valence s orbital was the critical factor, the trend of δ-C-H activations should be different due to relativistic effects.

3.3.2.9 Summary

By investigating n-C_4H_9ZrX and CH_3ZrX systems (X= H, CN, F, Cl, Br, I) in the singlet state following conclusions can be drawn:

- electron donations from the C-H-σ orbitals give the major contribution in cases of strong C-H activations.
- the more a C-H bond is activated, the more unpolar it gets.
- investigations of the excited state (singlet) is necessary. Perhaps in the CH_3ZrX systems both states (singlet and triplet) may compete in the transition state, in which reaction the sp^3-C-H bond is split. But in the n-C_4H_9ZrX system the excited state (singlet) is definitely preferred in sp^3-C-H bond splitting processes,

since hyperconjugations between the C-H bond and the Zr atom in the singlet state can probably overcome promotion energies and lead to lower activation barriers ($\Delta G^{\ddagger}$), which suggests a two-state reactivity (TSR).

3.4 Group 5 transition metal elements

3.4.1 Enthalpy comparison of the different states

Table 3.44: Enthalpy and IR frequency comparisons of the quartet and the doublet states of the CH_3NbX molecules, all the enthalpies are calculated at the B3LYP/def2-TZVP/def2-ecp levels (sums of electronic and thermal enthalpy) and presented as differences to the ground state at the corresponding absolute minimum of the molecules without zero-point corrections. IR column shows stretching frequencies of the most activated C-H bond, which stands trans to the Nb-X bond.

	quartet		doublet	
CH_3NbX	enthalpy	IR	enthalpy	IR
unit	kJ/mol	cm^{-1}	kJ/mol	cm^{-1}
-CN	0	2978	33.5	2918
-F	0	2938	32.5	2921
-Cl	0	2932	31.5	2891
-Br	0	2922	30.5	2884
-I	0	2890	29.5	2882

Enthalpies and IR frequencies of the CH_3NbX molecules (X= CN, F, Cl, Br, I) are summarized in Table 3.44, showing that the quartet state of the molecules is the ground state and the doublet state is the first excited state. Enthalpy comparison of the n-C_4H_9NbF molecules reveals the same pattern.

The quartet CH_3NbX molecules take staggered forms as their absolute minimum, but the doublet CH_3NbX molecules take eclipsed forms as their absolute minimum. The trans C-H bonds in the quartet state are only slightly activated, but are more strongly activated in the excited state. Conclusions about the quartet state will be explicitly described and differences between the two states will be briefly discussed.

3.4.2 The quartet state(ground state)

3.4.2.1 CH_3NbX system

The structure of the quartet CH_3NbF molecule is depicted in Figure 3.5. All the quartet CH_3NbX molecules (X=F, Cl, Br, I, CN) take staggered forms as absolute minimum. The trans C-H bond, which stands trans to the Nb-X bond, is more activated than the two cis C-H bonds. In all the molecules the cartesian axis are fixed as shown in Figure 3.5, the Nb atom lies in the origin, the C atom lies on the X-axis and the X-ligand lies in the XY-plane.

Figure 3.5: The structure of the CH_3NbF molecule optimized with the B3 method.

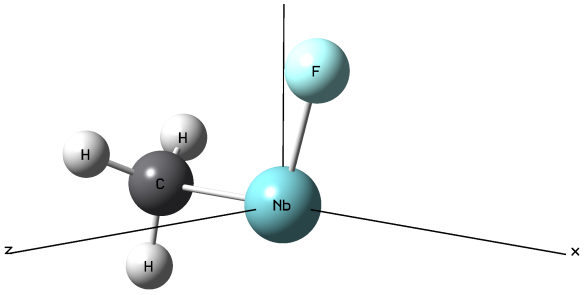

Analyse are done in the same way as shown in the Sec 3.3. Structure, bond-order and occupancy comparisons in the quartet state of the CH_3NbX molecules are shown in the appendix (Table A.1 and A.2) indicating that:

- the structure comparison shows that overlaps are not the only factors affecting C-H activations.
- the bond-order and occupancy comparisons give inconsistent conclusions.
  - The bond-order comparison shows that increasing delocalizations in both the α- and β-spin correlates with the C-H activation.
  - Analyse of the occupancy number show that occupancies of the C-H-σ^* orbital in the β-spin can be excluded as the reason for the C-H activation. Only occupancies of the C-H-σ orbital in the β-spin correlate properly with the C-H activation.

Studies of interactions between C-H-σ^* orbitals and occupied hybrid Nb orbitals in the α-spin shows that both the sum of the interactions and the individual interactions do not correlate properly with the C-H activation, therefore this type of interactions can be excluded as the main reason for C-H activations and will not be shown.
Interactions between the C-H-σ orbital and vacant hybrid Nb orbitals in the both spins are shown in the appendix (Table A.3). Conclusions drawn from this table is

that interactions between the C-H-σ and the Nb-X-σ^*-orbital in both spins should make the major contribution to C-H activations and the energy gap between the interacting orbitals is the origin for the C-H activation difference.
The NHO on the Nb atom side of the Nb-X-σ^*-orbital have a almost equal contribution of the 5s, $4d_{z^2}$, $4d_{x^2-y^2}$ and $4d_{xy}$ orbital of the Nb atom, hence which orbital is the most important one can not be identified.

3.4.2.2 C-H bond comparisons of the *n*-C_4H_9NbF and CH_3NbF molecules

Table 3.45: Details of interactions between the C-H-σ orbital and the vacant hybrid Nb orbital in the α-spin. IR column gives stretching frequencies of the C-H bond. ΔE^2_{ij} represents second-order perturbative estimations of the hyperconjugation, $\Delta\varepsilon_{ij}$ represents energy gaps of the two interacting NBOs, hyd. column shows hybridizations of the Nb orbital, which is participated in the interaction.

		NBO1			NBO2		
	IR	ΔE^2_{ij}	hyb.	$\Delta\varepsilon_{ij}$	ΔE^2_{ij}	hyb.	$\Delta\varepsilon_{ij}$
unit	cm^{-1}	kcal/mol		hartree	kcal/mol		hartree
Met^c	3046	0.07	$sd^{5.27}$	0.59	0.06	d	0.44
Met^t	2938	1.11	$sd^{5.27}$	0.59	1.72	d	0.44
But^α	2841	2.07	$sd^{2.08}$	0.50	1.90	d	0.41
But^δ	2798	4.58	$sd^{2.08}$	0.55	2.36	d	0.45

From analyse of structures, bond-orders and occupancies of the C-H bonds in the appendix (Table A.4) following conclusions can be drawn:

- In the *n*-C_4H_9NbF molecule both the α- and the δ-C-H bonds are activated, δ-C-H bonds are more activated. The Nb atom shows an unselective C-H activation pattern at the different positions.
- The structure comparison confirms the conclusion that overlaps alone can not be used to explain the C-H activation difference.
- The activation difference between the trans and the cis C-H bond in the CH_3NbF is induced by donations from the C-H-σ orbital into vacant Nb hybrid orbital in both spins.
- The activation difference between the δ- and α-C-H bond in the *n*-C_4H_9NbF molecule can be induced by all the interactions between the Nb atom and C-

H bond except the donation from occupied Nb hybrid orbital into the C-H-σ^*-orbital in β-spin system.

The NBO1 in Table 3.45 is a Nb-F-σ^* orbital except in the n-C_4H_9NbF, which is a hybrid Nb LP orbital with valence s and d orbital share. The NBO2 is a Nb LP orbital with main valence d orbital share. Only interactions between the C-H-σ orbital and the vacant hybrid Nb orbitals in the α-spin are shown in the table. Details of interactions between the C-H-σ orbital and the vacant hybrid Nb orbitals in the β-spin are more complicate but show a similar image as shown by the Table 3.45, therefore they are not shown here.
Other interactions are shown in the appendix (Table A.5 and A.6). Following conclusions can be drawn from analyse of the interactions.

- The trans and cis C-H activation difference in the CH_3NbF is induced by the donation from the C-H-σ orbital into a vacant Nb LP hybrid orbital in both spins.

- The C-H activation difference between the trans C-H bond in the CH_3NbF and the α-C-H bond in the n-C_4H_9NbF is raised by the shift of energy gaps of the interacting NBOs, as shown in the Table 3.45 and A.6.

- The activation difference between the δ- and α-C-H bond in the n-C_4H_9NbF molecule is not induced by the the shift of the energy gap of the interacting NBOs, but rather by the flexibility of the δ-C-H bond, which can make better overlap with Nb valence orbitals, compared to the α-C-H bond. The only interactions, which can be excluded as the origin for the C-H activation difference, are interactions between the C-H-σ^* orbital and the occupied hybrid Nb orbital in the β-spin system.

NPA comparison is carried out in the appendix (Table A.7), showing that in general the more a C-H bond is activated, the more nonpolar the C-H bonds get.

3.4.2.3 Group trends in the CH_3MF molecules

Analyse of group trends of C-H activations in the CH_3MF (M=V, Nb, Ta) molecules confirms the fact that interactions between the C-H-σ orbital and the vacant hybrid orbital of the metal atoms are the origin for the C-H activation difference.
Structure, bond-order and occupancy comparisons of the C-H bond in the CH_3MF

are shown in the appendix (Table A.8). Since interactions between the C-H-σ orbital and the vacant hybrid orbital in the β-spin are similar to that in the α-spin, here only interactions between the C-H-σ orbital and the vacant hybrid orbital in the α-spin are represented in Table 3.46. Interactions between the C-H-σ orbital and the vacant hybrid orbital in the β-spin are shown in the appendix (Table A.9).

In the table 3.46 the NBO1 orbital is an empty hybrid LP orbital of the metal atoms,

Table 3.46: Interactions between the C-H-σ orbital and the vacant hybrid orbital of the TM atoms in the α-spin of the CH_3MF molecules. NBO1 columns record calculated data of the NBO1, and so on. IR^t presents stretching frequencies of the trans C-H bond. The sum column gives sums of the both interactions, hyb. represents hybridizations of the vacant hybrid orbital of the Nb atom, which participates in the interaction. ΔE^2_{ij} gives second-order perturbative estimations of the hyperconjugation effect between the C-H-σ orbital and vacant valence orbital of the TM atom, $\Delta\varepsilon_{ij}$ gives energy gaps of the two interacting NBOs.

			NBO1: vacant LP			NBO2: M-F-σ^*		
CH_3MF	IR^t	sum	ΔE^2_{ij}	hyb.	$\Delta\varepsilon_{ij}$	ΔE^2_{ij}	hyb.	$\Delta\varepsilon_{ij}$
unit	cm^{-1}	kcal/mol	kcal/mol		hartree	kcal/mol		hartree
V	2993	0.89	0.20	$sd^{1.48}$	0.49	0.69	$sd^{5.45}$	0.52
Nb	2938	2.83	1.72	d	0.44	1.11	$sd^{5.27}$	0.59
Ta	2940	2.05	1.28	d	0.61	0.77	$sd^{7.18}$	0.87

which have a main valence d_{xy} character except in the CH_3VF. In the CH_3VF molecule the NBO1 has a strong valence s character, which is in agreement with that a 3d TM element prefers to use the valence s orbital to overlap with the C-H bond, but 4d and 5d TM elements prefer more to use valence d orbitals, since the diffuseness of the valence s and d orbital of 4d and 5d TM elements are similar, but the valence s orbital of 3d TM elements is more diffuse than the valence d orbitals.

The NBO2 orbitals in the table are M-F-σ^* orbitals, which have a main portion of metal valence orbitals $(0.33 * F - 0.94 * M)$. The hybrid orbital on the metal atom side, which forms the NBO2, have a almost equal portion of valence d_{xy}, d_{z^2}, $d_{x^2-y^2}$ orbitals and a smaller portion of the valence s orbital.

Both the sum of interactions and the individual interactions correlate properly with the C-H activation, as measured by the IR shifts. From the trend of the C-H activations one can draw the conclusion that only with the energy of valence s orbital the activation trend can be interpreted due to relativistic effects. Since in this case the interaction between the C-H-σ orbital and NBO2(with valence s orbital share) is comparatively weaker than that between the C-H-σ orbital and NBO1(with main valence d

orbital share), but the NBO2 can not be excluded as the reason for the C-H activation.

3.4.2.4 Group trends in the *n*-C_4H_9MF molecules

Group trends of C-H activations in the quartet n-C_4H_9MF (M=V, Nb, Ta) are analyzed in the same way. Structure, bond-order and occupancy comparisons of the most activated δ- and α-C-H bond are shown in the appendix (Table A.10 and A.11), showing that interactions between the C-H-σ and the vacant hybrid orbital of the metal atoms make probably the major contribution to C-H activations.

Details of interactions in the α-spin of the n-C_4H_9MF molecules are summarized in

Table 3.47: Details of interactions of the C-H-δ bond in the α-spin of the n-C_4H_9MF molecules. IR(δ) gives stretching frequencies of the δ-C-H bond. The C-H-σ orbital columns show calculated data related to the interaction between the C-H-σ and hybrid TM orbital in the α-spin, and so on. The NBO1 columns show calculated data of the NBO1, and so on. ΔE^2_{ij} gives second-order perturbative estimations of the hyperconjugation, hyb. shows hybridizations of the TM orbital, which is participated in the interaction.

		C-H-σ orbital				C-H-σ^* orbital	
		NBO1		NBO2		NBO3	
n-C_4H_9MF	IR(δ)	ΔE^2_{ij}	hyb.	ΔE^2_{ij}	hyb.	ΔE^2_{ij}	hyb.
unit	cm^{-1}	kcal/mol		kcal/mol			kcal/mol
V	2861	3.19	$sd^{1.43}$	3.06	$sd^{6.41}$	1.43	$sd^{8.31}$
Nb	2798	4.58	$sd^{2.08}$	2.36	d	3.18	$sd^{3.32}$
Ta	2809	3.02	$sd^{4.46}$	1.24	d	3.87	$sd^{1.96}$

the Table 3.47, all interactions of the α-spin of the n-C_4H_9MF molecules, which is stronger than 0.2 kcal/mol, are shown. Following conclusions can be drawn:

- The NBO2 can be excluded as the main reason for the C-H activation difference, since this interaction show opposed trends with the C-H activations. The NBO2 is a vacant hybrid LP orbital, which is mainly composed of valence d_{yz} and d_{xz} orbital of the metal atoms.

- The NBO1 is also a vacant hybrid LP orbital of the metal atoms, which is mainly composed of valence s and d_{xy} orbital of the metal atom. The interaction between the NBO1 and the C-H-σ orbital correlates approximately with the C-H activation, which implies that valence s orbital energy of the metal atoms is responsible for this interaction strength difference due to relativistic effects.

- The NBO3 is a occupied hybrid LP orbital of the metal atoms that is mainly composed of valence s, d_{xy}, $d_{x^2-y^2}$ orbital of the metal atoms, which has main portion of the valence $d_{x^2-y^2}$ orbital. The difference of the interaction between the NBO3 and C-H-σ^* orbital can be interpreted with the valence d-orbital energy of metal atom. Due to relativistic effects the d-orbital energy increases, which makes smaller energy gap between the NBO3 and C-H-σ^* orbital, on moving from the first to the third TM series.

The analyse of interactions of the α-C-H bond confirms (Table A.12 in the appendix) the conclusion drawn from the analysis of bond-order and occupancy that the activation difference between the δ-and α-C-H bond in the same molecule can be induced by all interactions between metal orbitals and the C-H orbitals except interactions between the C-H-σ^* orbital and valence metal orbitals in the β-spin.

3.4.3 The doublet state(first excited state)

3.4.3.1 CH_3NbX-system

The structure of the doublet CH_3NbF molecule is depicted in Figure 3.6. All the doublet CH_3NbX molecules (F, Cl, Br, I, CN) take the eclipsed form as the absolute minimum, a exception is that the Nb-CN bond and the cis C-H bond make a dihedral angle of 15.9° in the doublet CH_3NbCN molecule. The both trans C-H bonds, which stands trans to the Nb-X bond, are more activated than the cis C-H bond. In all the molecules the cartesian axis are fixed as shown in the Figure 3.6, the Nb atom lies in the origin, the C atom lies on the X-axis and the X-ligand lies in the XY-plane.

Figure 3.6: The structure of the CH_3NbF molecule optimized with the B3 method.

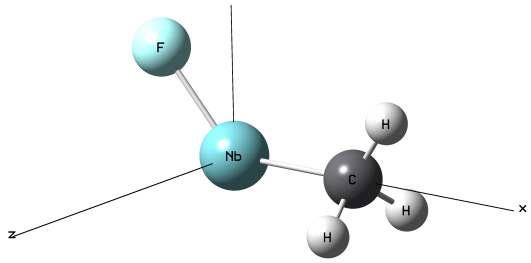

Analyse of the doublet CH_3NbX molecules are shown in the appendix (Table A.13 and A.14). Compared to the data of the quartet CH_3NbX molecules following conclusions can be drawn.

- Interactions between the C-H-σ orbital and vacant hybrid orbitals of the Nb atom in the both spin make the major contribution of the C-H activations in

the doublet CH_3NbX molecules. This conclusion is the same as got for the quartet CH_3NbX molecules. The vacant hybrid orbitals of the Nb atom can be a Nb-X-σ^* orbital or vacant hybrid Nb LP orbitals.

- Comparisons of the two states shows that interaction strengths between the Nb-X-σ^* orbital and the C-H-σ orbital in the both spins are only slightly changed, interactions between the C-H-σ orbital and the vacant hybrid Nb LP orbital in the α-spin, which have main d-orbital share, are strongly raised in the doublet state. In the doublet state both types of the above interactions can be the main reason for the C-H activations, but in the quartet state the interaction between the Nb-X-σ^* and the C-H-σ orbital can be surely identified as the main reason for the C-H activation.

- Analyse of the doublet CH_3NbX show also that the interaction between the Nb-CN-σ^* orbital and the C-H-σ orbital in the CH_3NbCN molecule is weaker than that in the other CH_3NbX molecules. However through π-backbonding of the cyanid group, interactions between the C-H-σ orbital and the vacant hybrid Nb LP orbital, which is mainly composed of valence d-orbitals, are strongly increased. Therefore the C-H activation in the CH_3NbCN molecule can be a coaction of the both type of interactions.

Comparisons of the C-H activations in the doublet n-C_4H_9NbF and CH_3NbF molecules are shown in the appendix (Table A.15,A.16, A.17 and A.18), showing that interactions between the C-H-σ orbital and vacant Nb hybrid LP orbitals are probably the crucial factor for the C-H activations.
NPA comparison of the atoms in the C-H bonds are shown in the appendix (Table A.19), showing that C-H bonds are in general more nonpolar with raising C-H activations.
Analyse of the group trend of C-H activations in the doublet CH_3MF (M=V, Nb, Ta) molecules are shown in the appendix (Table A.20 and A.21), indicating that interactions between the C-H-σ orbital and vacant hybrid LP orbital of the TM atoms determine the C-H activation. Compared to the ground state(quartet) the interaction strength between the M-X-σ^* and the C-H-σ orbitals decreases, but the interaction strength of the vacant hybrid LP orbital of the metal atoms, which is mainly of metal valence d orbital, increases. Therefore it shows a different trend of the C-H activation that the trans C-H bond is most activated in the CH_3TaF molecule in the doublet CH_3MF(M=V, Nb, Ta) molecules compared to the corresponding quartet molecules,

in which the most C-H activation of the trans C-H bond is occurred in the CH_3NbF molecule.
The same trend can be found also in the doublet n-C_4H_9MF (M=V, Nb, Ta), which are shown in the appendix (Table A.22, A.23, A.24 and A.25). It suggest that interactions of the valence d-orbital outweighs that of the valence s-orbital in these cases.

3.4.4 Summary

From above investigations following conclusions can be drawn.

- The group 5 TM elements show a unselective activation pattern of C-H bonds, both the α- and the δ-C-H bond can be activated.
- In general one can see that the more a C-H bond is activated, the more nonpolar is the C-H bond.
- A π-ligand in the CH_3NbX (X=CN) can make an impact on the metal valence orbitals though π-backbonding, which increases the interaction strength between the C-H-σ orbital and the vacant hybrid Nb LP orbital, which is mainly composed of valence d-orbitals.
- Interactions between the M-X-σ^* and the C-H-σ orbitals in general play an important role in the C-H activations. And it seems that the role played by metal valence s orbitals can as well not be neglected.
- The activation difference between the δ-and α-C-H bond in the same molecule is induced by the flexibility of the C-H bond not by the energy situation of the interacting orbitals. The investigation indicates also that impacts of the valence d orbitals of metal atoms on the activation of the α-C-H bond outweigh that of the valence s orbital, but the impact of the valence s orbital of metal atoms on the activation of the δ-C-H bond outweighes that of the valence d orbitals in the n-C_4H_9MF molecules.
- The C-H activation difference between the trans C-H bond in the CH_3NbF and the α-C-H bond in the n-C_4H_9NbF is induced by the shift of energy gaps of the interacting NBOs.

3.5 Group 6 transition metal elements

3.5.1 Enthalpy comparison of the different states

Table 3.48: Enthalpy and IR frequency comparisons of the CH_3MoX molecules in all the spin states, all the enthalpies are calculated at the B3LYP/def2-TZVP/def2-ecp levels (sums of electronic and thermal enthalpy) and presented as differences to the ground state at the corresponding absolute minimum of the molecules without zero-point corrections. IR column shows stretching frequencies of the most activated C-H bond, which stands trans to the Mo-X bond.

	quintet		triplet		singlet	
$MoCH_3X$	enthalpy	IR	enthalpy	IR	enthalpy	IR
unit	kJ/mol	cm^{-1}	kJ/mol	cm^{-1}	kJ/mol	cm^{-1}
-CN	0	2942	138.5	2948	214.2	3061
-I	0	2919	94.7	2537	161.3	2404
-Br	0	2914	91.2	2511	157.8	2374
-Cl	0	2916	86.9	2507	155.3	2367
-F	0	2902	86.3	2494	151.5	2333

Enthalpies and IR frequencies of the CH_3MoX molecules(X= CN, F, Cl, Br, I) are summarized in Table 3.48, showing that the quintet state of the molecules is the ground state and the triplet and the singlet state is the corresponding first and second excited state. Enthalpy comparisons of the n-C_4H_9MoF molecules reveals the same conclusion.

In the triplet and singlet states the CH_3MoX molecules take eclipsed forms as their absolute minimum except the CH_3MoCN molecule, which takes staggered forms as their absolute minimum. In the quintet state all of the CH_3MoX molecules take staggered forms as their absolute minimum. Since the trans C-H bonds in the quintet state are only slightly activated, but in the singlet state the trans C-H bond are more strongly activated than that in the quintet state, conclusions about the singlet state are explicitly described and differences to the other states will be just briefly discussed. In the investigation, the CH_3MoCN molecule will be firstly neglected except in the singlet state, since it takes different forms as the other molecules. One point worthily to mention is that a reverse ligand impacts on C-H activations is shown in the CH_3MoX molecules as shown in the molecules with group 4 and group 5 TM elements.

3.5.2 The singlet state(second excited state)

3.5.2.1 CH_3MoX-system

The structure of the singlet CH_3MoF-molecule is depicted in Figure 3.7. All the singlet CH_3MoX molecules (X=F, Cl, Br, I) take staggered forms as absolute minimum. The trans C-H bonds, which stand trans to the Mo-X bond, are very strongly activated. In all the molecules the cartesian axis are fixed as shown in Figure 3.7, the Mo atom lies in the origin, the C atom lies on the X-axis and the X-Ligand lies in the XY-plane.

Figure 3.7: The structure of the CH_3MoF molecule in the singlet state optimized with the B3 method.

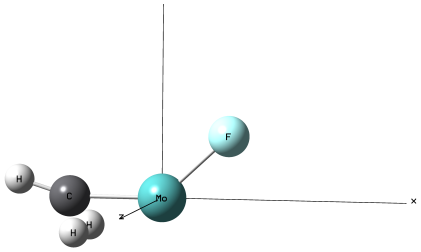

Structure, bond-order and occupancy comparisons of the trans C-H bond in the CH_3MoX molecules are shown in the appendix (Table A.26), indicating that C-H activations of the trans C-H bonds come with occupancy changes of both the C-H-σ^* and the C-H-σ orbitals. But analyse of interactions shows that interactions between C-H-σ^* orbital and occupied hybrid orbitals of the metal atom are 3 up to 5 times weaker than interactions between C-H-σ orbital and vacant hybrid orbitals of the metal atom, therefore the former should not be the main reason for the C-H activation and will just be shown in appendix (Table A.27). Here only interactions between C-H-σ orbital and vacant hybrid orbitals of the Mo atom are to be analyzed. The vacant hybrid orbitals of the metal atom can be M-X-σ^* orbitals with strong metal participation and vacant hybrid LP orbitals of the metal atom.

Interactions between C-H-σ orbitals and vacant hybrid orbitals of the Mo atom are shown in the Table 3.49, indicating that only the sum of the interactions correlates properly with the C-H activation. Since the interaction between the C-H-σ orbital and the NBO1 correlates approximately with the C-H activation, the accurate description of the NBO1 are summarized in the Table 3.50. The NBO1 is an antibonding (M-X-σ^*) orbital, which is composed of two hybrid orbitals ($0.88 * sd^{0.75}_{(Mo)} - 0.48 * sp^{5.45}_{(I)}$ in the CH_3MoI molecule), the NBO2 and NBO3 are empty metal d orbitals.

Table 3.49: Interactions between the C-H-σ orbital and vacant hybrid orbitals of the Mo atom in the CH_3MoX molecules. IR^t presents stretching frequencies of the trans C-H bond, hyb. represents hybridizations of the hybrid orbital of the Mo atom, which participates in the interaction. The NBO1 columns show calculated data of the NBO1, and so on. Sum column shows sums of the interactions. ΔE^2_{ij} gives second-order perturbative estimations of the hyperconjugation effect between the C-H-σ orbital and the vacant hybrid orbital of the Mo-atom.

			NBO1(M-X-σ^*)		NBO2(LP)		NBO3(LP)	
CH_3MoX	IR^t	sum	ΔE^2_{ij}	hyb.	ΔE^2_{ij}	hyb.	ΔE^2_{ij}	hyb.
unit	cm^{-1}	kcal/mol	kcal/mol		kcal/mol		kcal/mol	
I	2404	45.74	22.24	$sd^{0.75}$	18.99	d	4.51	d
Br	2374	49.51	26.27	$sd^{0.85}$	17.29	d	5.95	d
Cl	2367	50.88	27.60	$sd^{0.98}$	17.56	d	5.72	d
F	2333	51.02	25.45	$sd^{1.76}$	18.28	d	7.29	d

Table 3.50: Further details of the interaction between the C-H-σ orbital and the NBO1 in the CH_3MoX molecules. IR^t presents stretching frequencies of the C-H bond, ΔE^2_{ij} gives second-order perturbative estimations of the hyperconjugation effect between the C-H-σ orbital and the NBO1, $\Delta\varepsilon_{ij}$ gives energy gaps of the two interacting NBOs, hyb. represents hybridizations of the orbitals, s column records polarization coefficients of the Mo 5s orbital, $4d_{z^2}$ column shows polarization coefficients of the Mo $4d_{z^2}$ orbital, and so on. X(coe) column represents polarization coefficients of the X atom in the Mo-X antibonding orbital, and so on.

CH_3MoX	IR^t	ΔE^2_{ij}	$\Delta\varepsilon_{ij}$	hyb.	5s	$4d_{z^2}$	$4d_{xy}$	Mo(coe)	X(coe)
unit	cm^{-1}	kcal/mol	hartree				a.u.		
I	2404	22.24	0.60	$sd^{0.75}$	0.75	-0.30	0.55	0.88	-0.48
Br	2374	26.27	0.61	$sd^{0.85}$	0.73	-0.31	-0.58	0.89	-0.45
Cl	2367	27.60	0.62	$sd^{0.98}$	0.71	-0.33	-0.61	0.90	-0.44
F	2333	25.45	0.64	$sd^{1.76}$	0.60	-0.39	0.68	0.93	-0.36

From the Table 3.50 one can see that the C-H activation difference can not be induced by the energy gaps between the interacting orbitals, but rather by overlaps and the polarization coefficients of the Mo-X-σ orbital. The more the C-H bond is activated, the larger is the polarization coefficients of the NHOs of the Mo atom. It leads to the assumption that the polarization is another factor, which makes an important impact on C-H activations except energies of the interacting orbitals.

3.5.2.2 C-H bond comparison of the *n*-C_4H_9MoF and CH_3MoF molecules

Comparisons of structures, bond-orders and occupancies of the C-H bond are shown in the appendix (Table A.28), indicating that both occupancy changes of the C-H-σ- and C-H-σ^* orbital can induce the C-H activation, both of the interactions need to be investigated. Interactions between the C-H bond and the Mo atom are shown in

Table 3.51: Interactions between the C-H bond and the Mo atom. C-H-σ^* table shows calculated data of the C-H-$\sigma 1*$ orbital, and so on. Met^c row represents calculated data of the cis C-H bond in the CH_3MoF molecule, and so on. But$^\alpha$ row represents calculated data of the α-C-H bond in the *n*-C_4H_9MoF molecule, and so on. IR gives stretching frequencies of the C-H bond. Sum column shows sums of the two interactions, NBO1 columns show calculated data of the NBO1, and so on. ΔE^2_{ij} gives second-order perturbative estimations of the hyperconjugation effect, $\Delta\varepsilon_{ij}$ gives the energy gaps of the two interacting NBOs, hyb. represents hybridizations of the orbital.

C-H-σ^*			NBO1			NBO2		
	IR^t	sum	ΔE^2_{ij}	hyb.	$\Delta\varepsilon_{ij}$	ΔE^2_{ij}	hyb.	$\Delta\varepsilon_{ij}$
unit	cm^{-1}	kcal/mol	kcal/mol		a.u.	kcal/mol		a.u.
Met^c	3216	2.46	1.01	$sd^{1.80}$	0.59	1.45	$sd^{2.80}$	0.80
But$^\alpha$	2511	5.51	3.62	$sd^{3.97}$	0.46	1.89	d	0.47
But$^\delta$	2386	9.08	8.31	$sd^{3.97}$	0.43	0.77	d	0.44
Met^t	2333	13.65	10.33	$sd^{1.81}$	0.45	3.32	d	0.45

C-H-σ			NBO1		NBO2		NBO3	
	IR^t	sum	ΔE^2_{ij}	hyb.	ΔE^2_{ij}	hyb.	ΔE^2_{ij}	hyb.
unit	cm^{-1}	kcal/mol	kcal/mol		kcal/mol		kcal/mol	
Met^c	3216	0.09	0.03	$sd^{1.76}$	0.06	$sd^{2.80}$		
But$^\alpha$	2511	33.51	13.59	$sd^{3.12}$	14.54	d	5.38	$sd^{2.78}$
But$^\delta$	2386	57.34	30.33	$sd^{3.12}$	25.53	d	1.48	$sd^{2.78}$
Met^t	2333	51.02	25.45	$sd^{1.76}$	18.28	d	7.29	d

the Table 3.51. In the C-H-σ^* table all of the NBOs are occupied hybrid LP orbitals of the Mo atom. In the C-H-σ table the NBO1 of the CH_3MoF molecule and NBO3 of the *n*-C_4H_9MoF molecule are Mo-F-σ^* orbitals, all of the other NBOs are vacant hybrid LP orbitals of the Mo atom.
Following conclusions can be drawn:

- In cased of strong C-H bond activations, interactions between the C-H-σ orbitals and the vacant valence orbitals of the Mo atom are extensively stronger than interactions between the C-H-σ^* orbital and the occupied valence orbitals of the Mo atom, therefore can also be identified as the origin for the strong C-H activations.

- An exception is that the C-H activation difference between the δ-C-H bond in the n-C_4H_9MoF molecule and the trans C-H bond in the CH_3MoF molecule can only be understood with interactions between the C-H-σ^* orbital and the valence orbital of the Mo atom.

- In the CH_3MoF molecule the interaction between the C-H-σ orbital and the Mo-F-σ^* orbital is strong, and always as the origin for the C-H activation identified. But in the n-C_4H_9MoF molecule this type of the interaction is very weak compared to that in the CH_3MoF molecule, on the other side interaction strengths between the C-H-σ and the vacant hybrid LP orbitals of the Mo atom are strongly raised.

NPA comparison is carried in the appendix(Table A.29), showing that in general the more a C-H bond is activated, the more unpolar the C-H bond is and the less positive the H atom is.

3.5.2.3 Group trends in the CH_3MF molecules

Structure, bond-order and occupancy comparisons of the C-H bond in the CH_3MF (M=Cr, Mo, W) are shown in the appendix (Table A.30), indicating that both type of the interactions (between the C-H-σ orbital and vacant hybrid orbitals of the TM atoms and interactions between the C-H-σ^* orbital and occupied hybrid orbitals of the metal atoms) can induce C-H activations.
Both the sum of all the interactions and the leading hyperconjugation between the C-H-σ^* orbital and occupied hybrid orbitals of the metal atoms proportionate with the C-H activations. But since this type of the interactions are largely weaker than the other type of interactions, details of this type of the interactions will be just shown in the appendix (Table A.31) and can be excluded as the main factor for C-H activations.

Details of interactions between the C-H-σ orbital and the vacant hybrid orbital of the metal atoms in the CH_3MF molecules are shown in the 3.52, the NBO1 in the table is a M-F-σ^* orbital and the NBO2 is a vacant hybrid LP orbital of the metal atoms. One can see that the sum and the interaction between the C-H-σ orbital and the M-F-σ^* orbital does not proportionate with the C-H activation, only the interaction between the C-H-σ orbital and the vacant hybrid LP orbital of the metal atoms, which has the main valence d_{yz} character, correlates properly with the C-H activation.

Table 3.52: The leading interactions between the C-H-σ orbital and the vacant hybrid orbital of the TM atoms in the CH_3MF molecules. NBO1 columns record calculated data of the NBO1, and so on. IR^t presents stretching frequencies of the trans C-H bond. The sum column gives sums of the both interactions, hyb. represents hybridizations of the vacant hybrid orbital of the Nb atom, which participates in the interaction. ΔE^2_{ij} gives second-order perturbative estimations of the hyperconjugation effect between the C-H-σ orbital and vacant valence orbital of the TM atom, $\Delta\varepsilon_{ij}$ gives energy gaps of the two interacting NBOs.

			NBO1(M-F-σ^*)			NBO2(LP)		
CH_3MF	IR^t	sum	ΔE^2_{ij}	$\Delta\varepsilon_{ij}$	hyb.	ΔE^2_{ij}	$\Delta\varepsilon_{ij}$	hyb.
unit	cm^{-1}	kcal/mol	kcal/mol	hartree		kcal/mol	hartree	
Cr	2602	31.22	13.62	0.57	$sd^{1.18}$	11.06	0.44	d
Mo	2333	51.02	25.45	0.64	$sd^{1.76}$	18.28	0.41	d
W	2419	58.15	41.08	0.90	$sd^{2.52}$	16.95	0.41	d

Table 3.53: Interactions between the C-H-bond and the metal atoms in the n-C_4H_9MF molecules. In the δ-C-H bond columns calculated data of the δ-C-H bond are shown, and so on. IR gives stretching frequencies of the C-H bond, sum(ΔE^2_σ) give sums of all interactions, which is between the C-H-σ orbital and vacant hybrid orbitals of metal atoms; sum($\Delta E^2_{\sigma^*}$) give sums of all interactions, which is between the C-H-σ^* orbital and occupied hybrid orbitals of metal atoms.

	δ-C-H bond			α-C-H bond		
n-C_4H_9MF	IR	sum(ΔE^2_σ)	sum($\Delta E^2_{\sigma^*}$)	IR	sum(ΔE^2_σ)	sum($\Delta E^2_{\sigma^*}$)
unit	cm^{-1}	kcal/mol		cm^{-1}	kcal/mol	
Cr	2690	28.76	2.26	2816	13.42	1.28
Mo	2386	57.34	9.08	2511	33.51	5.71
W	2537	42.05	4.70	2403	54.32	7.21

3.5.2.4 Group trend in the *n*-C_4H_9MF molecules

Interactions between the C-H-bond and the metal atoms in the n-C_4H_9MF (M=Cr, Mo, W) molecules are summarized in the Table 3.53, showing that both the donation from the C-H-σ orbital and the donation into the C-H-σ^* orbital make a contribution to the C-H activation, which is consistent with conclusions obtained from bond-order and occupancy analysis of the C-H bond as shown in the appendix (Table A.32). But one can also see that interactions of the donation from the C-H-σ orbital overweighs that of the donation into the C-H-σ^* orbital (shown in the appendix in the Table A.33), the first type of the interactions should be the origin for the C-H activation

difference and need to be further investigated.

Table 3.54: Details of interactions between the C-H-σ orbital and vacant hybrid orbital of the TM atoms. δ-C-H bond columns give calculated data of the δ-C-H bond, and so on. The NBO1 row gives calculated data of the NBO1, and so on. IR$^{\delta}$ gives stretching frequencies of the δ-C-H bond, and so on. ΔE^2_{ij} gives second-order perturbative estimations of the hyperconjugation effect between the C-H-σ orbital and the vacant hybrid orbital of the TM atom, $\Delta\varepsilon_{ij}$ gives energy gaps of the two interacting NBOs, hyb. represents hybridizations of the orbitals.

					δ-C-H bond		α-C-H bond	
n-C_4H_9TMF	IR$^{\delta}$	IR$^{\alpha}$		hyb.	ΔE^2_{ij}	$\Delta\varepsilon_{ij}$	ΔE^2_{ij}	$\Delta\varepsilon_{ij}$
unit	cm^{-1}	cm^{-1}			kcal/mol	a.u.	kcal/mol	a.u.
Mo	2386	2511	NBO1	d	25.53	0.45	14.54	0.40
			NBO2	$sd^{3.12}$	30.33	0.49	13.59	0.43
			NBO3	$sd^{2.78}$	1.48	0.65	5.38	0.60
W	2537	2403	NBO1	d	1.28	0.45	28.06	0.39
			NBO2	d	1.26	0.47	13.85	0.40
			NBO3	$sd^{1.58}$	39.51	0.83	12.41	0.77

All of the individual interactions between the C-H-σ orbital and vacant hybrid orbital of the metal atoms in the n-C_4H_9MoF and n-C_4H_9WF molecules are summarized in the Table 3.54, showing that:

- compared the n-C_4H_9MoF molecule to the n-C_4H_9WF molecule,
  - corresponding to the δ-C-H bond, interaction strength, which is between the C-H-σ orbital and the vacant hybrid orbital with main valence d-orbital share of the metal atom, reduces strongly on moving from the molecule with 4d TM element to that with 5d TM element. But interaction strength, which is between the C-H-σ orbital and vacant hybrid orbitals with main valence s-orbital share of the TM atom, does not change very strongly.
  - corresponding to the α-C-H bond, interaction strength, which is between the C-H-σ orbital and vacant hybrid orbitals with main valence d-orbital share of the metal atom, increases strongly on moving from the molecule with 4d TM element to that with 5d TM element.
- the above observations imply that in the n-C_4H_9MF molecules vacant hybrid orbitals with main valence s-orbital share of the metal atoms interact preferably with the C-H-σ orbitals of the δ-C-H bond, but vacant hybrid orbitals with main

valence d-orbital share of the TM atoms interact preferably with the the C-H-σ orbitals of the α-C-H bond, which is consistent with the conclusion got from Section A.2.1.

- due to the relativistic effect, valence s orbital energy of Mo atom is higher than that of W atom, valence d orbital of the W atom is more diffuse than that of the Mo atom and valence d orbital energy of the Mo atom is lower than that of the W atom. This leads to the reduced C-H activation of the δ-C-H bond and increasing C-H activation of the the α-C-H bond on moving from the molecule with 4d TM element to that with 5d TM element. This explains also why 5d TM elements activate the α-C-H bond more strongly as 4d elements in n-C_4H_9MF molecules, which are found in the previous investigation of molecules with group 4 and group 5 TM elements.

- With the above reasons the inverse image that the α-C-H bond is more activated than the δ-C-H in the n-C_4H_9WF molecule, can be also be declared.

3.5.3 The quintet state(ground state)

The structure of the quintet CH_3MoF molecule is depicted in Figure 3.8. All the quintet CH_3MoX molecules (F, Cl, Br, I, CN) take staggered forms as the absolute minimum. The trans C-H bond, which stands trans to the Mo-X bond, is more activated than the cis C-H bonds. In all the molecules the cartesian axis are fixed as shown in Figure 3.8, the Mo atom lies in the origin, the C atom lies on the X-axis and the X-ligand lies in the XY-plane.

Figure 3.8: The structure of the CH_3MoF molecule optimized with the B3 method.

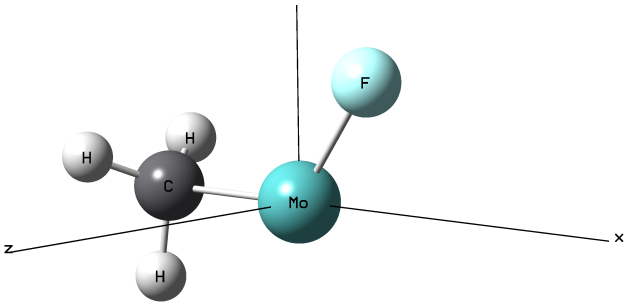

Analysis of the quintet CH_3MoX molecules are shown in the appendix (Table A.34 and A.35).

Compared to the singlet state of molecules following differences can be seen.

- The trans C-H bond in the quintet CH_3MoX molecules is only weakly activated, but in singlet CH_3MoX molecules the trans C-H bond is very strongly activated.

- Interactions between the C-H-σ orbital and vacant hybrid orbitals reduce about 8 times.
- Interactions between the C-H-σ^* orbital and occupied hybrid orbitals reduce about 3 times.

In the ground state (quintet state) the Mo atom shows a selective C-H activation pattern in the n-C_4H_9MoF molecule. The δ-C-H bond is strongly activated and the α-C-H bond is only weakly activated.
All information about the n-C_4H_9MoF molecule are summarized in the appendix (in the Table A.36, A.37 A.38 and A.39). One can see that interactions between the C-H-σ orbital and vacant hybrid orbitals make the major contribution to C-H activations. Compared to the singlet n-C_4H_9MoF molecule interactions between the C-H bond and the Mo atom are strongly reduced with reduce C-H activations, which implies that C-H activations should be induced by these interactions.
Information for investigations of group trends in the CH_3MX and n-C_4H_9MF (M=Cr, Mo ,W) molecules are shown in the appendix (in the Table A.36, A.36,A.36). Compared to the singlet state there are some difference to note, interactions between the C-H-σ orbital and vacant hybrid orbitals of the metal atoms change heavily, but the interactions between the C-H-σ^* orbital and occupied hybrid orbitals of the metal atoms change only very weakly.

3.5.4 The triplet state(first excited state)

Data of the triplet state are shown in the appendix (in the Section A.2.3), showing that interactions and C-H activations are very similar to the singlet state (second excited state), interactions between the C-H bond and the metal atoms weaken in general slightly.
During investigations of the CH_3MX molecules (in the appendix(Table A.46, A.47 and A.48) and group trends of C-H activations in the in the CH_3MF and n-C_4H_9MF molecules (in the appendix(Table A.54- A.59)), a question comes up that C-H activations can be more simply interpreted with interactions between the C-H-σ^* and the occupied hybrid orbital of the Mo atom. But this type of interactions is largely weaker than interactions between the C-H-σ and the vacant hybrid orbital of the Mo atom. Can a weak interaction outbalances a strong interaction, so as to determinate C-H activations?
Comparisons of the C-H bond in the n-C_4H_9MoF and the CH_3MoF molecules are

shown in the appendix (Table A.46, A.47 and A.48). Together with data of the singlet state it shows that interactions between the C-H-σ and the vacant hybrid orbital of the Mo atom vary strongly by C-H activations, but varies of interactions between the C-H-σ^* and the occupied hybrid orbital of the Mo atom are more weaker.

3.5.5 Summary

From the above investigations following conclusions can be drawn.

- The group 6 TM elements in the n-C_4H_9MF molecules show a unselective activation pattern of the C-H bond in the first and second excited state, but in the ground state(quintet state) they show a selective activation pattern that only the δ-C-H bond is strongly activated.
- In all the spin states it shows a reverse ligand impact on C-H activations as the molecules with group 4 and group 5 TM elements. This reverse ligand impact is probably due to polarizations of the metal atoms.
- In general one can see that the more a C-H bond is activated, the more nonpolar the C-H bond is and the less positive the H atom is.
- Interactions between the M-X-σ^* and the C-H-σ orbitals in general play a very important role in C-H activations. It implies that the valence s orbital of the atoms also have an impact on the C-H activation.
- Combined with the knowledge got from the section 3.3 and the above section, C-H activations can be splitted in two stages.
  - In the first stage only interactions between the C-H-σ^* and the occupied hybrid orbital of the metal atom are possible, which induce approaches of C-H bonds to metal atoms. These interactions are typically weak (in general $<$ 11kcal/mol), and in case of weak C-H activations this type of interactions should be the main reason for C-H activations.
  - Further approach of the C-H bond to metal atoms enables interactions between C-H-σ orbitals and vacant hybrid orbitals of the metal atom. The vacant hybrid orbitals of the metal atom can be M-X-σ^* orbitals and vacant hybrid LP orbitals of the metal atom. This type of interactions are typically

intense (up to 50 kcal/mol) in case of strong C-H activations and should be the main driving force to overcome pauli repulsions and ring pressure.

– In summary C-H activations are a coaction of the both type of interactions. In case of strong C-H activations the second type of interactions should dominantly impact C-H activations, so that low energy of vacant hybrid orbitals of the metal atom should benefit C-H activations.

3.6 Group 7 transition metal elements

3.6.1 Enthalpy comparison of the different states

Table 3.55: Enthalpy and IR frequency comparisons of the quartet and the doublet states of the CH_3TcX molecules, all the enthalpies are calculated at the B3LYP/def2-TZVP/def2-ecp levels (sums of electronic and thermal enthalpy) and presented as differences to the ground state at the corresponding absolute minimum of the molecules without zero-point corrections. IR column shows stretching frequencies of the most activated C-H bond, which stands trans to the Tc-X bond.

	quartet		doublet	
$MoCH_3X$	enthalpy	IR	enthalpy	IR
unit	kJ/mol	cm^{-1}	kJ/mol	cm^{-1}
CN	0	2945	59.2	2951
I	0	2936	60.9	2927
Br	0	2960	52.6	2922
Cl	0	2989	59.7	2909
F	0	2829	54.4	2829

Enthalpies and IR frequencies of the CH_3TcX molecules (X= CN, F, Cl, Br, I) are summarized in Table 3.55, showing that the quartet state of the molecules is the ground state and the doublet state is the corresponding first excited state. The other possible state is sextet, but in this state the molecules are unstable, therefore will not be considered. Enthalpy comparison of the *n*-C_4H_9TcF molecules reveals the same conclusion.

In the doublet state the CH_3TcX molecules take staggered forms as their absolute minimum, in the quartet state the molecules take distinct conformations as their absolute minimum. Since in the quartet state the trans C-H bonds of the molecules are only slightly activated, but in the doublet state the trans C-H bond are more activated, only conclusions about molecules in the doublet state are explicitly described and differences to the quartet state will be just briefly discussed.

3.6.2 The doublet state(first excited state)

3.6.2.1 CH_3TcX-system

The Figure 3.5 will be taken as the structure for the CH_3TcX-molecules and also the fixation of cartesian axis, only the Nb atom will be replaced to the Tc atom.

Structure, bond-order and occupancy comparisons of the trans C-H bond in the

Table 3.56: The leading interaction between the C-H-σ orbital and the vacant hybrid orbital of the Tc atom in the CH_3TcX molecules. α-spin table records interaction information in the α-spin, and so on. IR^t gives stretching frequencies of the trans C-H bonds. ΔE^2_{ij} column gives second-order perturbative estimations of the hyperconjugation, hyd. column shows hybridizations of the NHO of the metal atom, which is participated in the interaction, $\Delta\varepsilon_{ij}$ gives energy gaps of the interacting NBOs. Composition column shows orbital compositions of the Tc NHO. Sum column gives sums of this type of interactions. M(coe) column shows polarization coefficients of the M-F-σ^* orbital, and so on.

α-spin

	IR^t	sum	ΔE^2_{ij}	hyb.	$\Delta\varepsilon_{ij}$	composition	M(coe)	F(coe)
unit	cm^{-1}	kcal/mol	kcal/mol		hartree			
CN	2951	2.68	1.45	$sd^{1.45}$	0.65	$0.64*5s-0.56*4d_{x^2-y^2}-0.46*4d_{xy}$	0.84	-0.54
I	2927	2.08	2.08	$sd^{1.03}$	0.54	$-0.70*5s+0.51*4d_{x^2-y^2}+0.45*4d_{xy}$	0.85	-0.52
Br	2922	1.98	1.98	$sd^{0.81}$	0.55	$-0.74*5s+0.45*4d_{x^2-y^2}+0.49*4d_{xy}$	0.89	-0.45
Cl	2909	3.10	3.10	$sd^{1.54}$	0.54	$0.62*5s-0.46*4d_{x^2-y^2}-0.58*4d_{xy}$	0.88	-0.48
F	2829	5.04	5.04	$sd^{3.71}$	0.57	$-0.46*5s+0.78*4d_{xy}$	-0.92	0.38

β-spin

	IR^t	sum	ΔE^2_{ij}	hyb.	$\Delta\varepsilon_{ij}$	composition	M(coe)	F(coe)
unit	cm^{-1}	kcal/mol	kcal/mol		hartree			
CN	2951	1.44	1.25	$sd^{2.52}$	0.65	$0.53*5s-0.59*4d_{x^2-y^2}-0.44*4d_{z^2}$	0.85	-0.53
I	2927	2.23	1.26	$sd^{0.97}$	0.54	$0.71*5s-0.55*4d_{x^2-y^2}$	0.88	-0.48
Br	2922	2.48	2.48	$sd^{2.83}$	0.55	$-0.51*5s+0.45*4d_{x^2-y^2}+0.63*4d_{xy}$	0.89	-0.47
Cl	2909	2.88	2.00	$sd^{1.12}$	0.55	$0.68*5s-0.56*4d_{x^2-y^2}-0.35*4d_{xy}$	0.90	-0.45
F	2829	4.77	4.57	$sd^{4.18}$	0.58	$0.43*5s-0.37*4d_{z^2}+0.73*4d_{xy}$	-0.93	0.37

CH_3TcX molecules are shown in the appendix (Table A.60) indicating that the trans C-H bonds are only slightly activated in these molecules.

Analyse of interactions shows that interactions between the C-H-σ^* orbital and occupied hybrid orbitals of the Tc atom are two times weaker than interactions between the C-H-σ orbital and vacant hybrid orbitals of the Tc atom, and at the same time the first type of interactions does not correlate properly with the C-H activation strength, therefore should not be the main reason for the C-H activations and will be shown in the appendix (Table A.61). Here only interactions between C-H-σ orbital and vacant hybrid orbitals of the Tc atom are to be analyzed. The vacant hybrid orbitals of the metal atom can be M-X-σ^* orbitals and vacant hybrid LP orbitals of the metal atom. Interactions between C-H-σ orbital and vacant hybrids orbital of the Tc atom are

shown in the Table 3.56 indicating that both the sum of the interactions and the first leading interaction between the C-H-σ orbital and the vacant hybrid orbitals of the Tc atom, which are M-X-σ^* orbitals, correlate approximately with the C-H activation in both spin sets. But C-H activations are not induced by energy gaps between the interacting orbitals, but rather by overlaps and polarization coefficients of the Mo-X-σ orbital. The more the C-H bond is activated, the larger the polarization coefficients of the NHOs of the Mo atom is. It leads to the assumption that the polarization leads to better overlap between the interacting orbitals and makes an important impact on C-H activations.

3.6.2.2 C-H bond comparisons of the *n*-C_4H_9TcF and CH_3TcF molecules

Comparisons of the structures, bond-orders and occupancies of the C-H bond are shown in the appendix (Table A.62 and A.63) indicating that occupancy changes of both the C-H-σ- and C-H-σ^* orbitals can induce C-H activations.

Only the leading interaction between the C-H-σ orbital and the vacant Tc hybrid orbitals are shown here in the Table 3.57, the leading interaction between the C-H-σ^* orbital and the occupied Tc hybrid orbital are shown in the appendix (Table A.64).

Table 3.57: The leading interaction between the C-H-σ orbital and the vacant Tc hybrid orbital. Met^c row represents calculated data of the cis C-H bond in the CH_3TcF molecule, and so on. But$^\alpha$ row represents calculated data of the α-C-H bond in the n-C_4H_9TcF molecule, and so on. α-spin table gives calculated data in the α-spin of the molecules, and so on. IR gives stretching frequencies of the C-H bonds. ΔE^2_{ij} column gives second-order perturbative estimations of the hyperconjugation, hyd. column shows hybridizations of the NHO of the metal atom, which is participated in the interaction, $\Delta\varepsilon_{ij}$ gives energy gaps of the interacting NBOs. Composition column shows orbital compositions of the Tc NHO. Sum column gives sums of this type of interactions.

α-spin

	IR	sum	ΔE^2_{ij}	hyb.	$\Delta\varepsilon_{ij}$	composition
unit	cm^{-1}	kcal/mol	kcal/mol		hartree	
Met^c	3051	0.10	0.10	$sd^{3.31}$	0.58	$-0.48*5s-0.83*4d_{x^2-y^2}$
But$^\alpha$	2943	1.19	1.19	d	0.40	$-0.62*4d_{xz}+0.78*4d_{yz}$
Met^t	2829	5.04	5.04	$sd^{3.71}$	0.57	$0.46*5s+0.78*4d_{xy}$
But$^\delta$	2604	14.52	13.54	$sd^{1.11}$	0.65	$0.68*5s-0.65*4d_{x^2-y^2}$

β-spin

	IR	sum	ΔE^2_{ij}	hyb.	$\Delta\varepsilon_{ij}$	composition
unit	cm^{-1}	kcal/mol	kcal/mol		hartree	
Met^c	3051	1.98	1.09	d	0.43	$-0.81*4d_{xz}-0.57*4d_{yz}$
But$^\alpha$	2943	1.34	1.34	$sd^{2.59}$	0.46	$0.53*5s-0.45*4d_{xz}-0.60*4d_{yz}$
Met^t	2829	4.77	4.57	$sd^{4.18}$	0.58	$0.43*5s-0.37*4d_{z^2}+0.73*4d_{xy}$
But$^\delta$	2604	16.81	13.07	$sd^{4.44}$	0.63	$0.42*5s-0.53*4d_{x^2-y^2}-0.59*4d_{xy}$

Analyse of interactions shows that interactions between the C-H-σ^* orbital and the occupied hybrid orbital are dominant under weak C-H activations, but under strong C-H activations interactions between the C-H-σ orbital and vacant hybrid orbitals should be the crucial factor that impacts C-H activations.
The reason for raising of the C-H activations is not energy gaps of the interacting orbitals between the C-H-σ orbital and the vacant hybrid orbital. But in other sides energy gaps of the leading interaction between the C-H-σ^* orbital and the occupied hybrid orbital decreases with raising C-H activation, which can be seen in the appendix.
One explanation for this observation can be that energy gaps between the C-H-σ^* orbital and the occupied hybrid orbital is the reason for the initial approach of the C-H bond to the metal atom, which leads to better overlaps. But interactions between the C-H-σ^* orbital and the occupied hybrid orbital increase slowly with the approach of the C-H bond, interactions between the C-H-σ orbital and the vacant hybrid orbital increase very quickly. It leads to the conclusion that the real origin for the raising C-H activation is energy gaps between the C-H-σ^* orbital and the occupied hybrid orbital, which lead to quickly increases of overlap between the C-H-σ orbital and the vacant hybrid orbitals.
NPA comparison is carried in the appendix (Table A.65), showing that in general the more a C-H bond is activated, the less positive a H atom of the C-H bond is, the more unpolar the C-H bonds is.

3.6.2.3 Group trends in the CH_3MF molecules

Structure, bond-order and occupancy comparisons of the C-H bond in the CH_3MF (M=Mn, Tc, Re) are shown in the appendix (Table A.66) indicating that interactions between the C-H-σ orbital and the vacant hybrid orbitals of the metal atoms in both spins can induce the C-H activation difference of the trans C-H bond.

Interactions between the C-H-σ orbital and vacant hybrid orbital of the metal atoms are shown in the appendix (Table A.67) and they are more stronger than interactions between the C-H-σ^* and occupied hybrid orbitals of the metal atoms. Both the sum of all the interactions and the leading hyperconjugation between the C-H-σ orbital and vacant hybrid orbitals of the TM atoms proportionate with C-H activations. But one can also see that overlaps not energy gaps between interacting orbitals are the origin for the C-H activations.
The leading interaction between the C-H-σ^* orbital and occupied hybrid orbitals of

Table 3.58: The leading interaction between the C-H-σ^* orbital and the hybrid orbital of the metal atoms in the CH_3MF molecules. α-spin table records interaction information in the α-spin, and so on. IR^t gives stretching frequencies of the trans C-H bonds. ΔE_{ij}^2 column gives second-order perturbative estimations of the hyperconjugation, hyd. column shows hybridizations of the NHO of the metal atom, which is participated in the interaction, $\Delta\varepsilon_{ij}$ gives energy gaps of the interacting NBOs. Composition column shows orbital compositions of the Tc NHO. Sum column gives sums of this type of interactions.

α-spin

	IR	sum	ΔE_{ij}^2	hyb.	$\Delta\varepsilon_{ij}$	composition
unit	cm^{-1}	kcal/mol	kcal/mol		hartree	
Mn	2995	1.07	0.56	$sd^{3.04}$	0.75	$-0.50*4s-0.65*3d_{x^2-y^1}+0.45*3d_{z^2}$
Tc	2829	1.37	0.95	d	0.55	$-0.46*4d_{xy}-0.75*4d_{yz}$
Re	2584	3.18	2.11	$sd^{2.30}$	0.53	$-0.55*6s-0.59*5d_{x^2-y^2}+0.41*5d_{xy}$

β-spin

	IR	sum	ΔE_{ij}^2	hyb.	$\Delta\varepsilon_{ij}$	composition
unit	cm^{-1}	kcal/mol	kcal/mol		hartree	
Mn	2995	1.17	0.92	$sd^{6.80}$	0.63	$0.36*4s-0.57*3d_{x^2-y^2}+0.73*3d_{xy}$
Tc	2829	1.71	1.71	$sd^{6.83}$	0.54	$0.35*5s-0.62*4d_{x^2-y^2}-0.63*4d_{xy}$
Re	2584	2.44	2.04	$sd^{1.12}$	0.51	$0.68*6s-0.59*5d_{x^2-y^2}+0.32*5d_{z^2}$

the metal atoms in the CH_3MF molecules are shown here in the Table 3.58 indicating that energy gaps between the C-H-σ^* orbital and the occupied hybrid orbital decreases with raising C-H activations, which is the same as the previous section. With the same speculation as the previous section the group trends of C-H activations in the CH_3MF molecules can be explained: interactions between the C-H-σ^* orbital and occupied hybrid orbitals are weaker than interactions between the C-H-σ orbital and vacant hybrid orbitals, but they are the real origin for the initial approach of the C-H bond to the metal atoms.

3.6.2.4 Group trends in the *n*-C_4H_9MF molecules

Bond-order and occupancy analyse of the C-H bond as shown in the appendix (Table A.68) indicate that both donations from the C-H-σ orbital and donations into the C-H-σ^* orbital can be the reason for C-H activations.

The leading interaction between the C-H-σ orbital and the vacant hybrid orbital of the metal atoms in the *n*-C_4H_9MF (M=Mn, Tc, Re) molecules are summarized in the Table 3.59. The interactions, which lead to the donation from the C-H-σ orbital into the vacant metal hybrid orbitals should make the major contribution to C-H activations, since it is more stronger than interactions that lead to the donations from

Table 3.59: The leading interaction between the C-H-σ orbital and the vacant hybrid orbital of the metal atoms in the n-C_4H_9MF molecules. α-spin table records interaction information in the α-spin, and so on. IR gives stretching frequencies of the C-H bonds. ΔE^2_{ij} column gives second-order perturbative estimations of the hyperconjugation, hyd. column shows hybridizations of the NHO of the metal atom, which is participated in the interaction, $\Delta\varepsilon_{ij}$ gives energy gaps of the interacting NBOs. Composition column shows orbital compositions of the Tc NHO. Sum column gives sums of this type of interactions. M(coe) column shows polarization coefficients of the M-F-σ^* orbital, and so on.

α-spin

	IR	sum	ΔE^2_{ij}	hyb.	$\Delta\varepsilon_{ij}$	composition	M(coe)	F(coe)
unit	cm^{-1}	kcal/mol	kcal/mol		hartree			
Mn	2731	10.30	10.12	$sd^{0.95}$	0.59	$0.71*4s-0.61*3d_{x^2-y^2}$	-0.94	0.33
Tc	2604	14.52	13.54	$sd^{1.11}$	0.65	$0.68*5s-0.65*4d_{x^2-y^2}$	-0.94	0.35
Re	2481	23.23	21.96	$sd^{1.49}$	0.78	$0.63*6s-0.63*5d_{x^2-y^2}$	-0.93	0.38

β-spin

	IR	sum	ΔE^2_{ij}	hyb.	$\Delta\varepsilon_{ij}$	composition	M(coe)	F(coe)
unit	cm^{-1}	kcal/mol	kcal/mol		hartree			
Mn	2731	10.03	9.44	$sd^{1.25}$	0.62	$0.66*4s-0.67*3d_{x^2-y^2}$	-0.94	0.33
Tc	2604	16.81	13.07	$sd^{4.44}$	0.63	$0.42*5s-0.53*4d_{x^2-y^2}-0.59*4d_{xy}$	-0.93	0.38
Re	2481	22.39	21.03	$sd^{1.43}$	0.79	$0.64*6s-0.61*5d_{x^2-y^2}$	-0.93	0.37

the occupied metal hybrid orbitals into the C-H-σ^* orbital, which are shown in the appendix (Table A.70).

The group trends of C-H activations in the n-C_4H_9MF molecules can be also explained as the previous sections: interactions between the C-H-σ^* orbital and occupied hybrid orbitals are weaker than that between the C-H-σ orbital and vacant hybrid orbitals, but they are the real origin for the initial approach of the C-H bond to the metal atoms. Interaction strength between the C-H-σ orbital and vacant metal hybrid orbitals raises very quickly with the approach of the C-H bond to the metal atoms, and overlaps not the energy gaps of interacting orbitals are the reason for this quick raising of interaction strengths.

3.6.3 The quartet state(ground state)

All of data of quartet state are shown in the appendix (Section A.3.2).

The quartet CH_3TcX (X= CN, F, Cl, Br, I) molecules take a different conformation as their absolute minimum as their counterparts in the excited state(doublet state), a few of them take a conformation between a eclipsed and a staggered form due to unknown reasons, which can be seen in the Table A.71 in the appendix. This question about conformations will not be addressed here.

The C-H bonds of the molecules in the quartet state are less activated than that in the doublet state, this can also be observed in the previous sections that the C-H bonds are less activated in ground states than in excited states. Interactions between the C-H bonds and metal atoms increase in the excited state, and interactions between the C-H-σ orbital and vacant metal hybrid orbitals raise more quickly than that between the C-H-σ^* orbital and occupied metal hybrid orbitals. The raising of the interaction strength between the C-H-σ orbital and vacant metal hybrid orbitals should be induced by overlaps of the interacting orbitals, since energy gaps of the interaction orbitals are almost unaltered , however energy gaps between the C-H-σ^* orbital and occupied metal hybrid orbitals decrease with raising C-H activation compared the excited state with the ground state.
This is the same as in the previous sections: interactions between the C-H-σ orbital and vacant metal hybrid orbitals are very strong and should make the major contribution to C-H activations in cases of strong C-H activations, but the origin for this strong C-H activation should be energy gaps between the C-H-σ^* orbital and occupied metal hybrid orbitals, which lead to quick raise of orbital overlaps between the the C-H bond and the metal atoms.
NPA comparison in the quartet state is carried in the appendix (Table A.78), showing the same conclusion as in the doublet state.

3.6.4 Summary

From the above investigations following conclusions can be drawn.

- The group 7 TM elements in the n-C_4H_9MF molecules show a high selective activation pattern of the C-H bond in both the doublet and quartet states that δ-C-H bonds are very strongly activated and α-C-H bonds are almost untouched by the TM elements.

- The NPA comparisons show that in general the more a C-H bond is activated, the less positive the H atom of the C-H bond is, the more unpolar the C-H bonds gets.

- Under strong C-H activations interactions between the C-H-σ orbital and vacant metal hybrid orbitals are largely stronger than interactions between the C-H-σ^* orbital and occupied metal hybrid orbitals, therefore the first type of the interactions should make the major contribution to strong C-H activations. Analyse

of the interactions shows that quick raising of overlaps not decrease of energy gaps between the C-H-σ orbital and vacant metal hybrid orbitals are the reason for the raising interaction strength.

- With raising C-H activations, energy gaps between the C-H-σ^* orbital and the occupied metal hybrid orbitals decrease, which should lead to initial approaches of C-H bonds to metal atoms.

3.7 Group 8 transition metal elements

3.7.1 Enthalpy comparison of the different states

Table 3.60: Enthalpy and IR frequency comparison of the CH_3RuX molecules in different spin states, all the enthalpies are calculated at the B3LYP/def2-TZVP/def2-ecp levels (sums of electronic and thermal enthalpy) and presented as differences to the ground state at the corresponding absolute minimum of the molecules without zero-point corrections. IR column shows stretching frequencies of the most activated C-H bond, which stands trans to the Ru-X bond.

	quintet		triplet		singlet	
$RuCH_3X$	enthalpy	IR	enthalpy	IR	enthalpy	IR
unit	kJ/mol	cm^{-1}	kJ/mol	cm^{-1}	kJ/mol	cm^{-1}
F	0	2991	29.6	2876	118.9	2736
Cl	0	2996	9.6	2934	119.3	2867
Br	0	2997	5.8	2934	119.7	2866
I	0	2998	-1.9	2934	111.7	2904
CN	0	3000	-54.0	2966	91.6	3106

Enthalpies and IR frequencies of the CH_3RuX molecules (X= CN, F, Cl, Br, I) in different states are summarized in Table 3.60 showing that the quintet state is the ground state of the molecules and the triplet and singlet states are the corresponding first and second excited states except the CH_3RuCN and CH_3RuI molecules, which have triplet as the ground state. Enthalpy comparisons of the n-C_4H_9RuF molecules reveals that the singlet state is the second excited state of the molecule, the triplet state is the ground state, the enthalpy difference between the molecule of these two states is only 61.8kJ/mol.

C-H bonds are in general only slightly activated, since the trans C-H bond of the CH_3RuX molecules are most strongly activated in the singlet state, only analyse about the singlet state are explicitly described and differences to the quintet and triplet states will only be briefly discussed.

3.7.2 The singlet state(second excited state)

3.7.2.1 CH_3RuX-system

The Figure 3.5 can be taken as the structure for the CH_3RuX-molecules and also the fixation of cartesian axis, since all the CH_3RuX molecules (X= CN, F, Cl, Br, I) take staggered form as their absolute minimum, which is in line with the CH_3NbF molecule.

Structure, bond-order and occupancy comparisons of the trans C-H bond in the

Table 3.61: The leading interaction between the trans C-H bond(and cis C-H bond in case of CN as ligand) and hybrid orbitals of the Ru atom in the CH_3RuX molecules. C-H-σ table shows calculated data about the leading interaction between the C-H-σ orbital and the vacant hybrid orbital of the Ru atom in the CH_3RuX molecules, and so on. IR gives stretching frequencies of the trans C-H bonds. ΔE^2_{ij} column gives second-order perturbative estimations of the hyperconjugation, hyb. column shows hybridizations of the NHO of the metal atom, which is participated in the interaction, $\Delta\varepsilon_{ij}$ gives energy gaps of the interacting NBOs. Composition column shows orbital compositions of the NHO of the Ru atom. Sum column gives sums of this type of interactions. M(coe) column shows polarization coefficients of the M-F-σ^* orbital, and so on.

C-H-σ

	IR	sum	ΔE^2_{ij}	hyb.	$\Delta\varepsilon_{ij}$	composition	M(coe)	F(coe)
unit	cm^{-1}	kcal/mol	kcal/mol		hartree			
CN(trans C-H)	3106	1.34	1.17	$sd^{1.36}$	0.66	$0.65*5s-0.67*4d_{x^2-y^2}-0.28*4d_{z^2}$	0.82	-0.57
I	2904	2.09	1.18	$sd^{0.51}$	0.57	$0.81*5s+0.50*4d_{x^2-y^2}-0.28*4d_{xy}$	0.89	-0.46
Cl	2867	7.23	6.68	$sd^{5.46}$	0.52	$-0.39*5s+0.47*4d_{z^2}-0.68*4d_{xy}$	0.88	-0.48
Br	2866	6.28	5.88	$sd^{4.03}$	0.51	$-0.44*5s+0.42*4d_{x^2-y^2}-0.62*4d_{xy}$	0.87	-0.50
F	2736	16.07	15.23	$sd^{13.19}$	0.54	$0.26*5s-0.49*4d_{z^2}+0.81*4d_{xy}$	-0.91	0.40
CN(cis C-H)	2993	5.34	5.34	d	0.36	$0.98*4d_{xz}-0.19*4d_{yz}$		

C-H-σ^*

	IR	sum	ΔE^2_{ij}	hyb.	$\Delta\varepsilon_{ij}$	composition
unit	cm^{-1}	kcal/mol	kcal/mol		hartree	
CN(trans C-H)	3106	3.79	2.77	d	0.64	$-0.98*4d_{xy}-0.16*4d_{x^2-y^2}$
I	2904	3.54	2.06	d	0.58	$0.94*4d_{xz}-0.33*4d_{yz}$
Cl	2867	3.12	2.46	d	0.54	$0.55*4d_{z^2}-0.69*4d_{xy}-0.46*4d_{x^2-y^1}$
Br	2866	3.19	2.20	d	0.54	$-0.51*4d_{z^2}-0.59*4d_{xy}-0.44*4d_{xz}$
F	2736	4.17	2.79	d	0.50	$-0.63*4d_{z^2}-0.51*4d_{xy}-0.57*4d_{x^2-y^1}$
CN(cis C-H)	2993	1.57	0.56	$spd^{0.41}$	0.62	$-0.63*5s+0.22*4d_{z^2}+0.57*5p_y$

CH_3RuX molecules are shown in the appendix (Table A.85) indicating that the C-H activation of the trans C-H bonds can be probably induced by occupancy changes of the C-H-σ orbital. Since disagreement of calculated IR frequencies should be over $5cm^{-1}$, the strict sequence of the stretching frequencies of trans C-H bond in the CH_3RuBr and CH_3RuCl molecules should be not significant. There is one interesting point to note that the trans C-H bond is less activated than the cis C-H bond in the

CH_3RuCN molecule, which is contrary to all the previous investigations.
Analyse of interactions are shown in the Table 3.61 indicating that:

- Under weak C-H activations, interactions between the C-H-σ^* orbital and occupied hybrid LP orbitals of the Ru atom are stronger than those between the C-H-σ orbital and vacant hybrid orbitals indicating that the first type of the interactions should make the major contribution by weak C-H activations.

- Under strong C-H activations, the second type of the interactions are largely stronger than first type of the interactions, which indicates that the second type of the interactions should make the major contribution by strong C-H activations.

- The rise of interaction strengths between the C-H-σ orbital and vacant hybrid orbitals of the Ru atom is more likely induced by increasing overlaps of the interacting orbitals, therefore the raising of the interactions strength can not be the origin but rather the outcome of closer approaches of C-H bonds to metal atoms.

- Since only energy gaps between the C-H-σ^* orbital and vacant hybrid LP orbitals of the Ru atom show the right correlation with activations of trans C-H bonds, this type of interactions should be the origin for the closer approach of the C-H bond to the Ru atom that leads to increased overlaps of the orbitals.

In general the most important interaction for the trans C-H bond activation is the interaction between the C-H-σ orbital and Ru-X-σ^* orbital. This interaction is largely weakened in the CH_3RuCN molecule due to the high energy and the unfavored polarization of M-CN-σ^* orbital, which indicates that the Ru-CN-σ bond should be very stable. On the other hand this stable σ-bond should make the energy of the other occupied orbital higher, leading to smaller energy gaps between the C-H-σ^* orbital and occupied LP orbitals of the Ru atom, which can not be observed in the Table 3.61. This phenomenon can be explained by the π-backbonding of the cyanid group, which reduces the electronic density of the Ru atom leading to an increasing energy gap between the C-H-σ^* orbital and an occupied hybrid orbital of the Ru atom in the CH_3RuCN molecule. Meanwhile this π-backbonding can probably affect the energy of the M-CN-σ^* orbital, which leads to a varied C-H activation potential of cyanid group in comparison to the other σ-ligand(X= F, Cl, Br, I).
In the CH_3RuCN molecule the C-H activation distinction between cis- and trans C-H

bond can be explained by the π-backbonding of cyanid group. It lowers the energy of both the occupied and vacant orbitals of the Ru atom leading to the largely reduced energy gap between the cis C-H-σ orbital and vacant hybrid LP orbital of the Ru atom in comparison to the trans C-H bond.

3.7.2.2 C-H bond comparisons in the n-C_4H_9RuF and CH_3RuF molecules

Table 3.62: The leading interaction between the C-H-bond and the Ru atom. C-H-σ table shows calculated data about the leading interaction between the C-H-σ orbital and the occupied hybrid orbital of the Ru atom in the CH_3RuX molecules, and so on. Met^c row represents calculated data of the cis C-H bond in the CH_3RuF molecule, and so on. But^α row represents calculated data of the α-C-H bond in the n-C_4H_9RuF molecule, and so on. IR gives stretching frequencies of the C-H bonds. ΔE^2_{ij} column gives second-order perturbative estimations of the hyperconjugation, hyb. column shows hybridizations of the NHO of the metal atom, which is participated in the interaction, $\Delta\varepsilon_{ij}$ gives energy gaps of the interacting NBOs. Composition column shows orbital compositions of the Ru NHO. Sum column gives sums of this type of interactions. M(coe) column shows polarization coefficients of the M-F-σ^* orbital, and so on.

C-H-σ

	IR	sum	ΔE^2_{ij}	hyb.	$\Delta\varepsilon_{ij}$	composition	M(coe)	F(coe)
unit	cm^{-1}	kcal/mol	kcal/mol		hartree			
Met^c	3022	0.62	0.47	d	0.56	$0.49 * 4d_{z^2} - 0.80 * 4d_{x^2-y^2}$		
But^α	2976	1.26	0.72	$sd^{0.75}$	0.55	$0.75 * 5s - 0.59 * 4d_{yz}$		
Met^t	2736	16.07	15.23	d	0.54	$-0.49 * 4d_{z^2} + 0.81 * 4d_{xy}$	-0.91	0.40
But^δ	2342	63.85	45.22	$sd^{4.31}$	0.59	$0.43 * 5s - 0.62 * 4d_{x^2-y^2} - 0.44 * 4d_{z^2}$	-0.92	0.40

C-H-σ^*

	IR	sum	ΔE^2_{ij}	hyb.	$\Delta\varepsilon_{ij}$	composition
unit	cm^{-1}	kcal/mol	kcal/mol		hartree	
Met^c	3022	4.23	4.04	d	0.59	$0.96 * 4d_{xz} + 0.27 * 4d_{yz}$
But^α	2976	2.52	2.31	d	0.60	$0.94 * 4d_{xz} + 0.28 * 4d_{yz}$
Met^t	2736	4.17	2.79	d	0.50	$-0.63 * 4d_{z^2} - 0.57 * 4d_{x^2}$
But^δ	2342	7.66	6.95	d	0.47	$0.58 * 4d_{z^2} + 0.61 * 4d_{yz}$

Comparisons of structures, bond-orders and occupancies of the C-H bond are shown in the appendix (Table A.86 and A.87), indicating that occupancy changes of the C-H-σ-orbital should be the main factor that impacts C-H activations, and C-H activations correlate only properly with distance between the Ru and H atom.

The leading interaction between the C-H-bond and the Ru atom are shown here in Table 3.62, showing the same conclusion got from the previous section that interactions between the C-H-σ orbital and vacant hybrid LP orbitals of the Ru atom are largely stronger than that between the C-H-σ^* orbital and occupied hybrid LP orbitals, but

the energy gaps of the later type of interactions are the origin, why the C-H bonds approach closer to the Ru atom under stronger C-H activations.
NPA comparison is carried out in the appendix (Table A.88), showing that in general the more a C-H bond is activated, the more unpolar the C-H bond is.

3.7.2.3 Group trends in the CH_3MF molecules

In the absolute minimum of the CH_3OsF molecule as shown in the Figure 3.9, the Os atom shows a very strong C-H activation ability so that two hydrogen atoms of the methyl group move to the Os atom without an activation barrier. The CH_3FeF and CH_3RuF molecules take a normal structure as the the Figure 3.5.

Figure 3.9: The structure of the CH_3OsF molecule optimized with the B3 method.

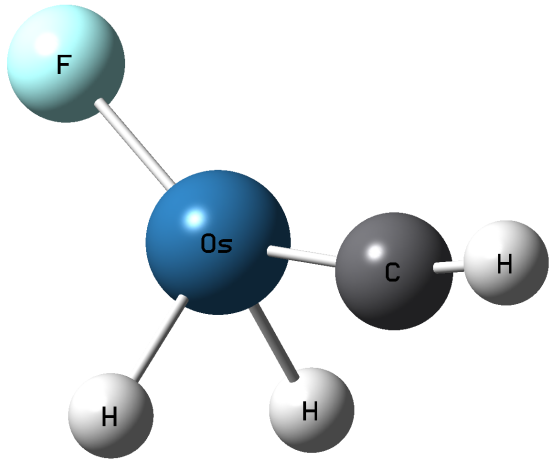

In order to compare the C-H activation ability of the Os atom to the Fe and Ru atoms in the CH_3MF (M=Fe, Ru, Os) molecules, the structure of the CH_3RuF is taken as the structure of the CH_3OsF molecule and only the Ru atom is replaced to the Os atom, since this geometry is not optimized in the artificial structure, no vibrational frequencies can be calculated.
Bond-order and occupancy comparisons of the C-H bond in the CH_3MF (M=Fe, Ru, Os) are shown in the appendix (Table A.89) indicating that both the donation from C-H-σ orbital into the metal atoms and donation from the metal atoms into the C-H-σ^* orbital can induce C-H activations of the trans C-H bonds.

The leading interactions between the trans C-H bond and the metal atoms in the CH_3MF molecules are shown in the Table 3.63 indicating that interactions between the C-H-σ orbital and vacant hybrid orbitals of the metal atoms are extensively stronger than that between the C-H-σ^* orbital and occupied hybrid orbitals. One can also see that the raising of interaction strengths between the C-H-σ orbital and the vacant hybrid orbital is rather due to overlaps than energy gaps of the interacting orbitals.
In this case energy gaps between the C-H-σ^* orbital and occupied hybrid orbitals also do not correlate properly with C-H activation, this is probably due to the fact that

Table 3.63: The leading interactions between the trans C-H bond and the metal atoms in the CH_3MF molecules. C-H-σ table records interactions between the C-H-σ orbital and the hybrid orbital of the metal atoms, and so on. IR^t gives stretching frequencies of the trans C-H bonds. ΔE^2_{ij} column gives second-order perturbative estimations of the hyperconjugation, hyb. column shows hybridizations of the NHO of the metal atom, which is participated in the interaction, $\Delta\varepsilon_{ij}$ gives energy gaps of the interacting NBOs. Composition column shows orbital compositions of the Ru NHO. Sum column gives sums of this type of interactions. M(coe) column shows polarization coefficients of the M-F-σ^* orbital, and so on.

C-H-σ

	IR	sum	ΔE^2_{ij}	hyb.	$\Delta\varepsilon_{ij}$	composition	M(coe)	F(coe)
unit	cm^{-1}	kcal/mol	kcal/mol		hartree			
Fe	2911	4.63	3.94	$sd^{2.68}$	0.50	$0.52*4s-0.46*3d_{x^2-y^2}+0.53*3d_{xy}$	-0.94	0.35
Ru	2736	16.07	15.23	$sd^{13.19}$	0.54	$0.81*4d_{xy}-0.49*4d_{z^2}$	-0.91	0.40
Os		31.02	29.91	$sd^{1.98}$	0.67	$0.57*6s+0.79*5d_{xy}$	-0.91	0.41

C-H-σ^*

	IR	sum	ΔE^2_{ij}	hyb.	$\Delta\varepsilon_{ij}$	composition
unit	cm^{-1}	kcal/mol	kcal/mol		hartree	
Fe	2911	2.73	0.99	d	0.62	$-0.41*4s+0.36*3d_{x^2-y^2}-0.72*3d_{xy}$
Ru	2736	4.17	2.79	d	0.50	$-0.63*4d_{z^2}-0.57*4d_{x^2-y^2}-0.51*4d_{xy}$
Os		6.46	4.92	$sd^{3.20}$	0.55	$0.49*6s-0.73*5d_{x^2-y^2}-0.48*5d_{xy}$

the CH_3OsF molecule accords an artificial molecule. Probably the closer a C-H bond approaches the metal atom, the lower are the energy gaps between the C-H-σ^* orbital and occupied hybrid orbitals of the metal atoms, which can be consistently observed in previous sections.

And one can also see that the hybrid orbitals of the Os atom overlap better with the C-H bond than that of the Ru atom, when the structure of the molecule is the same. It indicates that valence d-orbitals make an important contribution to the interactions, since valence d-orbitals of the 5d element are more diffuse than that of 4-d element due to relativistic effects.

3.7.2.4 Group trends in the n-C_4H_9MF molecules

Among the n-C_4H_9MF (M=Fe, Ru, Os) molecules, the n-C_4H_9FeF and n-C_4H_9RuF molecules take a normal structure as their local minimum, which is similar to the structure shown in the Figure 3.4, therefore this structure and the fixation of the cartesian axis will be taken for the molecules.

Figure 3.10: The structure of the n-C_4H_9OsF molecule optimized with the B3 method.

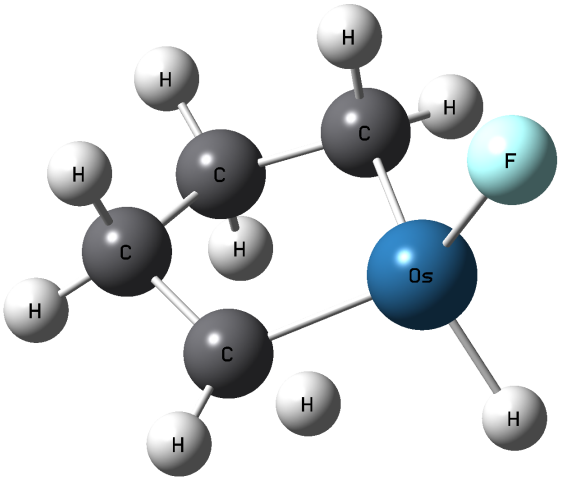

The Os atom in the n-C_4H_9OsF molecule shows a very strong C-H activation ability so that one hydrogen atoms of the δ-CH_3-group move to the Os atom without an activation barrier as shown in the Figure 3.10.
In order to compare the C-H activation ability of the Os atom with the Fe and Ru atoms, the n-C_4H_9OsF molecule takes the same structure of the n-C_4H_9RuF molecule, in which the Ru atom is replaced to the Os atom. For this non-optimized structure, again, no vibrational frequencies can be calculated.
Bond-order and occupancy analyse of the C-H bond as shown in the appendix (Table A.90) indicating that both donations from the C-H-σ orbital and donations into the C-H-σ^* orbital can be the reason for C-H activations.

The leading interaction between the C-H-bond and the hybrid orbitals of the metal atoms in the n-C_4H_9MF (M=Fe, Ru, Os) molecules are summarized in Table 3.64. The NBO1 in the C-H-σ-table represents a M-F-σ^*-orbital in the n-C_4H_9RuF and n-C_4H_9OsF molecules, NBO1 in the n-C_4H_9FeF and NBO2s are a vacant LP orbitals of the metal atoms. Interactions, which lead to donations from C-H-σ orbital into vacant metal hybrid orbitals, should make the major contribution to C-H activations, since they are largely stronger than interactions that lead to donations from occupied metal hybrid orbitals into the C-H-σ^* orbital.
Following conclusions can be drawn from the Table 3.64.

- The interaction between the M-F-σ^*-orbital and the C-H-σ orbital is in general the most important interaction for the C-H activations. By strong C-H activa-

Table 3.64: The leading interactions between the C-H bond and the metal atoms in the n-C_4H_9MF molecules. C-H-σ table records interactions between the C-H-σ orbital and the hybrid orbital of the metal atoms, and so on. NBO1 gives calculated data of the NBO1. IR gives stretching frequencies of the δ-C-H bonds. ΔE^2_{ij} column gives second-order perturbative estimations of the hyperconjugation, hyb. column shows hybridizations of the NHO of the metal atom, which is participated in the interaction, $\Delta\varepsilon_{ij}$ gives energy gaps of the interacting NBOs. Composition column shows orbital compositions of the Ru NHO. Sum column gives sums of this type of interactions.

C-H-σ

			NBO1			NBO2		
	IR	sum	ΔE^2_{ij}	hyb.	$\Delta\varepsilon_{ij}$	ΔE^2_{ij}	hyb.	$\Delta\varepsilon_{ij}$
unit	cm^{-1}	kcal/mol	kcal/mol		hartree	kcal/mol		hartree
Fe	2549	33.00	30.99	$sd^{0.76}$	0.51	1.92	$sd^{4.70}$	0.54
Ru	2342	63.85	45.22	$sd^{4.31}$	0.59	16.69	$sd^{0.75}$	0.60
Os		94.86	69.03	$sd^{2.81}$	0.79	25.41	$sd^{1.67}$	0.67

C-H-σ^*

	IR	sum	ΔE^2_{ij}	hyb.	$\Delta\varepsilon_{ij}$	composition
unit	cm^{-1}	kcal/mol	kcal/mol		hartree	
Fe	2549	6.82	6.23	d	0.50	$0.56 * 3d_{xy} - 0.46 * 3d_{x^2-y^2} - 0.42 * 3d_{xz}$
Ru	2342	7.66	6.95	$sd^{6.95}$	0.47	$0.58 * 4d_{z^2} + 0.61 * 4d_{yz} + 0.38 * 4d_{xy}$
Os		8.36	7.41	$sd^{7.18}$	0.45	$0.53 * 5d_{yz} + 0.60 * 4d_{z^2} + 0.37 * 4d_{xy}$

tions as in the n-C_4H_9RuF and n-C_4H_9OsF the vacant LP orbitals of the metal atoms can also make strong interaction with the C-H-σ orbital. It indicates that the C-H-σ orbital interacts more preferably with M-F-σ^*-orbitals than with vacant LP orbitals of the metal atoms, which may be due to the directions or diffuseness of the orbitals.

- Due to relativistic effects valence d-orbitals of a 5d-element are more diffuse than that of a 4d-element and the energy of valence d-orbitals of a 5d-element are higher than that of a 4d-element. This can explain why the interaction between the M-F-σ^*-orbital and the C-H-σ orbital is stronger but the energy gap is larger in the n-C_4H_9OsF molecule in comparison to that in the n-C_4H_9RuF molecule.

- The other conclusion is the same as the previous sections that the interactions, which lead to donations from the C-H-σ orbital into vacant metal hybrid orbitals make the major contribution to the C-H activation, since it is largely stronger than interactions that lead to donations from the occupied metal hybrid orbitals into the C-H-σ^* orbital. But only energy gaps between the C-H-σ^* orbital

and occupied metal hybrid orbitals correlate properly with the C-H activations, therefore the later type of interactions should be the origin, which brings the craft to lead closer approaches of the C-H bonds to the metal atoms.

3.7.3 The triplet state(first excited state) and quintet state(ground state)

All of the data of the triplet state and the quintet state are shown in the appendix (Section A.4.2 and A.4.3).
The C-H bonds of the CH_3RuX molecules in the triplet state are in general less activated than that in the singlet state, and in the quintet state all the C-H bond are almost inactivated. This pattern can also be observed in the previous investigations that the C-H bonds are in general less activated in ground states than in excited states. In general one can see that energy gaps between C-H bonds and hybrid orbitals of metal atoms are lower in excited states than that in lower excited states or ground states. But changes of energy gaps between the C-H-σ orbital and vacant hybrid orbitals of the metal atoms are small, whereas changes of energy gaps between the C-H-σ^* orbital and occupied hybrid orbitals are more significant.
NPA comparison of the molecules in the triplet state is carried out in the appendix (Table A.98), showing the same conclusion as in the singlet state.

3.7.4 Summary

From the above investigations following conclusions from the Section 3.6 can be confirmed.

- The NPA comparisons show that in general the more a C-H bond is activated, the less positive the H atom of the C-H bond is, the more unpolar the C-H bond is.

- Under strong C-H activations interactions between the C-H-σ orbital and vacant metal hybrid orbitals are largely stronger than interactions between the C-H-σ^* orbital and occupied metal hybrid orbitals, therefore the first type of the interactions should make the major contribution to the C-H activation. Analysis of the interactions shows that the quick raising of overlaps and not the decrease of energy gaps between the interacting orbitals are the reason for the increasing

interaction strength, hence this type of interactions can not be the origin for the closer approach of the C-H bond to the metal atoms in such cases.

- With increasing C-H activations, energy gaps between the C-H-σ^* orbital and occupied hybrid LP orbitals of metal atoms decrease and should can be the reason for the closer approaches of the C-H bonds to the metal atoms.

Following new conclusions can be drawn from the investigations.

- The group 8 TM elements in the quintet state (ground state) of n-C_4H_9MF molecules show a very weak activation potential. In the triplet state (first excited state) the Ru and Os atoms show a very strong C-H activation potential of the δ-C-H bond, but the Fe atom show a very weak activation potential. In the singlet state (second excited state) all the group 8 TM elements show a very strong activation potential. Therefore it is assumed that catalytic C-H functionalizations mediated group 8 transition metals should occur rather in low spin configurations.

- In comparison to the σ-ligands (F, Cl, Br, I) the CN^--group can via the π-backbonding, which reduces electronic density of the metal atom, lead to large the energy gap between C-H-σ^* orbital and an occupied hybrid orbital of the Ru atom in the CH_3RuCN molecule. And this π-backbonding can probably also affect the energy of the vacant M-CN-σ^* orbital, which leads to a varied C-H bond activation of CN^--group in comparison to the other X-groups.

- Due to relativistic effects valence d-orbitals of a 5d-element are more diffuse and energetically higher than that of a 4d-element. This can explain why the interaction between the M-F-σ^*-orbital and the C-H-σ orbital is stronger but the energy gap is larger in the n-C_4H_9OsF molecule in comparison to the n-C_4H_9RuF molecule.

- The interaction between the M-F-σ^*-orbital and the C-H-σ orbital is in general the most important interaction for the C-H activation. Under very strong C-H activations such as in the singlet state of the n-C_4H_9RuF and n-C_4H_9OsF molecules the vacant LP orbitals of the metal atoms can also make strong interaction with the C-H-σ orbital. It indicates that C-H-σ orbital interacts preferably with M-F-σ^*-orbitals than with vacant LP orbitals of the metal atoms, which can be due to directions or diffuseness of the orbitals.

3.8 Group 9 transition metal elements

3.8.1 Enthalpy comparison of the different spin states

Table 3.65: Enthalpy and IR frequency comparisons of the quartet and the doublet states of the CH_3RhX molecules, all the enthalpies are calculated at the B3LYP/def2-TZVP/def2-ecp levels (sums of electronic and thermal enthalpy) and presented as differences to the ground state at the corresponding absolute minimum of the molecules without zero-point corrections. IR column shows stretching frequencies of the most activated C-H bond, which stands trans to the Rh-X bond.

	quartet		doublet	
$MoCH_3X$	enthalpy	IR	enthalpy	IR
unit	kJ/mol	cm^{-1}	kJ/mol	cm^{-1}
CN	0	3116	106.6	2933
F	0	2999	23.9	2950
Cl	0	3095	45.6	2953
Br	0	3096	49.3	2950
I	0	3102	56.0	2949

Enthalpies and IR frequencies of the CH_3RhX molecules (X= CN, F, Cl, Br, I) are summarized in Table 3.65 showing that the quartet state of the molecules is the ground state and the doublet state is the excited state. Enthalpy comparisons of the n-C_4H_9RhF molecules reveals the same conclusion.
Since the trans C-H bonds in the CH_3RhX molecules are in general almost inactivated, only analyse about the doublet state are explicitly described, and differences to the quartet state will be just briefly discussed.

3.8.2 The doublet state (first excited state)

3.8.2.1 CH_3RhX-system

We take the Figure 3.5 as the structure for the CH_3RhX-molecules and also the fixation of the cartesian axis, since all the CH_3RhX molecules (X= CN, F, Cl, Br, I) take staggered form as their absolute minimum, which is similar to the CH_3NbF molecule. Structure, bond-order and occupancy comparisons of the trans C-H bond in the CH_3RhX molecules are shown in the appendix (Table A.112), which shows almost no clue about the main factor impacting C-H activation of the trans C-H bonds, perhaps due to the too small C-H activation differences. The discrepancies of calculated IR frequencies should be over $5cm^{-1}$, hence the sequence of the stretching frequencies of trans C-H bond in the CH_3RhX molecules should be critically used.

Table 3.66: The leading interactions between the C-H-σ^* orbital and the occupied hybrid orbital of the Rh atom in the CH_3RhX molecules. α-spin table records interactions in the α-spin system, and so on. IR gives stretching frequencies of the trans C-H bonds. ΔE_{ij}^2 column gives second-order perturbative estimations of the hyperconjugation, hyd. column shows hybridizations of the NHO of the metal atom, which is participated in the interaction, $\Delta\varepsilon_{ij}$ gives energy gaps of the interacting NBOs. Composition column shows orbital compositions of the Rh NHO. Sum column gives sums of this type of interactions.

α-spin						
	IR	sum	ΔE_{ij}^2	hyb.	$\Delta\varepsilon_{ij}$	composition
unit	cm^{-1}	kcal/mol	kcal/mol		hartree	
CN	2966	1.55	0.84	d	0.64	$0.99 * 4d_{xy}$
Cl	2953	1.70	1.08	d	0.63	$0.98 * 4d_{xy}$
I	2949	1.70	1.03	d	0.63	$0.98 * 4d_{xy}$
β-spin						
	IR	sum	ΔE_{ij}^2	hyb.	$\Delta\varepsilon_{ij}$	composition
unit	cm^{-1}	kcal/mol	kcal/mol		hartree	
CN	2966	1.45	0.88	d	0.63	$0.98 * 4d_{xy}$
Cl	2953	1.59	1.14	d	0.61	$0.95 * 4d_{xy}$
I	2949	1.64	1.12	d	0.61	$0.96 * 4d_{xy}$

Under weak C-H activations in this case interactions between the C-H-σ^* orbital and occupied hybrid LP orbitals of the Rh atom are stronger than that between the C-H-σ orbital and vacant Rh hybrid orbitals, therefore only the first type of interactions are shown here in Table 3.66, the later type of interactions are shown in the appendix

(Table A.113). Observations got from the Table 3.66 are that the Rh atom prefers to use occupied valence d orbitals to interact with the C-H-σ^* orbital by initial approaches of the C-H bond to the metal atom. In such case the later type of interactions are very weak, and the most important interaction of this type of interactions is in general the interaction between C-H-σ orbital and the Rh-X-σ^* orbital. This observation can also confirm the conclusions drawn from previous investigations.

3.8.2.2 Group trends in the CH_3MF molecules

Table 3.67: The leading interaction between the C-H-σ^* orbital and the hybrid orbital of the metal atoms in the CH_3MF molecules. α-spin table records interaction information in the α-spin, and so on. IR^t gives stretching frequencies of the trans C-H bonds. ΔE^2_{ij} column gives second-order perturbative estimations of the hyperconjugation, hyd. column shows hybridizations of the NHO of the metal atom, which is participated in the interaction, $\Delta\varepsilon_{ij}$ gives energy gaps of the interacting NBOs. Composition column shows orbital compositions of the Rh NHO. Sum column gives sums of this type of interactions.

α-spin

	IR	sum	ΔE^2_{ij}	hyb.	$\Delta\varepsilon_{ij}$	composition
unit	cm^{-1}	kcal/mol	kcal/mol		hartree	
Co	3079	0.79	0.45	d	0.74	$-0.98 * 3d_{xz}$
Rh	2950	1.78	1.21	d	0.62	$-0.96 * 4d_{xy}$
Ir	2259	7.76	3.64	$sd^{1.94}$	0.67	$0.58 * 6s + 0.60 * 5d_{z^2} - 0.48 * 5d_{xy}$

β-spin

	IR	sum	ΔE^2_{ij}	hyb.	$\Delta\varepsilon_{ij}$	composition
unit	cm^{-1}	kcal/mol	kcal/mol		hartree	
Co	3079	0.50	0.32	d	0.69	$0.76 * 3d_{yz} - 0.57 * 3d_{xz}$
Rh	2950	1.61	1.22	d	0.60	$-0.92 * 4d_{xy}$
Ir	2259	7.04	4.35	$sd^{4.23}$	0.49	$0.44 * 6s - 0.76 * 5d_{x^2-y^2} - 0.46 * 5d_{xy}$

Only the leading interaction between the C-H-σ^* orbital and hybrid orbitals of the metal atoms in the CH_3MF molecules are shown in the Table 3.67. Since interactions between the C-H-σ orbital and hybrid orbitals of the metal atoms are small except in the CH_3IrF molecule and do not correlate properly with C-H activations, therefore will only be shown in the appendix (Table A.115). Both interaction strength and energy gaps between the C-H-σ^* orbital and occupied hybrid orbital correlate properly with C-H actions. The only irregularity, which is occurred in energy gaps of the interaction in the α-spin, is probably due to different assignments of NBO processes, in the CH_3RhF molecules the orbital accords to a Rh-C-σ orbital, the corresponding orbitals in the CH_3IrF and CH_3CoF molecules are LP orbitals of the metal atoms.

Again the increased interaction between the C-H-σ^* and metal occupied orbital in the Ir case is the driving force for the metal atom and C-H bond coming close, then the increased overlap between C-H-σ and vacant metal-centered orbitals takes over and leads to the strong activations.

3.8.2.3 Group trends in the *n*-C_4H_9MF molecules

Structure, bond-order and occupancy analyse of the C-H bond in the *n*-C_4H_9MF molecules as shown in the appendix (Table A.116) indicating that both donations from the C-H-σ orbital and donations into the C-H-σ^* orbital can induce C-H activations.

Table 3.68: The leading interaction between the C-H-σ^* orbital and the hybrid orbital of the metal atoms in the *n*-C_4H_9MF molecules. IR gives stretching frequencies of the δ-C-H bonds. ΔE^2_{ij} column gives second-order perturbative estimations of the hyperconjugation, hyd. column shows hybridizations of the NHO of the metal atom, which is participated in the interaction, $\Delta\varepsilon_{ij}$ gives energy gaps of the interacting NBOs. Composition column shows orbital compositions of the Rh NHO. Sum column gives sums of this type of interactions.

α-spin						
	IR	sum	ΔE^2_{ij}	hyb.	$\Delta\varepsilon_{ij}$	composition
unit	cm^{-1}	kcal/mol	kcal/mol		hartree	
Co	2878	0.43	0.39	d	0.66	$0.71 * 3d_{z^2} - 0.55 * 3d_{yz}$
Rh	2465	5.38	4.91	d	0.52	$0.86 * 4d_{xy} - 0.45 * 4d_{yz}$
Ir	2326	8.85	8.02	d	0.49	$0.50 * 5d_{z^2} + 0.68 * 5d_{yz}$
β-spin						
	IR	sum	ΔE^2_{ij}	hyb.	$\Delta\varepsilon_{ij}$	composition
unit	cm^{-1}	kcal/mol	kcal/mol		hartree	
Co	2878	1.92	1.50	d	0.64	$-0.82 * 3d_{x^2-y^2} + 0.39 * 3d_{xy}$
Rh	2465	5.00	4.50	d	0.51	$0.71 * 4d_{yz} + 0.57 * 4d_{xy}$
Ir	2326	4.50	3.83	$sd^{7.18}$	0.48	$0.65 * 5d_{z^2} + 0.65 * 5d_{xy}$

The leading interaction between the C-H-σ^* orbital and the hybrid orbital of the metal atoms in the *n*-C_4H_9MF (M=Co, Rh, Ir) molecules are shown in Table 3.68. Interactions between the C-H-σ orbital and the vacant hybrid orbital of the metal atoms are shown in the appendix (Table A.117), although they are stronger than the first type of interactions, but with energy gaps between the interacting orbitals the question can not be explained, why the C-H bond tend to mover closer to the metal atom under stronger C-H activations. Only by using energy gaps between the C-H-

σ^* orbital and occupied hybrid LP orbitals of the metal atoms this question can be answered.

3.8.3 The quartet state (ground state)

All of data of the quartet state are shown in the appendix (A.5.2). C-H bonds of the CH_3RhX molecules in the quartet state are almost inactivated. Such pattern can also be observed in previous sections that C-H bonds are in general less activated in ground states than in excited states.
In comparison to the doublet state interactions between between C-H bonds and hybrid orbitals of metal atoms decrease largely, energy gaps between the C-H-σ orbital and vacant hybrid orbitals of the metal atoms change only slightly, energy gaps between the C-H-σ^* orbital and occupied hybrid orbitals increase more significantly, which can be identified as the origin for the C-H activation difference between different states.

3.8.4 Summary

From the above investigations firstly following conclusions from the previous sections can be confirmed.

- The NPA comparisons show that in general the more a C-H bond is activated, the less positive the H atom of the C-H bond is, the more unpolar the C-H bonds is.

- Only changes of energy gaps between the C-H-σ^* orbital and occupied metal hybrid orbitals correlate rightly with C-H activations indicating that interactions between the C-H-σ^* orbital and occupied metal hybrid orbitals are probably the origin for closer approach of a C-H bond to the metal atoms by C-H activations.

Following conclusions can be drawn from the investigation .

- The group 9 TM elements in the quartet state of n-C_4H_9MF molecules show a very weak activation potential, but in the doublet state Rh and Ir atoms shows a very strong activity of the δ-C-H bond and a very high selectivity that the α-C-H bond is almost inactivated, the Fe atom in the doublet state shows a less high activity and selectivity. Therefore it indicates that a C-H bond functionalization using Rh or Ir as catalyst are most probably occurred in the doublet state (excited state).

- By initial approach of a C-H bond to a metal atom occupied valence d-orbitals of the metal atoms are prefered to interact with C-H-σ^* orbital. In this stage interactions between the C-H-σ orbital and vacant hybrid orbitals of the metal atoms are still weak. With further approaching of the C-H bond to metal atoms the most important interaction of the later type of interactions, which is the occurred between the C-H-σ orbital and the M-F-σ^* orbital, increase more quickly than the first type of interactions.

3.9 Group 10 transition metal elements

3.9.1 Enthalpy comparisons of the different states

Table 3.69: Enthalpy and IR frequency comparisons of the CH_3PdX molecules in different states, all the enthalpies are calculated at the B3LYP/def2-TZVP/def2-ecp levels (sums of electronic and thermal enthalpy) and presented as differences to the ground state at the corresponding absolute minimum of the molecules without zero-point corrections. IR column shows stretching frequencies of the most activated C-H bond, which stands trans to the Pd-X bond.

	singlet		triplet	
CH_3PdX	enthalpy	IR	enthalpy	IR
unit	kJ/mol	cm^{-1}	kJ/mol	cm^{-1}
CN	0	2995	107.7	3030
F	0	2998	47.7	3016
Cl	0	2988	75.0	3022
Br	0	2985	81.3	3024
I	0	2982	89.0	3025

Enthalpies and IR frequencies of the CH_3PdX molecules (X= CN, F, Cl, Br, I) are summarized in Table 3.69, showing that the singlet state of the molecules is the ground state and the triplet state is the corresponding first excited state. This is unique in all the investigated CH_3MX molecules that the ground state of molecules is the state with the lower spin , and it shows a inverse ligand effects on the C-H activation in the different spin states.

Enthalpy comparisons of the n-C_4H_9PdF molecules reveals also that the singlet state is the ground state and the triplet state is the first excited state.

Since the trans C-H bonds of the CH_3PdX molecules are more activated in the singlet state (ground state), only the singlet state are explicitly analyzed.

3.9.2 The singlet state (ground state)

3.9.2.1 CH_3PdX-system

We take the Figure 3.5 as the structure of the CH_3PdX-molecules, since all the CH_3PdX molecules (X= CN, F, Cl, Br, I) take staggered form as their absolute minimum, which is similar to the CH_3NbF molecule.
Structure, bond-order and occupancy comparisons of the trans C-H bond in the CH_3PdX molecules are shown in the appendix (Table A.125) indicating that the C-H activation of the trans C-H bonds can be probably induced by occupancy changes of the C-H-σ orbital.
One can see that the Pd atom shows a very weak C-H activations potential in the molecules, which is inconsistent with the general knowledge that Pd atoms are the most used transition metal for catalytic C-H functionalization processes. This phenomenon probably indicates that the general usages of Pd containing catalysts for C-H functionalizations are due to high selectivities not activities of Pd atoms.
Investigations of interactions between trans C-H bond and the metal atom shows that

Table 3.70: The leading interactions between the C-H-σ^* orbital and the occupied hybrid orbital of the Pd atom in the CH_3PdX molecules. IR gives stretching frequencies of the trans C-H bonds. ΔE^2_{ij} column gives second-order perturbative estimations of the hyperconjugation, hyd. column shows hybridizations of the NHO of the metal atom, which is participated in the interaction, $\Delta\varepsilon_{ij}$ gives energy gaps of the interacting NBOs. Composition column shows orbital compositions of the Pd NHO. Sum column gives sums of this type of interactions.

			NBO1(LP)			NBO2(M-X-σ)		
	IR	sum	ΔE^2_{ij}	hyb.	$\Delta\varepsilon_{ij}$	ΔE^2_{ij}	hyb.	$\Delta\varepsilon_{ij}$
unit	cm^{-1}	kcal/mol	kcal/mol		hartree	kcal/mol		hartree
F	2998	2.77	1.45	d	0.66	0.88	$sd^{1.22}$	0.73
CN	2995	2.59	0.96	d	0.68	0.91	$sd^{1.33}$	0.75
Cl	2988	2.77	1.39	d	0.66	0.89	$sd^{1.47}$	0.74
Br	2985	2.81	1.38	d	0.66	0.86	$sd^{1.55}$	0.74
I	2982	2.80	1.34	d	0.66	0.80	$sd^{1.63}$	0.75

interactions between the C-H-σ^* orbital and the occupied hybrid orbital are stronger than interactions between the C-H-σ orbital and the vacant hybrid orbital, which is consistent with the conclusion drawn by the previous investigations that first type of interactions should make the major contribution under weak C-H activations, but is inconsistent with the conclusion got from the occupancy analysis.

Only the first type of interactions is shown here in the Table 3.70, the second type of interactions are shown in the appendix (Table A.126). The NBO1 in the Table 3.70 is a $4d_{xy}$ orbital of the Pd atom, NBO2 is a M-X-σ orbital. Since stretching frequencies of the trans C-H bond vary only slightly, interactions and energy gaps between the C-H-σ^* orbital and the occupied hybrid orbital is almost unvaried. However one can clearly recognize that the cyanid group via π-backbonding degrades the interactions between the C-H-σ^* orbital and the occupied LP orbitals of the Pd atom.

3.9.2.2 Group trends in the CH_3MF molecules

Structure, bond-order and occupancy comparisons of the C-H bond in the CH_3MF (M=Ni, Pd, Pt) are shown in the appendix (Table A.128) indicating that both donations from C-H-σ orbital into the metal atoms and donations from the metal atoms into the C-H-σ^* orbital can induce the C-H activation.

Table 3.71: The leading interaction between the trans C-H bond and the metal atoms in the CH_3MF molecules. C-H-σ table records interactions between the C-H-σ orbital and the hybrid orbital of the metal atoms, and so on. IR^t gives stretching frequencies of the trans C-H bonds. ΔE^2_{ij} column gives second-order perturbative estimations of the hyperconjugation, hyd. column shows hybridizations of the NHO of the metal atom, which is participated in the interaction, $\Delta\varepsilon_{ij}$ gives energy gaps of the interacting NBOs. Composition column shows orbital compositions of the Pd NHO. Sum column gives sums of this type of interactions. M(coe) column shows polarization coefficients of the M-F-σ^* orbital, and so on.

C-H-σ

	IR	sum	ΔE^2_{ij}	hyb.	$\Delta\varepsilon_{ij}$	composition	M(coe)	F(coe)
unit	cm^{-1}	kcal/mol	kcal/mol		hartree			
Ni	2958	2.20	1.86	$sd^{1.29}$	0.50	$0.66*4s-0.69*3d_{x^2-y^2}$	-0.92	0.40
Pd	2998	0.96	0.56	$sd^{1.00}$	0.54	$0.70*5s+0.69*4d_{x^2-y^2}$	-0.91	0.42
Pt	2909	4.25	4.18	$sd^{1.04}$	0.57	$0.64*6s-0.61*5d_{x^2-y^2}$	-0.88	0.47

C-H-σ^*

	IR	sum	ΔE^2_{ij}	hyb.	$\Delta\varepsilon_{ij}$	composition
unit	cm^{-1}	kcal/mol	kcal/mol		hartree	
Ni	2958	2.68	0.96	d	0.67	$-0.96*3d_{xy}$
Pd	2998	2.77	1.45	d	0.66	$-0.96*4d_{xy}$
Pt	2909	3.78	2.66	d	0.64	$-0.91*5d_{xy}$

The leading interaction between the trans C-H bond and the metal atoms in the CH_3MF molecules are shown in the Table 3.71 indicating that interactions between

the C-H-σ^* orbital and occupied hybrid orbitals of the metal atoms should be the origin for the C-H activation, since only strengths and energy gaps of this type of interactions correlate properly with the C-H activations. This observation confirms also the conclusion that interactions between the C-H-σ^* orbital and occupied hybrid orbital of the metal atoms should makes the major contribution under weak C-H activations.

3.9.2.3 Group trends in the *n*-C_4H_9MF molecules

Bond-order and occupancy analyse of the C-H bond in the *n*-C_4H_9MF molecules as shown in the appendix (Table A.129) indicating that both donations from the C-H-σ orbital and donations into the C-H-σ^* orbital can induce the C-H activations.

Table 3.72: The leading interaction between the C-H bond and the metal atoms in the *n*-C_4H_9MF molecules. C-H-σ table records interactions between the C-H-σ orbital and the hybrid orbital of the metal atoms, and so on. NBO1 gives calculated data of the NBO1. IR gives stretching frequencies of the δ-C-H bonds. ΔE^2_{ij} column gives second-order perturbative estimations of the hyperconjugation, hyd. column shows hybridizations of the NHO of the metal atom, which is participated in the interaction, $\Delta\varepsilon_{ij}$ gives energy gaps of the interacting NBOs. Composition column shows orbital compositions of the Pd NHO. Sum column gives sums of this type of interactions.

C-H-σ

	IR	sum	ΔE^2_{ij}	hyb.	$\Delta\varepsilon_{ij}$	composition	M(coe)	F(coe)
unit	cm^{-1}	kcal/mol	kcal/mol		hartree			
Ni	2596	23.90	23.72	$sd^{1.03}$	0.58	$-0.70*4s+0.70*3d_{x^2-y^2}$	-0.93	0.37
Pd	2525	30.11	30.08	$sd^{0.97}$	0.59	$-0.71*5s+0.69*4d_{x^2-y^2}$	-0.92	0.40
Pt	2064	68.39	67.85	$sd^{1.10}$	0.61	$-0.69*6s+0.69*3d_{x^2-y^2}$	-0.90	0.43

C-H-σ^*

	IR	sum	ΔE^2_{ij}	hyb.	$\Delta\varepsilon_{ij}$	composition
unit	cm^{-1}	kcal/mol	kcal/mol		hartree	
Ni	2596	7.56	6.65	d	0.52	$-0.91*3d_{yz}+0.30*3d_{xy}$
Pd	2525	9.07	8.15	d	0.54	$-0.92*4d_{yz}+0.39*4d_{xy}$
Pt	2064	20.02	18.70	d	0.49	$-0.92*5d_{yz}+0.37*5d_{xy}$

The leading interaction between the δ-C-H-bond and the metal atoms in the *n*-C_4H_9MF (M=Ni, Pd, Pt) molecules are summarized in the Table 3.72 indicating that strength of the both type of interactions correlate properly with C-H activation. The interactions, which lead to the donation from the C-H-σ orbital into vacant metal hybrid orbitals (with strong (n+1)s contribution) make the major contribution to the C-H activation, since it is more stronger than the interactions that lead to the donations from the occupied metal hybrid orbitals (almost pure metal nd type) into

the C-H-σ^* orbital. However with energy gaps of the both type of interactions the C-H activation difference can not be interpreted in this case.

3.9.3 The triplet state (first excited state)

All of data of the triplet state are shown in the appendix (A.6.2).
In the triplet state only interactions between the C-H-σ^* orbital and occupied hybrid orbital of the metal atoms in the α-spin and interactions between the C-H-σ orbital and vacant hybrid orbital of the metal atoms in the β-spin are significant, since all the valence d-orbital in the α-spin are occupied and only in the β-spin there are empty valence d-orbitals. Compared with molecules in the singlet state, strength of interactions decrease in the triplet state, but energy gaps of the second type of interactions decrease, which can be excluded as the reason for the weakened C-H activation in the triplet state. Only with the energy gaps between C-H-σ^* orbital and occupied hybrid orbital of the metal atoms the C-H activation difference in different spin states can be well interpreted.

3.9.4 Summary

With the investigations, firstly the following conclusions can be confirmed that under strong C-H activations interactions between the C-H-σ orbital and vacant metal hybrid orbitals are largely stronger than interactions between the C-H the C-H-σ^* orbital and occupied metal hybrid orbitals, therefore the first type of the interactions should make the major contribution to strong C-H activations. however only energy gaps between the C-H-σ^* orbital and occupied metal hybrid orbitals decrease with raising C-H activations, which should lead to the initial approach of the C-H bonds to the metal atoms.
Following new conclusions can be drawn from the investigation: The group 10 TM elements show a very weak activation potential except the Pt atom in the triplet state (first excited state) of n-C_4H_9MF molecules.
In the singlet state (ground state) all the group 10 transition metal show high activity and selectivity in the n-C_4H_9MF molecules. This phenomenon that the C-H bond is more activated in the ground state than in the excited state, is unique in all the investigations.

4 Conclusions and outlook

According to the NBO analysis, C-H activations can be approximately divided into three stages.

- In the first stage the C-H bond will be only weakly activated, it's calculated IR stretching frequency lies over 2950 cm^{-1} (the experimental frequency should be approximately over 2900 cm^{-1}).
  The hydrogen atom of the C-H bond approaches initially to metal atoms and interactions between C-H-σ^* orbital and occupied hybrid orbitals of the metal atom make the dominant contribution to C-H activations. Therefore high energies of occupied valence orbitals of the metal atom promotes the C-H activations. However this type of interactions increases largely slower than interactions between C-H-σ orbitals and M-F-σ^* orbitals.
  Such weak C-H activations mostly occur in the CH_3MX molecules, which M include all transition metal elements investigated in this thesis except group 6 elements.

- In the next stage with closer approach of C-H bonds to metal atoms, the later type of interactions have the dominant influence on C-H activations, the C-H bond will be strongly activated, it's calculated IR stretching frequency lies between 2500 to 2950 cm^{-1}.
  The latter type of interactions should make the major contribution to the C-H activations, however the rise of the interaction strength is due to increasing overlaps of the interacting orbitals. A strict decrease of the energy gaps of the interacting orbitals with the rise of the interaction strength, which proportionate with C-H activation, can not be observed.
  An interesting point is that the energy gaps of the first type interactions decrease with rise of the C-H activation strength in general and comparisons of C-H activations in different spin states show also that those energy gaps should be

the origin for the C-H activation difference. Therefore high energies of the the occupied hybrid orbitals of the metal atom should promote the C-H activations, but a low energy of the M-F-σ^* orbital can also contribute.
Such strong C-H activations can be observed in most of the n-C_4H_9MF molecules.

- With further approaches of C-H bonds to metal atoms, the C-H bonds will be further activated, it's calculated IR stretching frequency shifts under 2500 cm^{-1}, another important type of interactions between C-H-σ orbital and vacant hybrid LP orbitals come up beside the former two types of interactions. This indicates that M-F-σ^* orbitals are more favorable than vacant hybrid LP orbitals of the metal atoms to interact with the C-H-σ orbital.
Such very strong C-H activations can be observed for example in the singlet CH_3MX molecules (M is group 6 TM elements) and in the n-C_4H_9MF molecules, where M are electron rich group 6 to group 10 TM elements.

The investigations of CH_3MX molecules shows that ligand impacts on C-H activations can in general not be predicted, since there are two coadjutant factors, which make conflicting impacts on C-H activations. One of them is the energy of the M-X-σ^* orbital, the more electron negative the X-ligand is, the higher the energy gap between M-X-σ^* orbital and C-H-σ orbital gets leading to weaker interactions by same orbital overlaps. The other factor is polarizations of the M-X-σ^* orbital, which shows an opposite effect due to overlaps between the interacting orbitals.

The two-state reactivity (TSR) model proposes that a excited state can be less stable but more reactive than a ground state, because energy barriers associated with the rate-determining steps is lower. In the investigations one can see that energy differences between a spin state and the next excited states are about 50kJ/mol, however in the excited state hyperconjugations between the C-H bond and the metal atoms increase in about the same order or in most instances larger than the energy difference between two different spin states, except in molecules with group 10 transiton metal atoms. This indicates that C-H functionalization reactions should normally preferably occur in the excited state, since energy barriers associated with the rate-determining step is lower. The TSR mechanisms should be mainly a favored picture for catalytic C-H functionalization reactions mediated transition metal atoms.

Comparisons of NPAs of C-H bonds shows that the more a C-H bond is activated, the less positive is the H atom of the C-H bond, and in general more unpolar the C-H bond is. Since all hyperconjugations between C-H bonds and transition metal

atoms should lead to a reduction of the C-H bond polarity. In other sides experimental chemists generally use a proper base to abstract hydrogen atoms in order to accelerate catalytic C-H functionalization processes or modify reaction conditions. Is using a base to abstract the hydrogen atoms in such cases the right way?

In all the investigated molecules transition metals exhibit a formal oxidation state of 2+, therefore transition metals in other oxidation states can also be important for the C-H activation. In this thesis ligands are not completely investigated, oxygen-, nitrogen- and phosphor- containing ligands are especially desirable in the reactions. All these general research can lead to rational choices about how to modify existing catalysts and design new catalysts.

Dedication

This dissertation is dedicated to the support of my family.

My thanks and appreciation to Prof. Dr. Christoph van Wüllen for persevering with me as my advisor through out the time. He encouraged me to complete this research and write the dissertation. His generously shared knowledge, insights and advice supported and expanded my work.
I am grateful to Dr. Markus Mang who advised and supported my research.
My thanks must as well go to all persons who help me to write this dissertation, especially to Jonathan Meyer, Jie Tang and Patrick Jost.
The members of my dissertation committee, Prof. Dr. Markus Gerhards and Prof. Dr. Stefan Ernst, have generously given their time. I thank them for their contribution and their good-natured support.

5 Eidestattliche Erkärung

Hiermit erkläre ich, dass ich die vorliegende Arbeit selbständig angefertigt und keine anderen als die von mir anggegebenen Quellen und Hilfmittel benutzt habe.

Ich versichere außerdem, dass diese Dissertation weder in gleicher noch in anderer Form bereits in einem anderen Prüfverfahren vorgelegen hat.

Bibliography

[1] D. Schröder, H. Schwarz, *Proc. Natl. Acad. Sci. U. S. A.* **2008**, *105*, 18114–18119.

[2] R. G. Bergman, *Nature* **2007**, *446*, 391–393.

[3] J. A. Labinger, J. E. Bercaw, *Nature* **2002**, *417*, 507–514.

[4] M. Lersch, M. Tilset, *Chem. Rev.* **2005**, *105*, 2471–2526.

[5] X. Chen, J.-Q. Yu, *Angew. Chem. Int. Ed.* **2009**, *48*, 5094–5115.

[6] F. Shi, R. C. Larock, *Top. Curr. Chem.* **2010**, *292*, 123–164.

[7] W. Yoo, C. Li, *Top. Curr. Chem.* **2010**, *292*, 281–302.

[8] T. W. Lyons, M. S. Sanford, *Chem. Rev.* **2010**, *110*, 1147–1169.

[9] R. Giri, J. Liang, J.-Q. Yu, *Ang. Chem. Int. Ed.* **2005**, *44*, 7420–7424.

[10] J. F. Hartwig, *Nature* **2008**, *455*, 314–322.

[11] N. R. Deprez, M. S. Sanford, *J. Am. Chem. Soc.* **2009**, *131*, 11234–11241.

[12] N. Sasamoto, M. Sodeoka, *J. Am. Chem. Soc.* **2006**, *128*, 14010–14011.

[13] S. Lin, Z.-J. Shi, *J. Am. Chem. Soc.* **2008**, *130*, 12901–12903.

[14] M. R. Netherton, G. C. Fu, *J. Am. Chem. Soc.* **2001**, *123*, 10099–10100.

[15] D. Leow, G. Li, J.-Q. Yu, *Nature* **2012**, *486*, 518–522.

[16] D. Balcells, O. Eisenstein, *Chem. Rev.* **2010**, *110*, 749–823.

[17] Z. Boutadla, A. Poblador-Bahamonde, *Dalton Trans.* **2009**, 5820–5831.

[18] K. Mylvaganam, N. S. Hush, *J. Am. Chem. Soc.* **2000**, *122*, 2041–2052.

[19] E. M. Siegbahn, R. H. Crabtree, *J. Am. Chem. Soc.* **1996**, *118*, 4442–4450.

[20] H. Zhu, T. Ziegler, *Organometallics* **2007**, *26*, 2277–2284.

[21] H. Zhu, T. Ziegler, *Organometallics* **2008**, *27*, 1743–1749.

[22] H. Zhu, T. Ziegler, *Organometallics* **2009**, *28*, 2773–2777.

[23] H. Arakawa, W. Tumas, *Chem. Rev.* **2001**, *101*, 953–996.

[24] R. A. Periana, C. Jones, V. R. Ziatdinov, *J. Mol. Catal. A* **2004**, *220*, 7–25.

[25] T. M. Gilbert, T. Ziegler, *Organometallics* **2001**, *20*, 1183–1189.

[26] M. Ahlquist, W. A. Goddard, *Chem. Commun.* **2009**, *17*, 2373–2375.

[27] R. P. Muller, D. M. Philipp, *Top. Catal.* **2003**, *23*, 81–98.

[28] K. J. H. Young, R. A. Periana, *Chem. Commun.* **2009**, *22*, 3270–3272.

[29] S. Chempath, A. T. Bell, *J. Am. Chem. Soc.* **2006**, *128*, 4650–4657.

[30] A. J. Cowan, M. W. George, *Proc. Natl. Acad. Sci. U. S. A.* **2007**, *104*, 6933–6938.

[31] E. P. Wasserman, C. B. Moore, R. G. Bergman, *Science* **1992**, *255*, 315–318.

[32] W. H. Bernskoetter, C. K. Schauer, M. Brookhart, *Science* **2009**, *326*, 553–556.

[33] M. Brookhart, M. Green, *J. Organomet. Chem.* **1983**, *250*, 395–408.

[34] W. Scherer, G. S. McGrady, *Angew. Chem.* **2004**, *116*, 1816–1842.

[35] M. Brookhart, G. Parkin, *Proceedings of the National Academy of Sciences* **2007**, *104*, 6908–6914.

[36] Y. Zhang, J. C. Lewis, E. Oldfield, *Organometallics* **2006**, *25*, 3515–3519.

[37] W. E. Rhine, G. Stucky, S. W. Perterson, *J. Am. Chem. Soc.* **1975**, *97*, 6401–6406.

[38] R. M. Badger, *J. Chem. Phys.* **1935**, *3*, 710–714.

[39] D. C. McKean, *Int. J. Chem. Kinet.* **1989**, *21*, 445–464.

[40] W. E. Broderick, J. I. Legg, *Inorg. Chem.* **1991**, *30*, 3875–3881.

[41] G. von Frantzius, J. Grunenberg, *Organometallics* **2006**, *25*, 118–121.

[42] M. Bortolin, H. Ruegger, S. Trofimenko, *Organometallics* **1992**, *11*, 2514–2521.

[43] F. Weinhold, C. Landis, *Valency and Bonding*, Cambridge university press, Cambridge, **2005**.

[44] E. Glendening, F. Weinhold, *NBO 5.9*, **2009**, http://www.chem.wisc.edu/ nbo5.

[45] F. Weigend, H. Patzelt, R. Ahlrichs, *Chem. Phys. Lett.* **1998**, *294*, 143–152.

[46] D. Andrae, H. Preuß, *Theor. Chim. Acta* **1990**, *77*, 123–141.

[47] D. Schröder, H. Schwarz, *Acc. Chem. Res.* **2000**, *33*, 139–145.

[48] H. Hirao, S. Shaik, *J. Am. Chem. Soc.* **2006**, *128*, 8590–8606.

[49] S. Dhuri, Y. Wang, S. Shaik, *Angew. Chem. Int. Ed.* **2008**, *47*, 3356–3359.

[50] S. Dhuri, Y. Wang, S. Shaik, *Angew. Chem. Int. Ed.* **2009**, *48*, 1291–1295.

[51] D. Schröder, H. Schwarz, *J. Phys. Chem.* **1994**, *98*, 68–70.

[52] D. E. Clemmer, P. B. Armentrout, *J. Phys. Chem.* **1994**, *98*, 6522–6529.

[53] G. Raabe, J. Fleischhauer, *J. Am. Chem. Soc.* **1996**, *118*, 4622–4630.

[54] P. J. Wagner, B. J. Scheve, *J. Am. Chem. Soc.* **1977**, *99*, 1858–1863.

[55] V. Pophristic, L. Goodman, *Nature* **2001**, *411*, 565–568.

[56] F. Bohlmann, *Angew. Chem.* **1957**, *69*, 641–642.

[57] R. S. Mulliken, W. G. Brown, *J. Am. Chem. Soc.* **1941**, *63*, 41–56.

[58] R. S. Mulliken, *J. Chem. Phys.* **1393**, *7*, 339–352.

[59] M. Lein, *Coord. Chem. Rev.* **2009**, *253*, 625–634.

[60] S. E. Wheeler, W. D. Allen, *J. Am. Chem. Soc.* **2009**, *131*, 2547–2560.

[61] F. M. Bickelhaupt, E. J. Baerends, *Angew. Chem.-Int. Edit.* **2003**, *42*, 4183–4188.

[62] Y. Mo, W. Wu, J. Gao, *Angew. Chem.-Int. Edit.* **2004**, *43*, 1986–1990.

[63] Y. Mo, L. Song, Q. Zhang, *J. Am. Chem. Soc.* **2004**, *126*, 3974–3982.

[64] A. E. Reed, F. Weinhold, *J. Chem. Phys.* **1985**, *83*, 1736–1740.

[65] A. E. Reed, L. A. Curtiss, F. Weinhold, *Chem. Rev.* **1988**, *88*, 899–926.

[66] I. V. Alabugin, T. A. Zeidan, *J. Am. Chem. Soc.* **2002**, *124*, 3175–3185.

[67] F. Weinhold, C. Landis, *Discovery Chemistry With Natural Bond Orbitals*, Wileys, Hoboken, NJ, USA, **2012**.

[68] E. D. Glendening, F. Weinhold, *J. Comput. Chem.* **2013**, *34*, 1429–1437.

[69] A. E. Reed, F. Weinhold, *J. Chem. Phys.* **1985**, *83*, 735–746.

[70] F. Weinhold, J. E. Carpenter, *J. Mol. Struct.: THEOCHEM* **1988**, *165*, 189–202.

[71] P. Löwdin, *J. Chem. Phys.* **1950**, *18*, 365–375.

[72] K. C. Gross, P. G. Seybold, *Int. J. Quantum Chem.* **2001**, *85*, 569–579.

[73] P. Löwdin, *Phys. Rev.* **1955**, *97*, 1474–1489.

[74] F. Jensen, *Introduction to Computatioanl Chemistry*, Wileys, West Sussex, England, **2009**.

[75] K. Burke, *J. Chem. Phys.* **2012**, *136*, 150901–9.

[76] S. Grimme, *J. Comput. Chem.* **2004**, *25*, 1463–1473.

[77] S. Grimme, *J. Comput. Chem.* **2006**, *27*, 1787–1799.

[78] S. Grimme, J. Antony, H. Krieg, *J. Chem. Phys.* **2010**, *132*, 154104–19.

[79] S. Grimme, L. Goerigk, *J. Comput. Chem.* **2011**, *32*, 1456–1465.

[80] W. Hujo, S. Grimme, *J. Chem. Theory Comput.* **2012**, *9*, 308–315.

[81] J. Autschbach, *J. Chem. Phys.* **2012**, *136*, 150902–15.

[82] P. Pyykko, *Chem. Rev.* **1988**, *88*, 563–594.

[83] F. Weigend, R. Ahlrichs, *Phys. Chem. Chem. Phys.* **2005**, *7*, 3297–3305.

[84] F. Weigend, F. Furche, R. Ahlrichs, *J. Chem. Phys.* **2003**, *119*, 12753–12762.

[85] M. Dolg, H. Stoll, A. Savin, H. Preuss, *Theor. Chim. Acta* **1989**, *75*, 173–194.

[86] H. Krüger, E. Reyheller, personal communication.

[87] K. Bartl, A. Funk, M. Gerhards, *J. Chem. Phys.* **2008**, *129*, 234306–11.

[88] NIST, *precomputed vibrational scaling factors*, http://cccbdb.nist.gov/vibscalejust.asp.

[89] L. Andrews, *Organometallics* **2006**, *25*, 4040–4053.

TECHNISCHE UNIVERSITÄT
KAISERSLAUTERN

FACHBEREICH
CHEMIE

Appendix

C-H activation mediated Transition Metals

Dawei Zhao

Advisor: Prof. Dr. Christoph van Wüllen

appendix

A.1 Group 5 transition metal elements

A.1.1 The quartet state(ground state)

Table A.1: Structure and bond-order comparison of the CH_3NbX molecules. IR^t presents the stretching frequencies of the C-H bond that stands trans to the Nb-X bond, and so on. D(Nb-H^t) presents distances between the Nb atom and the H atom that belongs to the trans C-H bond, and so on. In the α-spin columns calculated data of the α-spin are given, and so on. BO^t column shows bond-orders of the trans C-H bond, and so on. Δ column shows bond-order differences of the cis and the trans C-H bonds in the same molecules.

CH_3NbX	IR^t	D(Nb-H^t)	IR^c	D(Nb-H^c)	D(Nb-C)
unit	cm^{-1}	pm	cm^{-1}	pm	pm
-CN	2978	273	3058	271	214
-F	2938	259	3046	280	215
-Cl	2932	262	3040	280	215
-Br	2922	261	3038	280	215
-I	2890	254	3044	281	215

			α-spin			β-spin		
CH_3NbX	IR^t	IR^c	BO^t	BO^c	Δ	BO^t	BO^c	Δ
unit	cm^{-1}	cm^{-1}	bond-order					
-CN	2978	3058	0.491	0.493	0.002	0.494	0.494	0
-F	2938	3046	0.491	0.494	0.004	0.492	0.497	0.005
-Cl	2932	3040	0.487	0.496	0.009	0.491	0.496	0.005
-Br	2922	3038	0.485	0.492	0.007	0.491	0.496	0.005
-I	2890	3044	0.483	0.495	0.012	0.489	0.496	0.008

Table A.2: Occupancy of the activated(trans) C-H bonds in the CH_3NbX molecules. In the α-spin columns occupancies of the C-H bond in the α-spin are given, and so on. IR^t presents stretching frequencies of the trans C-H bond. $Occ(\sigma)$ column gives occupancy changes relate to the CH_3NbF molecule in the C-H-σ(bonding) orbital, i.e. $Occ(\sigma) = Occ(\sigma_{(CH_3NbX)} - Occ(\sigma)_{(CH_3NbF)}$, and so on.

		α-spin		β-spin	
CH_3NbX	IR^t	$Occ(\sigma)$	$Occ(\sigma^*)$	$Occ(\sigma)$	$Occ(\sigma^*)$
unit	cm^{-1}	elemental charge			
-F	2938	0	0	0	0
-Cl	2932	0.003	0.004	-0.001	0
-Br	2922	0.003	0.005	-0.002	0
-I	2890	-0.005	0.003	-0.007	0

Table A.3: Interactions between the C-H-σ orbital and the vacant hybrid orbital of the Nb atom in the CH_3NbX molecules. β-spin table shows information of interactions in the β-spin, and so on. IR^t presents stretching frequencies of the C-H bond. NBO1 columns record calculated data of the NBO1, and so on. Hyb. column represents hybridizations of the vacant hybrid orbital of the Nb atom, which participates in the hyperconjugation. ΔE^2_{ij} gives second-order perturbative estimation of the hyperconjugation effect between the C-H-σ orbital and vacant hybrid orbitals of the Nb atom, $\Delta\varepsilon_{ij}$ gives energy gaps of the two interacting NBOs. The NBO1 is a vacant NB lone pair(LP) orbital with the main 4d orbital share, the NBO2 is a Nb-X-σ^* orbital, which has a main contribution of the Nb hybrid orbital(polarization coefficient>0.88).

β-spin		NBO1			NBO2		
CH_3NbX	IR^t	ΔE^2_{ij}	hyb.	$\Delta\varepsilon_{ij}$	ΔE^2_{ij}	hyb.	$\Delta\varepsilon_{ij}$
unit	cm^{-1}	kcal/mol		hartree	kcal/mol		hartree
-F	2938	1.70	$sd^{30.68}$	0.47	0.96	$sd^{4.42}$	0.62
-Cl	2932	1.04	$sd^{8.94}$	0.52	1.66	$sd^{2.58}$	0.57
-Br	2922	1.12	$sd^{99.99}$	0.52	1.99	$sd^{2.77}$	0.56
-I	2890	2.15	$sd^{52.68}$	0.46	2.25	$sd^{1.59}$	0.56
α-spin		NBO1			NBO2		
CH_3NbX	IR^t	ΔE^2_{ij}	hyb.	$\Delta\varepsilon_{ij}$	ΔE^2_{ij}	hyb.	$\Delta\varepsilon_{ij}$
unit	cm^{-1}	kcal/mol		hartree	kcal/mol		hartree
-F	2938	1.72	$sd^{99.99}$	0.44	1.11	$sd^{5.27}$	0.59
-Cl	2932	0.67	$sd^{99.99}$	0.41	1.86	$sd^{1.97}$	0.54
-Br	2922	0.23	$sd^{48.99}$	0.40	2.41	$sd^{1.65}$	0.53
-I	2890	1.28	$sd^{64.97}$	0.45	2.69	$sd^{1.94}$	0.52

Table A.4: Structure, bond-order and occupancy comparison of the n-C_4H_9NbF and CH_3NbF molecules. Met^t row represents calculated data of the trans C-H bond in the CH_3NbF molecule, and so on. But^δ row represents calculated data of the δ-C-H bond in the n-C_4H_9NbF molecule, and so on. IR gives stretching frequencies of the C-H bond. D(Nb-H) gives distances between the Nb atom and the H atom, which belongs to the activated C-H bond, and so on. In the α-spin columns calculated data of the α-spin are shown, and so on. BO column gives bond-orders of the C-H bond. Occ(σ) column gives occupancies of the C-H-σ orbital, Occ(σ^*) column presents occupancies of the C-H-σ^* orbital.

	IR	Nb-H	Nb-C
unit	cm^{-1}	pm	pm
Met^c	3046	280	215
Met^t	2938	259	215
But^α	2841	257	218
But^δ	2798	229	296

		α-spin			β-spin		
	IR	BO	Occ(σ)	Occ(σ^*)	BO	Occ(σ)	Occ(σ^*)
unit	cm^{-1}	a.u.					
Met^c	3046	0.494	0.998	0.011	0.497	0.992	0.001
Met^t	2938	0.491	0.983	0.002	0.492	0.986	0.001
But^α	2841	0.482	0.976	0.011	0.486	0.977	0.006
But^δ	2798	0.477	0.971	0.025	0.490	0.972	0.006

Table A.5: Interaction energy analysis of the n-C_4H_9NbF molecule. Met^c row represents calculated data of the cis C-H bond in the CH_3NbF molecule, and so on. But^α row represents calculated data of the α-C-H bond in the n-C_4H_9NbF molecule, and so on. IR gives stretching frequencies of the C-H bond. In the α-spin columns calculated data of the α-spin are shown, and so on. $\Delta E^2_{ij}(\sigma)$ presents sums of the second-order perturbative estimations of the hyperconjugation effects.

		α-spin		β-spin
	IR	$\Delta E^2_{ij}(\sigma)$	$\Delta E^2_{ij}(\sigma^*)$	$\Delta E^2_{ij}(\sigma)$
unit	cm^{-1}	kcal/mol		
Met^c	3046	0.13	2.63	1.09
Met^t	2938	2.83	0.32	2.66
But^α	2841	3.97	1.56	4.14
But^δ	2798	6.94	3.18	7.43

Table A.6: The leading interaction between the occupied Nb orbitals and the C-H-σ^* orbital in the α-spin of the n-C_4H_9NbF molecule. Met^c row represents calculated data of the cis C-H bond in the CH_3NbF molecule, and so on. But$^\alpha$ row represents calculated data of the α-C-H bond in the n-C_4H_9NbF molecule, and so on. IR gives the stretching frequencies of the C-H bond. ΔE^2_{ij} column gives second-order perturbative estimations of the hyperconjugation, $\Delta\varepsilon_{ij}$ column gives energy gaps of the two interacting NBOs, hyb. column shows hybridizations of the TM orbital, which is participated in the interaction. The composition column shows orbital compositions of the Nb hybrid orbital.

	IR	ΔE^2_{ij}	hyb.	$\Delta\varepsilon_{ij}$	composition
unit	cm^{-1}	kcal/mol		kcal/mol	
Met^c	3046	2.35	$sd^{99.99}$	0.57	$-0.42 * 4d_{yz} - 0.91 * 4d_{xz}$
Met^t	2938	0.32	$sd^{0.85}$	0.55	$0.72 * 5s + 0.60 * 4d_{z2}$
But$^\alpha$	2841	0.90	$sd^{99.99}$	0.53	$0.72 * 4d_{yz} + 0.68 * 4d_{xz}$
But$^\delta$	2798	3.18	$sd^{3.328}$	0.49	$0.48 * 5s + 0.65 * 4d_{xy} - 0.40 * 4d_{x^2-y^2}$

Table A.7: NPA comparison of the C-H bond in the CH_3NbX and n-C_4H_9NbF molecules. The trans C-H bond columns show calculated data of the trans C-H bond, and so on. IR gives the stretching frequencies of the C-H bonds, q(H) gives natural charges of the H atom of the C-H bond, and so on. $\Delta(q_H - q_C)$ gives natural charge differences between the H- and C-atoms of the C-H bond. Met^c row represents calculated data of the cis C-H bond in the CH_3NbF molecule, and so on. But$^\alpha$ row represents calculated data of the α-C-H bond in the n-C_4H_9NbF molecule, and so on.

	the trans-C-H bond				the cis-C-H bond		
CH_3NbX	IR	$\Delta(q_H - q_C)$	q(C)	q(H)	IR	$\Delta(q_H - q_C)$	q(H)
unit	cm^{-1}	a.u.			cm^{-1}	a.u.	
-CN	2978	1.327	-1.113	0.214	3058	1.351	0.238
-F	2938	1.292	-1.087	0.205	3046	1.302	0.215
-Cl	2932	1.327	-1.128	0.199	3040	1.361	0.233
-Br	2922	1.315	-1.120	0.195	3038	1.351	0.231
-I	2890	1.279	-1.081	0.198	3044	1.302	0.221

	IR	$\Delta(q_H - q_C)$	q(H)	q(C)
unit	cm^{-1}	a.u.		
Met^c	3046	1.302	0.215	-1.087
Met^t	2938	1.292	0.205	-1.087
But$^\alpha$	2841	1.070	0.190	-0.880
But$^\delta$	2798	0.733	0.148	-0.585

Table A.8: Analysis of group trend of the C-H activation in the CH_3MF molecules. α-spin columns give calculated data of α-spin, and so on. IR^t gives stretching frequencies of the C-H bond that stands trans to the M-X bond. $D(M\text{-}H^t)$ gives distances between the metal atom and the H atom that belongs to the trans C-H bond, D(M-C) gives distances between the metal atom and the C atom of the trans C-H bond. BO column gives C-H bond-orders of the trans C-H bond and $Occ(\sigma)$ column gives occupancies of the C-H-σ orbital.

				α-spin		β-spin	
CH_3MF	IR^t	$D(M\text{-}H^t)$	D(M-C)	BO	$Occ(\sigma)$	BO	$Occ(\sigma)$
unit	cm^{-1}	pm	pm	a.u.			
V	2993	268	209	0.493	0.993	0.497	0.994
Nb	2938	259	215	0.491	0.983	0.492	0.986
Ta	2940	260	216	0.490	0.984	0.492	0.986

Table A.9: Interactions between the C-H-σ orbital and the vacant hybrid orbital of the metal atoms in the β-spin of the CH_3MF molecules. NBO1 columns record calculated data of the NBO1, and so on. IR^t presents stretching frequencies of the trans C-H bond. The sum column gives sums of the interactions. hyb. represents hybridizations of the occupied NBO of the Nb atom, which participates in the hyperconjugation. ΔE^2_{ij} gives second-order perturbative estimations of the hyperconjugation effect, $\Delta\varepsilon_{ij}$ gives energy gaps of the two interacting NBOs.

			NBO1			NBO2		
CH_3NbX	IR^t	sum	ΔE^2_{ij}	hyb.	$\Delta\varepsilon_{ij}$	ΔE^2_{ij}	hyb.	$\Delta\varepsilon_{ij}$
unit	cm^{-1}	kcal/mol	kcal/mol		hartree	kcal/mol		hartree
V	2993	1.09	0.73	$sd^{5.44}$	0.50	0.36	$sd^{5.35}$	0.51
Nb	2938	2.66	1.70	$sd^{30.68}$	0.47	0.96	$sd^{4.42}$	0.62
Ta	2940	2.54	1.95	$sd^{33.87}$	0.53	0.59	$sd^{3.32}$	0.89

Table A.10: Group trends of the C-H activation in the n-C_4H_9MF molecules (structure) In the δ-C-H bond columns calculated data of the δ-C-H bond are represented, and so on. IR gives the stretching frequencies of the C-H bond. M-H gives distances between the metal atom and the H atom of the C-H bond, and so on.

	δ-C-H bond			α-C-H bond		
n-C_4H_9MF	IR	D(M-H)	D(M-C)	IR	D(M-H)	D(M-C)
unit	cm^{-1}	pm	pm	cm^{-1}	pm	pm
V	2861	217	271	2913	259	209
Nb	2798	229	296	2841	257	218
Ta	2809	241	320	2839	258	218

Table A.11: Bond-order and occupancy comparison of the C-H bond in the n-C_4H_9MF molecules. In the δ-C-H bond columns calculated data of the δ-C-H bond are shown, and so on. IR gives stretching frequencies of the C-H bond. BO(α) column gives bond-orders of the C-H bond in the α-spin, and so on. The α-spin columns give calculated data of the α-spin, and so on. Occ(σ) column gives occupancies of of the C-H-σ orbital, and so on.

	δ-C-H bond			α-C-H bond		
	IR	BO(α)	BO(β)	IR	BO(α)	BO(β)
unit	cm^{-1}	a.u.		cm^{-1}	a.u.	
V	2861	0.493	0.486	2913	0.489	0.490
Nb	2798	0.477	0.490	2841	0.482	0.486
Ta	2809	0.487	0.489	2839	0.481	0.486

	δ-C-H bond				α-C-H bond			
		α-spin		β-spin		α-spin		β-spin	
	IR	Occ(σ)	Occ(σ^*)	Occ(σ)	Occ(σ^*)	IR	Occ(σ)	Occ(σ^*)	Occ(σ)	Occ(σ^*)
unit	cm^{-1}	a.u.				cm^{-1}	a.u.			
V	2861	0.975	0.015	0.976	0.006	2913	0.985	0.007	0.985	0.005
Nb	2798	0.971	0.025	0.972	0.006	2841	0.976	0.011	0.977	0.006
Ta	2809	0.978	0.027	0.976	0.006	2839	0.976	0.012	0.978	0.005

Table A.12: Interactions of the α-C-H bond in the α-spin of the n-C_4H_9MF molecules.
C-H-σ^* orbital table gives information of interactions between the C-H-σ^* orbital and occupied hybrid orbital of the metal atoms, and so on. IR(α) gives stretching frequencies of the α-C-H bond. The NBO1 columns show calculated data of the NBO1, and so on. The sum column shows sums of the interactions. ΔE^2_{ij} gives the second-order perturbative estimation of the hyperconjugation, hyb. shows hybridizations of the TM orbital, which is participated in the interaction, $\Delta\varepsilon_{ij}$ gives energy gaps of the interacting orbitals.

C-H-σ orbital			NBO1			NBO2		
n-C_4H_9MF	IR(α)	sum	ΔE^2_{ij}	hyb.	$\Delta\varepsilon_{ij}$	ΔE^2_{ij}	hyb.	$\Delta\varepsilon_{ij}$
nit	cm^{-1}	kcal/mol	kcal/mol		hartree	kcal/mol		hartree
V	2913	1.75	0.34	$sd^{6.41}$	0.42	1.41	$sd^{1.43}$	0.45
Nb	2841	3.97	1.90	$sd^{36.82}$	0.41	2.07	$sd^{2.08}$	0.50
Ta	2839	4.07	2.31	$sd^{99.99}$	0.42	1.76	$sd^{4.46}$	0.64

CH-σ^* orbital			NBO1		NBO2		NBO3	
n-C_4H_9MF	IR(α)	sum	ΔE^2_{ij}	hyb.	ΔE^2_{ij}	hyb.	ΔE^2_{ij}	hyb.
unit	cm^{-1}	kcal/mol	kcal/mol		kcal/mol		kcal/mol	
V	2913	0.68	0.29	$sd^{99.99}$	0.12	$sd^{14.07}$	0.27	$sd^{8.31}$
Nb	2841	1.56	0.90	$sd^{99.99}$	0.33	$sd^{3.89}$	0.33	$sd^{3.32}$
Ta	2839	1.58	1.24	$sd^{42.79}$	0.25	$sd^{3.08}$	0.09	$sd^{1.96}$

A.1.2 The doublet state(first excited state)

Table A.13: Structure, bond-order and occupancy comparison of the CH_3NbX molecules. IR^t presents the stretching frequencies of the trans C-H bond, and so on. D(Nb-H^t) presents distances between the Nb atom and the H atom that belongs to the trans C-H bond, and so on. In the α-spin columns calculated data of the α-spin are given, and so on. BO^t column shows bond-orders of the trans C-H bond, and so on. Δ column shows bond-order differences between the cis and the trans C-H bonds in the same molecules. Occ(σ) column gives occupancy changes related to the CH_3NbF molecule in the C-H-σ orbital, i.e. $\mathrm{Occ}(\sigma) = \mathrm{Occ}(\sigma_{(CH_3NbX)} - \mathrm{Occ}(\sigma)_{(CH_3NbF)}$, and so on.

CH_3NbX	IR^t	D(Nb-H^t)	IR^c	D(Nb-H^c)	D(Nb-C)
unit	cm^{-1}	pm	cm^{-1}	pm	
F	2921	261	3137	288	212.5
CN	2918	253	3133	283	210.8
Cl	2891	254	3149	291	210.5
I	2884	253	3146	291	209.9
Br	2882	252	3151	292	209.9

			α-spin			β-spin		
CH_3NbX	IR^t	IR^c	BO^t	BO^c	Δ	BO^t	BO^c	Δ
unit	cm^{-1}	cm^{-1}	bond-order					
F	2921	3137	0.489	0.500	0.011	0.487	0.500	0.013
CN	2918	3133	0.486	0.496	0.010	0.487	0.498	0.011
Cl	2891	3149	0.482	0.500	0.018	0.484	0.500	0.016
I	2884	3146	0.484	0.500	0.016	0.484	0.500	0.016
Br	2882	3151	0.484	0.500	0.016	0.484	0.500	0.016

		α-spin		β-spin	
CH_3NbX	IR^t	Occ(σ)	Occ(σ^*)	Occ(σ)	Occ(σ^*)
unit	cm^{-1}	elemental charge			
F	2921	0	0	0	0
CN	2918	-0.0063	-0.0009	-0.0053	-0.0016
Cl	2891	-0.0079	0.0023	-0.0074	0.0023
I	2884	-0.0087	0.0013	-0.0066	0.0005
Br	2882	-0.0086	0.0012	-0.0068	0.0008

.

Table A.14: Interactions between the C-H-σ orbital and the vacant hybrid orbital of the Nb atom in the CH_3NbX molecules. α-spin table shows information of interactions in the α-spin, and so on. NBO1 columns record calculated data of the NBO1, and so on. IR^t column presents stretching frequencies of the C-H bond, sum column shows sums of all interactions, ΔE^2_{ij} gives second-order perturbative estimations of the hyperconjugation effect. hyb. column represents hybridizations of the occupied NBO of the Nb atom, which participates in the hyperconjugation. NBO1 is a Nb-X-σ^* orbital that has a main contribution of Nb hybrid orbital(polarization coefficient>0.89), which is mainly composed of the Nb 5s and $4d_{xy}$ orbital. NBO2 is a vacant Nb LP orbital, which is mainly composed of the $4d_{yz}$ and the $4d_{xz}$ orbitals.

α-spin			NBO1		NBO2		NBO3	
CH_3NbX	IR^t	sum	ΔE^2_{ij}	hyb.	ΔE^2_{ij}	hyb.	ΔE^2_{ij}	hyb.
unit	cm^{-1}	kcal/mol	kcal/mol		kcal/mol		kcal/mol	
F	2921	3.10	1.41	$sd^{3.37}$	1.45	$sd^{99.99}$	0.24	$sd^{6.44}$
CN	2918	4.45	0.62	$sd^{1.82}$	3.18	$sd^{36.08}$	0.65	$sd^{12.30}$
Cl	2891	4.85	2.49	$sd^{1.64}$	2.03	$sd^{99.99}$	0.33	$sd^{10.54}$
I	2884	5.20	2.57	$sd^{1.18}$	2.20	$sd^{76.59}$	0.43	$sd^{13.26}$
Br	2882	5.29	2.71	$sd^{1.39}$	2.16	$sd^{99.99}$	0.42	$sd^{10.93}$
β-spin			NBO1		NBO2		NBO3	
	IR^t	sum	ΔE^2_{ij}	hyb.	ΔE^2_{ij}	hyb.	ΔE^2_{ij}	hyb.
unit	cm^{-1}	kcal/mol	kcal/mol		kcal/mol		kcal/mol	
F	2921	3.39	1.33	$sd^{7.04}$	1.28	$sd^{99.99}$	0.78	$sd^{3.81}$
CN	2918	4.38	0.58	$sd^{2.45}$	3.15	$sd^{99.99}$	0.65	$sd^{28.21}$
Cl	2891	4.87	2.51	$sd^{3.01}$	1.70	$sd^{99.99}$	0.66	$pd^{7.06}$
I	2884	5.20	2.72	$sd^{2.04}$	1.80	$sd^{99.99}$	0.68	$pd^{7.00}$
Br	2882	5.38	2.77	$sd^{2.49}$	1.85	$sd^{99.99}$	0.76	$sd^{46.21}$

Table A.15: Structure comparison between the n-C_4H_9NbF and the CH_3NbF molecules. Met^t row represents calculated data of the trans C-H bond in the CH_3NbF molecule, and so on. But^δ row represents calculated data of the δ-C-H bond in the n-C_4H_9NbF molecule, and so on. IR gives stretching frequencies of the C-H bond. D(Nb-H) gives distances between the Nb atom and the H atom, which belongs to the C-H bond, and so on.

	IR	Nb-H	Nb-C
unit	cm^{-1}	pm	pm
Met^c	3137	288	212
Met^t	2921	261	212
But^α	2870	258	217
But^δ	2802	228	271

Table A.16: Bond-order and occupancy comparison of the C-H bond in the n-C_4H_9NbF and CH_3NbF molecules. Met^t row represents calculated data of the trans C-H bond in the CH_3NbF molecule, and so on. But^δ row represents calculated data of the δ-C-H bond in the n-C_4H_9NbF molecule, and so on. IR gives stretching frequencies of the C-H bond. In the α-spin columns calculated data of the α-spin are shown, and so on. BO column gives bond-orders of the C-H bond. Occ(σ) column gives occupancies of the C-H-σ orbital, and so on.

		α-spin			β-spin		
	IR	BO	Occ(σ)	Occ(σ^*)	BO	Occ(σ)	Occ(σ^*)
unit	cm^{-1}	a.u.					
Met^c	3137	0.500	0.994	0.001	0.500	0.996	0.001
Met^t	2921	0.489	0.983	0.005	0.487	0.984	0.005
But^α	2870	0.486	0.980	0.009	0.483	0.975	0.009
But^δ	2802	0.490	0.971	0.022	0.483	0.969	0.007

Table A.17: Interactions in the n-C_4H_9NbX and CH_3NbF molecules. Met^c row represents calculated data of the cis C-H bond in the CH_3NbF molecule, and so on. But^δ row represents calculated data of the δ-C-H bond in the n-C_4H_9NbF molecule, and so on. IR gives stretching frequencies of the C-H bond. In the α-spin columns calculated data of the α-spin are shown, and so on. $\Delta E^2_{ij}(\sigma)$ presents sums of the second-order perturbative estimation of the hyperconjugation effect between the C-H-σ and the Nb hybrid orbitals, and so on.

		α-spin		β-spin	
	IR	$\Delta E^2_{ij}(\sigma)$	$\Delta E^2_{ij}(\sigma^*)$	$\Delta E^2_{ij}(\sigma)$	$\Delta E^2_{ij}(\sigma^*)$
unit	cm^{-1}	kcal/mol			
Met^c	3137	0.31	0.04	0.47	0.04
Met^t	2921	3.10	1.26	3.39	0.92
But^α	2870	2.67	2.67	4.30	1.00
But^δ	2802	8.97	2.78	9.47	0.30

Table A.18: The first two leading interactions between the C-H-σ orbital and the vacant Nb hybrid orbital. Met^c row represents calculated data of the cis C-H bond in the CH_3NbF molecule, and so on. But$^\alpha$ row represents calculated data of the α-C-H bond in the n-C_4H_9NbF molecule, and so on. α-spin table records interaction information in the α-spin, and so on. NBO1 columns represents information of the NBO1, and so on. IR gives stretching frequencies of the C-H bonds. ΔE^2_{ij} column gives second-order perturbative estimations of the hyperconjugation, hyb. column shows hybridizations of the TM orbital, which is participated in the interaction. The composition column shows orbital compositions of the Nb hybrid orbital.

α-spin		NBO1			NBO2		
	IR	ΔE^2_{ij}	hyb.	composition	ΔE^2_{ij}	hyb.	composition
unit	cm^{-1}	kcal/mol			kcal/mol		
Met^c	3137	0.27	$sd^{3.37}$	$-0.47*5s+0.79*4d_{xy}$	0.04	$sd^{6.44}$	$0.36*5s-0.59*d_{x^2-y^2}+0.52*d_{xy}$
Met^t	2921	1.41	$sd^{3.37}$	$-0.47*5s+0.79*4d_{xy}$	1.45	$sd^{99.99}$	$-0.54*4d_{yz}+0.88*4d_{xz}$
But$^\alpha$	2870	0.60	$sd^{1.78}$	$0.59*5s-0.51*4d_{xy}$	2.07	$sd^{99.99}$	$-0.65*4d_{yz}+0.72*4d_{xz}$
But$^\delta$	2802	8.79	$sd^{1.78}$	$0.59*5s-0.51*4d_{xy}$	0.18	$sd^{6.78}$	$0.34*5s+0.75*4d_{z^2}$
β-spin		NBO1			NBO2		
	IR	ΔE^2_{ij}	hyb.	composition	ΔE^2_{ij}	hyb.	composition
unit	cm^{-1}	kcal/mol			kcal/mol		
Met^c	3137	0.25	$sd^{7.04}$	$0.43*5s+0.80*4d_{xy}$	0.22	$sd^{3.81}$	$0.52*4d_{yz}+0.43*4d_{xz}$
Met^t	2921	1.33	$sd^{7.04}$	$0.43*5s+0.80*4d_{xy}$	1.28	$sd^{99.99}$	$0.60*4d_{yz}-0.79*4d_{xz}$
But$^\alpha$	2870	2.47	$sd^{23.64}$	$-0.55*4d_{yz}-0.79*4d_{xz}$	1.34	$sd^{99.99}$	$-0.79*4d_{yz}+0.54*4d_{xz}$
But$^\delta$	2802	7.85	$sd^{2.27}$	$0.55*5s-0.66*4d_{xy}$	1.62	$sd^{4.14}$	$0.44*5s+0.72*4d_{xy}$

Table A.19: NPA comparison of the C-H bond in the n-C_4H_9NbF and the CH_3NbF molecules. The trans C-H bond columns show calculated data of the trans C-H bond, and so on. IR gives the stretching frequencies of the C-H bonds, q(H) gives natural charges of the H atom, which belongs to the C-H bond, and so on. $\Delta(q_H - q_C)$ gives natural charge differences between the H- and C-atoms. Met^c row represents calculated data of the cis C-H bond in the CH_3NbF molecule, and so on. But^α row represents calculated data of the α-C-H bond in the n-C_4H_9NbF molecule, and so on.

	the trans-C-H bond			the cis-C-H bond			
CH_3NbX	IR	$\Delta(q_H - q_C)$	q(H)	IR	$\Delta(q_H - q_C)$	q(H)	q(C)
unit	cm^{-1}	a.u.		cm^{-1}	a.u.		
F	2921	1.380	0.219	3137	1.403	0.242	-1.161
CN	2918	1.321	0.222	3133	1.343	0.244	-1.099
Cl	2891	1.338	0.217	3149	1.366	0.245	-1.121
I	2884	1.326	0.215	3146	1.356	0.245	-1.111
Br	2882	1.329	0.216	3151	1.359	0.246	-1.113

	IR	$\Delta(q_H - q_C)$	q(H)	q(C)
unit	cm^{-1}	a.u.		
Met^c	3137	1.403	0.242	-1.161
Met^t	2921	1.380	0.219	-1.161
But^α	2870	1.052	0.195	-0.857
But^δ	2802	0.794	0.184	-0.610

Table A.20: Analysis of group trends of the C-H activation in the CH_3MF molecules. IR^t gives stretching frequencies of the trans C-H bond. D(M-H^t) gives distances between the metal atom and the H atom that belongs to the trans C-H bond. D(M-C) gives distances between the metal atom and the C atom of the C-H bond. BO column gives C-H bond-orders of the trans C-H bond and Occ(σ) column gives occupancies of the C-H-σ orbital.

				α-spin		β-spin	
CH_3MF	IR^t	D(M-H^t)	D(M-C)	BO	Occ(σ)	BO	Occ(σ)
unit	cm^{-1}	pm	pm	a.u.			
V	2973	261	205	0.495	0.993	0.495	0.990
Nb	2921	261	213	0.489	0.983	0.487	0.984
Ta	2875	252	209	0.485	0.979	0.487	0.980

Table A.21: Interactions between the C-H-σ orbital and the vacant hybrid orbital of the metal atoms in the CH_3MF molecules. α-spin table records calculated data of the α-spin, and so on. NBO1 columns record calculated data of the NBO1, and so on. IR^t presents stretching frequencies of the C-H bond. Sum column shows sums of the interactions, ΔE^2_{ij} gives second-order perturbative estimations of the hyperconjugation effect, hyb. represents hybridizations of the vacant hybrid orbital of the metal atom, which participates in the hyperconjugation.

α-spin			NBO1		NBO2		NBO3	
CH_3MF	IR^t	sum	ΔE^2_{ij}	hyb.	ΔE^2_{ij}	hyb.	ΔE^2_{ij}	hyb.
unit	cm^{-1}	kcal/mol	kcal/mo		kcal/mol		kcal/mol	
V	2973	1.19	0.69	$sd^{3.06}$	0.36	$pd^{48.03}$	0.14	$sd^{28.12}$
Nb	2921	3.10	1.41	$sd^{3.37}$	1.45	$sd^{99.99}$	0.24	$sd^{6.44}$
Ta	2875	3.65	1.48	$sd^{5.67}$	1.83	$pd^{99.99}$	0.34	$sd^{39.04}$
β-spin								
V	2973	1.63	0.82	$sd^{7.33}$	0.81	$pd^{28.85}$		
Nb	2921	3.39	1.33	$sd^{7.04}$	1.28	$sd^{99.99}$	0.78	$sd^{3.81}$
Ta	2875	3.96	1.37	$sd^{5.70}$	1.65	$pd^{99.99}$	0.59	$sd^{5.51}$

Table A.22: Structure and bond-order comparison of the C-H activation in the n-C_4H_9MF molecules. In the δ-C-H bond columns calculated data of the δ-C-H bond are represented, and so on. IR gives the stretching frequencies of the C-H bonds. M-H gives distances between the metal atom and the H atom, which belongs to the C-H bond, and so on. BO(α) column gives bond-orders of the C-H bond in the α-spin, and so on.

	δ-C-H bond			in the α-C-H bond		
n-C_4H_9MF	IR	D(M-H)	D(M-C)	IR	D(M-H)	D(M-C)
unit	cm^{-1}	pm	pm	cm^{-1}	pm	pm
V	2863	218	261	2943	259	208
Nb	2802	228	271	2870	258	217
Ta	2768	229	273	2797	246	214

	δ-C-H bond			α-C-H bond		
	IR	BO(α)	BO(β)	IR	BO(α)	BO(β)
unit	cm^{-1}	a.u.	a.u.	cm^{-1}	a.u.	a.u.
V	2863	0.490	0.485	2943	0.491	0.489
Nb	2802	0.490	0.483	2870	0.486	0.483
Ta	2768	0.480	0.483	2797	0.477	0.479

Table A.23: Occupancy comparison of C-H bond in the n-C_4H_9MF molecules. The δ-C-H bond columns give calculated data of the δ-C-H bond, and so on. In the α-C-H bond columns calculated data of the α-C-H bond are shown, but only the occupancy changes related to the the δ-C-H bond in the same molecule are shown. α-spin columns show calculated data of the α-spin. IR gives stretching frequencies of the C-H bond. Occ(σ) column gives occupancies of the C-H-σ orbital, and so on.

	δ-C-H bond					α-C-H bond				
		α-spin		β-spin			α-spin		β-spin	
	IR	Occ(σ)	Occ(σ^*)	Occ(σ)	Occ(σ^*)	IR	Occ(σ)	Occ(σ^*)	Occ(σ)	Occ(σ^*)
unit	cm^{-1}	a.u.				cm^{-1}	a.u.			
V	2863	0.975	0.013	0.974	0.007	2943	0.012	-0.007	0.009	-0.001
Nb	2802	0.971	0.022	0.969	0.007	2870	0.010	-0.012	0.006	0.002
Ta	2768	0.966	0.014	0.968	0.017	2797	0.002	0.001	0.000	-0.006

Table A.24: Interactions in the n-C_4H_9MF molecules. δ-C-H bond columns give calculated data of the δ-C-H bond, and so on. IR gives the stretching frequencies of the C-H bond. In the α-spin columns calculated data of the α-spin are shown, and so on. $\Delta E^2_{ij}(\sigma)$ presents sums of the second-order perturbative estimation of the hyperconjugation effect between the C-H-σ orbital and the TM hybrid orbital.

	δ-C-H bond				α-C-H bond			
		α-spin		β-spin		α-spin		β-spin
	IR	$\Delta E^2_{ij}(\sigma)$	$\Delta E^2_{ij}(\sigma^*)$	$\Delta E^2_{ij}(\sigma)$	IR	$\Delta E^2_{ij}(\sigma)$	$\Delta E^2_{ij}(\sigma^*)$	$\Delta E^2_{ij}(\sigma)$
unit	cm^{-1}	kcal/mol			cm^{-1}	kcal/mol		
V	2863	6.91	1.38	6.95	2943	1.30	0.44	2.11
Nb	2802	8.97	2.78	9.47	2870	2.67	0.96	4.30
Ta	2768	10.79	1.37	10.84	2797	4.90	1.92	6.37

Table A.25: Further details of interactions between the C-H-σ and vacant metal hybrid orbitals in the β-spin of the n-C_4H_9MF molecules. IR(δ) gives stretching frequencies of the δ-C-H bond. NBO1 columns show calculated data of the NBO1, and so on. ΔE^2_{ij} and $\Delta\varepsilon_{ij}$ give the second-order perturbative estimations of the leading hyperconjugation and energy gaps between the interacting NBOs, hyb. shows hybridizations of the vacant hybrid orbital of the TM atom, which participate in the interaction.

		NBO1			NBO2		
n-C_4H_9MF	IR(δ)	ΔE^2_{ij}	hyb.	$\Delta\varepsilon_{ij}$	ΔE^2_{ij}	hyb.	$\Delta\varepsilon_{ij}$
unit	cm^{-1}	kcal/mol		hartree	kcal/mol		hartree
V	2863	5.31	$sd^{1.82}$	0.55	1.64	$sd^{2.77}$	0.53
Nb	2802	7.85	$sd^{2.27}$	0.58	1.62	$sd^{4.14}$	0.53
Ta	2768	9.53	$sd^{3.03}$	0.87	0.89	$sd^{38.57}$	0.57

A.2 Group 6 transition metal elements

A.2.1 The singlet state(second excited state)

Table A.26: Structure and bond-order comparison of the CH_3MoX molecules. IR^t presents the stretching frequencies of the C-H bond that stands trans to the Nb-X bond, and so on. D(Mo-H^t) presents distances between the Mo atom and the H atom that belongs to the trans C-H bond, and so on. BO^t column shows bond-orders of the trans C-H bond, and so on. Δ column shows bond-order differences of the cis and the trans C-H bonds in the same molecules. Occ(σ) column gives the occupancy in the C-H bonding orbital(occupied orbital), Occ(σ^*) column the occupancy in the C-H anti-bonding orbital(vacant orbital), In the trans C-H bond columns only occupancy changes related to the CH_3MoI molecule are shown, i.e. $Occ(\sigma) = Occ(\sigma_{(CH_3MoX)} - Occ(\sigma)_{(CH_3MoI)}$. In the cis C-H bond columns only occupancy changes realted to the trans C-H bond in the same molecule are shown, i.e. $Occ(\sigma) = Occ(\sigma_{(cis)} - Occ(\sigma)_{(trans)}$.

CH_3MoX	IR^t	D(Mo-H^t)	IR^c	D(Mo-H^c)	D(Mo-C)
unit	cm^{-1}	pm	cm^{-1}	pm	pm
CN	3061	275	2935	257	206
H	2592	215	3185	290	192
I	2404	204	3187	293	190
Br	2374	202	3194	293	189
Cl	2367	202	3200	294	189
F	2333	200	3216	293	188

CH_3MoX	IR^t	IR^c	BO^t	BO^c	Δ
unit	cm^{-1}	cm^{-1}	bond-order		
I	2404	3187	0.891	0.988	0.097
Br	2374	3194	0.884	0.989	0.105
Cl	2367	3200	0.883	0.989	0.107
F	2333	3216	0.879	0.995	0.116

	trans C-H bond			cis C-H bond		
CH_3MoX	IR	Occ(σ)	Occ(σ^*)	IR	Occ(σ)	Occ(σ^*)
unit	cm^{-1}	a.u.	a.u.	cm^{-1}	a.u.	a.u.
I	2404	0.000	0.000	3187	0.142	-0.042
Br	2374	-0.009	0.004	3194	0.151	-0.047
Cl	2367	-0.011	0.004	3200	0.153	-0.048
F	2333	-0.012	0.013	3216	0.153	-0.060

Table A.27: Interactions between the C-H-σ^* orbital and the occupied hybrid orbitals of the Mo atom in the CH_3MoX molecules. The NBO1 columns record calculated data of the NBO1, and so on. IR^t represents stretching frequencies of the C-H bond, hyb. represents hybridizations of the occupied NBO of the Mo atom, which participates in the interaction. ΔE^2_{ij} gives second-order perturbative estimations of the hyperconjugation effect between the C-H-σ^* orbital and the occupied valence orbital of the Mo atom, $\Delta\varepsilon_{ij}$ gives energy gaps of the two interacting NBOs. The NBO1 and the NBO2 are hybrid LP orbital of the Mo atoms. In the second table compositions of the NBO1 of the first table in the CH_3MoX molecules are shown. Composition column records orbital composition of hybrid LP orbital of the Mo atoms.

		NBO1			NBO2		
CH_3MoX	IR^t	ΔE^2_{ij}	hyb.	$\Delta\varepsilon_{ij}$	ΔE^2_{ij}	hyb.	$\Delta\varepsilon_{ij}$
unit	cm^{-1}	kcal/mol		hartree	kcal/mol		hartree
I	2404	8.54	$sd^{3.44}$	0.46	2.46	$sd^{99.99}$	0.45
Br	2374	8.81	$sd^{2.92}$	0.46	3.05	$sd^{99.99}$	0.45
Cl	2367	8.99	$sd^{2.57}$	0.46	3.06	$sd^{99.99}$	0.45
F	2333	10.33	$sd^{1.81}$	0.45	3.32	$sd^{99.99}$	0.45

CH_3MoX	IR^t	hyb.	composition
unit	cm^{-1}		
I	2404	$sd^{3.44}$	$0.47 * 5s + 0.57 * 4d_{z^2} + 0.47 * 4d_{xy} - 0.47 * 4d_{x^2-y^2}$
Br	2374	$sd^{2.92}$	$0.50 * 5s + 0.57 * 4d_{z^2} + 0.43 * 4d_{xy} - 0.48 * 4d_{x^2-y^2}$
Cl	2367	$sd^{2.57}$	$0.53 * 5s + 0.56 * 4d_{z^2} + 0.40 * 4d_{xy} - 0.49 * 4d_{x^2-y^2}$
F	2333	$sd^{1.81}$	$0.60 * 5s + 0.55 * 4d_{z^2} - 0.30 * 4d_{xy} - 0.50 * 4d_{x^2-y^2}$

Table A.28: structure, bond-order and occupancy comparison between the n-C_4H_9MoF and the CH_3MoF molecules. Met^c row represents calculated data of the cis C-H bond in the CH_3MoF molecule, and so on. But^α row represents calculated data of the α-C-H bond in the n-C_4H_9MoF molecule, and so on. IR gives stretching frequencies of the C-H bond. D(Mo-H) gives distances between the Mo atom and the H atom, and so on. The BO column gives bond-orders. Occ(σ) column gives occupancies of the C-H-σ-orbital, Occ(σ^*) column presents occupancies of the C-H-σ^*-orbital.

	IR	Mo-H	Mo-C	BO	Occ(σ)	Occ(σ^*)
unit	cm^{-1}	pm	pm		a.u.	
Met^c	3216	293	188	0.995	1.993	0.014
But^α	2511	211	203	0.907	1.857	0.041
But^δ	2386	206	231	0.937	1.842	0.056
Met^t	2333	200	188	0.879	1.839	0.073

Table A.29: NPA comparison of the C-H bond in the CH_3MoX and n-C_4H_9MoF molecules. The trans C-H bond columns show calculated data of the trans C-H bond, and so on. IR gives the stretching frequencies of the C-H bonds, q(H) gives natural charges of the H atom of the C-H bond, and so on. $\Delta(q_H - q_C)$ gives natural charge differences between the H- and C-atoms of the C-H bond. Met^c row represents calculated data of the cis C-H bond in the CH_3MoF molecule, and so on. But^α row represents calculated data of the α-C-H bond in the n-C_4H_9MoF molecule, and so on.

	the trans-C-H bond			the cis-C-H bond			
CH_3MoX	IR	$\Delta(q_H - q_C)$	q(H)	IR	$\Delta(q_H - q_C)$	q(H)	q(C)
unit	cm^{-1}	a.u.		cm^{-1}	a.u.		
I	2404	0.956	0.186	3187	1.011	0.241	-0.770
Br	2374	0.950	0.186	3194	1.006	0.242	-0.764
Cl	2367	0.955	0.187	3200	1.011	0.243	-0.768
F	2333	0.980	0.183	3216	1.043	0.246	-0.797

	IR	$\Delta(q_H - q_C)$	q(H)	q(C)
unit	cm^{-1}	a.u.		
Met^c	3216	1.043	0.246	-0.797
But^α	2511	0.779	0.180	-0.599
But^δ	2386	0.782	0.220	-0.562
Met^t	2333	0.980	0.183	-0.797

Table A.30: Structure, bond-order and occupancy comparison of the C-H bond in the CH_3MF molecules. IR^t gives stretching frequencies of the trans C-H bond, and so on. D(M-H) gives distances between the metal atom and the H atom that belongs to the C-H bond, D(M-C) gives distances between the metal atom and the C atom of the C-H bond. BO column gives C-H bond-orders of the C-H bond, Occ(σ) column gives occupancies of the C-H-σ orbital, and so on.

	trans C-H bond			cis C-H bond			
CH_3TMF	IR	D(M-H)	BO	IR	D(M-H)	BO	D(M-C)
unit	cm^{-1}	pm	a.u.	cm^{-1}	pm	a.u	pm
Cr	2602	197	0.926	3216	284	0.997	181
Mo	2333	200	0.879	3216	293	0.995	188
W	2419	205	0.893	3250	296	0.992	192

	trans C-H bond			cis C-H bond		
CH_3TMF	IR	Occ(σ)	Occ(σ^*)	IR	Occ(σ)	Occ(σ^*)
unit	cm^{-1}	a.u.	a.u.	cm^{-1}	a.u.	a.u.
Cr	2602	1.891	0.033	3216	1.994	0.008
Mo	2333	1.839	0.073	3216	1.993	0.014
W	2419	1.850	0.061	3250	1.992	0.009

Table A.31: Details of the leading interaction between the C-H-σ^* orbital and the occupied hybrid orbital of the Mo atom in the CH_3TMF molecules. IR^t presents stretching frequencies of the C-H bond, sum coulomb shows sums of all interaction between the C-H-σ^* orbital and the occupied hybrid orbital of the Mo atom, ΔE^2_{ij} gives second-order perturbative estimations of the hyperconjugation effect, $\Delta\varepsilon_{ij}$ gives energy gaps of the two interacting NBOs, hyb. represents hybridizations of the orbitals, Composition column records orbital compositions of the occupied hybrid orbital of the Mo atom.

CH_3TMF	IR^t	sum	ΔE^2_{ij}	$\Delta\varepsilon_{ij}$	hyb.	composition
unit	cm^{-1}	kcal/mol	kcal/mol	hartree		
Cr	2602	2.07	1.12	0.52	$sd^{4.23}$	$0.44 * s - 0.54 * d_{x^2-y^2} + 0.59 * d_{z^2}$
Mo	2333	13.65	10.33	0.45	$sd^{1.81}$	$0.60 * s - 0.50 * d_{x^2-y^2} + 0.55d*_{z^2}$
W	2419	11.11	7.09	0.47	$sd^{0.92}$	$0.72 * s - 0.49 * d_{x^2-y^2} + 0.43 * d_{z^2}$

Table A.32: Structure, bond-order and occupancy comparison of the C-H bond in the n-C_4H_9MF molecules. In the δ-C-H bond columns calculated data of the δ-C-H bond are represented, and so on. IR gives the stretching frequencies of the C-H bond. M-H gives distances between the metal atom and the H atom of the C-H bond, and so on. In the δ-C-H bond columns calculated data of the δ-C-H bond are shown, and so on. BO(α) column gives bond-orders of the C-H bond in the α-spin, and so on. Occ(σ) column gives occupancies of of the C-H-σ orbital, and so on.

	the δ-C-H bond			the α-C-H bond		
n-C_4H_9MF	IR	D(M-H)	D(M-C)	IR	D(M-H)	D(M-C)
unit	cm^{-1}	pm	pm	cm^{-1}	pm	pm
Cr	2690	198	232	2816	227	198
Mo	2386	206	231	2511	211	203
W	2537	206	241	2403	208	204

	δ-C-H bond				α-C-H bond			
n-C_4H_9MF	IR	BO	Occ(σ^*)	Occ(σ)	IR	BO	Occ(σ^*)	Occ(σ)
unit	cm^{-1}		a.u.		cm^{-1}		a.u.	
Cr	2690	0.946	1.913	0.026	2816	0.957	1.930	0.016
Mo	2386	0.937	1.842	0.056	2511	0.907	1.857	0.041
W	2537	0.965	1.882	0.044	2403	0.891	1.835	0.052

Table A.33: Comparison of the interactions between the C-H-σ^* orbital and occupied hybrid orbital of the metal atoms. δ-C-H bond columns give the calculated data of the δ-C-H bond, and so on. IR^{δ} gives the stretching frequency of the δ-C-H bond, IR^{α} gives the stretching frequency of the α-C-H bond. ΔE^2_{ij} gives second-order perturbative estimation of the hyperconjugation effect between the C-H-σ^* orbital and occupied hybrid orbital of the TM atom, $\Delta\varepsilon_{ij}$ gives the energy gap of the two interacting NBOs, hyb. represents the hybridization of the orbitals.

					δ-C-H bond		α-C-H bond	
n-C_4H_9TMF	IR^{δ}	IR^{α}		hyb.	ΔE^2_{ij}	$\Delta\varepsilon_{ij}$	ΔE^2_{ij}	$\Delta\varepsilon_{ij}$
unit	cm^{-1}	cm^{-1}			kcal/mol	hartree	kcal/mol	hartree
Mo	2386	2511	NBO1	$sd^{9.99}$	0.77	0.44	1.89	0.47
			NBO2	$sd^{3.97}$	8.31	0.43	3.62	0.46
W	2537	2403	NBO1	$sd^{34.05}$	1.97	0.44	4.09	0.44
			NBO2	$sd^{1.74}$	2.73	0.44	3.12	0.45

A.2.2 The quintet state(ground state)

Table A.34: Structure, bond-order and occupancy comparison of the CH_3MoX molecules. IR^t presents the stretching frequencies of the trans C-H bond, and so on. D(Mo-H^t) presents distances between the Mo atom and the H atom that belongs to the trans C-H bond, and so on. In the α-spin columns calculated data of the α-spin are given, and so on. BO^t column shows bond-orders of the trans C-H bond. Δ column shows bond-order differences between the cis and the trans C-H bonds in the same molecules. Occ(σ) column gives occupancy changes related to the CH_3MoF molecule in the C-H-σ orbital, i.e. $\mathrm{Occ}(\sigma) = \mathrm{Occ}(\sigma_{(CH_3MoX)} - \mathrm{Occ}(\sigma)_{(CH_3MoF)}$, and so on.

CH_3MoX	IR^t	D(Mo-H^t)	IR^c	D(Mo-H^c)	D(Mo-C)
unit	cm^{-1}	pm	cm^{-1}	pm	pm
CN	2942	260	3055	272	210
I	2919	257	3051	274	210
Cl	2916	256	3052	274	210
Br	2914	256	3052	274	210
F	2902	252	3052	276	210

			α-spin		β-spin	
CH_3MoX	IR^t	IR^c	BO^t	Δ	BO^t	Δ
unit	cm^{-1}	cm^{-1}	bond-order			
CN	2942	3055	0.491	0.006	0.492	0.003
I	2919	3051	0.487	0.010	0.490	0.006
Cl	2916	3052	0.486	0.010	0.490	0.006
Br	2914	3052	0.486	0.010	0.490	0.006
F	2902	3052	0.485	0.010	0.492	0.004

		α-spin		β-spin	
CH_3MoX	IR^t	Occ(σ)	Occ(σ^*)	Occ(σ)	Occ(σ^*)
unit	cm^{-1}	elemental charge			
CN	2942	0.0000	0.0000	0.0000	0.0000
I	2919	-0.0031	0.0004	-0.0030	0.0003
Cl	2916	-0.0041	0.0003	-0.0027	0.0001
Br	2914	-0.0043	0.0004	-0.0033	0.0002
F	2902	-0.0060	0.0004	-0.0016	0.0000

.

Table A.35: Interactions between the C-H-σ orbital and the vacant hybrid orbital of the Mo atom in the CH_3MoX molecules. α-spin table shows information of interactions in the α-spin, and so on. IR^t column presents stretching frequencies of the trans C-H bond, ΔE^2_{ij} gives second-order perturbative estimations of the hyperconjugation effect, $\Delta\varepsilon_{ij}$ gives energy gaps of the interacting NBOs, hyb. column represents hybridizations of the nature hybrid orbital(NHO) of the Mo atom, which participates in the hyperconjugation. Mo(coe) column represents polarization coefficients of the Mo atom in the Mo-X-σ^* orbital, and so on. Composition column shows orbital compositions of the NHO of the Mo atom. NBO1 columns record calculated data of the NBO1, and so on. Sum column shows sums of the interactions. NBO1 is a Mo-X-σ^* orbital, NBO2 is a vacant Mo LP orbital.

α-spin

CH_3MoX	IR^t	ΔE^2_{ij}	hyb.	$\Delta\varepsilon_{ij}$	Mo(coe)	X(coe)	composition
unit	cm^{-1}	kcal/mol		hartree			
CN	2942	1.98	$sd^{1.55}$	0.60	0.86	-0.51	$0.63*5s+0.55*4d_{xy}-0.48*4d_{x^2-y^2}$
I	2919	2.41	$sd^{1.08}$	0.51	0.86	-0.51	$-0.69*5s-0.55*4d_{xy}+0.43*4d_{x^2-y^2}$
Cl	2916	2.73	$sd^{1.56}$	0.53	0.89	-0.45	$0.62*5s+0.61*4d_{xy}-0.42*4d_{x^2-y^2}$
Br	2914	2.72	$sd^{1.32}$	0.52	0.88	-0.47	$0.65*5s+0.59*4d_{xy}-0.42*4d_{x^2-y^2}$
F	2902	3.18	$sd^{3.15}$	0.56	-0.93	0.37	$0.48*5s+0.72*4d_{xy}-0.35*4d_{x^2-y^2}$

β-spin

			NBO1			NBO2		
CH_3MoX	IR^t	sum	ΔE^2_{ij}	hyb.	$\Delta\varepsilon_{ij}$	ΔE^2_{ij}	hyb.	$\Delta\varepsilon_{ij}$
unit	cm^{-1}	kcal/mol	kcal/mol		hartree	kcal/mol		hartree
CN	2942	2.84	1.80	$sd^{2.37}$	0.64	1.04	$sd^{6.97}$	0.52
I	2919	3.34	2.36	$sd^{1.92}$	0.56	0.98	$sd^{8.51}$	0.52
Cl	2916	3.46	2.67	$sd^{2.88}$	0.58	0.79	$sd^{6.79}$	0.52
Br	2914	3.54	2.66	$sd^{2.41}$	0.57	0.88	$sd^{7.27}$	0.52
F	2902	3.43	3.02	$sd^{6.46}$	0.61	0.41	$sd^{4.59}$	0.54

Table A.36: Structure comparison between the n-C_4H_9MoF and the CH_3MoF molecules. Met^t row represents calculated data of the trans C-H bond in the CH_3MoF molecule, and so on. But^δ row represents calculated data of the δ-C-H bond in the n-C_4H_9MoF molecule, and so on. IR gives stretching frequencies of the C-H bond. D(Mo-H) gives distances between the Mo atom and the H atom, which belongs to the C-H bond, and so on.

	IR	Mo-H	Mo-C
unit	cm^{-1}	pm	pm
Met^c	3052	276	210
But^α	2972	269	215
Met^t	2902	252	210
But^δ	2778	217	282

Table A.37: Bond-order and occupancy comparison of the C-H bond in the n-C_4H_9MoF and CH_3MoF molecules. Met^t row represents calculated data of the trans C-H bond in the CH_3MoF molecule, and so on. But^δ row represents calculated data of the δ-C-H bond in the n-C_4H_9MoF molecule, and so on. IR gives stretching frequencies of the C-H bond. In the α-spin columns calculated data of the α-spin are shown, and so on. BO column gives bond-orders of the C-H bond. Occ(σ) column gives occupancies of the C-H-σ orbital, and so on.

		α-spin			β-spin		
	IR	BO	Occ(σ)	Occ(σ^*)	BO	Occ(σ)	Occ(σ^*)
unit	cm^{-1}	a.u.					
Met^c	3052	0.495	0.999	0.009	0.496	0.991	0.001
But^α	2972	0.491	0.994	0.011	0.489	0.983	0.005
Met^t	2902	0.485	0.983	0.007	0.492	0.983	0.001
But^δ	2778	0.475	0.968	0.024	0.482	0.970	0.006

Table A.38: The leading interaction between the C-H-σ orbital and the vacant Mo hybrid orbital. Met^c row represents calculated data of the cis C-H bond in the CH_3MoF molecule, and so on. But^α row represents calculated data of the α-C-H bond in the n-C_4H_9MoF molecule, and so on. α-spin table records interaction information in the α-spin, and so on. IR gives stretching frequencies of the C-H bonds. ΔE^2_{ij} column gives second-order perturbative estimations of the hyperconjugation, hyb. column shows hybridizations of the NHO of the metal atom, which is participated in the interaction, $\Delta\varepsilon_{ij}$ gives energy gaps of the interacting NBOs. Composition column shows orbital compositions of the Mo NHO. Sum column gives sums of this type of interactions.

α-spin

	IR	ΔE^2_{ij}	hyb.	$\Delta\varepsilon_{ij}$	composition
unit	cm^{-1}	kcal/mol		hartree	
Met^c	3052	0.14	$sd^{1.86}$	0.57	$-0.59*5s+0.75*4d_{x^2-y^2}$
But^α	2972	0.07	$sd^{2.07}$	0.56	$-0.57*5s+0.76*4d_{x^2-y^2}$
Met^t	2902	3.18	$sd^{3.15}$	0.56	$0.48*5s+0.72*4d_{xy}$
But^δ	2778	8.09	$sd^{1.67}$	0.62	$0.61*5s-0.61*4d_{x^2-y^2}$

β-spin

	IR	sum	ΔE^2_{ij}	hyb.	$\Delta\varepsilon_{ij}$	composition
unit	cm^{-1}	kcal/mol	kcal/mol		hartree	
Met^c	3052	1.31	0.83	$sd^{41.87}$	0.50	$-0.72*4d_{xz}+0.65*4d_{yz}$
But^α	2972	2.15	1.82	$sd^{18.15}$	0.48	$-0.85*4d_{xz}+0.40*4d_{yz}$
Met^c	2902	3.02	3.02	$sd^{6.46}$	0.61	$0.36*5s+0.75*4d_{xy}-0.44*4d_{z^2}$
But^δ	2778	8.43	7.16	$sd^{4.65}$	0.66	$0.42*5s-0.54*4d_{x^2-y^2}+0.54*4d_{xy}$

Table A.39: The leading interaction between the C-H-σ^* orbital and the Mo hybrid orbital in the α-spin. Met^c row represents calculated data of the cis C-H bond in the CH_3MoF molecule, and so on. But$^\alpha$ row represents calculated data of the α-C-H bond in the n-C_4H_9MoF molecule, and so on. IR gives stretching frequencies of the C-H bonds. ΔE^2_{ij} column gives second-order perturbative estimations of the hyperconjugation, hyb. column shows hybridizations of the NHO of the metal atom, which is participated in the interaction, $\Delta\varepsilon_{ij}$ gives energy gaps of the interacting NBOs. Composition column shows orbital compositions of the Mo NHO. Sum column gives sums of this type of interactions.

	IR	sum	ΔE^2_{ij}	hyb.	$\Delta\varepsilon_{ij}$	composition
unit	cm^{-1}	kcal/mol	kcal/mol		hartree	
Met^c	3052	2.35	2.01	$sd^{99.99}$	0.61	$0.93 * 4d_{xz} + 0.35 * 4d_{yz}$
But$^\alpha$	2972	1.89	1.62	$sd^{99.99}$	0.59	$0,92 * 4d_{xz} - 0.29 * 4d_{yz}$
Met^c	2902	1.54	1.54	$sd^{2.75}$	0.57	$0.51 * 5s + 0.64 * 4d_{xy}$
But$^\delta$	2778	3.82	3.05	$sd^{8.11}$	0.51	$0.32 * 5s - 0.60 * 4d_{yz} - 0.69 * 4d_{xy}$

Table A.40: NPA comparison of the C-H bond in the n-C_4H_9MoF and the CH_3MoF molecules. The trans C-H bond columns show calculated data of the trans C-H bond, and so on. IR gives the stretching frequencies of the C-H bonds, q(H) gives natural charges of the H atom, which belongs to the C-H bond, and so on. $\Delta(q_H - q_C)$ gives natural charge differences between the H- and C-atoms. Met^c row represents calculated data of the cis C-H bond in the CH_3MoF molecule, and so on. But$^\alpha$ row represents calculated data of the α-C-H bond in the n-C_4H_9MoF molecule, and so on.

	the trans-C-H bond			the cis-C-H bond			
CH_3MoX	IR	$\Delta(q_H - q_C)$	q(H)	IR	$\Delta(q_H - q_C)$	q(H)	q(C)
unit	cm^{-1}	a.u.		cm^{-1}	a.u.		
CN	2942	1.194	0.200	3055	1.216	0.222	-0.994
I	2919	1.205	0.196	3051	1.226	0.217	-1.009
Cl	2916	1.216	0.197	3052	1.236	0.217	-1.019
Br	2914	1.209	0.196	3052	1.231	0.218	-1.013
F	2902	1.249	0.198	3052	1.267	0.216	-1.051

	IR	$\Delta(q_H - q_C)$	q(H)	q(C)
unit	cm^{-1}	a.u.		
Met^c	3052	1.267	0.216	-1.051
But$^\alpha$	2972	0.949	0.190	-0.759
Met^t	2902	1.249	0.198	-1.051
But$^\delta$	2778	0.752	0.154	-0.598

Table A.41: Structure, bond-order and occupancy comparison of the C-H activation in the CH_3MF molecules. IR^t gives stretching frequencies of the trans C-H bond. D(M-H^t) gives distances between the metal atom and the H atom that belongs to the trans C-H bond. D(M-C) gives distances between the metal atom and the C atom of the C-H bond. BO column gives C-H bond-orders of the trans C-H bond and Occ(σ) column gives occupancies of the C-H-σ orbital.

				α-spin		β-spin	
CH_3MF	IR^t	D(M-H^t)	D(M-C)	BO	Occ(σ)	BO	Occ(σ)
unit	cm^{-1}	pm	pm	a.u.			
Cr	2972	256	204	0.491	0.991	0.496	0.991
Mo	2902	252	210	0.485	0.983	0.492	0.983
W	2888	251	211	0.485	0.980	0.491	0.982

Table A.42: The leading interaction between the C-H-σ orbital and the hybrid orbital of the metal atoms in the CH_3MF molecules.. α-spin table shows interaction information of the α-spin, and so on. IR gives stretching frequencies of the C-H bonds. ΔE^2_{ij} column gives second-order perturbative estimations of the hyperconjugation, hyb. column shows hybridizations of the NHO of the metal atom, which is participated in the interaction, $\Delta\varepsilon_{ij}$ gives energy gaps of the interacting NBOs. M(coe) represents polarization coefficients of the metal atom orbital in the M-F-σ^* orbital, composition column shows orbital compositions of the Mo hybrid orbital.

α-spin

	IR	ΔE^2_{ij}	hyb.	$\Delta\varepsilon_{ij}$	M(coe)	X(coe)	composition
unit	cm^{-1}	kcal/mol		hartree			
Cr	2972	1.36	$sd^{2.12}$	0.49	-0.93	0.36	$0.56*4s+0.58*3d_{xy}$
Mo	2902	3.18	$sd^{3.15}$	0.56	-0.93	0.37	$0.48*5s+0.72*4d_{xy}$
W	2888	3.21	$sd^{4.58}$	0.77	-0.93	0.37	$0.41*6s+0.79*5d_{xy}$

β-spin

	IR	ΔE^2_{ij}	hyb.	$\Delta\varepsilon_{ij}$	M(coe)	X(coe)	composition
unit	cm^{-1}	kcal/mol		hartree			
Cr	2972	1.56	$sd^{5.09}$	0.50			$0.40*4s+0.73*3d_{xy}$
Mo	2902	3.02	$sd^{6.46}$	0.61	-0.94	0.33	$0.36*5s+0.75*4d_{xy}$
W	2888	2.80	$sd^{4.81}$	0.83	-0.94	0.34	$0.41*6s+0.76*5d_{xy}$

Table A.43: Structure and bond-order and occupancy comparison of the C-H activation in the *n*-C_4H_9MF molecules. In the δ-C-H bond columns calculated data of the δ-C-H bond are represented, and so on. IR gives the stretching frequencies of the C-H bonds. M-H gives distances between the metal atom and the H atom, which belongs to the C-H bond, and so on. BO(α) column gives bond-orders of the C-H bond in the α-spin, and so on. α-spin columns show calculated data of the α-spin, and so on. Occ(σ) column gives occupancies of the C-H-σ orbital, and so on.

	δ-C-H bond			in the α-C-H bond		
n-C_4H_9MF	IR	D(M-H)	D(M-C)	IR	D(M-H)	D(M-C)
unit	cm^{-1}	pm	pm	cm^{-1}	pm	pm
Cr	2853	210	267	2984	261	206
Mo	2778	217	282	2972	269	215
W	2727	218	292	2962	271	216

	δ-C-H bond			α-C-H bond		
	IR	BO(α)	BO(β)	IR	BO(α)	BO(β)
unit	cm^{-1}	a.u.	a.u.	cm^{-1}	a.u.	a.u.
Cr	2853	0.483	0.490	2984	0.493	0.491
Mo	2778	0.475	0.482	2972	0.491	0.489
W	2727	0.479	0.481	2962	0.489	0.488

	δ-C-H bond					α-C-H bond				
		α-spin		β-spin			α-spin		β-spin	
	IR	Occ(σ)	Occ(σ^*)	Occ(σ)	Occ(σ^*)	IR	Occ(σ)	Occ(σ^*)	Occ(σ)	Occ(σ^*)
unit	cm^{-1}	a.u.				cm^{-1}	a.u.			
Cr	2853	0.974	0.014	0.976	0.006	2984	0.994	0.007	0.988	0.005
Mo	2778	0.968	0.024	0.970	0.006	2972	0.994	0.011	0.983	0.005
W	2727	0.966	0.034	0.967	0.007	2962	0.994	0.015	0.983	0.005

Table A.44: The leading interaction between the C-H-σ^* orbital and the Mo hybrid orbital in the α-spin of the *n*-C_4H_9MF molecules. IR gives stretching frequencies of the δ-C-H bonds. ΔE^2_{ij} column gives second-order perturbative estimations of the hyperconjugation, hyb. column shows hybridizations of the NHO of the metal atom, which is participated in the interaction, $\Delta\varepsilon_{ij}$ gives energy gaps of the interacting NBOs. Composition column shows orbital compositions of the Mo NHO. Sum column gives sums of this type of interactions.

	IR	sum	ΔE^2_{ij}	hyb.	$\Delta\varepsilon_{ij}$	composition
unit	cm^{-1}	kcal/mol	kcal/mol		hartree	
Cr	2853	1.72	1.35	$sd^{14.29}$	0.54	$0.25 * 4s - 0.54 * 3d_{yz} - 0.76 * 3d_{xy}$
Mo	2778	3.82	3.05	$sd^{2.75}$	0.51	$0.51 * 5s - 0.64 * 4d_{xy}$
W	2727	5.37	4.92	$sd^{5.15}$	0.50	$0.40 * 6s + 0.62 * 5d_{yz} + 0.61 * 5d_{xy}$

Table A.45: The leading interaction between the C-H-σ orbital and the vacant Mo hybrid orbital in the n-C_4H_9MF molecules. α-spin table records interaction information in the α-spin, and so on. IR gives stretching frequencies of the C-H bonds. ΔE^2_{ij} column gives second-order perturbative estimations of the hyperconjugation, hyb. column shows hybridizations of the NHO of the metal atom, which is participated in the interaction, $\Delta\varepsilon_{ij}$ gives energy gaps of the interacting NBOs. Composition column shows orbital compositions of the Mo NHO. Sum column gives sums of this type of interactions. M(coe) column shows polarization coefficients of the M-F-σ^* orbital, and so on.

α-spin

	IR	ΔE^2_{ij}	hyb.	$\Delta\varepsilon_{ij}$	composition	M(coe)	F(coe)
unit	cm^{-1}	kcal/mol		hartree			
Cr	2853	5.83	$sd^{1.21}$	0.57	$0.67*4s-0.65*3d_{x^2-y^2}$	-0.94	0.34
Mo	2778	8.09	$sd^{1.67}$	0.62	$0.61*5s-0.61*4d_{x^2-y^2}$	-0.94	0.35
W	2727	8.37	$sd^{2.60}$	0.77	$0.52*6s-0.56*5d_{x^2-y^2}+0.51*5d_{xy}$	-0.93	0.36

β-spin

	IR	sum	ΔE^2_{ij}	hyb.	$\Delta\varepsilon_{ij}$	composition	M(coe)	F(coe)
unit	cm^{-1}	kcal/mol	kcal/mol		hartree			
Cr	2853	6.59	5.36	$sd^{2.21}$	0.58	$0.55*4s-0.50*3d_{x^2-y^2}+0.51*3d_{xy}$		
Mo	2778	8.43	7.16	$sd^{4.65}$	0.66	$0.42*5s-0.54*4d_{x^2-y^2}+0.54*4d_{xy}$	-0.94	0.33
W	2727	9.66	7.63	$sd^{3.81}$	0.83	$0.45*6s-0.51*5d_{x^2-y^2}-0.59*5d_{xy}$	-0.94	0.34

A.2.3 The triplet state(first exited state)

Table A.46: Structure, bond-order and occupancy comparison of the CH_3MoX molecules. IR^t presents the stretching frequencies of the trans C-H bond, and so on. D(Mo-H^t) presents distances between the Mo atom and the H atom that belongs to the trans C-H bond, and so on. In the α-spin columns calculated data of the α-spin are given, and so on. BO^t column shows bond-orders of the trans C-H bond. Δ column shows bond-order differences between the cis and the trans C-H bonds in the same molecules. Occ(σ) column gives occupancy changes related to the CH_3MoF molecule in the C-H-σ orbital, i.e. $\mathrm{Occ}(\sigma) = \mathrm{Occ}(\sigma_{(CH_3MoX)} - \mathrm{Occ}(\sigma)_{(CH_3MoF)}$, and so on.

CH_3MoX	IR^t	D(Mo-H^t)	IR^c	D(Mo-H^c)	D(Mo-C)
unit	cm^{-1}	pm	cm^{-1}	pm	pm
CN	2948	260.6	3035	271.2	209.4
I	2537	208.3	3186	295.8	193.2
Br	2511	206.2	3196	296.2	192.7
Cl	2507	205.6	3202	296.4	192.7
F	2494	203.9	3220	296.6	192.5

			α-spin		β-spin	
CH_3MoX	IR^t	IR^c	BO^t	Δ	BO^t	Δ
unit	cm^{-1}	cm^{-1}	bond-order			
I	2537	3186	0.455	0.041	0.456	0.040
Br	2511	3196	0.452	0.044	0.452	0.046
Cl	2507	3202	0.451	0.045	0.451	0.046
F	2494	3220	0.450	0.046	0.451	0.046

		α-spin		β-spin	
CH_3MoX	IR^t	Occ(σ)	Occ(σ^*)	Occ(σ)	Occ(σ^*)
unit	cm^{-1}	a.u.			
I	2537	0.0000	0.0000	0.0000	0.0000
Br	2511	-0.0043	0.0015	-0.0038	0.0018
Cl	2507	-0.0051	0.0019	-0.0043	0.0021
F	2494	-0.0051	0.0038	-0.0037	0.0045

.

Table A.47: The leading interaction between the C-H-σ orbital and the vacant hybrid orbital of the Mo atom in the CH_3MoX molecules. α-spin table records interaction information in the α-spin, and so on. IR^t gives stretching frequencies of the trans C-H bonds. ΔE^2_{ij} column gives second-order perturbative estimations of the hyperconjugation, hyb. column shows hybridizations of the NHO of the metal atom, which is participated in the interaction, $\Delta\varepsilon_{ij}$ gives energy gaps of the interacting NBOs. Composition column shows orbital compositions of the Mo NHO. Sum column gives sums of this type of interactions. M(coe) column shows polarization coefficients of the M-F-σ^* orbital, and so on.

α-spin

	IR	sum	ΔE^2_{ij}	hyb.	$\Delta\varepsilon_{ij}$	composition	M(coe)	F(coe)
unit	cm^{-1}	kcal/mol	kcal/mol		hartree			
I	2537	19.38	13.16	$sd^{0.65}$	0.60	$-0.77*5s-0.61*4d_{xy}$	0.88	-0.48
Br	2511	21.65	14.97	$sd^{0.74}$	0.61	$-0.75*5s-0.63*4d_{xy}$	0.89	-0.45
Cl	2507	22.25	15.54	$sd^{0.84}$	0.62	$-0.73*5s-0.65*4d_{xy}$	0.90	-0.44
F	2494	22.49	14.80	$sd^{1.47}$	0.65	$-0.63*5s+0.72*4d_{xy}$	0.91	0.42

β-spin

	IR	sum	ΔE^2_{ij}	hyb.	$\Delta\varepsilon_{ij}$	composition	M(coe)	F(coe)
unit	cm^{-1}	kcal/mol	kcal/mol		hartree			
I	2537	20.54	12.46	$sd^{0.70}$	0.62	$-0.76*5s-0.60*4d_{xy}$	0.89	-0.45
Br	2511	22.56	14.18	$sd^{0.82}$	0.63	$-0.74*5s-0.63*4d_{xy}$	0.90	-0.43
Cl	2507	23.08	14.67	$sd^{0.95}$	0.64	$-0.71*5s-0.65*4d_{xy}$	0.91	-0.42
F	2494	22.30	13.76	$sd^{1.74}$	0.67	$-0.60*5s+0.72*4d_{xy}$	0.94	-0.34

Table A.48: The leading interaction between the C-H-σ^* orbital and the occupied hybrid orbital of the Mo atom in the CH_3MoX molecules. α-spin table records interaction information in the α-spin, and so on. IR^t gives stretching frequencies of the trans C-H bonds. ΔE^2_{ij} column gives second-order perturbative estimations of the hyperconjugation, hyb. column shows hybridizations of the NHO of the metal atom, which is participated in the interaction, $\Delta\varepsilon_{ij}$ gives energy gaps of the interacting NBOs. Composition column shows orbital compositions of the Mo NHO.

α-spin

	IR	ΔE^2_{ij}	hyb.	$\Delta\varepsilon_{ij}$	composition
unit	cm^{-1}	kcal/mol		hartree	
I	2537	3.04	$sd^{3.39}$	0.50	$0.48*5s+0.51*4d_{z^2}-0.54*d_{x^2-y^2}$
Br	2511	3.30	$sd^{2.90}$	0.50	$0.51*5s+0.51*4d_{z^2}-0.54*d_{x^2-y^2}$
Cl	2507	3.38	$sd^{2.54}$	0.50	$0.53*5s+0.51*4d_{z^2}-0.54*d_{x^2-y^2}$
F	2494	3.72	$sd^{1.72}$	0.49	$0.60*5s+0.50*4d_{z^2}-0.54*d_{x^2-y^2}$

β-spin

	IR	ΔE^2_{ij}	hyb.	$\Delta\varepsilon_{ij}$	composition
unit	cm^{-1}	kcal/mol		hartree	
I	2537	3.65	$sd^{3.12}$	0.46	$0.49*5s+0.65*4d_{z^2}-0.42*d_{x^2-y^2}$
Br	2511	3.97	$sd^{2.65}$	0.45	$0.52*5s+0.65*4d_{z^2}-0.43*d_{x^2-y^2}$
Cl	2507	4.06	$sd^{2.37}$	0.45	$0.54*5s+0.65*4d_{z^2}-0.43*d_{x^2-y^2}$
F	2494	4.50	$sd^{1.64}$	0.45	$0.61*5s+0.63*4d_{z^2}-0.43*d_{x^2-y^2}$

Table A.49: Structure comparison between the n-C_4H_9MoF and the CH_3MoF molecules. Met^t row represents calculated data of the trans C-H bond in the CH_3MoF molecule, and so on. But^δ row represents calculated data of the δ-C-H bond in the n-C_4H_9MoF molecule, and so on. IR gives stretching frequencies of the C-H bond. D(Mo-H) gives distances between the Mo atom and the H atom, which belongs to the C-H bond, and so on.

	IR	Mo-H	Mo-C
unit	cm^{-1}	pm	pm
Met^c	3220	297	192
But^α	2968	262	213
Met^c	2494	204	192
But^δ	2370	198	236

Table A.50: Bond-order and occupancy comparison of the C-H bond in the n-C_4H_9MoF and CH_3MoF molecules. Met^t row represents calculated data of the trans C-H bond in the CH_3MoF molecule, and so on. But^δ row represents calculated data of the δ-C-H bond in the n-C_4H_9MoF molecule, and so on. IR gives stretching frequencies of the C-H bond. In the α-spin columns calculated data of the α-spin are shown, and so on. BO column gives bond-orders of the C-H bond. Occ(σ) column gives occupancies of the C-H-σ orbital, and so on.

		α-spin			β-spin		
	IR	BO	Occ(σ)	Occ(σ^*)	BO	Occ(σ)	Occ(σ^*)
unit	cm^{-1}	a.u.					
Met^c	3220	0.496	0.997	0.006	0.497	0.996	0.006
But^α	2968	0.491	0.993	0.010	0.485	0.977	0.007
Met^t	2494	0.450	0.927	0.024	0.451	0.934	0.028
But^δ	2370	0.472	0.933	0.027	0.473	0.938	0.036

Table A.51: The leading interaction between the C-H-σ orbital and the vacant Mo hybrid orbital in the α-spin of the molecules. Met^c row represents calculated data of the cis C-H bond in the CH_3MoF molecule, and so on. But$^\alpha$ row represents calculated data of the α-C-H bond in the *n*-C_4H_9MoF molecule, and so on. IR gives stretching frequencies of the C-H bonds. ΔE^2_{ij} column gives second-order perturbative estimations of the hyperconjugation, hyb. column shows hybridizations of the NHO of the metal atom, which is participated in the interaction, $\Delta\varepsilon_{ij}$ gives energy gaps of the interacting NBOs. Composition column shows orbital compositions of the Mo NHO. Sum column gives sums of this type of interactions.

	IR	sum	ΔE^2_{ij}	hyb.	$\Delta\varepsilon_{ij}$	composition
unit	cm^{-1}	kcal/mol	kcal/mol		hartree	
Met^c	3220	0.03	0.03	$sd^{3.45}$	0.61	$-0.47 * 5s - 0.63 * 4d_{x^2-y^2} - 0.57 * 4d_{xy}$
But$^\alpha$	2968	0.40	0.40	$sd^{7.65}$	0.40	$0.34 * 5s - 0.28 * 4d_{xz} - 0.89 * 4d_{yz}$
Met^t	2494	22.49	14.80	$sd^{1.47}$	0.65	$-0.63 * 5s + 0.72 * 4d_{xy}$
But$^\delta$	2370	25.76	16.45	$sd^{7.65}$	0.46	$0.34 * 5s - 0.28 * 4d_{xz} - 0.89 * 4d_{yz}$

Table A.52: The leading interaction between the C-H-σ orbital and the vacant Mo hybrid orbital in the β-spin of the molecules. Met^c row represents calculated data of the cis C-H bond in the CH_3MoF molecule, and so on. But$^\alpha$ row represents calculated data of the α-C-H bond in the *n*-C_4H_9MoF molecule, and so on. NBO1 columns give calculated data of the NBO1, and so on. IR gives stretching frequencies of the C-H bonds. ΔE^2_{ij} column gives second-order perturbative estimations of the hyperconjugation, hyb. column shows hybridizations of the NHO of the metal atom, which is participated in the interaction, $\Delta\varepsilon_{ij}$ gives energy gaps of the interacting NBOs. Composition column shows orbital compositions of the Mo NHO. Sum column gives sums of this type of interactions. The NBO1 is a hybrid Mo LP orbital with main $4d_{xz}$ and $4d_{yz}$ orbital share. The NBO2 is a Mo-F-σ^* orbital except in the But$^\delta$ row.

			NBO1			NBO2		
	IR	sum	ΔE^2_{ij}	hyb.	$\Delta\varepsilon_{ij}$	ΔE^2_{ij}	hyb.	$\Delta\varepsilon_{ij}$
unit	cm^{-1}	kcal/mol	kcal/mol		hartree	kcal/mol		hartree
Met^t	3220	0						
But$^\alpha$	2968	3.24	3.01	$sd^{61.52}$	0.45	0.23	$sd^{8.87}$	0.46
Met^t	2494	22.30	7.13	$sd^{99.99}$	0.44	13.76	$sd^{1.74}$	0.67
But$^\delta$	2370	24.17	11.85	$sd^{31.34}$	0.48	11.13	$sd^{1.70}$	0.69

Table A.53: NPA comparison of the C-H bond in the n-C_4H_9MoF and the CH_3MoF molecules. The trans C-H bond columns show calculated data of the trans C-H bond, and so on. IR gives the stretching frequencies of the C-H bonds, q(H) gives natural charges of the H atom, which belongs to the C-H bond, and so on. $\Delta(q_H - q_C)$ gives natural charge differences between the H- and C-atoms. Met^c row represents calculated data of the cis C-H bond in the CH_3MoF molecule, and so on. But^α row represents calculated data of the α-C-H bond in the n-C_4H_9MoF molecule, and so on.

	the trans-C-H bond			the cis-C-H bond			
CH_3MoX	IR	$\Delta(q_H - q_C)$	q(H)	IR	$\Delta(q_H - q_C)$	q(H)	q(C)
unit	cm^{-1}	a.u.		cm^{-1}	a.u.		
I	2537	1.021	0.196	3186	1.066	0.241	-0.825
Br	2511	1.018	0.198	3196	1.062	0.242	-0.820
Cl	2507	1.023	0.199	3202	1.067	0.243	-0.824
F	2494	1.058	0.199	3220	1.106	0.247	-0.859

	IR	$\Delta(q_H - q_C)$	q(H)	q(C)
unit	cm^{-1}	a.u.		
Met^c	3220	1.106	0.247	-0.859
But^α	2968	0.888	0.196	-0.692
Met^t	2494	1.058	0.199	-0.859
But^δ	2370	0.799	0.202	-0.597

Table A.54: Structure, bond-order and occupancy comparison of the C-H activation in the CH_3MF molecules. IR^t gives stretching frequencies of the trans C-H bond. D(M-H^t) gives distances between the metal atom and the H atom that belongs to the trans C-H bond. D(M-C) gives distances between the metal atom and the C atom of the C-H bond. BO column gives C-H bond-orders of the trans C-H bond and Occ(σ) column gives occupancies of the C-H-σ orbital.

				α-spin		β-spin	
CH_3MF	IR^t	D(M-H^t)	D(M-C)	BO	Occ(σ)	BO	Occ(σ)
unit	cm^{-1}	pm	pm	a.u.			
Cr	2966	254	201	0.492	0.991	0.494	0.990
Mo	2494	204	192	0.450	0.927	0.451	0.934
W	2585	212	196	0.457	0.933	0.460	0.941

Table A.55: The leading interactions between the C-H-σ orbital and the hybrid orbital of the metal atoms in the CH_3MF molecules. α-spin table shows interaction information of the α-spin, and so on. IR gives stretching frequencies of the C-H bonds. ΔE^2_{ij} column gives second-order perturbative estimations of the hyperconjugation, hyb. column shows hybridizations of the NHO of the metal atom, which is participated in the interaction, $\Delta\varepsilon_{ij}$ gives energy gaps of the interacting NBOs. Sum column gives sums of this type of interactions. The NBO1 is a M-F-σ^* orbital, the NBO2 is a hybrid LP orbital of the metal atoms.

α-spin

			NBO1			NBO2		
	IR	sum	ΔE^2_{ij}	hyb.	$\Delta\varepsilon_{ij}$	ΔE^2_{ij}	hyb.	$\Delta\varepsilon_{ij}$
unit	cm^{-1}	kcal/mol	kcal/mol		hartree	kcal/mol		hartree
Cr	2966	1.58	1.58	$sd^{4.02}$	0.51			
Mo	2494	22.49	14.80	$sd^{1.47}$	0.65	7.69	$sd^{99.99}$	0.40
W	2585	26.35	18.12	$sd^{2.38}$	0.88	6.84	$sd^{99.99}$	0.41

β-spin

			NBO1			NBO2		
	IR	sum	ΔE^2_{ij}	hyb.	$\Delta\varepsilon_{ij}$	ΔE^2_{ij}	hyb.	$\Delta\varepsilon_{ij}$
unit	cm^{-1}	kcal/mol	kcal/mol		hartree	kcal/mol		hartree
Cr	2966	2.10	1.51	$sd^{2.71}$	0.53	0.59	$sd^{14.62}$	0.50
Mo	2494	22.30	13.76	$sd^{1.74}$	0.67	7.13	$sd^{99.99}$	0.44
W	2585	23.04	16.18	$sd^{2.72}$	0.89	6.34	$sd^{99.99}$	0.44

Table A.56: The leading interaction between the C-H-σ^* orbital and the hybrid orbital of the metal atoms in the α-spin of the CH_3MF molecules. IR gives stretching frequencies of the δ-C-H bonds. ΔE^2_{ij} column gives second-order perturbative estimations of the hyperconjugation, hyb. column shows hybridizations of the NHO of the metal atom, which is participated in the interaction, $\Delta\varepsilon_{ij}$ gives energy gaps of the interacting NBOs. Composition column shows orbital compositions of the Mo NHO. Sum column gives sums of this type of interactions.

	IR	sum	ΔE^2_{ij}	hyb.	$\Delta\varepsilon_{ij}$	composition
unit	cm^{-1}	kcal/mol	kcal/mol		hartree	
Cr	2966	0.76	0.76	$sd^{21.21}$	0.64	$-0.80 * 4s - 0.46 * 3d_{x^2-y^2}$
Mo	2494	4.78	3.72	$sd^{1.72}$	0.49	$0.60 * 5s - 0.54 * 4d_{x^2-y^2} + 0.50 * 4d_{z^2}$
W	2585	3.71	2.38	$sd^{0.92}$	0.52	$0.72 * 6s - 0.50 * 5d_{x^2-y^2} + 0.43 * 5d_{z^2}$

Table A.57: Structure and bond-order and occupancy comparison of the C-H activation in the *n*-C_4H_9MF molecules. In the δ-C-H bond columns calculated data of the δ-C-H bond are represented, and so on. IR gives the stretching frequencies of the C-H bonds. M-H gives distances between the metal atom and the H atom, which belongs to the C-H bond, and so on. BO(α) column gives bond-orders of the C-H bond in the α-spin, and so on. α-spin columns show calculated data of the α-spin, and so on. Occ(σ) column gives occupancies of the C-H-σ orbital, and so on.

	δ-C-H bond			in the α-C-H bond		
n-C_4H_9MF	IR	D(M-H)	D(M-C)	IR	D(M-H)	D(M-C)
unit	cm^{-1}	pm	pm	cm^{-1}	pm	pm
Cr	2624	194	231	2986	253	203
Mo	2370	198	236	2968	262	213
W	2611	212	251	2939	264	214

	δ-C-H bond			α-C-H bond		
	IR	BO(α)	BO(β)	IR	BO(α)	BO(β)
unit	cm^{-1}	a.u.	a.u.	cm^{-1}	a.u.	a.u.
Cr	2624	0.478	0.480	2986	0.491	0.488
Mo	2370	0.472	0.473	2968	0.491	0.485
W	2611	0.483	0.476	2939	0.488	0.485

	δ-C-H bond					α-C-H bond				
		α-spin		β-spin			α-spin		β-spin	
	IR	Occ(σ)	Occ(σ^*)	Occ(σ)	Occ(σ^*)	IR	Occ(σ)	Occ(σ^*)	Occ(σ)	Occ(σ^*)
unit	cm^{-1}	a.u.				cm^{-1}	a.u.			
Cr	2624	0.967	0.014	0.959	0.015	2986	0.990	0.008	0.988	0.010
Mo	2370	0.933	0.027	0.938	0.036	2968	0.993	0.010	0.977	0.007
W	2611	0.951	0.022	0.954	0.024	2939	0.987	0.012	0.978	0.007

Table A.58: The leading interaction between the C-H-σ^* orbital and the metal hybrid orbital in the n-C_4H_9MF molecules. IR gives stretching frequencies of the δ-C-H bonds. ΔE^2_{ij} column gives second-order perturbative estimations of the hyperconjugation, hyb. column shows hybridizations of the NHO of the metal atom, which is participated in the interaction, $\Delta\varepsilon_{ij}$ gives energy gaps of the interacting NBOs. Composition column shows orbital compositions of the Mo NHO. Sum column gives sums of this type of interactions.

α-spin	IR	sum	ΔE^2_{ij}	hyb.	$\Delta\varepsilon_{ij}$	composition
unit	cm^{-1}	kcal/mol	kcal/mol		hartree	
Cr	2624	1.72	0.97	$sd^{99.99}$	0.50	$0.88 * 3d_{yz} - 0.40 * 3d_{xy}$
Mo	2370	3.85	2.37	$sd^{3.63}$	0.45	$0.46 * 5s + 0.56 * 4d_{z^2} - 0.63 * 4d_{xy}$
W	2611	3.67	1.86	$sd^{13.60}$	0.47	$0.81 * 5d_{z^2} - 0.38 * 5d_{xy}$
β-spin	IR	sum	ΔE^2_{ij}	hyb.	$\Delta\varepsilon_{ij}$	composition
unit	cm^{-1}	kcal/mol	kcal/mol		hartree	
Cr	2624	1.12	1.12	$sd^{18.00}$	0.42	$0.52 * 3d_{z^2} + 0.81 * 3d_{xz}$
Mo	2370	5.00	5.00	$sd^{3.46}$	0.41	$0.47 * 5s + 0.85 * 4d_{z^2}$
W	2611	3.26	3.26	$sd^{1.36}$	0.44	$0.65 * 6s + 0.69 * 5d_{z^2}$

Table A.59: The first two leading interaction between the C-H-σ orbital and the vacant metal hybrid orbital in the n-C_4H_9MF molecules. α-spin table records interaction information in the α-spin, and so on. IR gives stretching frequencies of the C-H bonds. ΔE^2_{ij} column gives second-order perturbative estimations of the hyperconjugation, hyb. column shows hybridizations of the NHO of the metal atom, which is participated in the interaction, $\Delta\varepsilon_{ij}$ gives energy gaps of the interacting NBOs. Sum column gives sums of this type of interactions. The NBO1 is a M-F-σ^* orbital, the NBO2 is a hybrid LP orbital of the metal atoms.

α-spin

			NBO1			NBO2		
	IR	sum	ΔE^2_{ij}	hyb.	$\Delta\varepsilon_{ij}$	ΔE^2_{ij}	hyb.	$\Delta\varepsilon_{ij}$
unit	cm^{-1}	kcal/mol	kcal/mol		hartree	kcal/mol		hartree
Cr	2624	11.66	5.73	$sd^{2.70}$	0.60	5.93	$sd^{1.36}$	0.52
Mo	2370	25.76	9.31	$sd^{1.56}$	0.66	16.45	$sd^{7.65}$	0.46
W	2611	18.64	12.13	$sd^{0.81}$	0.81	6.51	$sd^{74.37}$	0.45

β-spin

			NBO1			NBO2		
	IR	sum	ΔE^2_{ij}	hyb.	$\Delta\varepsilon_{ij}$	ΔE^2_{ij}	hyb.	$\Delta\varepsilon_{ij}$
unit	cm^{-1}	kcal/mol	kcal/mol		hartree	kcal/mol		hartree
Cr	2624	14.33	7.07	$sd^{2.73}$	0.64	5.61	$sd^{31.69}$	0.54
Mo	2370	24.17	11.13	$sd^{1.70}$	0.69	11.85	$sd^{31.34}$	0.48
W	2611	19.72	11.58	$sd^{1.99}$	0.83	5.41	$sd^{99.99}$	0.48

A.3 Group 7 transition metal elements

A.3.1 The doublet state(first excited state)

Table A.60: Structure, bond-order and occupancy comparison of the CH_3TcX molecules. IR^t represents the stretching frequencies of the trans C-H bond, and so on. D(Tc-H^t) represents distances between the Tc atom and the H atom that belongs to the trans C-H bond, and so on. In the α-spin columns calculated data of the α-spin are given, and so on. BO^t column shows bond-orders of the trans C-H bond. Δ column shows bond-order differences between the cis and the trans C-H bonds in the same molecules. Occ(σ) column gives occupancy changes related to the CH_3TcF molecule in the C-H-σ orbital, i.e. $Occ(\sigma) = Occ(\sigma_{(CH_3TcX)} - Occ(\sigma)_{(CH_3TcCN)}$, and so on.

CH_3TcX	IR^t	D(Tc-H^t)	IR^c	D(Tc-H^c)	D(Tc-C)
unit	cm^{-1}	pm	cm^{-1}	pm	pm
CN	2951	254	3060	263	203
I	2927	256	3046	263	204
Br	2922	255	3043	265	204
Cl	2909	254	3044	266	204
F	2829	240	3051	268	202

			α-spin		β-spin	
CH_3TcX	IR^t	IR^c	BO^t	Δ	BO^t	Δ
unit	cm^{-1}	cm^{-1}	bond-order			
CN	2951	3060	0.490	0.006	0.493	-0.002
I	2927	3046	0.489	0.002	0.487	0.013
Br	2922	3043	0.489	0.009	0.488	0.005
Cl	2909	3044	0.486	0.001	0.492	0.007
F	2829	3051	0.483	0.010	0.483	0.013

		α-spin		β-spin	
CH_3TcX	IR^t	Occ(σ)	Occ(σ^*)	Occ(σ)	Occ(σ^*)
unit	cm^{-1}	a.u.			
CN	2951	0.000	0.000	0.000	0.000
I	2927	0.008	0.005	-0.004	0.000
Br	2922	0.008	0.005	-0.008	-0.002
Cl	2909	0.005	0.005	-0.006	0.001
F	2829	-0.005	0.003	-0.013	0.002

.

Table A.61: The leading interaction between the C-H-σ^* orbital and the occupied hybrid orbital of the Tc atom in the CH_3TcX molecules. α-spin table records interaction information in the α-spin, and so on. IR^t gives stretching frequencies of the trans C-H bonds. ΔE^2_{ij} column gives second-order perturbative estimations of the hyperconjugation, hyb. column shows hybridizations of the NHO of the metal atom, which is participated in the interaction, $\Delta\varepsilon_{ij}$ gives energy gaps of the interacting NBOs. Composition column shows orbital compositions of the Tc NHO. Sum column gives sums of this type of interactions.

α-spin

	IR^t	sum	ΔE^2_{ij}	hyb.	$\Delta\varepsilon_{ij}$	composition
unit	cm^{-1}	kcal/mol	kcal/mol		hartree	
CN	2951	0.30	0.19	$sd^{99.99}$	0.60	$0.90 * 4d_{xz} + 0.38 * 4d_{yz}$
I	2927	1.77	1.77	$sd^{8.65}$	0.59	$0.32 * 5s - 0.37 * 4d_{x^2-y^2} + 0.86 * 4d_{xy}$
Br	2922	1.78	1.78	$sd^{9.44}$	0.58	$0.31 * 5s - 0.42 * 4d_{x^2-y^2} + 0.85 * 4d_{xy}$
Cl	2909	1.70	1.70	$sd^{5.50}$	0.59	$0.39 * 5s - 0.49 * 4d_{x^2-y^2} + 0.77 * 4d_{xy}$
F	2829	1.37	0.95	$sd^{28.92}$	0.55	$-0.46 * 4d_{xy} - 0.75 * 4d_{yz}$

β-spin

	IR^t	sum	ΔE^2_{ij}	hyb.	$\Delta\varepsilon_{ij}$	composition
unit	cm^{-1}	kcal/mol	kcal/mol		hartree	
CN	2951	1.46	1.17	$sd^{27.94}$	0.58	$0.84 * 4d_{xy} - 0.30 * 4d_{x^2-y^2}$
I	2927	1.26	1.26	$sd^{6.68}$	0.57	$0.36 * 5s - 0.74 * 4d_{xz} - 0.58 * 4d_{yz}$
Br	2922	0.86	0.86	$sd^{99.99}$	0.55	$0.74 * 4d_{z^2} - 0.61 * 4d_{xy}$
Cl	2909	1.37	1.37	$sd^{4.13}$	0.57	$0.44 * 5s + 0.47 * 4d_{z^2} + 0.74 * 4d_{xy}$
F	2829	1.71	1.71	$sd^{6.83}$	0.54	$0.35 * 5s - 0.62 * 4d_{x^2-y^2} - 0.63 * 4d_{xy}$

Table A.62: Structure comparison between the n-C_4H_9TcF and the CH_3TcF molecules. Met^t row represents calculated data of the trans C-H bond in the CH_3TcF molecule, and so on. But^δ row represents calculated data of the δ-C-H bond in the n-C_4H_9TcF molecule, and so on. IR gives stretching frequencies of the C-H bond. D(Tc-H) gives distances between the Tc atom and the H atom, which belongs to the C-H bond, and so on.

	IR	Tc-H	Tc-C
unit	cm^{-1}	pm	pm
Met^c	3051	268	202
But^α	2943	257	207
Met^t	2829	240	202
But^δ	2604	201	249

Table A.63: Bond-order and occupancy comparison of the C-H bond in the n-C_4H_9TcF and CH_3TcF molecules. Met^t row represents calculated data of the trans C-H bond in the CH_3TcF molecule, and so on. But^δ row represents calculated data of the δ-C-H bond in the n-C_4H_9TcF molecule, and so on. IR gives stretching frequencies of the C-H bond. In the α-spin columns calculated data of the α-spin are shown, and so on. BO column gives bond-orders of the C-H bond. Occ(σ) column gives occupancies of the C-H-σ orbital, and so on.

		α-spin			β-spin		
	IR	BO	Occ(σ)	Occ(σ^*)	BO	Occ(σ)	Occ(σ^*)
unit	cm^{-1}	a.u.					
Met^c	3051	0.496	0.999	0.009	0.492	0.988	0.003
But^α	2943	0.489	0.986	0.009	0.487	0.987	0.010
Met^t	2829	0.486	0.975	0.005	0.483	0.978	0.008
But^δ	2604	0.476	0.953	0.016	0.473	0.954	0.023

Table A.64: The leading interaction between the C-H-σ^* orbital and the occupied Tc hybrid orbital in the α-spin of the molecules. Met^c row represents calculated data of the cis C-H bond in the CH_3TcF molecule, and so on. But^α row represents calculated data of the α-C-H bond in the n-C_4H_9TcF molecule, and so on. NBO1 columns give calculated data of the NBO1, and so on. α-spin table gives calculated data in the α-spin of the molecules, and so on. IR gives stretching frequencies of the C-H bonds. ΔE^2_{ij} column gives second-order perturbative estimations of the hyperconjugation, hyb. column shows hybridizations of the NHO of the metal atom, which is participated in the interaction, $\Delta\varepsilon_{ij}$ gives energy gaps of the interacting NBOs. Composition column shows orbital compositions of the Tc NHO. Sum column gives sums of this type of interactions.

α-spin

	IR	sum	ΔE^2_{ij}	hyb.	$\Delta\varepsilon_{ij}$	composition
unit	cm^{-1}	kcal/mol	kcal/mol		hartree	
Met^c	3051	2.14	1.99	$sd^{99.99}$	0.62	$0.94 * 4d_{xz} + 0.32 * 4d_{yz}$
But^α	2943	1.18	0.99	$sd^{83.53}$	0.57	$0.65 * 4d_{xz} + 0.53 * 4d_{yz} + 0.46 * 4d_{z^2}$
Met^t	2829	1.37	0.95	$sd^{28.92}$	0.55	$-0.46 * 4d_{xy} - 0.75 * 4d_{yz}$
But^δ	2604	2.10	1.41	$sd^{83.53}$	0.48	$0.65 * 4d_{xz} + 0.53 * 4d_{yz} + 0.46 * 4d_{z^2}$

β-spin

	IR	sum	ΔE^2_{ij}	hyb.	$\Delta\varepsilon_{ij}$	composition
unit	cm^{-1}	kcal/mol	kcal/mol		hartree	
Met^c	3051	0.59	0.59	$sd^{19.34}$	0.59	$-0.42 * 4d_{xz} + 0.64 * 4d_{yz} + 0.60 * 4d_{z^2}$
But^α	2943	1.29	1.29	$sd^{90.97}$	0.57	$0.73 * 4d_{xz} + 0.51 * 4d_{z^2}$
Met^t	2829	1.71	1.71	$sd^{6.83}$	0.54	$0.35 * 5s - 0.62 * 4d_{x^2-y^2} - 0.63 * 4d_{xy}$
But^δ	2604	3.80	3.68	$sd^{26.21}$	0.49	$-0.31 * 4d_{xz} + 0.72 * 4d_{yz} + 0.55 * 4d_{z^2}$

Table A.65: NPA comparison of the C-H bond in the n-C_4H_9TcF and the CH_3TcF molecules. The trans C-H bond columns show calculated data of the trans C-H bond, and so on. IR gives the stretching frequencies of the C-H bonds, q(H) gives natural charges of the H atom, which belongs to the C-H bond, and so on. $\Delta(q_H - q_C)$ gives natural charge differences between the H- and C-atoms. Met^c row represents calculated data of the cis C-H bond in the CH_3TcF molecule, and so on. But^α row represents calculated data of the α-C-H bond in the n-C_4H_9TcF molecule, and so on.

	the trans-C-H bond			the cis-C-H bond			
CH_3TcX	IR	$\Delta(q_H - q_C)$	q(H)	IR	$\Delta(q_H - q_C)$	q(H)	q(C)
unit	cm^{-1}	a.u.		cm^{-1}	a.u.		
CN	2951	1.081	0.203	3060	1.103	0.225	-0.878
I	2927	1.091	0.191	3046	1.124	0.224	-0.900
Br	2922	1.093	0.190	3043	1.118	0.215	-0.903
Cl	2909	1.114	0.196	3044	1.146	0.228	-0.918
F	2829	1.141	0.189	3051	1.166	0.214	-0.952

	IR	$\Delta(q_H - q_C)$	q(H)	q(C)
unit	cm^{-1}	a.u.		
Met^c	3051	1.166	0.214	-0.952
But^α	2943	0.822	0.188	-0.634
Met^t	2829	1.141	0.189	-0.952
But^δ	2604	0.793	0.185	-0.608

Table A.66: Structure, bond-order and occupancy comparison of the C-H activation in the CH_3MF molecules. IR^t gives stretching frequencies of the trans C-H bond. D(M-H^t) gives distances between the metal atom and the H atom that belongs to the trans C-H bond. D(M-C) gives distances between the metal atom and the C atom of the C-H bond. BO column gives C-H bond-orders of the trans C-H bond and Occ(σ) column gives occupancies of the C-H-σ orbital.

				α-spin		β-spin	
CH_3MF	IR^t	D(M-H^t)	D(M-C)	BO	Occ(σ)	BO	Occ(σ)
unit	cm^{-1}	pm	pm	a.u.			
Mn	2995	258	200	0.492	0.988	0.493	0.992
Tc	2829	240	202	0.483	0.975	0.483	0.978
Re	2584	217	199	0.466	0.948	0.466	0.948

Table A.67: The leading interactions between the C-H-σ orbital and the hybrid orbital of the metal atoms in the CH_3MF molecules. α-spin table records interaction information in the α-spin, and so on. IR^t gives stretching frequencies of the trans C-H bonds. ΔE_{ij}^2 column gives second-order perturbative estimations of the hyperconjugation, hyb. column shows hybridizations of the NHO of the metal atom, which is participated in the interaction, $\Delta\varepsilon_{ij}$ gives energy gaps of the interacting NBOs. Composition column shows orbital compositions of the Tc NHO. Sum column gives sums of this type of interactions. M(coe) column shows polarization coefficients of the M-F-σ^* orbital, and so on.

α-spin								
	IR	sum	ΔE_{ij}^2	hyb.	$\Delta\varepsilon_{ij}$	composition	M(coe)	F(coe)
unit	cm^{-1}	kcal/mol	kcal/mol		hartree			
Mn	2995	2.66	2.42	$sd^{5.18}$	0.50	$-0.40*4s+0.43*3d_{z^2}+0.79*3d_{xy}$	-0.94	0.34
Tc	2829	5.04	5.04	$sd^{3.71}$	0.57	$0.46*5s+0.78*4d_{xy}$	-0.92	0.38
Re	2584	17.36	16.73	$sd^{2.43}$	0.76	$-0.53*6s+0.79*5d_{xy}$	-0.92	0.39
β-spin								
	IR	sum	ΔE_{ij}^2	hyb.	$\Delta\varepsilon_{ij}$	composition	M(coe)	F(coe)
unit	cm^{-1}	kcal/mol	kcal/mol		hartree			
Mn	2995	1.25	1.25	$sd^{1.69}$	0.44	$0.61*4s-0.46*3d_{x^2-y^2}-0.63*3d_{xy}$		
Tc	2829	4.77	4.57	$sd^{4.18}$	0.58	$0.43*5s+0.37*4d_{z^2}+0.73*4d_{xy}$	-0.93	0.37
Re	2584	18.28	17.17	$sd^{4.19}$	0.77	$-0.43*6s+0.38*5d_{z^2}+0.81*5d_{xy}$	-0.92	0.39

Table A.68: Structure and bond-order and occupancy comparison of the C-H activation in the *n*-C_4H_9MF molecules. In the δ-C-H bond columns calculated data of the δ-C-H bond are represented, and so on. IR gives the stretching frequencies of the C-H bonds. M-H gives distances between the metal atom and the H atom, which belongs to the C-H bond, and so on. BO(α) column gives bond-orders of the C-H bond in the α-spin, and so on. α-spin columns show calculated data of the α-spin, and so on. Occ(σ) column gives occupancies of the C-H-σ orbital, and so on.

	δ-C-H bond			α-C-H bond		
n-C_4H_9MF	IR	D(M-H)	D(M-C)	IR	D(M-H)	D(M-C)
unit	cm^{-1}	pm	pm	cm^{-1}	pm	pm
Mn	2731	195	239	2967	248	198
Tc	2604	201	249	2943	257	207
Re	2481	200	239	2956	261	210

	δ-C-H bond			α-C-H bond		
	IR	BO(α)	BO(β)	IR	BO(α)	BO(β)
unit	cm^{-1}	a.u.	a.u.	cm^{-1}	a.u.	a.u.
Mn	2731	0.477	0.478	2967	0.493	0.489
Tc	2604	0.476	0.473	2943	0.489	0.487
Re	2481	0.461	0.461	2956	0.491	0.484

	δ-C-H bond					α-C-H bond				
		α-spin		β-spin			α-spin		β-spin	
	IR	Occ(σ)	Occ(σ^*)	Occ(σ)	Occ(σ^*)	IR	Occ(σ)	Occ(σ^*)	Occ(σ)	Occ(σ^*)
unit	cm^{-1}	a.u.				cm^{-1}	a.u.			
Mn	2731	0.962	0.013	0.967	0.018	2967	0.993	0.008	0.984	0.006
Tc	2604	0.953	0.016	0.954	0.023	2943	0.986	0.009	0.987	0.010
Re	2481	0.939	0.029	0.941	0.026	2956	0.992	0.010	0.976	0.009

Table A.69: The leading interaction between the C-H-σ orbital and the vacant hybrid orbital of the metal atoms in the n-C_4H_9MF molecules. α-spin table records interaction information in the α-spin, and so on. IR gives stretching frequencies of the C-H bonds. ΔE^2_{ij} column gives second-order perturbative estimations of the hyperconjugation, hyb. column shows hybridizations of the NHO of the metal atom, which is participated in the interaction, $\Delta\varepsilon_{ij}$ gives energy gaps of the interacting NBOs. Composition column shows orbital compositions of the Tc NHO. Sum column gives sums of this type of interactions. M(coe) column shows polarization coefficients of the M-F-σ^* orbital, and so on.

α-spin

	IR	sum	ΔE^2_{ij}	hyb.	$\Delta\varepsilon_{ij}$	composition	M(coe)	F(coe)
unit	cm^{-1}	kcal/mol		hartree				
Mn	2731	10.30	10.12	$sd^{0.95}$	0.59	$0.71*4s-0.61*3d_{x^2-y^2}$	-0.94	0.33
Tc	2604	14.52	13.54	$sd^{1.11}$	0.65	$0.68*5s-0.65*4d_{x^2-y^2}$	-0.94	0.35
Re	2481	23.23	21.96	$sd^{1.49}$	0.78	$0.63*6s-0.63*5d_{x^2-y^2}$	-0.93	0.38

β-spin

	IR	sum	ΔE^2_{ij}	hyb.	$\Delta\varepsilon_{ij}$	composition	M(coe)	F(coe)
unit	cm^{-1}	kcal/mol	kcal/mol		hartree			
Mn	2731	10.03	9.44	$sd^{1.25}$	0.62	$0.66*4s-0.67*3d_{x^2-y^2}$	-0.94	0.33
Tc	2604	16.81	13.07	$sd^{4.44}$	0.63	$0.42*5s-0.53*4d_{x^2-y^2}-0.59*4d_{xy}$	-0.93	0.38
Re	2481	22.39	21.03	$sd^{1.43}$	0.79	$0.64*6s-0.61*5d_{x^2-y^2}$	-0.93	0.37

Table A.70: The leading interaction between the C-H-σ^* orbital and the hybrid orbital of the metal atoms in the n-C_4H_9MF molecules. IR gives stretching frequencies of the δ-C-H bonds. ΔE^2_{ij} column gives second-order perturbative estimations of the hyperconjugation, hyb. column shows hybridizations of the NHO of the metal atom, which is participated in the interaction, $\Delta\varepsilon_{ij}$ gives energy gaps of the interacting NBOs. Composition column shows orbital compositions of the Tc NHO. Sum column gives sums of this type of interactions.

α-spin

	IR	sum	ΔE^2_{ij}	hyb.	$\Delta\varepsilon_{ij}$	composition
unit	cm^{-1}	kcal/mol	kcal/mol		hartree	
Mn	2731	1.32	1.23	$sd^{2.35}$	0.50	$0.46*3d_{z^2}-0.78*3d_{xy}$
Tc	2604	2.10	1.41	$sd^{83.55}$	0.48	$0.46*4d_{z^2}+0.65*4d_{xz}+0.53*4d_{yz}$
Re	2481	5.16	4.23	$sd^{30.65}$	0.48	$0.56*5d_{z^2}+0.68*5d_{yz}$

β-spin

	IR	sum	ΔE^2_{ij}	hyb.	$\Delta\varepsilon_{ij}$	composition
unit	cm^{-1}	kcal/mol	kcal/mol		hartree	
Mn	2731	2.59	1.98	$sd^{8.76}$	0.48	$0.32*4s+0.71*3d_{z^2}-0.46*3d_{xy}$
Tc	2604	3.80	3.68	$sd^{26.21}$	0.49	$0.55*4d_{z^2}+0.72*4d_{yz}$
Re	2481	3.39	3.39	$sd^{3.26}$	0.45	$0.48*6s+0.36*5d_{z^2}+0.70*5d_{xy}$

A.3.2 The quartet state(ground state)

Table A.71: Structure, bond-order and occupancy comparison of the CH_3TcX molecules. IR^t represents the stretching frequencies of the trans C-H bond, and so on. D(Tc-H^t) represents distances between the Tc atom and the H atom that belongs to the trans C-H bond, and so on. A(X-Tc-C-H^t) represents dihedral angles of the X-Tc-C-H^t group. In the α-spin columns calculated data of the α-spin are given, and so on. BO^t column shows bond-orders of the trans C-H bond. Δ column shows bond-order differences between the cis and the trans C-H bonds in the same molecules. Occ(σ) column gives occupancy changes related to the CH_3TcF molecule in the C-H-σ orbital, i.e. $\mathrm{Occ}(\sigma) = \mathrm{Occ}(\sigma_{(CH_3TcX)} - \mathrm{Occ}(\sigma)_{(CH_3TcCl)}$, and so on.

CH_3TcX	IR^t	D(Tc-H^t)	IR^c	D(Tc-H^c)	D(Tc-C)	A(X-Tc-C-H^t)
unit	cm^{-1}	pm	cm^{-1}	pm	pm	°
Cl	2989	247	3124	273	203	-146
Br	2960	260	3111	266	205	-121
CN	2945	255	3063	262	204	-165
I	2936	253	3121	274	204	-122
F	2829	241	3055	270	203	-167

			α-spin		β-spin	
CH_3TcX	IR^t	IR^c	BO^t	Δ	BO^t	Δ
unit	cm^{-1}	cm^{-1}	bond-order			
Cl	2989	3124	0.496	0.001	0.487	0.013
Br	2960	3111	0.494	0.005	0.489	0.005
CN	2945	3063	0.494	0.003	0.491	0.002
I	2936	3121	0.493	0.005	0.486	0.012
F	2829	3055	0.484	0.012	0.486	0.008

		α-spin		β-spin	
CH_3TcX	IR^t	Occ(σ)	Occ(σ^*)	Occ(σ)	Occ(σ^*)
unit	cm^{-1}	a.u.			
Cl	2989	0.000	0.000	0.000	0.000
Br	2960	-0.003	-0.001	0.001	0.000
CN	2945	-0.006	-0.002	-0.001	-0.003
I	2936	-0.004	-0.001	-0.001	0.001
F	2829	-0.020	0.002	-0.004	0.001

Table A.72: The leading interaction between the C-H-σ orbital and the vacant hybrid orbital of the Tc atom in the CH_3TcX molecules. α-spin table records interaction information in the α-spin, and so on. IR gives stretching frequencies of the trans C-H bonds. ΔE_{ij}^2 column gives second-order perturbative estimations of the hyperconjugation, hyb. column shows hybridizations of the NHO of the metal atom, which is participated in the interaction, $\Delta\varepsilon_{ij}$ gives energy gaps of the interacting NBOs. Composition column shows orbital compositions of the Tc NHO. Sum column gives sums of this type of interactions. M(coe) column shows polarization coefficients of the M-F-σ^* orbital, and so on.

α-spin

	IR	sum	ΔE_{ij}^2	hyb.	$\Delta\varepsilon_{ij}$	composition	M(coe)	F(coe)
unit	cm^{-1}	kcal/mol	kcal/mol		hartree			
Cl	2989	0.37	0.37	$sd^{1.00}$	0.54	$-0.70*5s+0.49*4d_{x^2-y^2}+0.48*4d_{xy}$	0.87	-0.49
Br	2960	0.80	0.80	$sd^{0.86}$	0.52	$-0.73*5s+0.52*4d_{x^2-y^2}+0.42*4d_{xy}$	0.86	-0.51
CN	2945	1.15	1.15	$sd^{1.27}$	0.63	$0.66*5s-0.59*4d_{x^2-y^2}-0.38*4d_{xy}$	0.84	-0.55
I	2936	1.00	1.00	$sd^{0.74}$	0.53	$-0.75*5s+0.49*4d_{x^2-y^2}+0.42*4d_{xy}$	0.84	-0.54
F	2829	4.17	4.17	$sd^{1.98}$	0.57	$-0.57*5s+0.36*4d_{x^2-y^2}+0.68*4d_{xy}$	-0.92	0.38

β-spin

	IR	sum	ΔE_{ij}^2	hyb.	$\Delta\varepsilon_{ij}$	composition
unit	cm^{-1}	kcal/mol	kcal/mol		hartree	
Cl	2989	3.29	1.90	$sd^{99.99}$	0.47	$0.83*4d_{xz}+0.50*4d_{yz}$
Br	2960	3.02	1.35	$sd^{24.19}$	0.46	$0.84*4d_{xz}+0.48*4d_{yz}$
CN	2945	2.75	1.47	$sd^{14.16}$	0.47	$0.90*4d_{xz}+0.29*4d_{x^2-y^2}$
I	2936	3.69	1.47	$sd^{99.99}$	0.47	$0.84*4d_{xz}+0.48*4d_{yz}$
F	2829	5.07	4.65	$sd^{8.46}$	0.58	$-0.32*5s-0.81*4d_{xy}+0.43*4d_{z^2}$

Table A.73: The leading interaction between the C-H-σ^* orbital and the occupied hybrid orbital of the Tc atom in the CH_3TcX molecules.

α-spin

	IR	sum	ΔE_{ij}^2	hyb.	$\Delta\varepsilon_{ij}$	composition
unit	cm^{-1}	kcal/mol	kcal/mol		hartree	
Cl	2989	1.76	0.98	$sd^{76.58}$	0.63	$-0.92*4d_{xz}+0.31*4d_{xy}$
Br	2960	1.73	1.05	$sd^{99.99}$	0.63	$1.00*4d_{xz}$
CN	2945	1.29	1.29	$sd^{20.26}$	0.61	$-0.32*4d_{x^2-y^2}+0.91*4d_{xy}$
I	2936	1.64	0.92	$sd^{99.99}$	0.62	$1.00*4d_{xz}$
F	2829	1.78	1.78	$sd^{4.45}$	0.57	$0.48*5s+0.62*4d_{z^2}-0.72*4d_{yz}$

β-spin

	IR	sum	ΔE_{ij}^2	hyb.	$\Delta\varepsilon_{ij}$	composition
unit	cm^{-1}	kcal/mol	kcal/mol		hartree	
Cl	2989	0.64	0.64	$sd^{3.22}$	0.56	$0.48*5s+0.51*4d_{z^2}+0.65*4d_{xy}$
Br	2960	0.88	0.88	$sd^{3.87}$	0.56	$0.45*5s+0.52*4d_{z^2}+0.70*4d_{xy}$
CN	2945	0.15	0.09	$sd^{0.85}$	0.85	$0.54*5s-0.58*4d_{x^2-y^2}-0.44*4d_{xy}$
I	2936	0.92	0.92	$sd^{4.92}$	0.55	$0.40*5s+0.53*4d_{z^2}+0.72*4d_{xy}$
F	2829	0.91	0.91	$sd^{83.45}$	0.51	$-0.40*4d_{z^2}+0.62*4d_{yz}+0.45*4d_{xz}$

Table A.74: Structure comparison between the n-C_4H_9TcF and the CH_3TcF molecules. Met^t row represents calculated data of the trans C-H bond in the CH_3TcF molecule, and so on. But^δ row represents calculated data of the δ-C-H bond in the n-C_4H_9TcF molecule, and so on. IR gives stretching frequencies of the C-H bond. D(Tc-H) gives distances between the Tc atom and the H atom, which belongs to the C-H bond, and so on.

	IR	Tc-H	Tc-C
unit	cm^{-1}	pm	pm
Met^c	3055	270	203
But^α	2948	256	207
Met^t	2829	241	203
But^δ	2544	199	252

Table A.75: Bond-order and occupancy comparison of the C-H bond in the n-C_4H_9TcF and CH_3TcF molecules. Met^t row represents calculated data of the trans C-H bond in the CH_3TcF molecule, and so on. But^δ row represents calculated data of the δ-C-H bond in the n-C_4H_9TcF molecule, and so on. IR gives stretching frequencies of the C-H bond. In the α-spin columns calculated data of the α-spin are shown, and so on. BO column gives bond-orders of the C-H bond. Occ(σ) column gives occupancies of the C-H-σ orbital, and so on.

		α-spin			β-spin		
	IR	BO	Occ(σ)	Occ(σ^*)	BO	Occ(σ)	Occ(σ^*)
unit	cm^{-1}	a.u.					
Met^c	3055	0.496	0.999	0.008	0.494	0.990	0.002
But^α	2948	0.492	0.994	0.011	0.485	0.981	0.011
Met^t	2829	0.484	0.978	0.009	0.486	0.978	0.005
But^δ	2544	0.463	0.955	0.030	0.473	0.952	0.017

Table A.76: The leading interaction between the C-H-σ orbital and the vacant Tc hybrid orbital. Met^c row represents calculated data of the cis C-H bond in the CH_3TcF molecule, and so on. But$^\alpha$ row represents calculated data of the α-C-H bond in the n-C_4H_9TcF molecule, and so on. IR gives stretching frequencies of the C-H bonds. ΔE^2_{ij} column gives second-order perturbative estimations of the hyperconjugation, hyb. column shows hybridizations of the NHO of the metal atom, which is participated in the interaction, $\Delta\varepsilon_{ij}$ gives energy gaps of the interacting NBOs. Composition column shows orbital compositions of the Tc NHO. Sum column gives sums of this type of interactions.

α-spin

	IR	sum	ΔE^2_{ij}	hyb.	$\Delta\varepsilon_{ij}$	composition
unit	cm^{-1}	kcal/mol	kcal/mol		hartree	
Met^c	3055	0.11	0.11	$sd^{1.57}$	0.59	$0.62*5s+0.71*4d_{x^2-y^2}$
But$^\alpha$	2948	0.04	0.04	$sd^{1.12}$	0.58	$0.68*5s-0.64*4d_{x^2-y^2}$
Met^t	2829	4.17	4.17	$sd^{1.98}$	0.57	$-0.57*5s+0.36*4d_{x^2-y^2}+0.68*4d_{xy}$
But$^\delta$	2544	13.99	13.99	$sd^{1.12}$	0.63	$0.68*5s-0.64*4d_{x^2-y^2}$

β-spin

	IR	sum	ΔE^2_{ij}	hyb.	$\Delta\varepsilon_{ij}$	composition
unit	cm^{-1}	kcal/mol	kcal/mol		hartree	
Met^c	3055	1.52	1.04	$sd^{99.99}$	0.44	$0.78*4d_{xz}-0.62*4d_{yz}$
But$^\alpha$	2948	2.53	2.01	$sd^{2.00}$	0.47	$0.57*5s+0.51*4d_{z^2}-0.57*4d_{xz}$
Met^t	2829	5.07	4.65	$sd^{8.46}$	0.58	$-0.32*5s+0.43*4d_{z^2}+0.81*4d_{xy}$
But$^\delta$	2544	16.82	11.89	$sd^{4.03}$	0.64	$0.44*5s-0.53*4d_{x^2-y^2}-0.58*4d_{xy}$

Table A.77: The leading interaction between the C-H-σ^* orbital and the occupied Tc hybrid orbital in the α-spin of the molecules. Met^c row represents calculated data of the cis C-H bond in the CH_3TcF molecule, and so on. But$^\alpha$ row represents calculated data of the α-C-H bond in the n-C_4H_9TcF molecule, and so on. NBO1 columns give calculated data of the NBO1, and so on. IR gives stretching frequencies of the C-H bonds. ΔE^2_{ij} column gives second-order perturbative estimations of the hyperconjugation, hyb. column shows hybridizations of the NHO of the metal atom, which is participated in the interaction, $\Delta\varepsilon_{ij}$ gives energy gaps of the interacting NBOs. Composition column shows orbital compositions of the Tc NHO. Sum column gives sums of this type of interactions.

	IR	sum	ΔE^2_{ij}	hyb.	$\Delta\varepsilon_{ij}$	composition
unit	cm^{-1}	kcal/mol	kcal/mol		hartree	
Met^c	3055	2.17	1.94	$sd^{99.99}$	0.63	$0.95*4d_{xz}-0.28*4d_{yz}$
But$^\alpha$	2948	1.51	1.51	$sd^{27.36}$	0.59	$0.49*4d_{z^2}+0.78*4d_{xz}$
Met^t	2829	1.78	1.78	$sd^{4.45}$	0.57	$0.43*5s+0.62*4d_{z^2}-0.72*4d_{yz}$
But$^\delta$	2544	5.61	5.17	$sd^{17.33}$	0.50	$0.81*4d_{xy}-0.51*4d_{yz}$

Table A.78: NPA comparison of the C-H bond in the n-C_4H_9TcF and the CH_3TcF molecules. The trans C-H bond columns show calculated data of the trans C-H bond, and so on. IR gives the stretching frequencies of the C-H bonds, q(H) gives natural charges of the H atom, which belongs to the C-H bond, and so on. $\Delta(q_H - q_C)$ gives natural charge differences between the H- and C-atoms. Met^c row represents calculated data of the cis C-H bond in the CH_3TcF molecule, and so on. But^α row represents calculated data of the α-C-H bond in the n-C_4H_9TcF molecule, and so on.

	the trans-C-H bond			the cis-C-H bond			
CH_3TcX	IR	$\Delta(q_H - q_C)$	q(H)	IR	$\Delta(q_H - q_C)$	q(H)	q(C)
unit	cm^{-1}	a.u.		cm^{-1}	a.u.		
Cl	2989	1.098	0.213	3124	1.112	0.227	-0.885
Br	2960	1.098	0.205	3111	1.117	0.224	-0.893
CN	2945	1.090	0.204	3063	1.106	0.220	-0.886
I	2936	1.075	0.201	3121	1.097	0.223	-0.874
F	2829	1.150	0.188	3055	1.175	0.213	-0.962

	IR	$\Delta(q_H - q_C)$	q(H)	q(C)
unit	cm^{-1}	a.u.		
Met^c	3055	1.175	0.213	-0.962
But^α	2948	0.825	0.188	-0.637
Met^t	2829	1.150	0.188	-0.962
But^δ	2544	0.792	0.178	-0.614

Table A.79: Structure, bond-order and occupancy comparison of the C-H activation in the CH_3MF molecules. IR^t gives stretching frequencies of the trans C-H bond. D(M-H^t) gives distances between the metal atom and the H atom that belongs to the trans C-H bond. D(M-C) gives distances between the metal atom and the C atom of the C-H bond. BO column gives C-H bond-orders of the trans C-H bond and Occ(σ) column gives occupancies of the C-H-σ orbital.

				α-spin		β-spin	
CH_3MF	IR^t	D(M-H^t)	D(M-C)	BO	Occ(σ)	BO	Occ(σ)
unit	cm^{-1}	pm	pm	a.u.			
Mn	3002	253	198	0.495	0.994	0.495	0.991
Tc	2829	241	203	0.484	0.978	0.486	0.978
Re	2603	217	200	0.464	0.945	0.494	0.954

Table A.80: The leading interactions between the C-H-σ orbital and the hybrid orbital of the metal atoms in the CH_3MF molecules. α-spin table records interaction information in the α-spin, and so on. IR^t gives stretching frequencies of the trans C-H bonds. ΔE^2_{ij} column gives second-order perturbative estimations of the hyperconjugation, hyb. column shows hybridizations of the NHO of the metal atom, which is participated in the interaction, $\Delta\varepsilon_{ij}$ gives energy gaps of the interacting NBOs. Composition column shows orbital compositions of the Tc NHO. Sum column gives sums of this type of interactions. M(coe) column shows polarization coefficients of the M-F-σ^* orbital, and so on.

α-spin

	IR	sum	ΔE^2_{ij}	hyb.	$\Delta\varepsilon_{ij}$	composition	M(coe)	F(coe)
unit	cm^{-1}	kcal/mol	kcal/mol		hartree			
Mn	3002	1.23	1.01	$sd^{16.66}$	0.48	$0.24*4s+0.95*3d_{xy}$	-0.95	0.32
Tc	2829	4.17	4.17	$sd^{1.98}$	0.57	$-0.57*5s+0.36*4d_{x^2-y^2}+0.68*4d_{xy}$	-0.92	0.38
Re	2603	18.17	17.52	$sd^{2.10}$	0.73	$0.57*6s-0.68*5d_{x^2-y^2}+0.45*5d_{xy}$	-0.91	0.41

β-spin

	IR	sum	ΔE^2_{ij}	hyb.	$\Delta\varepsilon_{ij}$	composition	M(coe)	F(coe)
unit	cm^{-1}	kcal/mol	kcal/mol		hartree			
Mn	3002	1.71	1.71	$sd^{3.78}$	0.49	$0.45*4s-0.80*3d_{x^2-y^2}$		
Tc	2829	5.07	4.65	$sd^{8.46}$	0.58	$-0.32*5s+0.43*4d_{z^2}+0.81*4d_{xy}$	-0.93	0.37
Re	2603	15.52	14.95	$sd^{0.94}$	0.77	$0.71*6s-0.54*5d_{x^2-y^2}+0.32*5d_{xy}$	-0.93	0.38

Table A.81: The leading interactions between the C-H-σ^* orbital and the hybrid orbital of the metal atoms in the CH_3MF molecules. α-spin table records interaction information in the α-spin, and so on. IR^t gives stretching frequencies of the trans C-H bonds. ΔE^2_{ij} column gives second-order perturbative estimations of the hyperconjugation, hyb. column shows hybridizations of the NHO of the metal atom, which is participated in the interaction, $\Delta\varepsilon_{ij}$ gives energy gaps of the interacting NBOs. Composition column shows orbital compositions of the Tc NHO. Sum column gives sums of this type of interactions.

α-spin

	IR	sum	ΔE^2_{ij}	hyb.	$\Delta\varepsilon_{ij}$	composition
unit	cm^{-1}	kcal/mol	kcal/mol		hartree	
Mn	3002	1.14	0.81	$sd^{0.72}$	0.69	$-0.75*4s+0.57*3d_{x^2-y^2}$
Tc	2829	1.78	1.78	$sd^{4.45}$	0.57	$0.43*5s+0.62*4d_{z^2}-0.72*4d_{yz}$
Re	2603	3.12	2.25	$sd^{2.88}$	0.55	$-0.50*6s+0.79*5d_{xy}+0.31*5d_{z^2}$

β-spin

	IR	sum	ΔE^2_{ij}	hyb.	$\Delta\varepsilon_{ij}$	composition
unit	cm^{-1}	kcal/mol	kcal/mol		hartree	
Mn	3002	0.51	0.41	$sd^{13.78}$	0.60	$0.25*4s-0.85*3d_{xy}$
Tc	2829	0.91	0.91	$sd^{83.45}$	0.51	$-0.40*4d_{z^2}+0.62*4d_{yz}+0.45*4d_{xz}$
Re	2603	2.31	2.12	$sd^{3.84}$	0.49	$-0.45*6s+0.39*5d_{z^2}+0.79*5d_{xy}$

Table A.82: Structure and bond-order and occupancy comparison of the C-H activation in the *n*-C_4H_9MF molecules. In the δ-C-H bond columns calculated data of the δ-C-H bond are represented, and so on. IR gives the stretching frequencies of the C-H bonds. M-H gives distances between the metal atom and the H atom, which belongs to the C-H bond, and so on. BO(α) column gives bond-orders of the C-H bond in the α-spin, and so on. α-spin columns show calculated data of the α-spin, and so on. Occ(σ) column gives occupancies of the C-H-σ orbital, and so on.

	δ-C-H bond			α-C-H bond		
n-C_4H_9MF	IR	D(M-H)	D(M-C)	IR	D(M-H)	D(M-C)
unit	cm^{-1}	pm	pm	cm^{-1}	pm	pm
Mn	2880	211	255	2986	257	202
Tc	2544	199	252	2948	256	207
Re	2542	202	256	2965	260	210

	δ-C-H bond			α-C-H bond		
	IR	BO(α)	BO(β)	IR	BO(α)	BO(β)
unit	cm^{-1}	a.u.		cm^{-1}	a.u.	
Mn	2880	0.484	0.486	2986	0.493	0.489
Tc	2544	0.463	0.473	2948	0.492	0.485
Re	2542	0.457	0.468	2965	0.491	0.485

	δ-C-H bond					α-C-H bond				
		α-spin		β-spin			α-spin		β-spin	
	IR	Occ(σ)	Occ(σ^*)	Occ(σ)	Occ(σ^*)	IR	Occ(σ)	Occ(σ^*)	Occ(σ)	Occ(σ^*)
unit	cm^{-1}	a.u.				cm^{-1}	a.u.			
Mn	2880	0.974	0.009	0.976	0.014	2986	0.993	0.007	0.987	0.007
Tc	2544	0.955	0.030	0.952	0.017	2948	0.994	0.011	0.981	0.011
Re	2542	0.949	0.036	0.946	0.021	2965	0.994	0.012	0.977	0.007

Table A.83: The leading interaction between the C-H-σ orbital and the vacant hybrid orbital of the metal atoms in the n-C_4H_9MF molecules. α-spin table records interaction information in the α-spin, and so on. IR gives stretching frequencies of the C-H bonds. ΔE^2_{ij} column gives second-order perturbative estimations of the hyperconjugation, hyb. column shows hybridizations of the NHO of the metal atom, which is participated in the interaction, $\Delta\varepsilon_{ij}$ gives energy gaps of the interacting NBOs. Composition column shows orbital compositions of the Tc NHO. Sum column gives sums of this type of interactions. M(coe) column shows polarization coefficients of the M-F-σ^* orbital, and so on.

α-spin

	IR	ΔE^2_{ij}	hyb.	$\Delta\varepsilon_{ij}$	composition	M(coe)	F(coe)	
unit	cm^{-1}	kcal/mol		hartree				
Mn	2880	5.71	5.55	$sd^{0.64}$	0.56	$0.77*4s-0.59*3d_{x^2-y^2}$	-0.95	0.33
Tc	2544	13.99	13.99	$sd^{1.12}$	0.63	$0.68*5s-0.64*4d_{x^2-y^2}$	-0.93	0.36
Re	2542	18.68	18.48	$sd^{1.64}$	0.74	$0.61*6s-0.62*5d_{x^2-y^2}-0.35*5d_{xy}$	-0.92	0.39

β-spin

	IR	sum	ΔE^2_{ij}	hyb.	$\Delta\varepsilon_{ij}$	composition	M(coe)	F(coe)
unit	cm^{-1}	kcal/mol	kcal/mol		hartree			
Mn	2880	6.37	5.20	$sd^{2.43}$	0.63	$0.53*4s-0.56*3d_{x^2-y^2}+0.51*5d_{xy}$	-0.95	0.33
Tc	2544	16.82	11.89	$sd^{4.03}$	0.64	$0.44*5s-0.53*4d_{x^2-y^2}-0.58*4d_{xy}$	-0.93	0.36
Re	2542	20.27	17.17	$sd^{1.72}$	0.78	$0.60*6s-0.60*5d_{x^2-y^2}-0.41*5d_{xy}$	-0.93	0.37

Table A.84: The leading interaction between the C-H-σ^* orbital and the Tc hybrid orbital in the n-C_4H_9MF molecules. IR gives stretching frequencies of the δ-C-H bonds. ΔE^2_{ij} column gives second-order perturbative estimations of the hyperconjugation, hyb. column shows hybridizations of the NHO of the metal atom, which is participated in the interaction, $\Delta\varepsilon_{ij}$ gives energy gaps of the interacting NBOs. Composition column shows orbital compositions of the Tc NHO. Sum column gives sums of this type of interactions.

α-spin	IR	sum	ΔE^2_{ij}	hyb.	$\Delta\varepsilon_{ij}$	composition
unit	cm^{-1}	kcal/mol	kcal/mol		hartree	
Mn	2880	0.95	0.59	$sd^{99.99}$	0.58	$0.93*3d_{xz}-0.27*3d_{xy}$
Tc	2544	5.61	5.17	$sd^{17.33}$	0.50	$0.81*4d_{xy}-0.51*4d_{yz}$
Re	2542	6.80	6.10	$sd^{7.97}$	0.60	$0.33*6s+0.76*5d_{yz}+0.49*5d_{xy}$

β-spin	IR	sum	ΔE^2_{ij}	hyb.	$\Delta\varepsilon_{ij}$	composition
unit	cm^{-1}	kcal/mol	kcal/mol		hartree	
Mn	2880	1.29	1.29	$sd^{6.03}$	0.47	$0.37*4s+0.82*3d_{z^2}$
Tc	2544	1.87	1.87	$sd^{20.50}$	0.44	$0.62*4d_{z^2}+0.63*4d_{xz}$
Re	2542	2.41	2.41	$sd^{1.77}$	0.45	$0.60*6s+0.70*5d_{z^2}$

A.4 Group 8 transition metal elements

A.4.1 The singlet state(second excited state)

Table A.85: Structure, bond-order and occupancy comparison of the CH_3RuX molecules. IR represents the stretching frequencies of the C-H bond. D(Ru-H^t) represents distances between the Ru atom and the H atom that belongs to the trans C-H bond, and so on. The trans C-H bond columns give calculated data of the trans C-H bond, the cis C-H bond columns give changes related to the trans C-H bond in the same molecule. BO column shows bond-orders of the C-H bond. Occ(σ) column gives occupancies of the C-H bond. In the cis C-H bond columns only differences between cis and the trans C-H bond are shown, i.e. $X = X_{(\text{trans C-H bond})} - X_{(\text{cis C-H bond})}$.

CH_3RuX	IR^t	D(Ru-H^t)	IR^c	D(Ru-H^c)	D(Ru-C)
unit	cm^{-1}	pm	cm^{-1}	pm	pm
CN	3106	259	2993	253	200
I	2904	252	3100	269	199
Cl	2867	242	3020	263	198
Br	2866	243	3087	256	198
F	2736	222	3022	266	196

	trans C-H bond				cis C-H bond			
CH_3RuX	IR	BO	Occ(σ)	Occ(σ^*)	IR	BO	Occ(σ)	Occ(σ^*)
unit	cm^{-1}		a.u.		cm^{-1}		a.u.	
CN	3106	0.989	1.990	0.011	2993	0.013	0.039	0.005
I	2904	0.985	1.982	0.014	3100	-0.010	-0.016	0.006
Cl	2867	0.971	1.959	0.011	3020	-0.022	-0.034	-0.002
Br	2866	0.973	1.960	0.012	3087	-0.021	-0.035	0.001
F	2736	0.952	1.931	0.017	3022	-0.039	-0.064	-0.001

Table A.86: Structure comparison between the n-C_4H_9RuF and the CH_3RuF molecules. Met^t row represents calculated data of the trans C-H bond in the CH_3RuF molecule, and so on. But^δ row represents calculated data of the δ-C-H bond in the n-C_4H_9RuF molecule, and so on. IR gives stretching frequencies of the C-H bond. D(Ru-H) gives distances between the Ru atom and the H atom, which belongs to the C-H bond, and so on.

	IR	Ru-H	Ru-C
unit	cm^{-1}	pm	pm
Met^c	3022	266	196
But^α	2976	260	205
Met^t	2736	222	196
But^δ	2342	189	208

Table A.87: Bond-order and occupancy comparison of the C-H bond in the n-C_4H_9RuF and CH_3RuF molecules. IR gives stretching frequencies of the C-H bond.

	IR	BO	Occ(σ)	Occ(σ^*)
unit	cm^{-1}		a.u.	
Met^c	3022	0.991	1.995	0.018
But$^\alpha$	2976	0.984	1.987	0.017
Met^t	2736	0.952	1.931	0.017
But$^\delta$	2342	0.910	1.856	0.060

Table A.88: NPA comparison of the C-H bond in the n-C_4H_9RuF and the CH_3RuF molecules. The trans C-H bond columns show calculated data of the trans C-H bond, and so on. IR gives the stretching frequencies of the C-H bonds, q(H) gives natural charges of the H atom, which belongs to the C-H bond, and so on. $\Delta(q_H - q_C)$ gives natural charge differences between the H- and C-atoms.

	the trans-C-H bond			the cis-C-H bond			
CH_3RuX	IR	$\Delta(q_H - q_C)$	q(H)	IR	$\Delta(q_H - q_C)$	q(H)	q(C)
unit	cm^{-1}	a.u.		cm^{-1}	a.u.		
CN	3106	1.048	0.205	2993	1.099	0.256	-0.843
I	2904	0.990	0.177	3100	1.028	0.215	-0.813
Cl	2867	0.988	0.182	3020	0.999	0.193	-0.806
Br	2866	0.979	0.183	3087	0.999	0.203	-0.796
F	2736	0.972	0.170	3022	0.991	0.189	-0.802

	IR	$\Delta(q_H - q_C)$	q(H)	q(C)
unit	cm^{-1}	a.u.		
Met^c	3022	0.991	0.189	-0.802
But$^\alpha$	2976	0.659	0.170	-0.489
Met^t	2736	0.972	0.170	-0.802
But$^\delta$	2342	0.689	0.204	-0.485

.

Table A.89: Bond-order and occupancy comparison of the C-H activation in the CH_3MF molecules. Trans C-H bond columns give calculated data of the trans C-H bond. IR gives stretching frequencies of the C-H bond. D(M-H^t) gives distances between the metal atom and the H atom that belongs to the trans C-H bond. D(M-C) gives distances between the metal atom and the C atom of the C-H bond. BO column gives C-H bond-orders of the trans C-H bond and Occ(σ) column gives occupancies of the C-H-σ orbital.

	trans C-H bond				cis C-H bond			
CH_3MF	IR	BO	Occ(σ)	Occ(σ^*)	IR	BO	Occ(σ)	Occ(σ^*)
unit	cm^{-1}		a.u.		cm^{-1}		a.u.	
Fe	2911	0.987	1.978	0.009	3124	1.000	1.997	0.003
Ru	2736	0.952	1.931	0.017	3022	0.991	1.995	0.018
Os		0.933	1.901	0.027		0.992	1.988	0.015

Table A.90: Bond-order and occupancy comparison of the C-H activation in the n-C_4H_9MF molecules. In the δ-C-H bond columns calculated data of the δ-C-H bond are represented, and so on. IR gives the stretching frequencies of the C-H bonds. M-H gives distances between the metal atom and the H atom, which belongs to the C-H bond, and so on. BO(α) column gives bond-orders of the C-H bond in the α-spin, and so on. α-spin columns show calculated data of the α-spin, and so on. Occ(σ) column gives occupancies of the C-H-σ orbital, and so on.

	δ-C-H bond				α-C-H bond			
n-C_4H_9MF	IR	BO	Occ(σ)	Occ(σ^*)	IR	BO	Occ(σ)	Occ(σ^*)
unit	cm^{-1}		a.u.		cm^{-1}		a.u.	
Fe	2549	0.955	1.880	0.042	2742	0.961	1.946	0.021
Ru	2342	0.910	1.856	0.060	2976	0.984	1.987	0.017
Os		0.905	1.836	0.070		0.983	1.987	0.022

A.4.2 The triplet state(first excited state)

Table A.91: Structure, bond-order and occupancy comparison of the CH_3RuX molecules. IR^t represents the stretching frequencies of the trans C-H bond, and so on. D(Ru-H^t) represents distances between the Ru atom and the H atom that belongs to the trans C-H bond, and so on. In the α-spin columns calculated data of the α-spin are given, and so on. BO^t column shows bond-orders of the trans C-H bond. Δ column shows bond-order differences between the cis and the trans C-H bonds in the same molecules. Occ(σ) column gives occupancy changes related to the CH_3RuF molecule in the C-H-σ orbital, i.e. $Occ(\sigma) = Occ(\sigma_{(CH_3RuX)} - Occ(\sigma)_{(CH_3RuCN)}$, and so on.

CH_3RuX	IR^t	D(Ru-H^t)	IR^c	D(Ru-H^c)	D(Ru-C)
unit	cm^{-1}	pm	cm^{-1}	pm	pm
CN	2966	254	3067	259	201
I	2934	249	3129	269	199
Br	2934	250	3129	268	199
Cl	2934	250	3130	268	199
F	2876	243	3043	264	200

			α-spin		β-spin	
CH_3RuX	IR^t	IR^c	BO^t	Δ	BO^t	Δ
unit	cm^{-1}	cm^{-1}	bond-order			
CN	2966	3067	0.494	0.004	0.493	0.000
I	2934	3129	0.494	0.004	0.488	0.010
Br	2934	3129	0.494	0.004	0.488	0.010
Cl	2934	3130	0.494	0.004	0.488	0.009
F	2876	3043	0.489	0.008	0.488	0.008

		α-spin		β-spin	
CH_3RuX	IR^t	Occ(σ)	Occ(σ^*)	Occ(σ)	Occ(σ^*)
unit	cm^{-1}	a.u.			
CN	2966	0.000	0.000	0.000	0.000
I	2934	0.002	0.001	-0.009	0.001
Br	2934	0.002	0.001	-0.009	0.001
Cl	2934	0.003	0.001	-0.008	0.001
F	2876	-0.007	0.001	-0.010	-0.001

Table A.92: The leading interaction between the C-H-σ orbital and the vacant hybrid orbital of the Ru atom in the CH_3RuX molecules. α-spin table records interaction information in the α-spin, and so on. IR gives stretching frequencies of the trans C-H bonds. ΔE_{ij}^2 column gives second-order perturbative estimations of the hyperconjugation, hyb. column shows hybridizations of the NHO of the metal atom, which is participated in the interaction, $\Delta\varepsilon_{ij}$ gives energy gaps of the interacting NBOs. Composition column shows orbital compositions of the Ru NHO. Sum column gives sums of this type of interactions. M(coe) column shows polarization coefficients of the M-F-σ^* orbital, and so on.

α-spin

	IR	sum	ΔE_{ij}^2	hyb.	$\Delta\varepsilon_{ij}$	composition	M(coe)	F(coe)
unit	cm^{-1}	kcal/mol	kcal/mol		hartree			
CN	2966	0.99	0.85	$sd^{1.01}$	0.64	$0.69*5s-0.63*4d_{x^2-y^2}$	0.83	-0.56
I	2934	0.60	0.50	$sd^{0.63}$	0.54	$-0.78*5s+0.56*4d_{x^2-y^2}$	0.85	-0.53
F	2876	1.89	1.84	$sd^{1.41}$	0.55	$0.62*5s-0.55*4d_{x^2-y^2}+0.48*4d_{xy}$	-0.92	0.42

β-spin

	IR	sum	ΔE_{ij}^2	hyb.	$\Delta\varepsilon_{ij}$	composition	M(coe)	F(coe)
unit	cm^{-1}	kcal/mol	kcal/mol		hartree			
CN	2966	1.19	1.06	$sd^{2.93}$	0.64	$0.50*5s-0.61*4d_{x^2-y^2}-0.44*4d_{z^2}$	0.84	-0.54
I	2934	2.63	1.59	$sd^{85.52}$	0.41	$0.81*4d_{xz}+0.58*4d_{yz}$		
F	2876	2.94	2.85	$sd^{6.34}$	0.55	$0.36*5s-0.45*4d_{z^2}+0.69*4d_{xy}$	-0.92	0.40

Table A.93: The leading interaction between the C-H-σ^* orbital and the occupied hybrid orbital of the Ru atom in the CH_3RuX molecules.

α-spin

	IR	sum	ΔE_{ij}^2	hyb.	$\Delta\varepsilon_{ij}$	composition
unit	cm^{-1}	kcal/mol	kcal/mol		hartree	
CN	2966	1.79	1.29	$sd^{45.19}$	0.62	$0.95*4d_{xy}$
I	2934	1.73	0.90	$sd^{99.99}$	0.62	$0.98*4d_{xz}$
F	2876	2.01	1.44	$sd^{12.27}$	0.60	$0.95*4d_{z^2}$

β-spin

	IR	sum	ΔE_{ij}^2	hyb.	$\Delta\varepsilon_{ij}$	composition
unit	cm^{-1}	kcal/mol	kcal/mol		hartree	
CN	2966	1.42	1.16	$sd^{99.99}$	0.59	$0.87*4d_{xy}-0.43*4d_{z^2}$
I	2934	1.50	0.66	$sd^{99.99}$	0.58	$-0.58*4d_{xz}+0.81*4d_{yz}$
F	2876	1.23	0.99	$sd^{99.99}$	0.56	$-0.67*4d_{xy}-0.61*4d_{xy}$

Table A.94: Structure comparison between the n-C_4H_9RuF and the CH_3RuF molecules. Met^t row represents calculated data of the trans C-H bond in the CH_3RuF molecule, and so on. But^δ row represents calculated data of the δ-C-H bond in the n-C_4H_9RuF molecule, and so on. IR gives stretching frequencies of the C-H bond. D(Ru-H) gives distances between the Ru atom and the H atom, which belongs to the C-H bond, and so on.

	IR	Ru-H	Ru-C
unit	cm^{-1}	pm	pm
Met^c	3043	264	200
But^α	2946	249	204
Met^t	2876	243	200
But^δ	2580	195	240

Table A.95: Bond-order and occupancy comparison of the C-H bond in the n-C_4H_9RuF and CH_3RuF molecules. Met^t row represents calculated data of the trans C-H bond in the CH_3RuF molecule, and so on. But^δ row represents calculated data of the δ-C-H bond in the n-C_4H_9RuF molecule, and so on. IR gives stretching frequencies of the C-H bond. In the α-spin columns calculated data of the α-spin are shown, and so on. BO column gives bond-orders of the C-H bond. Occ(σ) column gives occupancies of the C-H-σ orbital, and so on.

		α-spin			β-spin		
	IR	BO	Occ(σ)	Occ(σ^*)	BO	Occ(σ)	Occ(σ^*)
unit	cm^{-1}	a.u.					
Met^c	3043	0.497	0.999	0.007	0.496	0.996	0.008
But^α	2946	0.493	0.993	0.009	0.484	0.976	0.009
Met^t	2876	0.489	0.986	0.006	0.488	0.982	0.004
But^δ	2580	0.469	0.953	0.023	0.467	0.946	0.019

Table A.96: The leading interaction between the C-H-σ orbital and the vacant Ru hybrid orbital. Met^c row represents calculated data of the cis C-H bond in the CH_3RuF molecule, and so on. But$^\alpha$ row represents calculated data of the α-C-H bond in the n-C_4H_9RuF molecule, and so on. α-spin table gives calculated data in the α-spin of the molecules, and so on. IR gives stretching frequencies of the C-H bonds. ΔE^2_{ij} column gives second-order perturbative estimations of the hyperconjugation, hyb. column shows hybridizations of the NHO of the metal atom, which is participated in the interaction, $\Delta\varepsilon_{ij}$ gives energy gaps of the interacting NBOs. Composition column shows orbital compositions of the Ru NHO. Sum column gives sums of this type of interactions. M(coe) column shows polarization coefficients of the M-F-σ^* orbital, and so on.

α-spin

	IR	sum	ΔE^2_{ij}	hyb.	$\Delta\varepsilon_{ij}$	composition	M(coe)	F(coe)
unit	cm^{-1}	kcal/mol	kcal/mol		hartree			
Met^c	3043	0.26	0.21	$sd^{1.40}$	0.59	$-0.65*5s-0.72*4d_{x^2-y^2}$		
But$^\alpha$	2946	0.13	0.07	$sd^{1.02}$	0.58	$0.70*5s-0.67*4d_{x^2-y^2}$	-0.93	0.38
Met^t	2876	1.89	1.84	$sd^{1.41}$	0.55	$0.62*5s-0.55*4d_{x^2-y^2}$	-0.92	0.42
But$^\delta$	2580	15.51	15.42	$sd^{1.02}$	0.62	$0.70*5s-0.67*4d_{x^2-y^2}$	-0.93	0.38

β-spin

	IR	sum	ΔE^2_{ij}	hyb.	$\Delta\varepsilon_{ij}$	composition	M(coe)	F(coe)
unit	cm^{-1}	kcal/mol	kcal/mol		hartree			
Met^c	3043	0.68	0.22	$sd^{5.48}$	0.58	$-0.39*5s-0.79*4d_{x^2-y^2}+0.46*4d_{z^2}$		
But$^\alpha$	2946	2.75	2.44	$sd^{4.44}$	0.42	$0.43*5s-0.59*4d_{x^2-y^2}-0.51*4d_{xy}$		
Met^t	2876	2.94	2.85	$sd^{6.34}$	0.55	$0.36*5s-0.45*4d_{x^2-y^2}+0.69*4d_{xy}$	-0.92	0.40
But$^\delta$	2580	17.53	17.17	$sd^{2.08}$	0.62	$0.57*5s-0.69*4d_{x^2-y^2}-0.38*4d_{z^2}$	-0.93	0.37

Table A.97: The leading interaction between the C-H-σ^* orbital and the occupied Ru hybrid orbital in the the molecules.

α-spin

	IR	sum	ΔE^2_{ij}	hyb.	$\Delta\varepsilon_{ij}$	composition
unit	cm^{-1}	kcal/mol	kcal/mol		hartree	
Met^c	3043	1.80	1.51	$sd^{99.99}$	0.63	$-0.94*4d_{xz}-0.33*4d_{yz}$
But$^\alpha$	2946	1.13	0.83	$sd^{23.29}$	0.62	$0.80*4d_{z^2}+0.50*4d_{xz}$
Met^t	2876	2.01	1.44	$sd^{12.27}$	0.60	$0.95*4d_{z^2}+0.32*4d_{yz}$
But$^\delta$	2580	4.43	3.49	$sd^{25.47}$	0.53	$0.68*4d_{xy}+0.66*4d_{yz}$

β-spin

	IR	sum	ΔE^2_{ij}	hyb.	$\Delta\varepsilon_{ij}$	composition
unit	cm^{-1}	kcal/mol	kcal/mol		hartree	
Met^c	3043	1.94	1.65	$sd^{99.99}$	0.60	$-0.95*4d_{xz}-0.31*4d_{yz}$
But$^\alpha$	2946	1.02	0.79	$sd^{99.99}$	0.58	$0.67*4d_{xz}+0.44*4d_{z^2}-0.44*4d_{xy}$
Met^t	2876	1.23	0.99	$sd^{99.99}$	0.56	$-0.61*4d_{z^2}-0.67*4d_{xy}$
But$^\delta$	2580	2.55	1.74	$sd^{9.93}$	0.49	$0.55*4d_{z^2}+0.74*4d_{xy}$

Table A.98: NPA comparison of the C-H bond in the n-C_4H_9RuF and the CH_3RuF molecules. The trans C-H bond columns show calculated data of the trans C-H bond, and so on. IR gives the stretching frequencies of the C-H bonds, q(H) gives natural charges of the H atom, which belongs to the C-H bond, and so on. $\Delta(q_H - q_C)$ gives natural charge differences between the H- and C-atoms. Met^c row represents calculated data of the cis C-H bond in the CH_3RuF molecule, and so on. But^α row represents calculated data of the α-C-H bond in the n-C_4H_9RuF molecule, and so on.

	the trans-C-H bond				the cis-C-H bond			
CH_3RuX	IR	$\Delta(q_H - q_C)$	q(H)		IR	$\Delta(q_H - q_C)$	q(H)	q(C)
unit	cm^{-1}	a.u.			cm^{-1}	a.u.		
CN	2966	0.987	0.190		3067	1.012	0.215	-0.797
I	2934	0.973	0.192		3129	0.998	0.217	-0.781
Br	2934	0.978	0.192		3129	1.005	0.219	-0.786
Cl	2934	0.985	0.192		3130	1.013	0.220	-0.793
F	2876	1.018	0.180	3043	1.036	0.198	-0.838	

	IR	$\Delta(q_H - q_C)$	q(H)	q(C)
unit	cm^{-1}	a.u.		
Met^c	3043	1.036	0.198	-0.838
But^α	2946	0.793	0.189	-0.604
Met^t	2876	1.018	0.180	-0.838
But^δ	2580	0.716	0.186	-0.530

Table A.99: Structure, bond-order and occupancy comparison of the C-H activation in the CH_3MF molecules. IR^t gives stretching frequencies of the trans C-H bond. D(M-H^t) gives distances between the metal atom and the H atom that belongs to the trans C-H bond. D(M-C) gives distances between the metal atom and the C atom of the C-H bond. BO column gives C-H bond-orders of the trans C-H bond and Occ(σ) column gives occupancies of the C-H-σ orbital.

				α-spin		β-spin	
CH_3MF	IR^t	D(M-H^t)	D(M-C)	BO	Occ(σ)	BO	Occ(σ)
unit	cm^{-1}	pm	pm	a.u.			
Fe	3002	257	197	0.499	0.998	0.495	0.990
Ru	2876	243	200	0.489	0.986	0.488	0.982
Os	2423	204	194	0.451	0.926	0.454	0.935

Table A.100: The leading interactions between the C-H-σ orbital and the hybrid orbital of the metal atoms in the CH_3MF molecules. α-spin table records interaction information in the α-spin, and so on. IR^t gives stretching frequencies of the trans C-H bonds. ΔE^2_{ij} column gives second-order perturbative estimations of the hyperconjugation, hyb. column shows hybridizations of the NHO of the metal atom, which is participated in the interaction, $\Delta\varepsilon_{ij}$ gives energy gaps of the interacting NBOs. Composition column shows orbital compositions of the Ru NHO. Sum column gives sums of this type of interactions. M(coe) column shows polarization coefficients of the M-F-σ^* orbital, and so on.

α-spin

	IR	sum	ΔE^2_{ij}	hyb.	$\Delta\varepsilon_{ij}$	composition	M(coe)	F(coe)
unit	cm^{-1}	kcal/mol	kcal/mol		hartree			
Fe	3002	0.64	0.35	$sd^{0.16}$	0.54	$0.90*4s-0.31*3d_{x^2-y^2}$		
Ru	2876	1.89	1.84	$sd^{1.41}$	0.55	$0.62*5s+0.48*4d_{xy}-0.55*4d_{x^2-y^2}$	-0.92	0.42
Os	2423	28.65	27.07	$sd^{2.13}$	0.70	$-0.56*6s+0.77*5d_{xy}$	-0.90	0.43

β-spin

	IR	sum	ΔE^2_{ij}	hyb.	$\Delta\varepsilon_{ij}$	composition	M(coe)	F(coe)
unit	cm^{-1}	kcal/mol	kcal/mol		hartree			
Fe	3002	1.11	1.06	$sd^{99.99}$	0.42	$0.98*3d_{xy}$		
Ru	2876	2.94	2.85	$sd^{6.34}$	0.55	$-0.42*4d_{x^2-y^2}-0.45*4d_{z^2}+0.69*4d_{xy}$	-0.92	0.40
Os	2423	26.09	23.65	$sd^{2.42}$	0.73	$-0.53*6s+0.76*5d_{xy}$	-0.91	0.40

Table A.101: The leading interactions between the C-H-σ^* orbital and the hybrid orbital of the metal atoms in the CH_3MF molecules. α-spin table records interaction information in the α-spin, and so on. IR^t gives stretching frequencies of the trans C-H bonds. ΔE^2_{ij} column gives second-order perturbative estimations of the hyperconjugation, hyb. column shows hybridizations of the NHO of the metal atom, which is participated in the interaction, $\Delta\varepsilon_{ij}$ gives energy gaps of the interacting NBOs. Composition column shows orbital compositions of the Ru NHO. Sum column gives sums of this type of interactions.

α-spin

	IR	sum	ΔE^2_{ij}	hyb.	$\Delta\varepsilon_{ij}$	composition
unit	cm^{-1}	kcal/mol	kcal/mol		hartree	
Fe	3002	0.75	0.57	$sd^{99.99}$	0.75	$0.98*3d_{xy}$
Ru	2876	2.01	1.44	$sd^{12.27}$	0.60	$0.95*4d_{z^2}$
Os	2423	5.10	2.74	$sd^{3.43}$	0.52	$0.47*6s-0.68*5d_{x^2-y^2}+0.41*5d_{xy}$

β-spin

	IR	sum	ΔE^2_{ij}	hyb.	$\Delta\varepsilon_{ij}$	composition
unit	cm^{-1}	kcal/mol	kcal/mol		hartree	
Fe	3002	0.15	0.09	$sd^{5.62}$	0.68	$0.39*4s-0.78*3d_{x^2-y^2}+0.48*3d_{z^2}$
Ru	2876	1.23	0.99	$sd^{99.99}$	0.56	$-0.61*4d_{z^2}-0.67*4d_{xy}$
Os	2423	4.66	3.58	$sd^{2.10}$	0.48	$0.57*6s-0.66*5d_{x^2-y^2}+0.40*5d_{xy}$

Table A.102: Structure and bond-order and occupancy comparison of the C-H activation in the *n*-C_4H_9MF molecules. In the δ-C-H bond columns calculated data of the δ-C-H bond are represented, and so on. IR gives the stretching frequencies of the C-H bonds. M-H gives distances between the metal atom and the H atom, which belongs to the C-H bond, and so on. BO(α) column gives bond-orders of the C-H bond in the α-spin, and so on. α-spin columns show calculated data of the α-spin, and so on. Occ(σ) column gives occupancies of the C-H-σ orbital, and so on.

	δ-C-H bond			α-C-H bond		
n-C_4H_9MF	IR	D(M-H)	D(M-C)	IR	D(M-H)	D(M-C)
unit	cm^{-1}	pm	pm	cm^{-1}	pm	pm
Fe	2910	229	304	2972	251	198
Ru	2580	195	240	2946	249	204
Os		195	240		249	204

	δ-C-H bond			α-C-H bond		
	IR	BO(α)	BO(β)	IR	BO(α)	BO(β)
unit	cm^{-1}	a.u.		cm^{-1}	a.u.	
Fe	2910	0.491	0.492	2972	0.492	0.490
Ru	2580	0.469	0.467	2946	0.493	0.484
Os		0.457	0.459		0.491	0.481

	δ-C-H bond					α-C-H bond				
		α-spin		β-spin			α-spin		β-spin	
	IR	Occ(σ)	Occ(σ^*)	Occ(σ)	Occ(σ^*)	IR	Occ(σ)	Occ(σ^*)	Occ(σ)	Occ(σ^*)
unit	cm^{-1}	a.u.				cm^{-1}	a.u.			
Fe	2910	0.984	0.007	0.987	0.010	2972	0.992	0.007	0.985	0.005
Ru	2580	0.953	0.023	0.946	0.019	2946	0.993	0.009	0.976	0.009
Os		0.943	0.033	0.937	0.021		0.994	0.011	0.971	0.010

Table A.103: The leading interaction between the C-H-σ orbital and the vacant hybrid orbital of the metal atoms in the n-C_4H_9MF molecules. α-spin table records interaction information in the α-spin, and so on. IR gives stretching frequencies of the C-H bonds. ΔE^2_{ij} column gives second-order perturbative estimations of the hyperconjugation, hyb. column shows hybridizations of the NHO of the metal atom, which is participated in the interaction, $\Delta\varepsilon_{ij}$ gives energy gaps of the interacting NBOs. Composition column shows orbital compositions of the Ru NHO. Sum column gives sums of this type of interactions. M(coe) column shows polarization coefficients of the M-F-σ^* orbital, and so on.

α-spin

	IR	sum	ΔE^2_{ij}	hyb.	$\Delta\varepsilon_{ij}$	composition	M(coe)	F(coe)
unit	cm^{-1}	kcal/mol	kcal/mol		hartree			
Fe	2910	1.71	1.58	$sd^{0.10}$	0.50	$0.95*4s+0.21*3d_{z^2}$		
Ru	2580	15.51	15.42	$sd^{1.02}$	0.62	$0.70*5s-0.67*4d_{x^2-y^2}$	-0.93	0.38
Os		22.38	22.11	$sd^{1.30}$	0.72	$0.65*6s-0.68*5d_{x^2-y^2}$	-0.92	0.40

β-spin

	IR	sum	ΔE^2_{ij}	hyb.	$\Delta\varepsilon_{ij}$	composition	M(coe)	F(coe)
unit	cm^{-1}	kcal/mol	kcal/mol		hartree			
Fe	2910	2.08	1.97	$sd^{10.28}$	0.52	$-0.61*3d_{z^2}-0.56*3d_{x^2-y^2}$		
Ru	2580	17.53	17.17	$sd^{2.08}$	0.62	$0.57*5s-0.69*4d_{x^2-y^2}$	-0.93	0.37
Os		23.26	22.82	$sd^{1.63}$	0.74	$0.61*6s-0.68*5d_{x^2-y^2}$	-0.92	0.39

Table A.104: The leading interaction between the C-H-σ^* orbital and the hybrid orbital of the metal atoms in the n-C_4H_9MF molecules. IR gives stretching frequencies of the δ-C-H bonds. ΔE^2_{ij} column gives second-order perturbative estimations of the hyperconjugation, hyb. column shows hybridizations of the NHO of the metal atom, which is participated in the interaction, $\Delta\varepsilon_{ij}$ gives energy gaps of the interacting NBOs. Composition column shows orbital compositions of the Ru NHO. Sum column gives sums of this type of interactions.

α-spin

	IR	sum	ΔE^2_{ij}	hyb.	$\Delta\varepsilon_{ij}$	composition
unit	cm^{-1}	kcal/mol	kcal/mol		hartree	
Fe	2910	0.70	0.48	$sd^{99.99}$	0.65	$-0.75*3d_{z^2}-0.61*3d_{x^2-y^2}$
Ru	2580	4.43	3.49	$sd^{25.47}$	0.53	$0.68*4d_{xy}+0.66*4d_{yz}$
Os		6.65	5.44	$sd^{16.19}$	0.51	$-0.65*5d_{xy}-0.69*5d_{yz}$

β-spin

	IR	sum	ΔE^2_{ij}	hyb.	$\Delta\varepsilon_{ij}$	composition
unit	cm^{-1}	kcal/mol	kcal/mol		hartree	
Fe	2910	0.96	0.80	$sd^{97.48}$	0.61	$0.51*3d_{z^2}-0.85*3d_{yz}$
Ru	2580	2.55	1.74	$sd^{9.93}$	0.49	$0.55*4d_{z^2}+0.74*4d_{xy}$
Os		2.78	1.57	$sd^{1.63}$	0.48	$0.61*6s-0.68*5d_{x^2-y^2}$

A.4.3 The quintet state(ground state)

Table A.105: Structure, bond-order and occupancy comparison of the CH_3RuX molecules. IR^t represents the stretching frequencies of the trans C-H bond, and so on. D(Ru-H^t) represents distances between the Ru atom and the H atom that belongs to the trans C-H bond, and so on.

CH_3RuX	IR^t	D(Ru-H^t)	IR^c	D(Ru-H^c)	D(Ru-C)
unit	cm^{-1}	pm	cm^{-1}	pm	pm
CN	3000	267	3096	266	209
I	2998	267	3081	265	209
Br	2997	267	3079	265	208
Cl	2996	267	3077	266	208
F	2991	267	3071	267	208

Table A.106: Structure, bond-order and occupancy comparison of the C-H activation in the CH_3MF molecules. trans-C-H bond columns give calculated data of the trans C-H bond, and so on. IR gives stretching frequencies of the C-H bond. D(M-H) gives distances between the metal atom and the H atom. D(M-C) gives distances between the metal atom and the C atom of the C-H bond. α-spin columns give calculated data of the α-spin, and so on. BO column gives C-H bond-orders of the trans C-H bond. Occ(σ) column gives occupancies of the C-H-σ orbital, and so on.

	trans-C-H bond		cis-C-H bond		
CH_3MF	IR	D(M-H)	IR	D(M-H)	D(M-C)
unit	cm^{-1}	pm	cm^{-1}	pm	pm
Fe	3075	262	3007	261	201
Ru	2991	267	3071	267	208
Os	2990	266	3070	269	208

		α-spin			β-spin		
CH_3MF	IR^t	BO	Occ(σ)	Occ(σ^*)	BO	Occ(σ)	Occ(σ^*)
unit	cm^{-1}	a.u.					
Fe	3075	0.500	0.999	0.002	0.497	0.992	0.001
Ru	2991	0.498	0.999	0.005	0.491	0.983	0.002
Os	2990	0.497	0.999	0.006	0.489	0.978	0.002

Table A.107: The leading interactions between the C-H-σ orbital and the hybrid orbital of the metal atoms in the CH_3MF molecules. α-spin table records interaction information in the α-spin, and so on. IR^t gives stretching frequencies of the trans C-H bonds. ΔE_{ij}^2 column gives second-order perturbative estimations of the hyperconjugation, hyb. column shows hybridizations of the NHO of the metal atom, which is participated in the interaction, $\Delta\varepsilon_{ij}$ gives energy gaps of the interacting NBOs. Composition column shows orbital compositions of the Ru NHO. Sum column gives sums of this type of interactions. M(coe) column shows polarization coefficients of the M-F-σ^* orbital, and so on.

α-spin

	IR	sum	ΔE_{ij}^2	hyb.	$\Delta\varepsilon_{ij}$	composition
unit	cm^{-1}	kcal/mol	kcal/mol		hartree	
Fe	3075	0.07	0.07	$sd^{0.10}$	0.55	$-0.95*4s-0.25*3d_{x^2-y^2}$
Ru	2991	0.05	0.05	$sd^{0.30}$	0.62	$0.87*5s+0.39*4d_{x^2-y^2}$
Os	2990	0.22	0.22	$sd^{0.77}$	0.80	$0.77*6s+0.52*5d_{x^2-y^2}$

β-spin

	IR	sum	ΔE_{ij}^2	hyb.	$\Delta\varepsilon_{ij}$	composition	M(coe)	F(coe)
unit	cm^{-1}	kcal/mol	kcal/mol		hartree			
Fe	3075	0.89	0.64	$sd^{44.57}$	0.42	$0.98*3d_{xz}$		
Ru	2991	3.37	1.57	$sd^{11.94}$	0.48	$0.33*4d_{z^2}+0.89*4d_{xy}$		
Os	2990	3.79	1.96	$sd^{4.28}$	0.53	$-0.43*6s+0.86*5d_{xy}$	-0.93	0.36

Table A.108: The leading interactions between the C-H-σ^* orbital and the hybrid orbital of the metal atoms in the CH_3MF molecules. α-spin table records interaction information in the α-spin, and so on. IR^t gives stretching frequencies of the trans C-H bonds. ΔE_{ij}^2 column gives second-order perturbative estimations of the hyperconjugation, hyb. column shows hybridizations of the NHO of the metal atom, which is participated in the interaction, $\Delta\varepsilon_{ij}$ gives energy gaps of the interacting NBOs. Composition column shows orbital compositions of the Ru NHO. Sum column gives sums of this type of interactions.

α-spin

	IR	sum	ΔE_{ij}^2	hyb.	$\Delta\varepsilon_{ij}$	composition
unit	cm^{-1}	kcal/mol	kcal/mol		hartree	
Fe	3075	0.54	0.40	$sd^{99.99}$	0.78	$0.99*3d_{xz}$
Ru	2991	1.06	0.86	$sd^{99.99}$	0.71	$0.99*4d_{xz}$
Os	2990	1.95	1.23	$sd^{99.99}$	0.72	$0.99*5d_{xz}$

β-spin

	IR	sum	ΔE_{ij}^2	hyb.	$\Delta\varepsilon_{ij}$	composition
unit	cm^{-1}	kcal/mol	kcal/mol		hartree	
Fe	3075	0.04	0.04	$sd^{99.99}$	0.66	$0.99*3d_{yz}$
Ru	2991	0.35	0.19	$sd^{99.99}$	0.64	$0.99*4d_{yz}$
Os	2990	0.50	0.46	$sd^{1.24}$	0.65	$0.67*6s-0.52*5d_{x^2-y^2}+0.51*5d_{z^2}$

Table A.109: Structure and bond-order and occupancy comparison of the C-H activation in the *n*-C_4H_9MF molecules. In the δ-C-H bond columns calculated data of the δ-C-H bond are represented, and so on. IR gives the stretching frequencies of the C-H bonds. M-H gives distances between the metal atom and the H atom, which belongs to the C-H bond, and so on. BO(α) column gives bond-orders of the C-H bond in the α-spin, and so on. α-spin columns show calculated data of the α-spin, and so on. Occ(σ) column gives occupancies of the C-H-σ orbital, and so on.

	δ-C-H bond			α-C-H bond		
n-C_4H_9MF	IR	D(M-H)	D(M-C)	IR	D(M-H)	D(M-C)
unit	cm^{-1}	pm	pm	cm^{-1}	pm	pm
Fe	2961	240	313	2975	257	201
Ru	2954	255	329	2965	263	209
Os	2927	254	335	2979	264	209

	δ-C-H bond			α-C-H bond		
	IR	BO(α)	BO(β)	IR	BO(α)	BO(β)
unit	cm^{-1}	a.u.		cm^{-1}	a.u.	
Fe	2961	0.494	0.496	2975	0.494	0.490
Ru	2954	0.493	0.493	2965	0.493	0.485
Os	2927	0.494	0.489	2979	0.491	0.489

	δ-C-H bond					α-C-H bond				
		α-spin		β-spin			α-spin		β-spin	
	IR	Occ(σ)	Occ(σ^*)	Occ(σ)	Occ(σ^*)	IR	Occ(σ)	Occ(σ^*)	Occ(σ)	Occ(σ^*)
unit	cm^{-1}	a.u.				cm^{-1}	a.u.			
Fe	2961	0.994	0.008	0.985	0.006	2975	0.994	0.006	0.986	0.005
Ru	2954	0.994	0.009	0.980	0.006	2965	0.995	0.009	0.977	0.006
Os	2927	0.994	0.011	0.977	0.006	2979	0.995	0.011	0.978	0.005

Table A.110: The leading interaction between the C-H-σ orbital and the vacant hybrid orbital of the metal atoms in the n-C_4H_9MF molecules. α-spin table records interaction information in the α-spin, and so on. IR gives stretching frequencies of the C-H bonds. ΔE^2_{ij} column gives second-order perturbative estimations of the hyperconjugation, hyb. column shows hybridizations of the NHO of the metal atom, which is participated in the interaction, $\Delta\varepsilon_{ij}$ gives energy gaps of the interacting NBOs. Composition column shows orbital compositions of the Ru NHO. Sum column gives sums of this type of interactions. M(coe) column shows polarization coefficients of the M-F-σ^* orbital, and so on.

α-spin

	IR	sum	ΔE^2_{ij}	hyb.	$\Delta\varepsilon_{ij}$	composition	M(coe)	F(coe)
unit	cm^{-1}	kcal/mol	kcal/mol		hartree			
Fe	2961	0.23	0.23	$sd^{0.11}$	0.57	$0.94*4s+0.26*3d_{x^2-y^2}$	-0.89	0.45
Ru	2954	0.06	0.06	$sd^{0.30}$	0.64	$-0.87*5s+0.24*4d_{z^2}$	-0.88	0.48
Os	2927	0.06	0.06	$sd^{0.60}$	0.88	$-0.79*6s-0.50*5d_{x^2-y^2}$		

β-spin

	IR	sum	ΔE^2_{ij}	hyb.	$\Delta\varepsilon_{ij}$	composition
unit	cm^{-1}	kcal/mol	kcal/mol		hartree	
Fe	2961	1.99	1.99	$sd^{0.45}$	0.48	$0.81*4s-0.50*3d_{x^2-y^2}$
Ru	2954	2.02	2.02	$sd^{0.43}$	0.49	$0.82*5s+0.41*4d_{z^2}$
Os	2927	2.81	2.46	$sd^{0.57}$	0.47	$0.79*6s+0.41*5d_{z^2}$

Table A.111: The leading interaction between the C-H-σ^* orbital and the hybrid orbital of the metal atoms in the n-C_4H_9MF molecules. IR gives stretching frequencies of the δ-C-H bonds. ΔE^2_{ij} column gives second-order perturbative estimations of the hyperconjugation, hyb. column shows hybridizations of the NHO of the metal atom, which is participated in the interaction, $\Delta\varepsilon_{ij}$ gives energy gaps of the interacting NBOs. Composition column shows orbital compositions of the Ru NHO. Sum column gives sums of this type of interactions.

α-spin

	IR	sum	ΔE^2_{ij}	hyb.	$\Delta\varepsilon_{ij}$	composition
unit	cm^{-1}	kcal/mol	kcal/mol		hartree	
Fe	2961	0.78	0.41	$sd^{10.84}$	0.70	$-0.87*3d_{x^2-y^2}+0.34*3d_{z^2}$
Ru	2954	1.31	0.63	$sd^{6.80}$	0.66	$0.48*4d_{z^2}-0.63*4d_{x^2-y^2}$
Os	2927	2.36	1.21	$sd^{2.93}$	0.64	$0.50*6s-0.50*5d_{x^2-y^2}-0.53*5d_{xz}$

β-spin

	IR	sum	ΔE^2_{ij}	hyb.	$\Delta\varepsilon_{ij}$	composition
unit	cm^{-1}	kcal/mol	kcal/mol		hartree	
Fe	2961	0				
Ru	2954	0.20	0.20	$sd^{99.99}$	0.60	$0.58*4d_{z^2}+0.74*4d_{yz}$
Os	2927	0.16	0.16	$sd^{99.99}$	0.57	$0.65*5d_{z^2}+0.67*5d_{yz}$

A.5 Group 9 transition metal elements

A.5.1 The doublet state(first excited state)

Table A.112: Structure, bond-order and occupancy comparison of the CH_3RhX molecules. IR^t represents the stretching frequencies of the trans C-H bond, and so on. D(Rh-H^t) represents distances between the Rh atom and the H atom that belongs to the trans C-H bond, and so on. In the α-spin columns calculated data of the α-spin are given, and so on. BO^t column shows bond-orders of the trans C-H bond, and so on. Occ(σ) column gives occupancy changes related to the CH_3RhF molecule in the C-H-σ orbital, i.e. $Occ(\sigma) = Occ(\sigma_{(CH_3RhX)} - Occ(\sigma)_{(CH_3RhCN)}$, and so on.

CH_3RhX	IR^t	D(Rh-H^t)	IR^c	D(Rh-H^c)	D(Rh-C)
unit	cm^{-1}	pm	cm^{-1}	pm	pm
CN	2966	249	3090	260	200
Cl	2953	248	3080	259	199
F	2950	250	3071	258	199
Br	2950	247	3080	259	199
I	2949	246	3081	260	199

			α-spin		β-spin	
CH_3RhX	IR^t	IR^c	BO^t	BO^c	BO^t	BO^c
unit	cm^{-1}	cm^{-1}	bond-order			
CN	2966	3090	0.495	0.498	0.495	0.498
Cl	2953	3080	0.493	0.498	0.493	0.498
F	2950	3071	0.493	0.498	0.493	0.498
Br	2950	3080	0.493	0.498	0.493	0.498
I	2949	3081	0.493	0.498	0.493	0.498

		α-spin		β-spin	
CH_3RhX	IR^t	Occ(σ)	Occ(σ^*)	Occ(σ)	Occ(σ^*)
unit	cm^{-1}	a.u.			
CN	2966	0.000	0.000	0.000	0.000
Cl	2953	-0.001	0.001	-0.002	0.001
F	2950	-0.001	0.001	-0.002	0.001
Br	2950	-0.002	0.001	-0.002	0.001
I	2949	-0.002	0.001	-0.002	0.001

.

Table A.113: The leading interaction between the C-H-σ orbital and the vacant hybrid orbital of the Rh atom in the CH_3RhX molecules. α-spin table records interaction information in the α-spin, and so on. IR gives stretching frequencies of the trans C-H bonds. ΔE^2_{ij} column gives second-order perturbative estimations of the hyperconjugation, hyb. column shows hybridizations of the NHO of the metal atom, which is participated in the interaction, $\Delta\varepsilon_{ij}$ gives energy gaps of the interacting NBOs. Composition column shows orbital compositions of the Rh NHO. Sum column gives sums of this type of interactions. M(coe) column shows polarization coefficients of the M-F-σ^* orbital, and so on.

α-spin

	IR	sum	ΔE^2_{ij}	hyb.	$\Delta\varepsilon_{ij}$	composition	M(coe)	F(coe)
unit	cm^{-1}	kcal/mol	kcal/mol		hartree			
CN	2966	0.77	0.59	$sd^{0.95}$	0.65	$0.71*5s-0.66*4d_{x^2-y^2}$	0.83	-0.56
Cl	2953	0.78	0.64	$sd^{0.81}$	0.54	$-0.74*5s+0.64*4d_{x^2-y^2}$	0.87	-0.48
I	2949	0.81	0.65	$sd^{0.67}$	0.54	$-0.77*5s-0.61*4d_{x^2-y^2}$	0.84	-0.54

β-spin

	IR	sum	ΔE^2_{ij}	hyb.	$\Delta\varepsilon_{ij}$	composition	M(coe)	F(coe)
unit	cm^{-1}	kcal/mol	kcal/mol		hartree			
CN	2966	1.34	0.63	$sd^{3.13}$	0.61	$0.49*5s-0.68*4d_{x^2-y^2}-0.51*4d_{z^2}$	0.82	-0.57
Cl	2953	1.09	0.91	$sd^{3.05}$	0.52	$-0.49*5s+0.65*4d_{x^2-y^2}+0.50*4d_{z^2}$	0.86	-0.50
I	2949	1.02	0.86	$sd^{2.23}$	0.52	$-0.55*5s+0.65*4d_{x^2-y^2}+0.46*4d_{z^2}$	0.83	-0.55

Table A.114: Structure, bond-order and occupancy comparison of the C-H activation in the CH_3MF molecules. IR^t gives stretching frequencies of the trans C-H bond.
BO column gives C-H bond-orders of the trans C-H bond and Occ(σ) column gives occupancies of the C-H-σ orbital.

				α-spin			β-spin		
CH_3MF	IR^t	D(M-H^t)	D(M-C)	BO	Occ(σ)	Occ(σ^*)	BO	Occ(σ)	Occ(σ^*)
unit	cm^{-1}	pm	pm			a.u.			
Co	3079	253	193	0.500	0.998	0.002	0.497	0.992	0.002
Rh	2950	250	199	0.493	0.993	0.005	0.493	0.992	0.005
Ir	2259	193	191	0.441	0.907	0.025	0.443	0.917	0.026

Table A.115: The leading interaction between the C-H-σ orbital and the hybrid orbital of the metal atoms in the CH_3MF molecules. α-spin table records interaction information in the α-spin, and so on. IR^t gives stretching frequencies of the trans C-H bonds. ΔE_{ij}^2 column gives second-order perturbative estimations of the hyperconjugation, hyb. column shows hybridizations of the NHO of the metal atom, which is participated in the interaction, $\Delta\varepsilon_{ij}$ gives energy gaps of the interacting NBOs. Composition column shows orbital compositions of the Rh NHO. Sum column gives sums of this type of interactions. M(coe) column shows polarization coefficients of the M-F-σ^* orbital, and so on.

α-spin

	IR	sum	ΔE_{ij}^2	hyb.	$\Delta\varepsilon_{ij}$	composition	M(coe)	F(coe)
unit	cm^{-1}	kcal/mol	kcal/mol		hartree			
Co	3079	0.85	0.46	$sd^{8.54}$	0.46	$-0.32*4s-0.82*3d_{x^2-y^2}+0.46*3d_{z^2}$		
Rh	2950	0.67	0.54	$sd^{1.15}$	0.54	$0.68*5s-0.67*4d_{x^2-y^2}$	-0.92	0.40
Ir	2259	37.67	35.63	$sd^{1.65}$	0.64	$0.61*6s+0.75*5d_{xy}$	-0.90	0.44

β-spin

	IR	sum	ΔE_{ij}^2	hyb.	$\Delta\varepsilon_{ij}$	composition		
unit	cm^{-1}	kcal/mol	kcal/mol		hartree			
Co	3079	0.79	0.63	$sd^{31.36}$	0.41	$-0.80*3d_{xz}-0.52*3d_{yz}$		
Rh	2950	1.34	0.87	$sd^{5.40}$	0.52	$0.39*5s-0.54*4d_{z^2}-0.64*4d_{x^2-y^2}$	-0.90	0.43
Ir	2259	34.79	31.43	$sd^{1.49}$	0.66	$0.63*6s+0.73*5d_{xy}$	-0.91	0.42

Table A.116: Structure and bond-order and occupancy comparison of the C-H activation in the *n*-C_4H_9MF molecules. In the δ-C-H bond columns calculated data of the δ-C-H bond are represented, and so on. IR gives the stretching frequencies of the C-H bonds. M-H gives distances between the metal atom and the H atom, which belongs to the C-H bond, and so on. BO(α) column gives bond-orders of the C-H bond in the α-spin, and so on. α-spin columns show calculated data of the α-spin, and so on. Occ(σ) column gives occupancies of the C-H-σ orbital, and so on.

	δ-C-H bond			α-C-H bond		
n-C_4H_9MF	IR	D(M-H)	D(M-C)	IR	D(M-H)	D(M-C)
unit	cm^{-1}	pm	pm	cm^{-1}	pm	pm
Co	2878	217	301	2964	244	195
Rh	2465	183	243	3005	254	202
Ir	2326	184	226	3004	258	205

	δ-C-H bond			α-C-H bond		
	IR	BO(α)	BO(β)	IR	BO(α)	BO(β)
unit	cm^{-1}	a.u.		cm^{-1}	a.u.	
Co	2878	0.494	0.492	2964	0.491	0.491
Rh	2465	0.462	0.462	3005	0.492	0.492
Ir	2326	0.460	0.467	3004	0.492	0.492

	δ-C-H bond					α-C-H bond				
		α-spin		β-spin			α-spin		β-spin	
	IR	Occ(σ)	Occ(σ^*)	Occ(σ)	Occ(σ^*)	IR	Occ(σ)	Occ(σ^*)	Occ(σ)	Occ(σ^*)
unit	cm^{-1}	a.u.				cm^{-1}	a.u.			
Co	2878	0.976	0.007	0.989	0.013	2964	0.990	0.008	0.985	0.006
Rh	2465	0.945	0.027	0.939	0.028	3005	0.994	0.009	0.993	0.009
Ir	2326	0.936	0.040	0.908	0.028	3004	0.994	0.009	0.994	0.010

Table A.117: The leading interaction between the C-H-σ orbital and the vacant hybrid orbital of the metal atoms in the n-C_4H_9MF molecules. α-spin table records interaction information in the α-spin, and so on. IR gives stretching frequencies of the C-H bonds. ΔE^2_{ij} column gives second-order perturbative estimations of the hyperconjugation, hyb. column shows hybridizations of the NHO of the metal atom, which is participated in the interaction, $\Delta\varepsilon_{ij}$ gives energy gaps of the interacting NBOs. Composition column shows orbital compositions of the Rh NHO. Sum column gives sums of this type of interactions. M(coe) column shows polarization coefficients of the M-F-σ^* orbital, and so on.

α-spin

	IR	sum	ΔE^2_{ij}	hyb.	$\Delta\varepsilon_{ij}$	composition	M(coe)	F(coe)
unit	cm^{-1}	kcal/mol		hartree				
Co	2878	2.75	2.36	$sd^{0.05}$	0.52	$0.97*4s-0.19*3d_{x^2-y^2}$		
Rh	2465	16.70	16.60	$sd^{0.98}$	0.61	$0.71*5s-0.68*4d_{x^2-y^2}$	-0.93	0.38
Ir	2326	29.01	28.69	$sd^{1.06}$	0.70	$0.69*6s-0.67*5d_{x^2-y^2}$	-0.91	0.40

β-spin

	IR	sum	ΔE^2_{ij}	hyb.	$\Delta\varepsilon_{ij}$	composition	M(coe)	F(coe)
unit	cm^{-1}	kcal/mol	kcal/mol		hartree			
Co	2878	1.15	0.86	$sd^{31.91}$	0.44	$-0.50*3d_{z^2}-0.43*3d_{x^2-y^2}-0.64*3d_{xy}$		
Rh	2465	20.65	18.53	$sd^{3.81}$	0.56	$0.45*5s-0.67*4d_{x^2-y^2}-0.48*4d_{z^2}$	-0.92	0.40
Ir	2326	33.01	30.84	$sd^{1.09}$	0.71	$0.69*6s-0.66*5d_{x^2-y^2}$	-0.92	0.40

A.5.2 The quartet state(ground state)

Table A.118: Structure, bond-order and occupancy comparison of the CH_3RuX molecules. IR^t represents the stretching frequencies of the trans C-H bond, and so on. D(Ru-H^t) represents distances between the Ru atom and the H atom that belongs to the trans C-H bond, and so on.

CH_3RuX	IR^t	D(Ru-H^t)	IR^c	D(Ru-H^c)	D(Ru-C)
unit	cm^{-1}	pm	cm^{-1}	pm	pm
CN	3116	267	3019	260	211
I	3102	262	3004	262	206
Br	3096	262	3002	261	206
Cl	3095	262	3002	261	206
F	2999	262	3092	261	205

Table A.119: Structure, bond-order and occupancy comparison of the C-H activation in the CH_3MF molecules. trans-C-H bond columns give calculated data of the trans C-H bond, and so on. IR gives stretching frequencies of the C-H bond. D(M-H) gives distances between the metal atom and the H atom. D(M-C) gives distances between the metal atom and the C atom of the C-H bond. α-spin columns give calculated data of the α-spin, and so on. BO column gives C-H bond-orders of the trans C-H bond. Occ(σ) column gives occupancies of the C-H-σ orbital, and so on.

	trans-C-H bond		cis-C-H bond		
CH_3MF	IR	D(M-H)	IR	D(M-H)	D(M-C)
unit	cm^{-1}	pm	cm^{-1}	pm	pm
Co	3081	256	3081	255	195
Rh	2999	262	3092	261	205
Ir	2983	260	3109	267	204

		α-spin			β-spin		
CH_3MF	IR^t	BO	Occ(σ)	Occ(σ^*)	BO	Occ(σ)	Occ(σ^*)
unit	cm^{-1}	a.u.					
Co	3081	0.500	0.999	0.002	0.496	0.989	0.001
Rh	2999	0.498	1.000	0.004	0.490	0.982	0.003
Ir	2983	0.498	0.999	0.005	0.484	0.972	0.004

Table A.120: The leading interactions between the C-H-σ orbital and the hybrid orbital of the metal atoms in the CH_3MF molecules. α-spin table records interaction information in the α-spin, and so on. IR^t gives stretching frequencies of the trans C-H bonds. ΔE^2_{ij} column gives second-order perturbative estimations of the hyperconjugation, hyb. column shows hybridizations of the NHO of the metal atom, which is participated in the interaction, $\Delta\varepsilon_{ij}$ gives energy gaps of the interacting NBOs. Composition column shows orbital compositions of the Ru NHO. Sum column gives sums of this type of interactions. M(coe) column shows polarization coefficients of the M-F-σ^* orbital, and so on.

α-spin

	IR	sum	ΔE^2_{ij}	hyb.	$\Delta\varepsilon_{ij}$	composition
unit	cm^{-1}	kcal/mol	kcal/mol		hartree	
Co	3081	0.05	0.05	$sd^{0.07}$	0.57	$-0.96*4s-0.21*3d_{x^2-y^2}$
Rh	2999	0				
Ir	2983	0.19	0.19	$sd^{0.46}$	0.78	$-0.82*6s-0.45*5d_{x^2-y^2}$

β-spin

	IR	sum	ΔE^2_{ij}	hyb.	$\Delta\varepsilon_{ij}$	composition
unit	cm^{-1}	kcal/mol	kcal/mol		hartree	
Co	3081	1.50	0.78	$sd^{61.32}$	0.39	$0.98*3d_{xz}$
Rh	2999	3.94	1.76	$sd^{10.07}$	0.46	$-0.30*5s+0.90*4d_{xy}$
Ir	2983	4.15	2.38	$sd^{2.30}$	0.52	$0.55*6s+0.80*5d_{xy}$

Table A.121: The leading interactions between the C-H-σ^* orbital and the hybrid orbital of the metal atoms in the CH_3MF molecules. α-spin table records interaction information in the α-spin, and so on. IR^t gives stretching frequencies of the trans C-H bonds. ΔE^2_{ij} column gives second-order perturbative estimations of the hyperconjugation, hyb. column shows hybridizations of the NHO of the metal atom, which is participated in the interaction, $\Delta\varepsilon_{ij}$ gives energy gaps of the interacting NBOs. Composition column shows orbital compositions of the Ru NHO. Sum column gives sums of this type of interactions.

α-spin

	IR	sum	ΔE^2_{ij}	hyb.	$\Delta\varepsilon_{ij}$	composition
unit	cm^{-1}	kcal/mol	kcal/mol		hartree	
Co	3081	0.41	0.32	$sd^{99.99}$	0.79	$0.99*3d_{xz}$
Rh	2999	1.19	0.77	$sd^{99.99}$	0.71	$0.99*4d_{xz}$
Ir	2983	1.66	1.02	$sd^{99.99}$	0.72	$0.99*5d_{xz}$

β-spin

	IR	sum	ΔE^2_{ij}	hyb.	$\Delta\varepsilon_{ij}$	composition
unit	cm^{-1}	kcal/mol	kcal/mol		hartree	
Co	3081	0.09	0.09	$sd^{4.46}$	0.78	$0.43*4s+0.78*3d_{x^2-y^2}-0.45*3d_{z^2}$
Rh	2999	0.85	0.51	$sd^{99.99}$	0.65	$0.60*4d_{xz}+0.80*4d_{yz}$
Ir	2983	1.02	0.51	$sd^{1.94}$	0.66	$0.58*6s-0.55*5d_{x^2-y^2}+0.51*5d_{z^2}$

Table A.122: Structure and bond-order and occupancy comparison of the C-H activation in the *n*-C_4H_9MF molecules. In the δ-C-H bond columns calculated data of the δ-C-H bond are represented, and so on. IR gives the stretching frequencies of the C-H bonds. M-H gives distances between the metal atom and the H atom, which belongs to the C-H bond, and so on. BO(α) column gives bond-orders of the C-H bond in the α-spin, and so on. α-spin columns show calculated data of the α-spin, and so on. Occ(σ) column gives occupancies of the C-H-σ orbital, and so on.

	δ-C-H bond			α-C-H bond		
n-C_4H_9MF	IR	D(M-H)	D(M-C)	IR	D(M-H)	D(M-C)
unit	cm^{-1}	pm	pm	cm^{-1}	pm	pm
Co	2939	229	309	2970	251	196
Rh	2927	246	331	2968	256	206
Ir	2806	231	322	2932	256	204

	δ-C-H bond			α-C-H bond		
	IR	BO(α)	BO(β)	IR	BO(α)	BO(β)
unit	cm^{-1}	a.u.	a.u.	cm^{-1}	a.u.	a.u.
Co	2939	0.493	0.490	2970	0.494	0.490
Rh	2927	0.493	0.494	2968	0.493	0.482
Ir	2806	0.492	0.489	2932	0.492	0.476

	δ-C-H bond					α-C-H bond				
		α-spin		β-spin			α-spin		β-spin	
Co	2939	0.993	0.009	0.979	0.007	2970	0.994	0.006	0.987	0.008
Rh	2927	0.994	0.012	0.979	0.007	2968	0.995	0.008	0.973	0.007
Ir	2806	0.993	0.016	0.975	0.015	2932	0.995	0.010	0.960	0.007

Table A.123: The leading interaction between the C-H-σ orbital and the vacant hybrid orbital of the metal atoms in the n-C_4H_9MF molecules. α-spin table records interaction information in the α-spin, and so on. IR gives stretching frequencies of the C-H bonds. ΔE^2_{ij} column gives second-order perturbative estimations of the hyperconjugation, hyb. column shows hybridizations of the NHO of the metal atom, which is participated in the interaction, $\Delta\varepsilon_{ij}$ gives energy gaps of the interacting NBOs. Composition column shows orbital compositions of the Ru NHO. Sum column gives sums of this type of interactions.

α-spin

	IR	ΔE^2_{ij}	hyb.	$\Delta\varepsilon_{ij}$	composition	
unit	cm^{-1}	kcal/mol		hartree		
Co	2939	0.43	0.43	$sd^{0.09}$	0.57	$0.95*4s+0.23*3d_{x^2-y^2}$
Rh	2927	0.22	0.22	$sd^{0.18}$	0.69	$0.92*5s+0.30*4d_{z^2}$
Ir	2806	0.38	0.38	$sd^{0.48}$	0.83	$-0.82*6s-0.48*5d_{x^2-y^2}$

β-spin

			NBO1			NBO2		
	IR	sum	ΔE^2_{ij}	hyb.	$\Delta\varepsilon_{ij}$	ΔE^2_{ij}	hyb.	$\Delta\varepsilon_{ij}$
unit	cm^{-1}	kcal/mol	kcal/mol		hartree	kcal/mol		hartree
Co	2939	3.00	1.88	$sd^{0.64}$	0.44	1.07	$sd^{35.68}$	0.51
Rh	2927	2.15	1.26	$sd^{0.13}$	0.51	0.35	$sd^{84.94}$	0.46
Ir	2806	2.94	1.25	$sd^{1.57}$	0.46	1.31	$sd^{19.36}$	0.37

Table A.124: The leading interaction between the C-H-σ^* orbital and the hybrid orbital of the metal atoms in the n-C_4H_9MF molecules. IR gives stretching frequencies of the δ-C-H bonds. ΔE^2_{ij} column gives second-order perturbative estimations of the hyperconjugation, hyb. column shows hybridizations of the NHO of the metal atom, which is participated in the interaction, $\Delta\varepsilon_{ij}$ gives energy gaps of the interacting NBOs. Composition column shows orbital compositions of the Ru NHO. Sum column gives sums of this type of interactions.

α-spin

	IR	sum	ΔE^2_{ij}	hyb.	$\Delta\varepsilon_{ij}$	composition
unit	cm^{-1}	kcal/mol	kcal/mol		hartree	
Co	2939	1.03	0.46	$sd^{14.68}$	0.72	$-0.83*3d_{x^2-y^2}+0.37*3d_{z^2}$
Rh	2927	1.87	0.94	$sd^{15.88}$	0.67	$0.90*4d_{xy}+0.28*4d_{z^2}$
Ir	2806	4.02	3.44	$sd^{2.71}$	0.66	$0.52*6s-0.72*5d_{x^2-y^2}$

β-spin

	IR	sum	ΔE^2_{ij}	hyb.	$\Delta\varepsilon_{ij}$	composition
unit	cm^{-1}	kcal/mol	kcal/mol		hartree	
Co	2939	0.22	0.13	$sd^{26.28}$	0.64	$0.80*3d_{xz}+0.44*3d_{z^2}$
Rh	2927	0.39	0.32	$sd^{99.99}$	0.60	$0.46*4d_{xz}+0.88*4d_{yz}$
Ir	2806	3.19	3.00	$sd^{3.19}$	0.61	$0.49*6s-0.54*5d_{x^2-y^2}+0.51*5d_{xy}$

A.6 Group 10 transition metal elements

A.6.1 The singulet state(ground state)

Table A.125: Structure, bond-order and occupancy comparison of the CH_3PdX molecules. IR represents the stretching frequencies of the C-H bond. D(Pd-H^t) represents distances between the Pd atom and the H atom that belongs to the trans C-H bond, and so on. The trans C-H bond columns give calculated data of the trans C-H bond, the cis C-H bond columns give changes related to the trans C-H bond in the same molecule. BO column shows bond-orders of the C-H bond. Occ(σ) column gives occupancies of the C-H bond.

CH_3PdX	IR^t	D(Pd-H^t)	IR^c	D(Pd-H^c)	D(Pd-C)
unit	cm^{-1}	pm	cm^{-1}	pm	pm
F	2998	247	3124	253	197
CN	2995	243	3134	258	199
Cl	2988	243	3126	255	198
Br	2985	242	3125	256	198
I	2982	240	3124	257	198

	trans C-H bond				cis C-H bond			
CH_3PdX	IR	BO	Occ(σ)	Occ(σ^*)	IR	BO	Occ(σ)	Occ(σ^*)
unit	cm^{-1}		a.u.		cm^{-1}		a.u.	
F	2998	0.995	1.989	0.008	3124	0.997	1.998	0.008
CN	2995	0.995	1.986	0.007	3134	0.997	1.998	0.007
Cl	2988	0.988	1.986	0.008	3126	0.997	1.998	0.008
Br	2985	0.988	1.985	0.008	3125	0.997	1.998	0.008
I	2982	0.987	1.985	0.009	3124	0.997	1.999	0.008

.

Table A.126: The leading interaction between the C-H-σ orbital and the vacant hybrid orbital of the Pd atom in the CH_3PdX molecules. IR gives stretching frequencies of the trans C-H bonds. ΔE^2_{ij} column gives second-order perturbative estimations of the hyperconjugation, hyb. column shows hybridizations of the NHO of the metal atom, which is participated in the interaction, $\Delta\varepsilon_{ij}$ gives energy gaps of the interacting NBOs. Composition column shows orbital compositions of the Pd NHO. Sum column gives sums of this type of interactions. M(coe) column shows polarization coefficients of the M-F-σ^* orbital, and so on.

	IR	sum	ΔE^2_{ij}	hyb.	$\Delta\varepsilon_{ij}$	composition	M(coe)	F(coe)
unit	cm^{-1}	kcal/mol	kcal/mol		hartree			
F	2998	0.96	0.56	$sd^{1.00}$	0.54	$0.70*5s-0.69*4d_{x^2-y^2}$	0.91	0.42
CN	2995	1.42	1.04	$sd^{0.88}$	0.65	$0.73*5s-0.67*4d_{x^2-y^2}$	0.83	0.56
Cl	2988	1.32	1.05	$sd^{0.78}$	0.56	$-0.75*5s+0.65*4d_{x^2-y^2}$	0.87	0.49
Br	2985	1.35	1.08	$sd^{0.72}$	0.56	$-0.76*5s+0.64*4d_{x^2-y^2}$	0.86	0.52
I	2982	1.36	1.09	$sd^{0.68}$	0.57	$-0.77*5s+0.62*4d_{x^2-y^2}$	0.83	0.55

Table A.127: NPA comparison of the C-H bond in the CH_3PdF molecules. The trans C-H bond columns show calculated data of the trans C-H bond, and so on. IR gives the stretching frequencies of the C-H bonds, q(H) gives natural charges of the H atom, which belongs to the C-H bond, and so on. $\Delta(q_H - q_C)$ gives natural charge differences between the H- and C-atoms. Met^c row represents calculated data of the cis C-H bond in the CH_3PdF molecule, and so on.

	trans-C-H bond			cis-C-H bond			
CH_3PdX	IR	$\Delta(q_H - q_C)$	q(H)	IR	$\Delta(q_H - q_C)$	q(H)	q(C)
unit	cm^{-1}	a.u.		cm^{-1}	a.u.		
F	2998	0.838	0.179	3124	0.863	0.204	-0.659
CN	2995	0.842	0.188	3134	0.867	0.213	-0.654
Cl	2988	0.813	0.180	3126	0.838	0.205	-0.633
Br	2985	0.813	0.181	3125	0.837	0.205	-0.632
I	2982	0.827	0.183	3124	0.849	0.205	-0.644

Table A.128: Bond-order and occupancy comparison of the C-H activation in the CH_3MF molecules. Trans C-H bond columns give calculated data of the trans C-H bond. IR gives stretching frequencies of the C-H bond. D(M-H^t) gives distances between the metal atom and the H atom that belongs to the trans C-H bond. D(M-C) gives distances between the metal atom and the C atom of the C-H bond. BO column gives C-H bond-orders of the trans C-H bond and Occ(σ) column gives occupancies of the C-H-σ orbital.

	trans C-H bond				cis C-H bond			
CH_3MF	IR	BO	Occ(σ)	Occ(σ^*)	IR	BO	Occ(σ)	Occ(σ^*)
unit	cm^{-1}		a.u.		cm^{-1}		a.u.	
Ni	2958	0.988	1.982	0.007	3108	0.998	1.999	0.006
Pd	2998	0.995	1.989	0.008	3124	0.997	1.998	0.008
Pt	2909	0.979	1.971	0.011	3089	0.994	1.998	0.013

Table A.129: Bond-order and occupancy comparison of the C-H activation in the n-C_4H_9MF molecules. In the δ-C-H bond columns calculated data of the δ-C-H bond are represented, and so on. IR gives the stretching frequencies of the C-H bonds. M-H gives distances between the metal atom and the H atom, which belongs to the C-H bond, and so on. BO(α) column gives bond-orders of the C-H bond in the α-spin, and so on. α-spin columns show calculated data of the α-spin, and so on. Occ(σ) column gives occupancies of the C-H-σ orbital, and so on.

	δ-C-H bond				α-cis C-H bond			
n-C_4H_9MF	IR	BO	Occ(σ)	Occ(σ^*)	IR	BO	Occ(σ)	Occ(σ^*)
unit	cm^{-1}		a.u.		cm^{-1}		a.u.	
Ni	2596	0.936	1.908	0.041	3023	0.987	1.986	0.014
Pd	2525	0.936	1.893	0.046	3041	0.986	1.987	0.016
Pt	2064	0.893	1.813	0.094	3043	0.984	1.988	0.018

A.6.2 The quartet state(first exited state)

Table A.130: Structure, bond-order and occupancy comparison of the CH_3PdX molecules. IR^t represents the stretching frequencies of the trans C-H bond, and so on. D(Pd-H^t) represents distances between the Pd atom and the H atom that belongs to the trans C-H bond, and so on.

CH_3PdX	IR^t	D(Pd-H^t)	IR^c	D(Pd-H^c)	D(Pd-C)
unit	cm^{-1}	pm	cm^{-1}	pm	pm
CN	3030	256	3148	264	212
I	3025	258	3128	262	208
Br	3024	257	3129	262	208
Cl	3022	256	3127	262	207
F	3016	254	3118	262	206

Table A.131: Structure, bond-order and occupancy comparison of the C-H activation in the CH_3MF molecules. trans-C-H bond columns give calculated data of the trans C-H bond, and so on. IR gives stretching frequencies of the C-H bond. D(M-H) gives distances between the metal atom and the H atom. D(M-C) gives distances between the metal atom and the C atom of the C-H bond. α-spin columns give calculated data of the α-spin, and so on. BO column gives C-H bond-orders of the trans C-H bond. Occ(σ) column gives occupancies of the C-H-σ orbital, and so on.

	trans-C-H bond		cis-C-H bond		
CH_3MF	IR	D(M-H)	IR	D(M-H)	D(M-C)
unit	cm^{-1}	pm	cm^{-1}	pm	pm
Ni	3007	250	3085	254	193
Pd	3016	254	3118	262	206
Pt	2974	254	3146	266	201

		α-spin			β-spin		
CH_3MF	IR^t	BO	Occ(σ)	Occ(σ^*)	BO	Occ(σ)	Occ(σ^*)
unit	cm^{-1}	a.u.					
Ni	3007	0.500	1.000	0.002	0.492	0.987	0.003
Pd	3016	0.500	1.000	0.003	0.487	0.980	0.003
Pt	2974	0.498	0.999	0.005	0.482	0.969	0.005

Table A.132: The leading interactions between the C-H-σ orbital and the hybrid orbital of the metal atoms in the CH_3MF molecules. α-spin table records interaction information in the α-spin, and so on. IR^t gives stretching frequencies of the trans C-H bonds. ΔE^2_{ij} column gives second-order perturbative estimations of the hyperconjugation, hyb. column shows hybridizations of the NHO of the metal atom, which is participated in the interaction, $\Delta\varepsilon_{ij}$ gives energy gaps of the interacting NBOs. Composition column shows orbital compositions of the Pd NHO. Sum column gives sums of this type of interactions. M(coe) column shows polarization coefficients of the M-F-σ^* orbital, and so on.

α-spin

	IR	ΔE^2_{ij}	hyb.	$\Delta\varepsilon_{ij}$	composition
unit	cm^{-1}	kcal/mol	kcal/mol		hartree
Ni	3007	0.06	$sd^{0.06}$	0.55	$0.96 * 4s + 0.18 * 3d_{x^2-y^2}$
Pd	3016	0			
Pt	2974	0.12	$sd^{0.31}$	0.75	$0.87 * 6s + 0.39 * 5d_{x^2-y^2}$

β-spin

			NBO1			NBO2		
	IR	sum	ΔE^2_{ij}	hyb.	$\Delta\varepsilon_{ij}$	ΔE^2_{ij}	hyb.	$\Delta\varepsilon_{ij}$
unit	cm^{-1}	kcal/mol	kcal/mol		hartree	kcal/mol		hartree
Ni	3007	2.67	2.15	$sd^{3.93}$ 3.93	0.47	0.48	$sd^{3.57}$	0.49
Pd	3016	4.75	2.91	$sd^{13.96}$ 13.96	0.45	1.45	$sd^{29.94}$	0.46
Pt	2974	4.48	2.63	$sd^{1.08}$ 1.08	0.52	1.70	$sd^{99.98}$	0.36

Table A.133: The leading interactions between the C-H-σ^* orbital and the hybrid orbital of the metal atoms in the CH_3MF molecules. α-spin table records interaction information in the α-spin, and so on. IR^t gives stretching frequencies of the trans C-H bonds. ΔE^2_{ij} column gives second-order perturbative estimations of the hyperconjugation, hyb. column shows hybridizations of the NHO of the metal atom, which is participated in the interaction, $\Delta\varepsilon_{ij}$ gives energy gaps of the interacting NBOs. Composition column shows orbital compositions of the Pd NHO. Sum column gives sums of this type of interactions.

α-spin

	IR	sum	ΔE^2_{ij}	hyb.	$\Delta\varepsilon_{ij}$	composition
unit	cm^{-1}	kcal/mol	kcal/mol		hartree	
Ni	3007	0.47	0.47	$sd^{74.57}$	0.79	$0.98 * 3d_{xy}$
Pd	3016	0.84	0.48	$sd^{8.91}$	0.70	$-0.43 * 4d_{xz} - 0.76 * 4d_{x^2-y^2}$
Pt	2974	1.39	0.84	$sd^{99.99}$	0.72	$0.99 * 5d_{xz}$

β-spin

	IR	sum	ΔE^2_{ij}	hyb.	$\Delta\varepsilon_{ij}$	composition
unit	cm^{-1}	kcal/mol	kcal/mol		hartree	
Ni	3007	1.17	0.76	$sd^{3.57}$	0.77	$-0.47 * 4s - 0.64 * 3d_{x^2-y^2} + 0.48 * 3d_{z^2}$
Pd	3016	1.04	0.71	$sd^{29.94}$	0.75	$-0.47 * 4d_{z^2} + 0.84 * 4d_{x^2-y^2}$
Pt	2974	1.51	0.49	$sd^{2.40}$	0.81	$-0.54 * 6s - 0.66 * 5d_{x^2-y^2} - 0.43 * 5d_{xy}$

Table A.134: Structure and bond-order and occupancy comparison of the C-H activation in the *n*-C_4H_9MF molecules. In the δ-C-H bond columns calculated data of the δ-C-H bond are represented, and so on. IR gives the stretching frequencies of the C-H bonds. M-H gives distances between the metal atom and the H atom, which belongs to the C-H bond, and so on. BO(α) column gives bond-orders of the C-H bond in the α-spin, and so on. α-spin columns show calculated data of the α-spin, and so on. Occ(σ) column gives occupancies of the C-H-σ orbital, and so on.

	δ-C-H bond			α-C-H bond		
n-C_4H_9MF	IR	D(M-H)	D(M-C)	IR	D(M-H)	D(M-C)
unit	cm^{-1}	pm	pm	cm^{-1}	pm	pm
Ni	2944	236	313	3058	248	194
Pd	2962	253	332	3023	259	209
Pt	2699	213	307	3048	258	205

	δ-C-H bond				α-C-H bond		
	IR	BO(α)	BO(β)		IR	BO(α)	BO(β)
unit	cm^{-1}	a.u.			cm^{-1}	a.u.	
Ni	2944	0.493	0.490	3058		0.495	0.492
Pd	2962	0.493	0.490	3023		0.494	0.491
Pt	2699	0.496	0.490	3048		0.492	0.490

	δ-C-H bond					α-C-H bond				
		α-spin		β-spin			α-spin		β-spin	
	IR	Occ(σ)	Occ(σ^*)	Occ(σ)	Occ(σ^*)	IR	Occ(σ)	Occ(σ^*)	Occ(σ)	Occ(σ^*)
unit	cm^{-1}	a.u.				cm^{-1}	a.u.			
Ni	2944	0.993	0.009	0.986	0.008	3058	0.995	0.006	0.991	0.007
Pd	2962	0.994	0.010	0.985	0.006	3023	0.995	0.007	0.990	0.008
Pt	2699	0.993	0.021	0.943	0.011	3048	0.995	0.009	0.986	0.006

Table A.135: The leading interaction between the C-H-σ orbital and the vacant hybrid orbital of the metal atoms in the n-C_4H_9MF molecules. α-spin table records interaction information in the α-spin, and so on. IR gives stretching frequencies of the C-H bonds. ΔE^2_{ij} column gives second-order perturbative estimations of the hyperconjugation, hyb. column shows hybridizations of the NHO of the metal atom, which is participated in the interaction, $\Delta\varepsilon_{ij}$ gives energy gaps of the interacting NBOs. Composition column shows orbital compositions of the Pd NHO. Sum column gives sums of this type of interactions.

α-spin

	IR	sum	ΔE^2_{ij}	hyb.	$\Delta\varepsilon_{ij}$	composition
unit	cm^{-1}	kcal/mol		hartree		
Ni	2944	0.46	0.46	$sd^{0.06}$	0.58	$-0.96*4s-0.17*3d_{x^2-y^2}$
Pd	2962	0.26	0.26	$sd^{0.12}$	0.70	$-0.94*5s-0.23*4d_{x^2-y^2}$
Pt	2699	0.41	0.41	$sd^{0.31}$	0.77	$-0.87*6s-0.38*5d_{x^2-y^2}$

β-spin

			NBO1			NBO2		
	IR	sum	ΔE^2_{ij}	hyb.	$\Delta\varepsilon_{ij}$	ΔE^2_{ij}	hyb.	$\Delta\varepsilon_{ij}$
unit	cm^{-1}	kcal/mol	kcal/mol		hartree	kcal/mol		hartree
Ni	2944	1.51	0.72	$sd^{0.71}$	0.45	0.79	$sd^{3.11}$	0.49
Pd	2962	1.46	0.71	$sd^{0.10}$	0.54	0.49	$sd^{13.31}$	0.43
Pt	2699	7.40	7.23	$sd^{0.33}$	0.48	0.17	$sd^{10.66}$	0.55

Table A.136: The leading interaction between the C-H-σ^* orbital and the hybrid orbital of the metal atoms in the n-C_4H_9MF molecules. IR gives stretching frequencies of the δ-C-H bonds. ΔE^2_{ij} column gives second-order perturbative estimations of the hyperconjugation, hyb. column shows hybridizations of the NHO of the metal atom, which is participated in the interaction, $\Delta\varepsilon_{ij}$ gives energy gaps of the interacting NBOs. Composition column shows orbital compositions of the Pd NHO. Sum column gives sums of this type of interactions.

α-spin

	IR	sum	ΔE^2_{ij}	hyb.	$\Delta\varepsilon_{ij}$	composition
unit	cm^{-1}	kcal/mol	kcal/mol		hartree	
Ni	2944	0.93	0.39	$sd^{34.00}$	0.73	$-0.92*3d_{x^2-y^2}+0.21*3d_{z^2}$
Pd	2962	1.33	0.47	$sd^{47.11}$	0.68	$-0.78*4d_{x^2-y^2}-0.57*4d_{xy}$
Pt	2699	5.63	4.79	$sd^{4.72}$	0.64	$0.42*6s-0.36*5d_{x^2-y^2}+0.77*5d_{z^2}$

β-spin

	IR	sum	ΔE^2_{ij}	hyb.	$\Delta\varepsilon_{ij}$	composition
unit	cm^{-1}	kcal/mol	kcal/mol		hartree	
Ni	2944	0.56	0.42	$sd^{62.05}$	0.65	$-0.57*3d_{x^2+z}+0.69*3d_{xy}$
Pd	2962	0.36	0.25	$sd^{99.99}$	0.63	$-0.71*4d_{z^2}+0.39*4d_{xy}$
Pt	2699	1.54	0.82	$sd^{99.99}$	0.62	$0.93*5d_{xz}+0.38*5d_{z^2}$

CV – DAWEI ZHAO

Name: Dawei Zhao
Marital Status: single
Nationality: Chinese
e-mail: daweiberlin@yahoo.de

HIGHER EDUCATION:

06/10-Present PhD studies in Theoretic Chemistry, Department of Chemistry, Technical University Kaiserslautern.
Advisor: Prof. Dr. Christopher van. Wüllen.
Focus on C-H activation mediated transition metal.

02/10-02/05 Diplom studies in Department of Chemistry, Technical University Berlin,
Grade: GPA 1.7 (1.0 highest – 4.0 lowest mark).
Advisor: Prof. Dr. Otto Dopfer.
Thesis: Structure and infrared spectra of protonated polycyclic aromatic hydrocarbon molecules.

SCHOOL:

1991 – 1993 Automatic productprocess, Technical University South China
1988 – 1991 Senior High School, Beijing.

EMPLOYMENT:

1993 – 2001 Computer associated work in Beijing.

LANGUAGES: Chinese – mother tongue
Deutsch – fluent (reading & oral)
English – fluent (reading & written)

HOBBIES: Yoga, Reading, Music

PUBLICATIONS:

1) Dawei Zhao, Judith Langer, Jos Oomens, and Otto Dopfer, *Journal of Chemical Physics*, **2009**, 131,184307:Infrared spectra of protonated polycyclic aromatic hydrocarbon molecules: Azulene

AWARDS AND HONORS:

Scholarship Klaus-Koch-Stiftung (2005)

REFERENCES:

Prof. Dr. Christoph van Wüllen
FACHBEREICH CHEMIE - THEORETISCHE CHEMIE
TECHNISCHE UNIVERSITÄT KAISERSLAUTERN
ERWIN-SCHRÖDINGER-STRAßE 52
67663 KAISERSLAUTERN
TEL.: +49-(0)631-205-2749
MAIL:VANWULLEN@CHEMIE.UNI-KL.DE

PROF. DR. OTTO DOPFER
TECHNISCHE UNIVERSITÄT BERLIN
HARDENBERGSTRAßE 36
EUGENE-PAUL-WIGNER GEBÄUDE
10623 BERLIN
TELEFON: +49 - (0)30 - 314 23017
MAIL: dopfer@physik.tu-berlin.de